Analysis of earthquake-triggered landslides in the South of Iberia:

Testing the use of the Newmark's method at different scales

MARTÍN JESÚS RODRÍGUEZ PECES

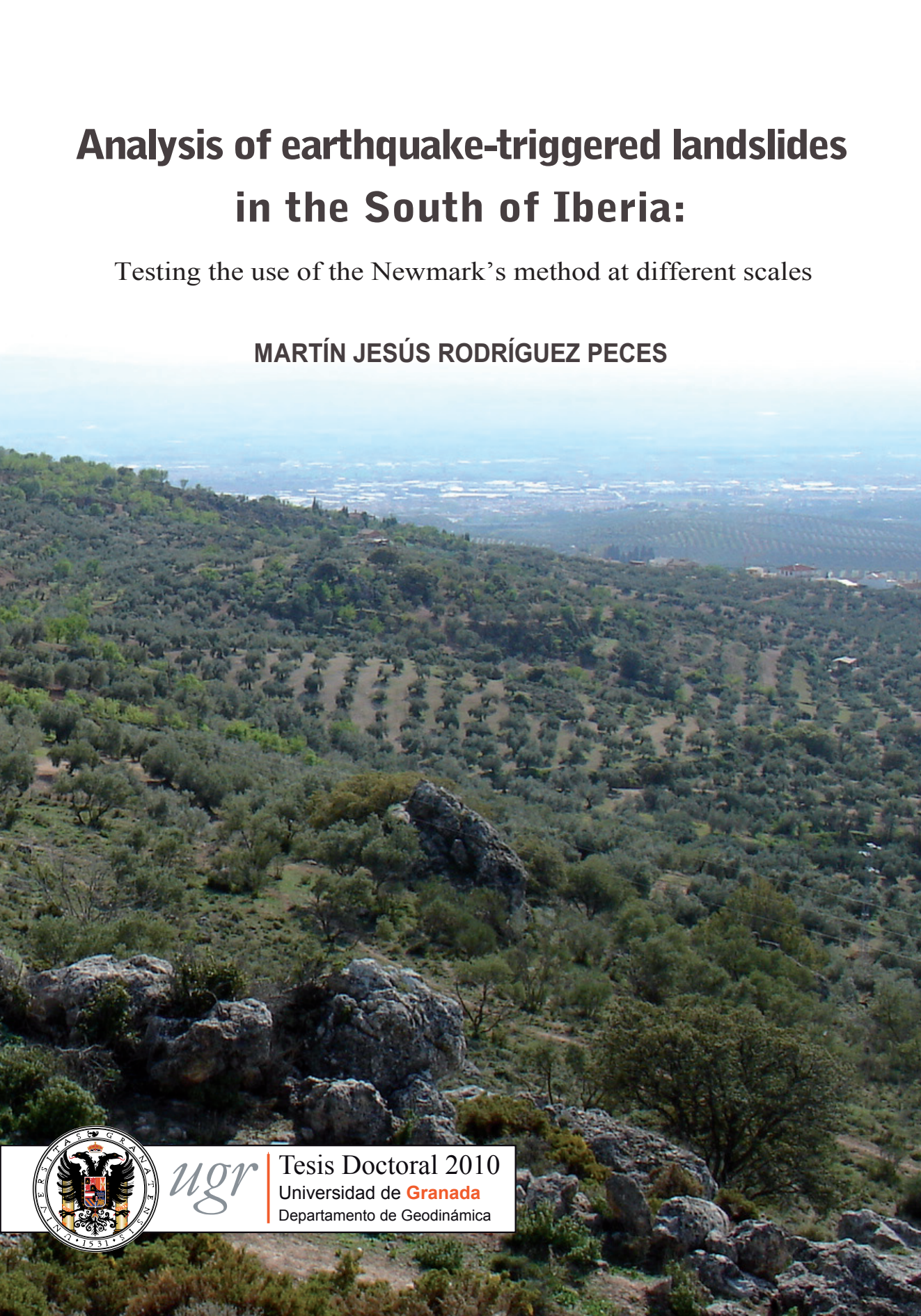

ugr
Tesis Doctoral 2010
Universidad de Granada
Departamento de Geodinámica

Editor: Editorial de la Universidad de Granada
Autor: Martín Jesús Rodríguez Peces
D.L.: GR 3794-2010
ISBN: 978-84-693-6019-4

ANALYSIS OF EARTHQUAKE-TRIGGERED LANDSLIDES IN THE SOUTH OF IBERIA:
TESTING THE USE OF THE NEWMARK'S METHOD AT DIFFERENT SCALES

BY

MARTÍN JESÚS RODRÍGUEZ PECES

Ph.D. Thesis – Tesis Doctoral

Departamento de Geodinámica

UNIVERSIDAD DE GRANADA

2010

Departamento de Geodinámica
Universidad de Granada

ANALYSIS OF EARTHQUAKE-TRIGGERED LANDSLIDES IN THE SOUTH OF IBERIA:
TESTING THE USE OF THE NEWMARK'S METHOD AT DIFFERENT SCALES

Memoria de Tesis Doctoral presentada por el Licenciado en Geología D. Martín Jesús Rodríguez Peces para optar al Grado de Doctor por la Universidad de Granada

Granada, Julio de 2010

Fdo. Martín Jesús Rodríguez Peces

VºBº del Director

VºBº del Director

Fdo. Dr. José Miguel Azañón Hernández

Fdo. Dr. Julián García Mayordomo

VºBº del Director

Fdo. Dr. Antonio Jabaloy Sánchez

Agradecimientos

Este trabajo de investigación ha sido realizado gracias a una Beca de Formación de Personal Docente e Investigador asociada al Proyecto de Investigación de Excelencia P05-RNM-0327 concedida por la Junta de Andalucía, a los recursos materiales del Grupo de investigación RNM-149 y del Departamento de Geodinámica de la Universidad de Granada y a los proyectos TOPOIBERIA CONSOLIDER-INGENIO2010 CSD2006-00041, MMA083/2007, CGL2008-03249/BTE y FASE-GEO CGL2009-09726.

Deseo expresar mi más sincero agradecimiento a José Miguel Azañón Hernández, a Julián García Mayordomo y a Antonio Jabaloy Sánchez por aceptar mi propuesta para trabajar con ellos, así como por realizar sus respectivas tareas como tutores y supervisores de la presente Tesis Doctoral. Gracias a sus sugerencias e ideas ya que han contribuido a enriquecer gran parte de este trabajo. Además agradezco especialmente a Julián García Mayordomo por haberse involucrado en este proyecto, a pesar de encontrarse lejos de Granada.

Un agradecimiento especial para José Jesús Martínez Díaz y Meaza Tsige por su apoyo en los primeros momentos de la tesis y por proporcionarme información muy valiosa sobre la Cuenca de Lorca (modelo digital de elevaciones, ortofotos e informes geotécnicos).

Gracias también a Juan Miguel Insua Arévalo ya que, además de ser un excelente profesor y haber contribuido notablemente a mi formación académica, he tenido el placer de compartir algunas jornadas de campo (¡y pulgas!).

Especial agradecimiento a Francisco Javier Roldán García y a Carlos Marín Lechado del Instituto Geológico y Minero de España por facilitarme los nuevos mapas geológicos continuos del área de Sierra Nevada y Granada, incluso antes de estar finalizados.

También mis agradecimientos van dirigidos a Antonio Azor Pérez y Juan Jiménez Pintor por permitirme hacer uso de la información recogida en la tesis de máster dedicada al estudio del deslizamiento de Güevéjar. También agradezco a Carlos Sanz de Galdeano su confianza al prestarme parte de la bibliografía consultada.

Muchas gracias a José Luis Pérez García de la Universidad de Jaén por haber sacado tiempo para ayudarme con los datos del escáner laser terrestre, a pesar de sus otras obligaciones.

Mi gratitud a todos los investigadores y trabajadores de las unidades de investigación de inestabilidades del terreno y de peligrosidad sísmica del BRGM

(Orleans, Francia) por su estupenda acogida durante mi breve estancia, especialmente a Gilles Grandjean que se interesó por mi trabajo desde el principio facilitándome los medios materiales (¡con despacho propio incluido!) durante mi estancia y a Daniel Monfort Clement que, como español exiliado, me ayudó múltiples veces con el idioma.

Gracias también a la larga lista de compañeros becarios, contratados y doctores que en mayor o en menor medida han compartido su tiempo durante estos cuatro años de tesis (¡y de cafés!). Todos ellos sabrán quienes son. Un agradecimiento especial a Mercedes Vázquez y María Luján, compañeras de despacho de "becarios", por sus ánimos y consejos.

Una mención especial a José Alberto, compañero y amigo desde el primer día que nos conocimos (buscando la desaparecida G-16), con el que he compartido esta aventura granadina durante estos 10 años de geología. Tenemos una bajada del Jorado pendiente.

A mis compañeros de promoción de la licenciatura, tanto los que terminaron como los que se quedaron en el camino a descansar.

A los buenos amigos "dominicos" (Rafa, Mario, Carlos, Juanma) que aunque estén lejos siempre estarán cerca.

Tampoco quiero olvidarme de mis compañeros del último Máster de Ingeniería Geológica de la Universidad Complutense de Madrid, en especial de Marta, Mariajo y Mariela con las que tantas horas de trabajos en grupo compartí desde la distancia.

También agradezco el apoyo recibido de mis amigos canarios desde las regiones ultraperiféricas, sobre todo a Orlando que logró que durante mis cortas vacaciones me olvidase temporalmente de las obligaciones del trabajo.

Por último, quiero agradecer en gran medida a mi familia por haberme permitido llegar hasta aquí y por darme ánimos para seguir adelante con la siguiente etapa de la vida. Y a mi querida Leti por tener que soportarme día a día cuando estaba cerca y echarme de menos cuando estaba lejos. A todos ellos va especialmente dedicada la presente Tesis Doctoral.

“La ciencia no consiste sólo en saber lo que debe o puede hacerse, sino también en saber lo que podría hacerse aunque quizá no debiera hacerse”

Fray Guillermo de Baskerville
(El nombre de la rosa)

TABLE OF CONTENTS

ABSTRACT

In this Ph.D. Thesis, a comprehensive methodology has been developed and tested in order to assess the potential earthquake-triggered slope instabilities at different scales. This methodology was applied at a regional scale in order to obtain regional hazard maps in terms of Newmark displacement as a first step in studying earthquake-triggered slope instabilities at specific locations. The Newmark displacement represents the expected slope displacement due to strong ground motion. The construction of the Newmark displacement map is based on GIS technology (ArcGIS 9.3) and results from computing several sets of maps. The first aim of this calculation is to obtain a critical acceleration map –i.e., the minimum horizontal seismic acceleration to overcome shear resistance and initiate sliding, provided the static safety factor is known. The second aim is to estimate Newmark displacement combining the critical acceleration map with a peak ground acceleration map (PGA) by means of an empirical relationship.

To produce the critical acceleration (a_c) map, a lithological map is firstly arranged from digital geological maps from the Institute of Geology and Mines of Spain (IGME). Strength parameters –specific weight, cohesion and friction angle– are assigned to each lithological unit based on a database derived from geotechnical bibliography as well as from available geotechnical tests. Then, a map of static safety factors was estimated considering an infinite-slope limit equilibrium model. Finally, the safety factor map is combined with a slope map to produce a critical acceleration map, which can be regarded as a map of seismic landslide susceptibility.

To estimate the Newmark displacements, different seismic input scenarios are considered: probabilistic, pseudo-probabilistic and deterministic. The former scenario considers hazard maps in terms of peak ground acceleration (PGA) corresponding to different return periods (or exceedance probability levels) commonly used in the engineering design of structures. Pseudo-probabilistic seismic scenarios are considered assuming the occurrence of the most probable earthquake for a specific return period at every location, while the deterministic scenarios are devised by considering the complete rupture of the main active faults in the study area. Input PGA values are originally referred to rock conditions, so it was necessary to consider the influence of local site effects (soil and topography factors) in the amplification of strong ground motion. Soil amplification factors are adopted from previous studies concerning seismic hazard in the south Spain (RISMUR and SISMOSAN projects), while the topographic factor has been particularly evaluated in this Ph.D. Thesis considering the slope and relative height of the ridges, following Eurocode-8 provisions. Finally, amplified PGA scenario maps are computed with the critical acceleration map by means of a regression equation that correlates Newmark displacement to the critical acceleration ratio (a_c/PGA).

The proposed methodology has been firstly used to perform a regional hazard assessment of earthquake-triggered slope instabilities in the Lorca and Granada basins and the Sierra Nevada Range. These regions are one of the most seismically active areas of the Iberian Peninsula. Three significant seismic series have recently struck the Lorca Basin: 1999 Mula (M_w=4.8, I_{EMS}=VI), 2002 Bullas (M_w=5.0, I_{EMS}=V) and 2005 La Paca (M_w=4.8, I_{EMS}=VI-VII). Despite their small magnitude, these earthquakes produced significant damage on buildings, as well as they induced the well-known Bullas and La Paca rock slides. In the Granada Basin, several slope instabilities (mainly rock falls and landslides) can be related to historical earthquakes, such as the 1884 Arenas del Rey earthquake (M_w~6.5, I_{MSK}=X), as well as to instrumental ones (e.g. 1956 Albolote earthquake).

The resulting Newmark displacement maps show that seismically-induced landslide hazard in the Lorca and Granada Basins and Sierra Nevada Range can be considered as low. However, the occurrence of widespread slope instabilities across these areas is expected if a low-frequency but powerful earthquake (M_w>6.6) related to the rupture of one of the main active faults in the area takes place. In addition, this approach has allow to identify disrupted-type slides as the most likely earthquake-triggered slope instability in Lorca and Granada basins and Sierra Nevada Range. These instabilities seem to be related to a threshold Newmark displacement of 2 cm or even smaller.

A detailed study of the 2002 Bullas and 2005 La Paca rock slides have been performed in order to evaluate the applicability of the developed method at different scales. In this sense, it has been showed in this Ph.D. Thesis that the evaluation of earthquake-triggered landslides at a regional scale can produce wrong estimates of Newmark displacements. Nevertheless, the regional scale maps are useful to show in a preliminarily way the areas with the highest susceptibility and hazard that can be interesting for subsequent site-specific studies at a larger scale. A critical Newmark displacement value of 3 cm has been obtained as the minimum threshold to trigger disrupted-type slope instabilities similar to the 2002 Bullas and 2005 La Paca rock slides. The results obtained at a sub-regional scale agreed with those obtained in these slides at a site scale.

A new approach is also proposed in this Ph.D. Thesis to reassess the magnitude and epicentral location of pre-instrumental earthquakes by means of the implementation of the Newmark's method in the study of singular earthquake-triggered landslides. This methodology has been applied succesfully to the Güevéjar landslide that was triggered both by the 1755 Lisbon and 1884 Arenas del Rey historical earthquakes. A minimum M_w 8.5 and an epicentral distance from the Güevéjar landslide of 580 km have been estimated for the 1755 Lisbon earthquake. For the case of the 1884 Arenas del Rey earthquake, the estimated minimum magnitude was M_w 6.5 and the epicentral distance from the Güevéjar landslide was 55 km. In both cases, the results agree with the magnitude and epicentral location suggested by other authors. In addition, it has been confirmed that the 1884 Arenas del Rey earthquake was most likely related to the rupture of the Ventas de Zafarraya Fault.

Finally, the Newmark's method is also applied successfully to consider the potencial seismic reactivation and testing the efficiency of slope stabilisation measures of present-day slope instabilities (e.g. Güevéjar and Diezma landslides). This approach provides minimum magnitudes at different epicentral distances that are required to overcome the critical acceleration value and thus to trigger the instability. It has been found that the Güevéjar and Diezma landslides would be very likely reactivated by an earthquake related to the rupture of some of the active faults in the Granada Basin (e.g. Granada, Atarfe and Santa Fe faults).

RESUMEN

En esta Tesis Doctoral se ha desarrollado y puesto a prueba una metodología integral con objeto de evaluar las potenciales inestabilidades de ladera provocadas por terremotos considerando diferentes escalas. Esta metodología ha sido aplicada a escala regional con la finalidad de obtener mapas de peligrosidad en términos de desplazamiento de Newmark como primer paso en el estudio de las inestabilidades de ladera inducidas por terremotos en emplazamientos concretos. El desplazamiento de Newmark representa una aproximación al desplazamiento esperado en una ladera debido al movimiento del terreno. La construcción de los mapas de desplazamiento de Newmark se realiza con un sistema de información geográfica (ArcGIS 9.3.) y resulta de combinar una serie de mapas con dos propósitos principales. El primero es el de obtener un mapa de aceleración crítica (la aceleración sísmica mínima necesaria para superar la resistencia al corte e iniciar el desplazamiento) a partir del factor de seguridad estático. El segundo objetivo es estimar el valor de desplazamiento de Newmark combinando el mapa de aceleración crítica con el mapa de aceleración sísmica máxima (*PGA*) mediante el uso de una relación empírica.

Para generar el mapa de aceleración crítica (a_c), se ha compuesto un mapa litológico a partir de los mapas geológicos digitales del Instituto Geológico y Minero de España (IGME). A cada unidad litológica se le asignaron valores de parámetros resistentes (peso específico, cohesión y ángulo de rozamiento interno) derivados de una base de datos construida a partir de bibliografía geotécnica así como de ensayos geotécnicos disponibles. A continuación, se calculó un mapa de factores de seguridad estáticos considerando un modelo de equilibrio límite de talud infinito. Por último, el mapa de factores de seguridad se combinó con el mapa de pendientes para obtener el mapa de aceleración crítica, que puede considerarse como un índice de susceptibilidad a inestabilidades inducidas sísmicamente.

Para estimar los desplazamientos de Newmark se han considerado diferentes escenarios sísmicos: probabilistas, pseudo-probabilistas y deterministas. Los primeros consideran mapas de peligrosidad sísmica en términos de aceleración sísmica máxima (*PGA*) correspondientes a diferentes periodos de retorno (o niveles de probabilidad de excedencia) de uso habitual en ingeniería para el diseño de infraestructuras. Los escenarios sísmicos pseudo-probabilistas han sido considerados asumiendo que el terremoto más probable para un periodo de retorno determinado puede ocurrir en cualquier punto del área de estudio, mientras que los escenarios deterministas se obtuvieron considerando que un terremoto máximo relacionado con la rotura completa de las principales fallas activas tiene lugar en el área de estudio. Los valores de *PGA* están referidos para basamento rocoso, así que han sido corregidos para tener en cuenta los efectos de amplificación del suelo y topográfica. Los factores de amplificación del suelo han sido tomados de estudios previos concernientes a la peligrosidad sísmica en el sur de España (proyectos RISMUR y SISMOSAN),

mientras que el factor de amplificación topográfico ha sido evaluado particularmente en esta Tesis Doctoral considerando la pendiente y la altura relativa de las crestas montañosas, siguiendo las recomendaciones del Eurocódigo 8. Por último, los mapas de *PGA* amplificada correspondientes a de cada escenario considerado se combinaron con el mapa de aceleración crítica por medio de una ecuación de regresión que correlaciona los desplazamientos de Newmark con la razón de aceleración crítica (a_c/PGA).

La metodología propuesta se ha empleado en primer lugar para realizar una evaluación regional de la peligrosidad de las inestabilidades de ladera producidas por terremotos en las cuencas de Lorca y de Granada y en Sierra Nevada. Estos territorios son las áreas con mayor actividad sísmica histórica e instrumental en el sur de la Península Ibérica. Recientemente, tres series sísmicas significativas han afectado a la Cuenca de Lorca: Mula en 1999 (M_w=4.8, I_{EMS}=VI), Bullas en 2002 (M_w=5.0, I_{EMS}=V) y La Paca en 2005 (M_w=4.8, I_{EMS}=VI-VII). A pesar de tener una magnitud relativamente pequeña, estos terremotos produjeron importantes daños en las edificaciones y provocaron los desprendimientos rocosos de Bullas y La Paca, respectivamente. En la Cuenca de Granada se han producido importantes inestabilidades de ladera (principalmente, desprendimientos y deslizamientos) relacionados con terremotos históricos, como el de Arenas del Rey en 1884 (M_w~6.5, I_{MSK}=X), y también con terremotos instrumentales (ej. Albolote en 1956).

Los mapas de desplazamiento de Newmark resultantes muestran que la peligrosidad del fenómeno de movimientos de ladera inducidos por efecto sísmico en las cuencas de Lorca y Granada y en Sierra Nevada se puede considerar como baja. Sin embargo, es de esperar que se produzcan inestabilidades de ladera de manera generalizada en dichas areas, si se produce un gran terremoto (M_w>6.6) en relación con la rotura de alguna de las principales fallas activas de la zona. Además, este método ha permitido identificar las inestabilidades de tipo disgregado como las inestabilidades de ladera provocadas por terremotos más probables en las cuencas de Lorca y Granada y en Sierra Nevada. Estas inestabilidades parecen estar relacionadas con un desplazamiento de Newmark mínimo de 2 cm o incluso más pequeño.

Se ha realizado un estudio detallado de los desprendimientos de rocas de Bullas en 2002 y de La Paca en 2005 con la finalidad de evaluar la aplicabilidad del método de Newmark a diferentes escalas. En este sentido, en esta Tesis Doctoral se ha puesto en evidencia que la evaluación de inestabilidades de ladera causadas por terremotos a escala regional puede mostrar resultados erróneos en el cálculo de los desplazamientos de Newmark. Sin embargo, los mapas a escala regional son útiles para mostrar de forma preliminar las áreas con mayor susceptibilidad y peligrosidad que pueden ser interesantes para futuros estudios a una escala mayor. Se ha obtenido un valor crítico de desplazamiento de Newmark de 3 cm como el umbral mínimo para causar inestabilidades de ladera de tipo disgregado similares a los desprendimientos rocosos de Bullas en 2002 y La Paca en 2005. Los resultados obtenidos a escala sub-regional están de acuerdo con los obtenidos en estas inestabilidades a una escala local.

En esta Tesis Doctoral también se ha propuesto un nuevo procedimiento para reevaluar la magnitud y la localización epicentral de terremotos pre-instrumentales por medio de la aplicación del método de Newmark en el estudio de determinadas inestabilidades de ladera inducidas por terremotos. Esta metodología se ha aplicado con éxito para el deslizamiento de Güevéjar que fue inducido por los terremotos históricos de Lisboa en 1755 y Arenas del Rey en 1884. Se ha estimado una magnitud mínima de M_w 8.5 y una distancia epicentral al deslizamiento de Güevéjar de 580 km para el terremoto de Lisboa de 1755. Para el caso del terremoto de Arenas del Rey en 1884, la magnitud mínima estimada fue de M_w 6.5 y la distancia epicentral al deslizamiento de Güevéjar fue de 55 km. En ambos casos, los resultados coinciden con la magnitud y la localización epicentral sugeridas por otros autores. Además, se ha corroborado que el terremoto de Arenas del Rey en 1884 estuvo relacionado muy probablemente con la rotura de la Falla de Ventas de Zafarraya.

Por último, en esta Tesis Doctoral se estudia la posible reactivación sísmica de inestabilidades de ladera actuales (ej., deslizamientos de Güevéjar y de Diezma), así como se comprueba la eficacia de las medidas de estabilización de laderas empleadas en ellas. Esta aplicación proporciona las magnitudes mínimas a diferentes distancias epicentrales requeridas para superar el valor de la aceleración crítica y por lo tanto para desencadenar la inestabilidad. Se ha encontrado que los deslizamientos de los Güevéjar y de Diezma podrían ser reactivados muy probablemente por un terremoto relacionado con la rotura de alguna de las fallas activas presentes en la Cuenca de Granada.

PART ONE

1

Introduction

1.1. Interest of the topic

Ground shaking is considered the primary cause of damage, loss of life and injuries due to earthquakes. However, earthquakes are one of the most relevant triggering factors of ground failures (e.g. landslides, liquefaction and surface fault rupture). In this sense, slope movements are often the major second cause of the greatest damage, human and material losses when an earthquake occurs (cf. Bird and Bommer, 2004). For instance, about 56% of the total cost of the damage caused during the 1964 Alaska earthquake was due to earthquake-induced slope failures (Youd, 1978). While the ground shaking is mainly related to structural damage and collapse of buildings in urban areas, earthquake-triggered landslides are less likely to cause structural damage, but are frequently the cause of major disruptions of life-lines (e.g. roads, railways, power lines, gas pipes, water channels, etc.) and, therefore, are crucial in permitting a rapid response of emergency services in the aftermath of a seismic event. Landslides can also produce dramatic changes in the landscape even far away from the earthquake epicentre. In particular, catastrophic floods can occur by rupture of dams formed by landslides blocking a river valley. A recent unfortunate example is the M_w 7.9, 2008 Wenchuan earthquake in Eastern China (USGS, 2008). Landslides, rock falls and debris flows induced by this earthquake damaged or destroyed several mountain roads and railways and buried buildings in the Beichuan-Wenchuan area, cutting off access to the region and difficulting the rescue operations for several days. Landslides also dammed several rivers, creating more than 32 barrier lakes that threatened about 700,000 people upstream and downstream (Xu et al., 2009; Yin et al., 2009).

Nevertheless, earthquake-triggered slope instabilities are not well understood. In fact, the study of seismically-induced slope instabilities is a complex issue where different factors have to be taken into account. These factors are related to the characteristics of strong ground-motion (e.g. earthquake magnitude and distance to epicentre, soil and topographic amplification), specific parameters of the slope resistance (e.g. safety factor), initial stability conditions (e.g. dry or saturated ground conditions), type of slope failure (e.g. landslides, rock falls) and deformational behaviour of the materials against the seismic vibration (e.g. liquefaction, collapses). In addition, it raises a number of uncertainties surrounding earthquake-triggered slope instabilities, such as: the number and distribution of instabilities depending on the magnitude of the earthquake, the slope-instability type that takes place, the hazard of

these instabilities, the behaviour of geological materials in relation to earthquakes, the possible reactivation of previous instabilities, etc.

Study of earthquake-triggered slope-instability phenomenon is particularly interesting in areas with a moderate-high seismic activity. In Spain, the Lorca and Granada basins (Murcia and Granada provinces, respectively) are both good examples because they are the areas with the highest historical and instrumental seismic activity. In the past 10 years, three seismic series have affected the Lorca Basin and adjacent areas: 1999 Mula (M_w=4.8, I_{EMS}=VI), 2002 Bullas (M_w=5.0, I_{EMS}=V) and 2005 La Paca (M_w=4.8, I_{EMS}=VII). Despite its relatively small size, these earthquakes caused a number of significant damage to buildings and caused several slope instabilities, mainly rock falls and rock slides (Buforn et al., 2005, 2006; Benito et al., 2007). In the Granada Basin, the most relevant earthquake-triggered slope-instability cases are related to historical earthquakes, such as the 1884 Arenas del Rey (I_{EMS}=X, M_w~6.5). These slope instabilities comprise mainly landslides and rock falls (Muñoz and Udías, 1981). In addition, there are some cases in the instrumental period (e.g. 1956 Albolote earthquake with M_w=4.9 and I_{EMS}=VIII) which was also related to the occurrence of rock falls (IGME and Diputación de Granada, 2007). Moreover, Lorca and Granada basins are surrounding by several ranges, some of which have the highest reliefs of Iberian Peninsula (Sierra Nevada Range). In these mountainous areas, there is no historical evidence of earthquake-triggered slope instabilities. However, these areas with steep slopes are the place where relevant slope instabilities occurred in the past and some of them were likely induced by earthquakes.

1.2. State of the art on earthquake-triggered landslides

The phenomenology of landslides triggered by earthquakes has been thoroughly studied by Keefer (1984, 2002) and Rodríguez et al. (1999). These authors studied the instabilities attributed to several historical earthquakes from different regions where seismic activity is high. These regions were chosen to represent a wide variety of different seismic scenarios and geological and geographical features. These works concluded that the most common type of earthquake-triggered slope instabilities (landslides s.l.) are rock falls, disrupted soil slides, rock slides and debris flows. In general, earthquakes as small as magnitude M~4.0 can trigger these types of landslides. Moreover, complex landslides can also take place involving two or more types of these movements in both rocks and soils. Additionally, they found a positive correlation between the abundance of landslides and the area affected by them, with earthquake magnitude; although variations due to either specific geological and terrain conditions or seismic parameters are noted. They also found that seismic reactivation of previous slope instabilities occurred when the instabilities were in metastable conditions (safety factor close to one). Concerning the hazard, over 90% of the slope instabilities induced by earthquakes that have caused human and economic losses are due to rock avalanches, fast debris flows and rock falls. This is because the involved materials can travel long distances (up to several kilometres) at high speed over relatively gentle slopes.

Earthquake-triggered landslides have also been studied from the point of view of spatial prediction and regional hazard assessment. In these regional works, geographical information systems (GIS) are intensively used for combining geological information with terrain models and seismic input by means of different approaches (cf. Van Westen, 2000 and 2004). It is relevant to notice that most of these methods concern only to landslide susceptibility assessment and not to hazard assessment. In addition, few of them consider the seismicity as a triggering factor.

A first method is based on direct determination of the landslide susceptibility using a heuristic qualitative approach by means of geomorphological maps. In these maps, an area is considered susceptible to landslides when the terrain conditions at that site are comparable to those in an area where a slide has occurred. This method implies the elaboration of a landslide inventory by an expert that performs a direct relationship between the occurrence of slope failures and determinant terrain parameters. In this sense, this approach has an important degree of subjectivity. For this reason, it is mostly used in regional scale studies (e.g. 1:100,000-1:250,000) as a first rough estimate of landslide susceptibility.

Others approaches are based on an indirect determination of susceptibility by statistical and deterministic models. Statistical quantitative approaches are based on predictive modelling through the application of logistic regression analysis (bivariate or multivariate) or neural network analysis. In contrast to the previous approach, these methods are highly objective because correlate quantitatively determinant factors and the distribution of landslides and provide predictions for the landslide susceptibility. However, some doubts arise in the selection criteria of the causative terrain factors. In this case, these approaches are mainly used to estimate the landslide susceptibility at a intermediate regional scale (e.g. 1:25,000-1:50,000).

Application of deterministic models in landslide susceptibility and hazard studies has some advantages with respect to the other approaches. Deterministic methods are based on limit equilibrium or numerical models widely used in geotechnical engineering to calculate the stability of slopes. The input data in these models are physically-based parameters, such as geotechnical, hydrological and strong ground motion parameters. In this sense, this approach is the only that allow for incorporating as a triggering factor the seismic accelerations in the stability calculations. However, a high spatial variability of these parameters implies that these models should be used for detailed studies at large scales (e.g. 1:2,000-1:10,000). Nevertheless, specific deterministic models (e.g. infinite-slope model) can be applied successfully at regional scale as long as the quality of the input data is good.

The most common deterministic approach followed in earthquake-triggered landslides hazard assessment deal with the Newmark's sliding rigid-block model (Newmark, 1965). This method was originally developed as a simple approach to evaluate the effects of earthquakes on the stability of earth dams and embankments. A ground-motion record (accelerogram) is used to obtain a rapid estimate of the

expected displacement during an earthquake. About 20 years later, some authors applied successfully the Newmark's methodology to natural slopes (e.g., Wilson and Keefer, 1983, Wieczoreck et al., 1985; Wilson and Keefer, 1985). Wilson and Keefer (1983) study a landslide triggered by the 1979 Coyote Creek (California) earthquake. This slide was located close to an accelerometer, and the landslide displacement predicted by the Newmark's method using the recorded accelerations agreed well with the observed displacement. This approach using acceleration-time records have been also used by Wieczoreck et al. (1985) to empirically predict and map earthquake-triggered landslides in San Mateo County (California). These authors verify the feasibility of the Newmark's method in the field in the aftermath of a seismic event and concluded that this method draws reasonable good predictions of coseismic downward slope displacement. However, these studies can only be performed when ground-motion records are available, and reliable cause-and-effect relationships between specific earthquakes and landslides are easy to demonstrate. In the opposite cases, it is necessary to dismiss the influence of other triggering factors (e.g., intense rainfall, erosion) by means of slope stability back-analyses.

Jibson (1993) reviewed the Newmark's method and proposed a new simplified procedure to estimate the Newmark displacement in case that a ground-motion record is not available at the specific slope instability location. This author developed a regression equation to estimate Newmark displacement –i.e. the expected theoretical displacement of the slope due to ground motion; using seismic parameters, such as Arias Intensity (Arias, 1970) and critical acceleration –i.e. the minimum seismic acceleration value that initiates the slope instability (these concepts are discussed in more detail in Chapter 3). Following this approach, Newmark's method has also been used in site-specific studies in order to analyse the hypothetical seismic origin of particular landslides associated to known historical earthquakes (e.g., Jibson and Keefer, 1993) or to paleoseismic events (cf. Jibson, 1996).

With the recent development of geographical information systems (GIS), several authors have begun to use widely the deterministic Newmark's method to study earthquake-induced instabilities at a regional scale (e.g. Luzi and Pergalani, 1996; Van Westen and Terlien, 1996; Mankelow and Murphy, 1998; Jibson et al., 2000; Luzi and Pergalani, 2000; Luzi et al., 2000; Capalongo et al., 2002; Carro et al., 2003; Chen et al., 2004; among others). Some of these works are limited to obtain the safety factor and critical acceleration, while the most recent estimate directly the Newmark displacement associated to the earthquake.

Luzi and Pergalani (1996) performed one of the first studies that used the Newmark's method by means of a GIS to evaluate earthquake-induced landslide susceptibility. These authors obtained different safety factor and critical acceleration maps using the infinite-slope and ordinary limit equilibrium methods. However, Newmark displacement maps were estimated considering accelerograms recorded in distant areas assuming that could be representative of the study area.

Van Westen and Terlien (1996) were mostly concerned with implementing the variability of input parameters, mainly geotechnical variables, into the computation of a safety factor map. They assume that geotechnical and hydrologic properties are random variables and so can be expressed by probability-density distributions. In addition, they estimate the seismic acceleration and even site effects considering the occurrence of a great earthquake. However, the variability of this determinant input parameter was not analysed. Resulting safety factor maps showed the unstable areas in terms of probability that safety factor is lower than 1. The main problem of this procedure was that they were not able to estimate a critical acceleration value and, therefore, a Newmark displacement.

Following this probabilistic extension of the Newmark's method, Mankelow and Murphy (1998) developed an earthquake-triggered landslide hazard map for the 1989 Loma Prieta (California) earthquake in terms of probability that a slope will exceed a certain critical value of Newmark displacement and thus fail. The Newmark displacement was calculated by means of the empirical relationship suggested by Jibson (1993). These authors also derived hazard maps for a likely future earthquake scenario.

Luzi et al. (2000) improved the error evaluation due to spatial variability of the geotechnical parameters by means of Monte Carlo simulation and first-order second-moment method. Using these probabilistic approaches, they derived a critical acceleration map and the probability of failure associated with each slope. However, rocky slopes are deliberately excluded from the analysis, with the consequent limitation that only about 20% of the study area was analysed. Moreover, most of the paper concerns to discussions on the statistical technique, paying less attention to considering a suitable input seismic acceleration, which was used for these authors to estimate the map of probability of failure.

Jibson et al. (2000) developed a new implementation of the Newmark's method by means of a GIS using data from the 1994 Northridge earthquake that triggered landslides in the Oat Mountain region, California (Harp and Jibson, 1996). In this case, the variability of geotechnical parameters is not evaluated. These authors considered that the absolute value assigned to the shear strength is less important than the relative strength differences between lithological units, essentially if those differences are reasonably well constrained in a regional scale. They also proposed a new regression equation to estimate the Newmark displacement using the Arias Intensity (Arias, 1970) as a strong ground motion parameter. They compared the resulting landslide hazard maps to the actual inventory of triggered landslides showing satisfactory results. In addition, these authors developed a probability function relating the predicted Newmark displacements to the probability of failure of landslides.

Capalongo et al. (2002) used a probabilistic approach similar to Mankelow and Murphy (1998) to assess earthquake-triggered landslide hazard at a regional scale during the 1980 Irpinian earthquake (Italy). In this case, these authors have considered

the Monte Carlo simulation to take into account errors and/or uncertainties in the input parameters. The Newmark displacement and the probability of failure were estimated using the method suggested by Jibson et al. (2000). However, these authors used a digital elevation model relatively large (30 m pixel size) which is not useful to model adequately the deep slope changes of the rock materials. In fact, they noticed that very few critical Newmark displacements were predicted in rocky slopes, despite landslides were common on such slopes.

Carro et al. (2003) studied the landslides triggered by the 1997 Umbria-Marche earthquake (Italy) comparing different empirical relationships to estimate Newmark displacement from several strong-ground motion parameters. They conclude that Arias Intensity gave the best results, while peak ground acceleration (PGA) was a conservative strong-ground motion parameter. In addition, they found that the best empirical relationship to estimate the Newmark displacement was the one suggested by Jibson et al. (2000).

Chen et al. (2004) were the first that implemented the topographic amplification of ground motion in earthquake-triggered landslide hazard assessment. They used the landslide inventory related to the 1999 Chi-Chi earthquake to obtain probability functions on Newmark displacement versus proportion of slope failures following the method suggested by Jibson et al. (2000).

Despite the limitations and assumptions discussed above, the Newmark's method remains one of the most common approach followed in earthquake-triggered landslides assessment at present-day (e.g. Rapolla et al., 2010; Tselentis and Danciu, 2010; Wang and Lin, 2010). However, most of these works concern only to landslide susceptibility assessment and not to hazard assessment. Moreover, some relevant doubts arises from the implementation of the Newmark's method developed in these studies, mainly related to the reliability of the input seismic scenarios and/or the resolution of the digital elevation models.

1.2.1. Regional assessment of earthquake-triggered landslide hazard in Spain

Even though in Spain a great number of studies dealing with regional landslide assessment exist (e.g. Ayala Carcedo and Corominas, 2002), those specifically focussed on analysing the seismic factor are very few: García-Mayordomo (1998, 1999), Coral Moncayo (2002); Mulas et al. (2001, 2003), Figueras et al. (2005), Delgado et al. (2006). All these works are based on the Newmark's method and most of them make use of geographical information systems (Idrissi or ArcGIS).

García-Mayordomo (1998, 1999) analysed the stability of two particular slope models widely distributed across the Alcoy Basin (Alicante, East Spain), finding that critical accelerations as low as 0.03g to 0.04g could potentially trigger landslides. In the same area, Delgado et al. (2006), after modelling the natural variability of

geotechnical parameters by means of a Monte Carlo analysis, obtained a set of maps in terms of the probability associated to a critical acceleration lower than 0.1g for dry and saturated conditions. He determined a very good correlation between high probability areas and the distribution of actual known slope instabilities triggered by the 1620 Alcoy (I_{MSK}=VIII) and 1945 Onteniente (m_{bLg}=4.0, I_{MSK}=VII) earthquakes. Both García-Mayordomo (1999) and Delgado et al. (2006) studies indicate that earthquake-triggered landslides in the Alcoy Basin appear to be a frequent and repeated phenomena.

Coral Moncayo (2002) and Figueras et al. (2005) works, performed in Andorra (Pyrenees), are particularly outstanding for assessing earthquake-triggered landslide hazard in terms of the probability of failure as a function of Newmark displacement. However, it is important to notice that this assessment was eventually done using the Jibson et al. (2000) equation derived from 1994 Northridge earthquake data. Newmark displacement is calculated from empirical relationships with Arias Intensity, as well as from real accelerograms consistent with the 475-year return period in the area (PGA~0.1g), and assuming a critical acceleration of 0.01g. They finally concluded that the probability of failure is only significant for slopes greater than 40º.

Mulas et al. (2001 and 2003) works in the valleys of Gállego and Caldarés rivers (central Pyrenees) deal with designing a specific methodology for the quantitative assessment of slope instability levels against the seismic phenomena. Instability levels are derived from a matrix that combines discrete values of a variable dependant on aseismic factors (e.g. slope, lithology) with another variable dependant on seismic soil response; which is also a function of macroseismic intensity. For intensity levels between VI and VIII (presumably related to the 500-year return period), the authors found out that the areas with the highest levels of instability coincided with the higher parts of the valleys, in contrast with the location of currently known instabilities.

1.3. Objectives

The study of seismicity and slope instabilities are usually investigated separately using different methodology approaches. For this reason, this Ph.D. Thesis make use of tools and models commonly used in both engineering geology and earthquake engineering fields in order to consider the interaction between seismic events and the occurrence of slope instabilities.

The main aim of this Ph.D. Thesis is the development, testing and application of a methodology for the assessment of potential earthquake-triggered slope instabilities at different scales in the Betic Cordillera, particularly in the area of the Lorca Basin and the eastern sector of the Granada Basin and Sierra Nevada Range. These areas have been selected considering that they are the most seismically active in Spain.

The specific objectives of this Ph.D. Thesis are:

- Development of a comprehensive methodology to evaluate earthquake-triggered slope instabilities at regional scale by means of a geographic information system (GIS).

- Considering specific earthquake scenarios significant for civil protection and engineering purposes as seismic input, as well as strong ground-motion site effects, namely soil and topographic amplification.

- Developing a simple tool to estimate the topographic amplification by means of a GIS and digital elevation models.

- Identifying the most likely unstable areas corresponding to different seismic scenarios (probabilistic, pseudo-probabilistic and deterministic) and determining the areas where the seismicity could contribute to reactivate slope instabilities or generate new ones, as well as to identify the most likely involved landslide typology.

- Regional estimation of the critical acceleration and Newmark displacement values at areas where particular cases of known earthquake-triggered slope instabilities took place.

- Evaluating the applicability of the proposed methodology at different scales (regional, sub-regional and site scales) in order to determine which is most suitable for assessing the earthquake-induced landslide phenomenon.

- Identifying determinant parameters in stability of significant earthquake-triggered slope instabilities cases.

- Constraining pre-instrumental and historical earthquake parameters, such as magnitude and epicentral location, by means of detailed slope-stability analyses.

- Estimation of the most likely seismic sources of reactivation for selected slope instabilities

- Testing the efficiency of slope stabilisation measures in significant slope instabilities considering a possible future seismic reactivation.

1.4. Thesis structure

The structure of the Thesis is based on the observations, results and conclusions obtained from the research studies carried out in the Lorca and Granada basins and Sierra Nevada Range by the author of this thesis and other co-workers. These studies have resulted in several research papers that have been submitted to international journals included in the Science Citation Index (SCI). Some of them are already published. These papers have been separated and organised into different chapters of the Thesis.

The manuscript is organized into four main parts, which comprise 10 chapters, followed by the Appendixes and References sections. In particular, the first part (Chapters 1 and 2) is organized as follows:

- **Chapter 1** provides an introduction, showing the importance of the study of earthquake-triggered landslides in seismically-active areas. A brief background on this topic is also described, both worldwide and in the particular case of Spain. In this chapter, the main objectives of the thesis are presented. Finally, the contents of each chapter are summarized.

- **Chapter 2** describes the geological and seismotectonic setting of the Betic Cordillera, as well as the main faults located in the Lorca and Granada basins regarding to their potential seismic hazard.

The second part of the thesis (**Chapter 3**) focuses on a comprehensive development of the methodology used in the forthcoming chapters. Therefore, this chapter shows the different steps followed to obtain the critical acceleration and Newmark displacement values. Moreover, implementations of the input seismic scenarios and strong ground-motion site effects (soil and topographic amplifications) are also explained. The third part deals with different applications and testing of the methodology introduced in Chapter 3 to some specific areas of the Betic Cordillera (Lorca and Granada basins and Sierra Nevada Range). This part is structured as follows:

- **Chapter 4**: "Regional hazard assessment of earthquake-triggered slope instabilities considering site effects and seismic scenarios: Application to the Lorca Basin (Eastern Betic Cordillera, SE Spain)". The proposed methodology has been applied to the Lorca Basin in order to obtain a regional view of earthquake-triggered slope instabilities based on the occurrence of specific seismic scenarios. Comparison between the obtained Newmark displacement maps and the location of known earthquake-triggered rock slides in the area has resulted in a new Newmark displacement threshold for disrupted-type slope instabilities. This chapter has been submitted to Soil Dynamics and Earthquake Engineering.

- **Chapter 5**: "Regional hazard assessment of seismically-induced slope instabilities in Sierra Nevada Range (Betic Cordillera, South Spain) simulating the occurrence of a maximum magnitude earthquake related to the Padul Fault". In this chapter, a comparison between the Newmark displacement map and an inventory of slope instabilities in Sierra Nevada Range has been performed at a regional scale. This approach allows for identifying areas where the seismicity might reactivate old slope instabilities or generate new ones, as well as to identify the involved landslide typology. This chapter has been submitted to Comptes Rendus Geoscience.

- **Chapter 6**: "Applicability of Newmark's method at regional, sub-regional and site scales: seismically-induced SW Bullas and La Paca rock-slide cases (Murcia, SE

Spain)". The applicability of the proposed methodology to assess seismically-induced slope instabilities at different scales has been investigated in this chapter. Two rock slides cases triggered by recent seismic events in Lorca Basin (2002 SW Bullas and 2005 La Paca earthquakes) have been studied in detail at site scale to be compared with regional and sub-regional results in order to determine what is most suitable. This chapter has been submitted to Journal of Geotechnical and Geoenvironmental Engineering.

- **Chapter 7**: "Constraining pre-instrumental earthquake parameters from slope stability back-analysis: Paleoseismic reconstruction of the Güevéjar landslide during the 1st November 1755 Lisbon and 25th December 1884 Arenas del Rey earthquakes". In this chapter stability back-analyses of the Güevéjar landslide (Granada Basin) during the 1755 Lisbon and 1884 Arenas del Rey earthquakes have been performed. Critical acceleration values required to trigger this landslide have been estimated, and from these data the most likely magnitude and epicentral location for the 1755 Lisbon and 1884 Arenas del Rey earthquakes has been inferred. The stability of the present-day Guevéjar landslide is also evaluated. This chapter has been accepted for publication in Quaternary International (Special Issue on Palaeoseismology).

- **Chapter 8**: "Effectiveness of deep drainage wells as a slope stabilization measure: The reactivation of the Diezma landslide (Southern Spain)". A complete evolution of the history of failures of the Diezma landslide has been performed in relation to the construction of the A-92 motorway and the occurrence of periods of heavy rainfalls. In this case, seismicity has been considered as a triggering mechanism in a possible future landslide reactivation in order to test the feasibility of slope stabilisation measures. This chapter has been submitted to Bulletin of Engineering Geology and the Environment.

In the fourth part of the Thesis, general conclusions and future perspectives on earthquake-triggered landslide research are presented. This part is organized as follows:

- **Chapter 9** summarizes the most relevant conclusions and their implications in the knowledge of the seismically-induced landslides. This chapter has been also translated to Spanish (**Capítulo 9**).

- **Chapter 10** highlights some aspects of the earthquake-triggered slope instabilities investigation that could be potential research lines on this topic in the future.

In order to keep the original structure of the published and submitted papers, all the sections of these manuscripts are maintained except the references, which are all put together in the References section in order to follow a formal format of a thesis volume. In addition, the figure numbers kept their original form, so the numbering refers to the figures included in each chapter.

2

Geological, tectonic and seismic context

2.1. Regional Geology

The Central and Eastern Betic Cordillera is located in southern and southeastern Spain, respectively. The Betic Cordillera, together with the Rif Chain (Africa) form the western end of the Mediterranean Alpine orogenic belt developed by the convergence between the African and Eurasian Plates during the Late Mesozoic and Cenozoic. In the last 9 Ma (Late Miocene to present), African and Eurasian plates have undergone a process of convergence with a NW-SE trend that generated the present-day relief.

The Betic Cordillera (Fig. 2-1) comprises three main domains (Fallot, 1948): the External Betic Zones (or South-Iberian Domain), the Campo de Gibraltar Complex and the Internal Betic Zones (or Alborán Domain). Intramontane basins filled by Neogene-Quaternary sedimentary deposits are developed over these domains.

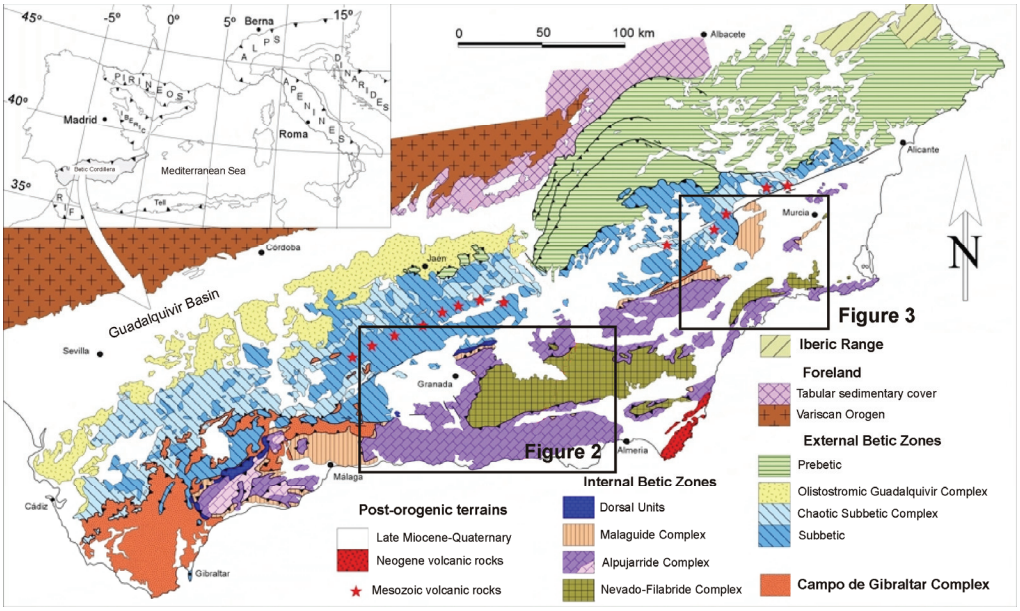

Figure 2-1. General geological map of the Betic Cordillera which shows the extent of the outcrops of each of the different units (modified from Vera, 2004). It also shows the areas corresponding to figures 2-2 and 2-3.

The External Betic Zones (or South-Iberian Domain) are constituted by sedimentary rocks deposited in the southern and eastern paleomargin of the Iberian Massif during the Mesozoic and part of the Cenozoic. Traditionally, it is subdivided into Prebetic at the north and Subbetic at the south (García-Hernández et al., 1980). In general, the Prebetic is characterized by shallow shelf facies (limestones and dolomites) and even continental facies (sandstones and shales), while the Subbetic presents pelagic facies (limestones and marls). The Prebetic and Subbetic show a typical thrust and fold belt structure related to the external zones of mountain ranges (García Dueñas, 1967; Sanz de Galdeano, 1973). In addition, much of the Subbetic outcrops correspond to Chaotic Subbetic Complexes (García Cortés et al., 1991; Pérez-López and Sanz de Galdeano, 1994) consisting of olistoliths formed by Mesozoic and Cenozoic rocks within a Triassic sediment matrix. The materials belonging to the External Betic Zones were deformed between the Late Burdigalian and Early Tortonian times developing mainly compressive structures with N and NW trend. This strong deformation constitutes a thrust and fold belt of ENE-WSW trend (Vera, 2004).

The Campo de Gibraltar Complex comprises sediments with flysch facies that probably was extended along the northern edge of the African Plate (Martín-Algarra, 1987; Sanz de Galdeano and Vera, 1992). These marine sediments consist of Cretaceous-Paleogene succession of clays, marls and turbiditic sandstones belonging to the sedimentary cover of an oceanic crust (or a thinned continental crust). These sediments mainly outcrop along the contact between the External and Internal Zones. The Campo de Gibraltar units are currently thrusting on the External Betic Zones.

The Internal Betic Zones (or Alborán Domain) are formed by sedimentary and metamorphic rocks of Paleozoic to Triassic age which were deformed in a wide range of pressure and temperature conditions during the Alpine orogeny (Fontboté, 1986). Three main superposed tectonic complexes have been recognized, from bottom to top: the Nevado-Filábride Complex (Egeler, 1963), the Alpujárride Complex (Van Bemmelen, 1927) and the Maláguide Complex (Blumenthal, 1927). These complexes are separated by large extensional detachments that accommodate a ENE-WSW extension of the Alborán Domain (García-Dueñas and Martínez-Martínez, 1988, Galindo-Zaldívar et al., 1989, Platt and Vissers, 1989; Aldaya et al., 1991, García-Dueñas et al., 1992; Jabaloy et al., 1993, Lonergan and Platt, 1995, González-Lodeiro et al., 1996, Martínez-Martínez et al., 2002, Booth-Rea et al. 2002, Booth-Rea, 2004, Booth-Rea et al., 2004). The Nevado-Filábride Complex is constituted mainly by graphitic micasquists with quartzites, amphibolites, gneisses and marbles. The Alpujárride Complex is composed by metapelites (schist, phyllites and quartzites) and carbonate rocks (limestones and dolomites). In general, the Maláguide Complex consists of limestones and dolomites, and phyllites, sandstones and conglomerates, which have virtually not undergone alpine metamorphism. Between the Maláguide Complex and the Campo de Gibraltar Complex appear the Dorsal Units. These Mesozoic and Tertiary carbonate materials constituted the sedimentary cover of the Maláguide Complex.

The Betic Cordillera emerged in the Late Miocene, progressively isolating different Neogene-Quaternary intramontane basins (Montenat et al., 1990; Sanz de Galdeano and Vera, 1991, 1992; Vera, 2000). In the central sector of the Betic Cordillera stand out the Granada, Guadix-Baza and Ugíjar Basins (Fig. 2-2), while in the eastern sector the Tabernas, Vera, Lorca, Mula and Fortuna basins, the Guadalentín Depression, etc. are relevant (Fig. 2-3). The geometry and Neogene-Quaternary evolution of these basins are mainly related to the activity of major fault zones with normal and strike-slip movement. These faults cross much of the Betic Cordillera with NE-SW and NW-SE main trend (Bousquet, 1979; Sanz de Galdeano, 1983; Silva et al., 1993, Sanz de Galdeano and López Garrido, 2000; Galindo Zaldívar et al., 2001; Meijninger and Vissers, 2006). Several outcrops of volcanic rocks are directly related to the formation and evolution of the intramontane basins in the Eastern Betic Cordillera. These rocks have an age ranging from the Late Tortonian (9 Ma) to the Pleistocene (1 Ma) (Nobel et al., 1981; Turner et al., 1999; Cesare et al., 2003). The most recent are located in the easternmost part (Campo de Cartagena and Mazarrón).

2.2. Tectonic setting

The Betic Cordillera was built on by the convergence and collision between the African and European plates, which took place in the Early Miocene, forming the present contact between the Internal and External Zones during the Middle Burdigalian (Lonergan and Platt, 1994). In the eastern sector of the Betic Cordillera (Fig. 2-3), this contact is not straight and is partly covered by Neogene-Quaternary sediments. The current geometry of the region indicates that the External Zones thrusted on the Internal Zones (Fernández-Fernández, 2003). In the Central Betic Cordillera, this contact is straight with a general NE-SW trend and it is covered by sediments of the Granada Basin (Fig. 2-2).

Sanz de Galdeano (1983) distinguished several active fault systems on a regional basis: N70°E to E-W, NW-SE and NNE-SSW to NE-SW. He also concluded that during the Middle Miocene the horizontal compression trend was WNW-ESE and it was related to the activation of the N70ºE to E-W faults as dextral and the NW-SE faults as sinistral. The neotectonic period started in the Tortonian coinciding with a change in the convergence trend between the Iberian and African plates. This change caused a rotation of the subhorizontal compression from WNW-ESE to NNW-SSE and NW-SE (Sanz de Galdeano, 1983; Ott d'Estevou and Montenat, 1985; Sanz de Galdeano, 1990; Galindo-Zaldivar et al., 1993; Herraiz et al., 2000). Because of this change of trend, the N70ºE to E-W faults were blocked or reactivated as thrust or normal faults. In addition, NE-SW to NNE-SSW left-lateral strike-slip faults were generated working as the conjugated system of the NW-SE right-lateral strike-slip faults. In the Central Betic Cordillera, there was also a NE-SW extension that resulted in the development of NW-SE normal faults. This new trend of shortening was associated with long-range E-W folds during the Tortonian-Messinian boundary (Weijermars et al., 1985; Martínez-Martínez et al., 2002; Sanz de Galdeano and

Alfaro, 2004). The folding extended to Pleistocene (Johnson, 1997) and even at present-day (Marín-Lechado et al., 2002). There is a close relationship between high mountain elevations of the Internal Betic Zones and the formation of these large folds, because the ranges are associated with major antiforms. Some examples of these folds are Sierra Nevada, Filabres, Tejeda, Gador and Contraviesa ranges that are located in the Central Betic Cordillera (Fig. 2-2). These ranges correspond to the core of the major antiforms cited above. In the eastern sector, the Estancias, Tercia and Espuña Ranges are also the core of large-scale antiformal structures (Fig. 2-3).

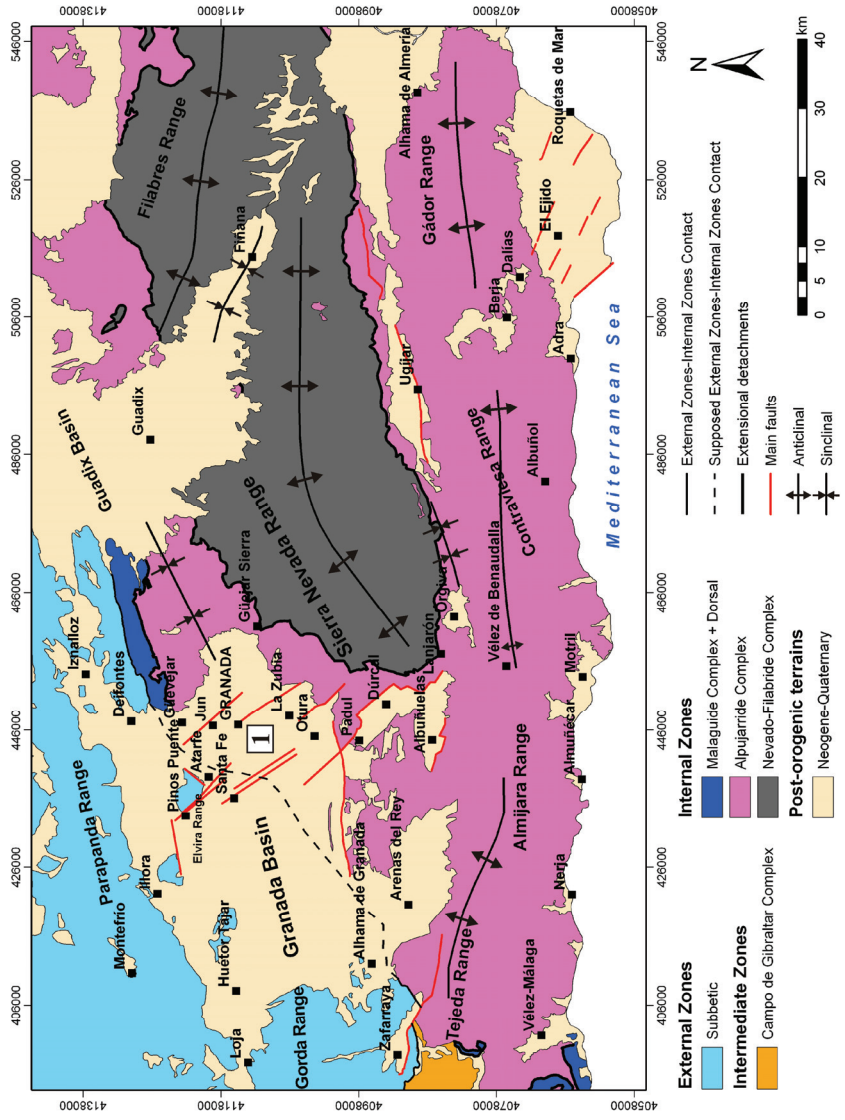

Figure 2-2. Simplified geological map of the central sector of the Betic Cordillera which shows the extent of the outcrops of each of the different units. 1: Main active faults located in the eastern border of the Granada Basin.

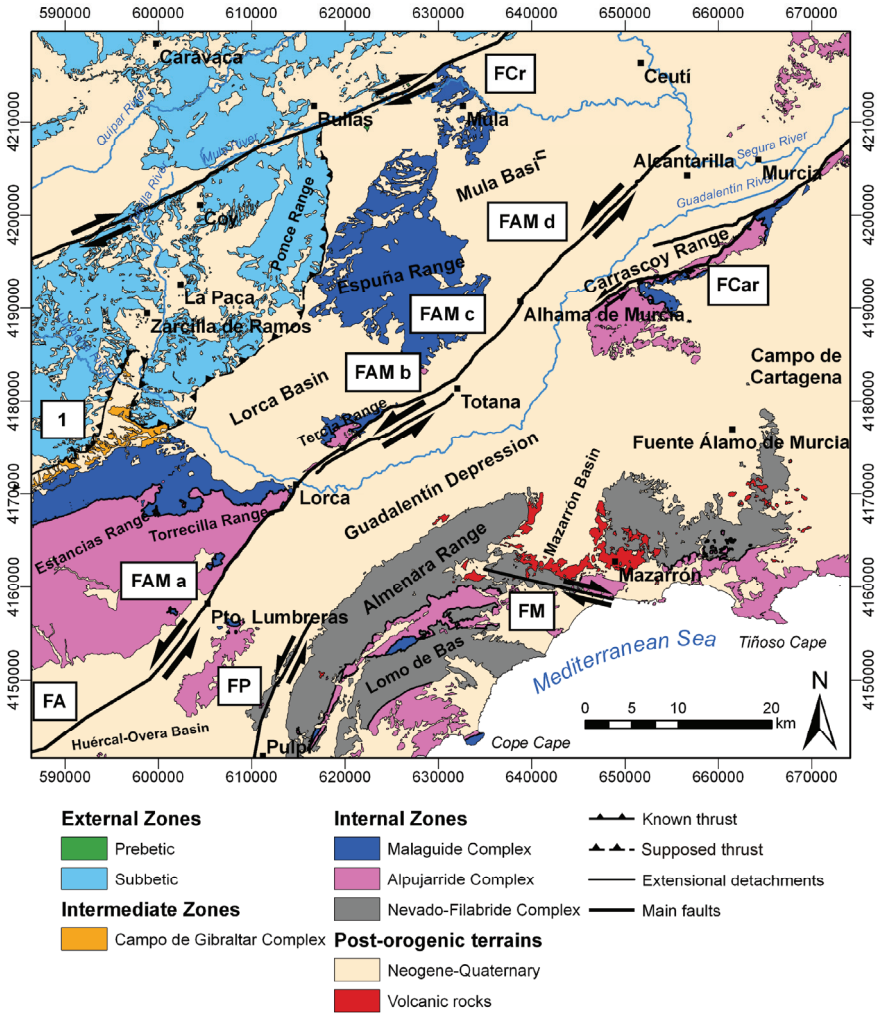

Figure 2-3. Simplified geological map of the eastern sector of the Betic Cordillera that shows the extent of the outcrops of the different units. 1: Internal Zones-External Zones Contact, FCR: Crevillente Fault, FCar: Carrascoy Fault, FM: Moreras Fault, FAM: Alhama de Murcia Fault (a: Pto. Lumbreras- Lorca segment; b: Lorca-Totana segment; c: Totana-Alhama segment; d: Alhama-Alcantarilla segment).

2.3. Seismicity

The boundary between the African and Eurasian plates in the Western Mediterranean is defined by a broad zone of deformation and strain partitioning. The location and nature of the contact between the two plates is widely discussed (e.g. Udías and Buforn, 1991; Buforn et al., 1995; Stich et al., 2003; Buforn et al., 2004; Fadil et al., 2006; Serpelloni et al., 2007). This region corresponds to the transition from an oceanic boundary (between the Azores islands and the Gorringe Bank) to a continental boundary at the Strait of Gibraltar (Fig. 2-4). The plate boundary is very

well delimited by the earthquake epicentre locations in the oceanic part, from the Azores islands (around 25º W) along the Gloria Fault to approximately 12º W (west of the Strait of Gibraltar). Near the Gorringe Bank region (12º W to 6º W), the concentration of earthquakes is higher (Buforn et al., 1995) corresponding to the epicentral area of great earthquakes (M_w>6.0), such as the 1755 Lisbon earthquake (I_{EMS}=XI-XII, M_w~8.5). From the east of the Strait of Gibraltar to the western part of Algeria (6º W to 4º E), the seismicity is distributed diffusely in a relative wide belt around the presumed present-day plate contact and earthquakes occur as well in the foreland at significant distances (over 300 km) from the plate boundary zone. This area is known as the Iberia-Maghreb region and comprise the south of Spain, the Alborán Sea, North of Morocco, Algeria and Tunisia. In this area, the distribution of the seismicity shows scattered seismic swarms and it is not clearly aligned with the actual contact between the African and Eurasian plates.

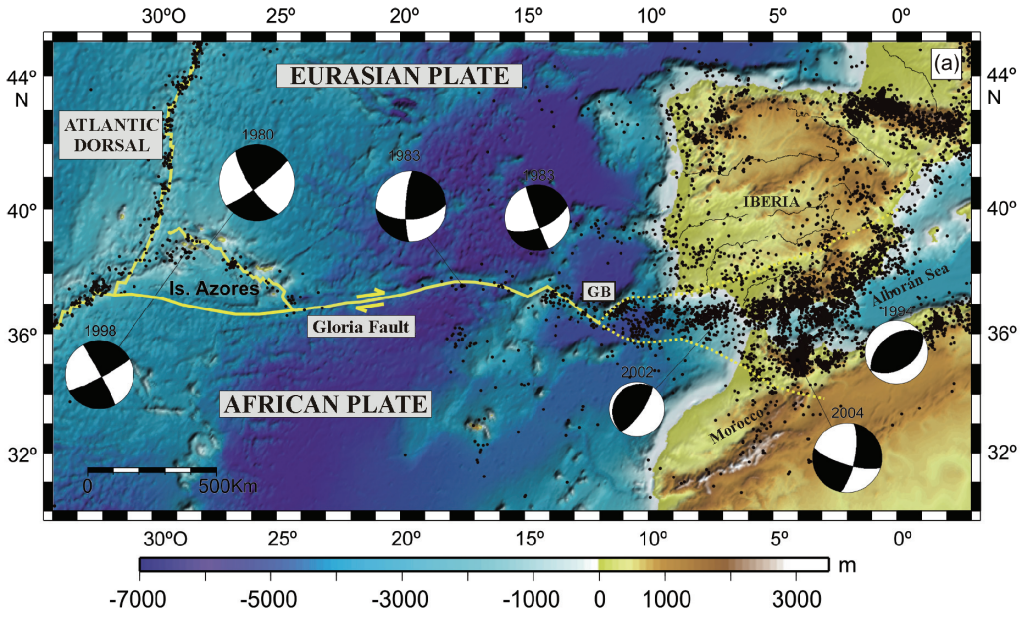

Figure 2-4: Regional seismicity in the boundary between the African and Eurasian plates (modified from Fernández-Ibáñez, 2007). Only magnitude ≥ 2.5 events are plotted. The focal mechanisms correspond to earthquakes of magnitude M_w>5.5 recorded in the region over the past two decades. They show in general the changes of the stress state from west to east. The dashed line marks the region where the seismicity is widely distributed and the plate boundary is diffuse. GB: Gorringe Bank.

In the Iberia-Maghreb region, the most active seismic areas are located at South and Southeast of the Iberian Peninsula and at the Alborán Sea region (Fig. 2-4). Focal depth distribution displays abundant shallow crustal earthquakes (<40 km), but also intermediate seismic events (40-150 km) and few deep earthquakes (~630 km) (Buforn et al., 1991, 2004). However, the seismic activity in this area is mostly confined to shallow crustal levels at depths smaller than 15 km (Fernández-Ibáñez and Soto, 2007). The seismicity is characterised by low-intermediate magnitude

earthquakes (M_w<5.5), but there are some recent seismic events that overcome this magnitude threshold (e.g. 2004 Alhucemas earthquake with M_w 6.3). Moreover, some high magnitude earthquakes (M_w>6.0) have also occurred at this area in historical times (Vidal, 1986; Martínez Solares and Mezcua 2002; Stich et al., 2003; Mezcua et al., 2004; Buforn et al., 2005): 1518 Vera earthquake (I=IX), 1522 Alhama de Almería earthquake (M_w~6.5), 1680 Málaga earthquake (M_w~6.8), 1804 Almería earthquake (M_w~6.7), 1829 Torrevieja earthquake (M_w~6.6), 1884 Arenas del Rey earthquake (M_w~6.5), 1910 Adra earthquake (M_w=6.1) and 1911 Torres de Cotillas earthquake (M_s~5.7).

In this context, the Betic Cordillera and, particularly, the Lorca and Granada basins are distinguished by a moderate-high seismic activity. In fact, these basins are the areas with the highest historical and instrumental seismic activity in Spain. Since the beginning of the instrumental record in the region in the 1920's, a large number of earthquakes have been recorded in the Betic Cordillera, although all of them of low to moderate magnitude (m_b<5.5) (De Miguel et al., 1989). However, several significant historical earthquakes took place at these areas (e.g. 1884 Arenas del Rey).

2.3.1 Eastern Betic Cordillera (Lorca Basin)

The Eastern Betic Cordillera, particularly the Lorca Basin and surroundings, shows a distributed seismicity with shallow earthquakes and magnitudes usually smaller than 5.0, at least for the time of recordings. However, the occurrence of earthquakes with intensity between VIII and X (Fig. 2-5) is known from historical times (Martínez Solares and Mezcua, 2002). The most significant seismic events felt in the Lorca Basin area are 1579 Lorca (I_{MSK}=VII) and 1674 Lorca (I_{MSK}=VIII) earthquakes. In the instrumental period, the most damaging earthquake was the 1948 Cehegín earthquake (I_{MSK}=VIII, m_b=5.0). Apart from this earthquake, the instrumental catalogue of the area contains 15 earthquakes felt with MSK intensities between VI and VII (Martínez Solares and Mezcua, 2002). The Eastern Betic Cordillera has been also the place where great historical earthquakes took place, such as the 1829 Torrevieja earthquake with an intensity of I_{EMS}=IX-X (Fig. 2-5).

From the point of view of earthquake environmental effects, the most interesting seismic events are the recent 1999 Mula (M_w=4.8, I_{EMS}=VI), 2002 Bullas (M_w=5.0, I_{EMS}=VI) and 2005 La Paca (M_w=4.8, I_{EMS}=VII) earthquakes (Buforn et al., 2005; Murphy, 2005; Buforn et al., 2006; Benito et al., 2007). These earthquakes, in contrast to other studies, account for descriptions of specific cases of triggered slope instabilities –mainly rock falls and rock slides. These slope instabilities will be described with more detail in Chapter 6.

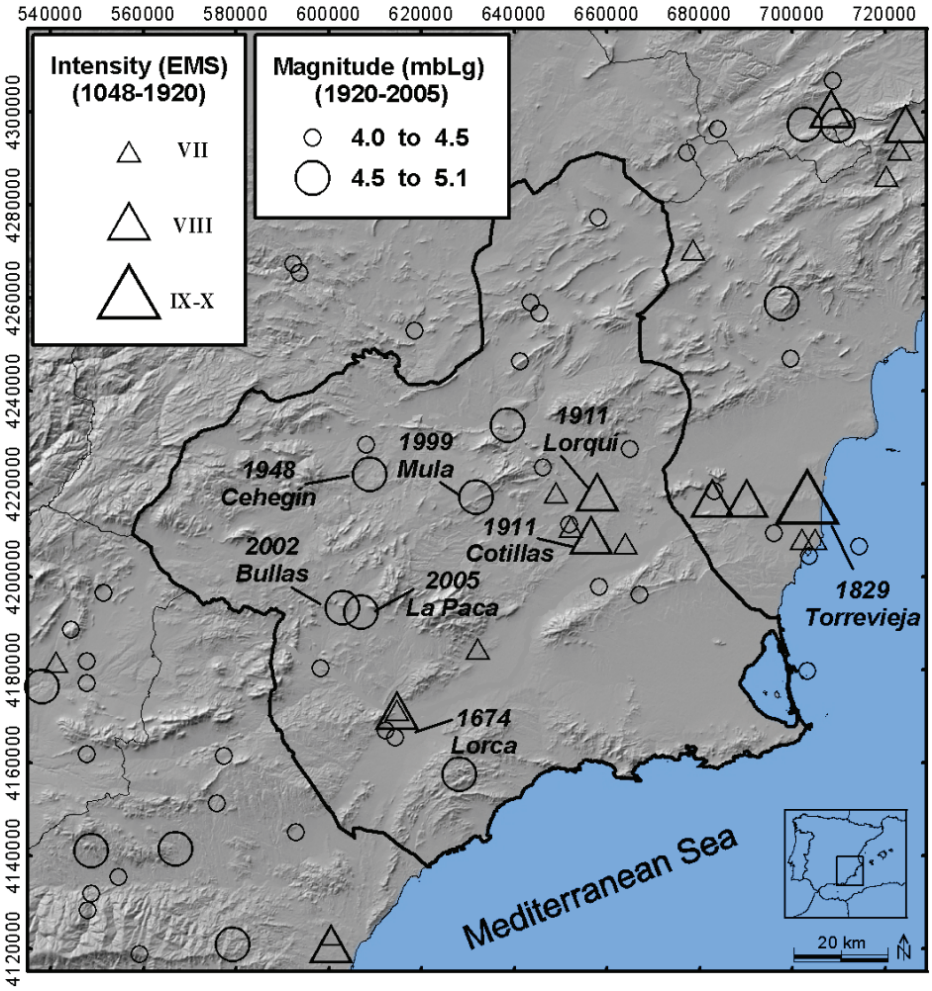

Figure 2-5: Distribution of main historical and instrumental seismicity in the Eastern Betic Cordillera, particularly around the Lorca Basin (Murcia Region) (modified from García-Mayordomo et al., 2007).

2.3.1.1. The 1999 Mula seismic series

The 1999 Mula seismic series begun with a precursor event the 2nd of February of 1999 at 3:22 (UCT) with a magnitude m_b=4.3. The main event occurred the same day at 13:45 (UCT) with magnitude M_w=4.8 (Buforn et al. 2005). Aftershocks followed during the next days, some of them at a great distance from the main epicentre (Fig. 2-6). The events were very shallow (h< 5 km), except the precursor event that was located at 7 km depth. The focal mechanisms calculated for these events indicate two sets of possible faults: one with a NW-SE strikes and dippping towards the SW, and another set striking E-W and dippping towards the south. Both sets show a reverse component of movement (Stich et al., 2003).

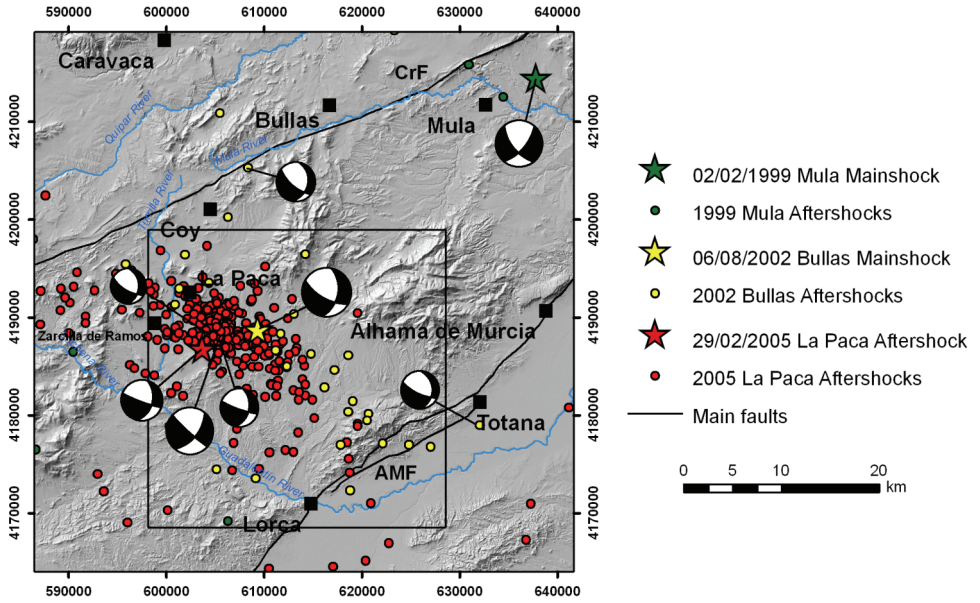

Figure 2-6: Epicentres and focal mechanisms of the mainshocks and aftershocks for the 1999 Mula, 2002 Bullas and 2005 La Paca series. Only magnitude ≥ 2.0 events are plotted. Size of the focal mechanisms is proportional to magnitude (Stich et al., 2003, 2006 and Benito et al., 2007)

2.3.1.2. The 2002 SW Bullas seismic series

The main event of the 2002 SW Bullas seismic series took place the 6th of August of 2002 at 6:16 (UCT) with a magnitude M_w=5.0 (Buforn et al., 2005). The depth of the whole series is formed by shallow events with depths lower than 11 km (Buforn et al., 2005. Several aftershocks followed the main event during August and September, which are grouped in two main populations (Fig. 2-6). The population with a great number of events follows a NW-SE straight trend in the middle of the Lorca Basin and stops at the Alhama de Murcia Fault zone. The second population of events follows a N-S alignment northwards of the main event epicentre. The main population of events defines a line parallel to the strikes of the normal faults that bound the Lorca Basin. The focal mechanisms indicate normal faulting either striking NW-SE and dipping towards the SW or striking N-S and dipping towards the east (Stich et al., 2003; Benito et al., 2007).

2.3.1.3. The 2005 La Paca seismic series

The 2005 La Paca seismic series occurred after three years of low seismic activity. The series began with several precursors of low magnitude during the 1st to 3rd of February of 2005. The epicentres of the precursors define a ENE-WSW alignment (Fig. 2-6). The main event took place on the 3rd of February of 2005 at 11:40 (UCT) with a magnitude M_w=4.8 (Benito et al., 2007). Taking into account the calculated depth of the aftershocks, they define a ENE-WSW striking surface with a

strong dip towards the SSE. The focal mechanism of the main event shows one plane with a WNW-ESE strike and dipping towards the south (Stich et al., 2006; Benito et al., 2007) that is very similar to the surface defined by the epicentres of the events of the series. Assuming this surface as the most likely fault plane whose movement produced the seismic series, the focal mechanism indicates that the movement was a left-lateral strike-slip one with a small normal component.

2.3.2 Central Betic Cordillera (Granada Basin)

In the Central Betic Cordillera, the present-day seismicity is also characterized by shallow earthquakes and low to moderate magnitudes ($M_b \leq 5.5$; De Miguel et al., 1989), but the earthquake epicentres are concentrated along the western and southern borders of the Sierra Nevada Range. These borders represent the contact with the Neogene-Quaternary sediments of the Granada Basin, which is the most seismically active area in Spain. In general, the seismicity associated to these borders is related to active normal faults with different trends, but particularly with a NW-SE strike (Martínez-Martínez et al., 2006). These active faults are described in more detail in section 2.4.2.

In the Granada Basin, the earthquakes have been mainly distributed in the upper crust, between 9 and 16 km depth at the eastern part, and between 9 and 25 km in the western part (Morales et al., 1997). Although no moderate-to-large magnitude seismic events have been recorded in the Granada Basin during the instrumental period (since 1983), such occurrences should not be excluded given the existence of various historical earthquakes. The most important historical earthquakes occurred during the period between the XV and the XIX centuries (Vidal, 1986; López Casado et al., 2001; Feriche and Botari, 2002): 1431 Granada (I_{EMS}=IX), 1526 Granada (I_{EMS}=VIII), 1806 Pinos Puente (I_{EMS}=IX) and 1884 Arenas del Rey (I_{EMS}=X). The last significant seismic events occurred in the Granada Basin are the Albolote 1956 and Jayena 1984 earthquakes with magnitude M_w=4.9 and M_w=5.0 (Vidal, 1986; Morales et al., 1996), respectively.

From the point of view of environmental effects, several historical reports demonstrate that most of the landslides phenomena occurring on the Granada Basin are related to some of the major historical earthquakes. The most significant is the 1884 Arenas del Rey earthquake (I_{EMS}=X, M_w~6.5), which induced several slope instabilities such as the Güevéjar landslide (Jiménez Pintor and Azor, 2006), rock falls and rock avalanches produced in Alhama de Granada and Albuñuelas villages and even some liquefaction phenomena (Muñoz and Udías, 1981; IGME and Diputación de Granada, 2007). A detailed description of the major historical earthquakes that trigger slope instabilities in the Granada Basin is developed in Chapter 7.

2.4. Main faults and Seismic hazard

2.4.1. Eastern Betic Cordillera (Lorca Basin)

Major faults located in the Eastern Betic Cordillera comprise significant fault zones which are recognizable on the surface with lengths of at least 30 km and, in most cases by more than 50 km. Exceptionally, they are recognized over distances of 100 km. Examples of such faults are the Crevillente, Alhama de Murcia, Palomares, Carrascoy and Las Moreras faults (Fig. 2-3 and 2-7). These faults have a predominant NE-SW to ENE-WSW trend, while the Las Moreras and Palomares fault have WNW-ESE and NNE- SSW trend, respectively. In general, they are strike-slip faults with left-lateral displacement. The Crevillente and Alhama de Murcia faults delimite the NW and SE margins of the Lorca Basin, respectively (Fig. 2-3 and 2-7). The Lorca Basin has been interpreted as a pull-apart basin where the fault systems had a significant influence on Neogene basin sedimentation and were periodically active during the Miocene (Montenat and Ott d'Estevou, 1999).

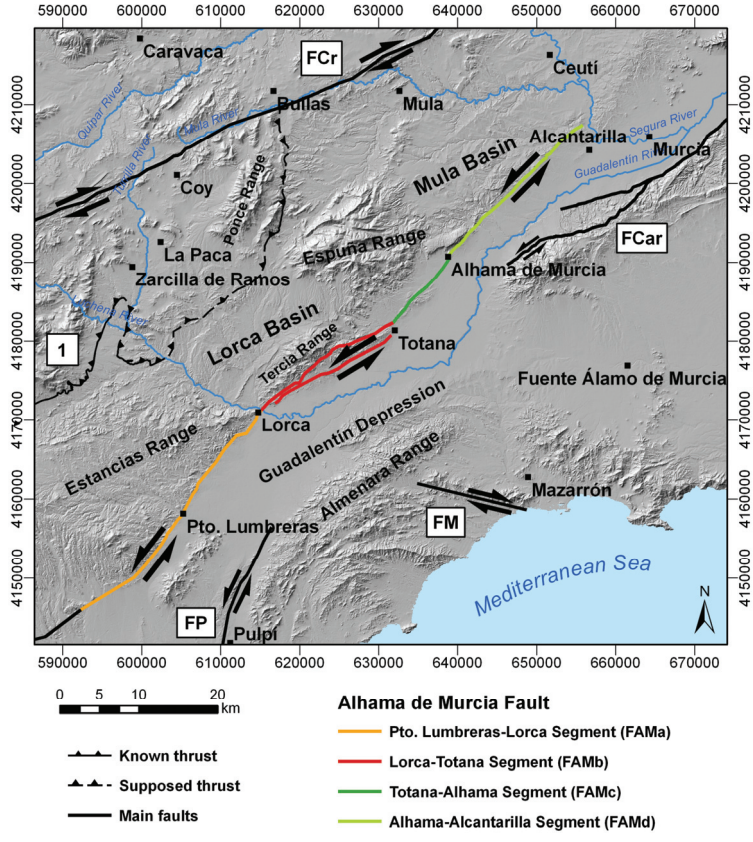

Figure 2-7. Shaded relief map of the Eastern Betic Cordillera showing major faults location. 1: External Zones-Internal Zones Contact, FCr: Crevillente Fault, FCar: Carrascoy Fault, FM: Las Moreras Fault and FAM: Alhama de Murcia Fault. The four fault segments of the FAM are also shown.

2.4.1.1. Crevillente Fault

The Crevillente Fault (FCr) is a large right-lateral strike-slip fault with a general NE-SW and ENE-WSW trend (Sanz de Galdeano, 1983). It comprises a fault zone of variable width between 1 and 5 km, frequently interrupted by faults with NW-SE and N-S trend. In the Early Tortonian, due to the rotation of the trend of maximum shortening of the orogen to NNW-SSE and NW-SE, the Crevillente Fault began to work as a transpressive strike-slip fault with dextral and reverse regimes (Sanz de Galdeano, 1990; Nieto and Rey, 2003). Even though the Crevillente Fault was essentially active in the Early-Middle Pleistocene, many authors have related the 1999 Mula earthquake (M_w=4.8) to this fault (Martínez-Díaz et al., 2002; Sanz de Galdeano and Buforn, 2005).

2.4.1.2. Alhama de Murcia Fault

The Alhama de Murcia Fault (FAM) is an about 80 km long active fault with a NE-SW trend (Gauyau et al., 1977; Bousquet, 1979; Martínez-Díaz, 1998; Masana et al., 2004). The main trace of Alhama de Murcia Fault is recognized almost without any interruption since the northern limit of the Huércal-Overa Basin to the surroundings of the Murcia City (Fig. 2-7). The fault zone has a width generally less than 1 km, with the exception of the section that limits the southern edge of the Lorca Basin, where there are two main branches of deformation defining a width of about 3-4 km. This fault has been active since Serravallian times with a sinistral-reverse kinematic that can still be observed during the Quaternary (Montenat et al., 1990; Martínez-Díaz, 1998; Martínez-Díaz, 2000; Martínez-Díaz, 2002). In fact, the Alhama de Murcia Fault has the highest seismic potential in the Betic Cordillera. This active fault has been responsible of earthquakes in historical times (Martínez-Díaz et al., 2001). In addition, some instrumental earthquakes with seismic effects on buildings (e.g. 1977 Lorca and 1981 Totana earthquakes) were related to Alhama de Murcia Fault (Mezcua et al., 1984; Rodríguez-Estrella and Almoguera, 1986; Rodríguez-Estrella and Mancheño, 1993). Furthermore, palaeoseismological research based on trenching analysis has associated the occurrence of at least three M_w=6.5-7.0 earthquakes in the last 27,000 years related to the activity of this fault (Martínez-Díaz and Hernández-Enrile, 1999; Hernández-Enrile et al., 2000; Masana et al., 2004).

The Alhama de Murcia Fault is divided into four segments from SW to NE (Fig. 2-7): the Puerto Lumbreras-Lorca, Lorca-Totana, Totana-Alhama de Murcia and Alhama de Murcia-Alcantarilla (Silva et al., 1992; Martínez-Díaz, 1998; Martínez-Díaz y Hernández-Enrile, 1999; García-Mayordomo, 2005). The Puerto Lumbreras-Lorca and Lorca-Totana segments are the most tectonically active and their earthquake recurrence has been estimated in less than 10,000 years (García-Mayordomo, 2005). For this reason these fault segments should be considered in any seismic hazard study developed in the Lorca Basin area.

a) Puerto Lumbreras-Lorca Segment (FAM a):

The Puerto Lumbreras-Lorca segment (Fig. 2-7) has a surface trace of about 28 km (Silva et al., 2003, García-Mayordomo, 2005) with a general trend of N45ºE and it is located in the contact between the southeast edge of Estancias Range and the Guadalentín Depression.

The most recent activity of the Puerto Lumbreras-Lorca segment was at least during the Late Pleistocene (Silva, 1994; Silva et al., 1997; Silva et al., 2003). The slip rate of this segment during this period was estimated at 0.41 m/ka (García-Mayordomo, 2005). The movement of the Alhama de Murcia Fault in this segment is purely lateral strike-slip. The distribution of earthquake epicentres along this segment is very scarce, except for one important group of earthquakes with magnitudes greater than 3.5 located in the north eastern part (SW Lorca group) (García-Mayordomo, 2005). The seismicity is associated with small displacements in depth of the main fault and with NE-SW secondary faults located within the deformation zone of the fault.

The maximum moment magnitude of an earthquake related to the complete rupture of the Puerto Lumbreras-Lorca segment (28 km) is estimated at M_w 6.76 (García-Mayordomo, 2005) using the empirical relationship suggested by Wells and Coppersmith (1994). Since deformations have not been recognized in Holocene deposits and the slip-rate of this fault segment is high (0.41 m/ka), the recurrence of such event has been estimated at 7,000-10,000 years (García-Mayordomo, 2005).

b) Lorca-Totana Segment (FAM b):

The Lorca-Totana segment (Fig. 2-7) has about 23 km long (Martínez-Díaz and Hernández-Enrile, 1991, 1992, 1999) but the trace of Alhama de Murcia Fault splits into two branches with opposite senses of dipping: La Tercia Fault (or North of Lorca Fault) to the north and Guadalentín Fault (or South of Lorca Fault) to the south (Silva 1994, Martínez-Díaz, 1998). The complete deformation zone comprises a width of about 3-4 km. The kinematics of the La Tercia Fault is mainly reverse, while the Guadalentín Fault is mainly left-lateral strike-slip with a reverse component.

The recent activity of the Lorca-Totana segment has been evident at least during the Middle Pleistocene in La Tercia Fault, and during the Holocene in the Guadalentín Fault (Armijo, 1977; Silva, 1994; Martínez-Díaz, 1998; Martínez-Díaz and Hernández-Enrile, 1999; Martínez-Díaz et al., 2001). According to Masana et al. (2004) and García-Mayordomo (2005), the maximum slip rate related to the Guadalentín Fault is 0.30 m/ka.

The analysis of seismicity along this segment indicates that the occurrence of seismic activity may also be due to movements of NW-SE and N-S faults that are located in the deformation area of the Alhama de Murcia Fault. However, the maximum magnitude of an event related to the rupture of the total length of this

segment (23 km) is estimated at 6.66 (Garcia-Mayordomo, 2005) using the Wells and Coppersmith (1994) relationship. From palaeoseismicity data of Masana et al. (2004), considerations about the number of earthquakes in different time intervals and the slip rate of the segment, an average recurrence period of 2,000 to 5,000 years has been estimated for such events (Garcia-Mayordomo, 2005).

c) Totana-Alhama Segment (FAM c):

The Totana-Alhama segment (Fig. 2-7) is the shortest one with 12 km length (Martínez-Díaz, 1998; Martínez-Díaz and Hernández-Enrile, 1999). In this case, the trace of the Alhama de Murcia Fault is frequently interrupted and displaced by small NW-SE and N-S faults.

The activity of the Alhama de Murcia fault in this segment has been only found in Lower-Middle Pleistocene deposits (ITGE, 1991). Moreover, the occurrence of seismicity along this segment is rather low and has no evidence of seismotectonic relations (García-Mayordomo, 2005).

Nevertheless, considering the maximum surface length of the fault traces (about 5 km), the moment magnitude of an earthquake related to the rupture of this length have been estimated of M_w 5.89 (García-Mayordomo, 2005) based on the Wells and Coppersmith (1994) empirical equations. According to the age of the last evidence of deformation, the recurrence of such events should be at least several tens of thousands of years (García-Mayordomo, 2005).

d) Alhama-Alcantarilla Segment (FAM d):

In the Alhama-Alcantarilla segment (Fig. 2-7), of about 23 km long (Martínez-Díaz and Hernández-Enrile, 1999), the trace of the Alhama de Murcia Fault is located in the contact between the Mula Basin and the Guadalentín Depression. In this case, the fault trace is also interrupted by NW-SE and N-S fault systems.

The most recent activity of this segment of the Alhama de Murcia Fault has been found only in Lower-Middle Pleistocene deposits (ITGE, 1991). The occurrence of seismicity, although more abundant than in the Totana-Alhama segment, is still quite low (García-Mayordomo, 2005).

According to the maximum surface length of this fault segment (approximately 17 km), a moment magnitude of an earthquake related to the rupture of this length is estimated of M_w 6.51 (García-Mayordomo, 2005). Considering the absence of Holocene deformation, the average recurrence period of this maximum earthquake is estimated at 13, 000 to 35,000 years (García-Mayordomo, 2005).

2.4.2. Central Betic Cordillera (Granada Basin)

The major faults in the Central Betic Cordillera are located in the Granada Basin (Fig. 2-8). This basin is delimited by E-W faults along the southern boundary (e.g. Ventas de Zafarraya Fault) and NW-SE faults at its western and eastern margins (Fig. 2-8). In general, these faults have normal kinematics and medium to steep dips towards the SW (Sanz de Galdeano, 1996; Doblas et al., 1997; Sanz de Galdeano and López Garrido, 2000; Sanz de Galdeano, 2001a, 2001b; Sanz de Galdeano et al., 2003; Martínez-Martínez et al., 2006; Rodríguez-Fernández and Sanz de Galdeano, 2006). Most of the active faults are concentrated at the eastern margin of the basin (e.g. Granada, Padul, Santa Fe and Atarfe faults) and have been recording movements since Late Miocene. Moreover, some of these faults have a significant steadily microseismicity (Muñoz et al., 2002). This fault system located on the eastern border of Granada Basin is responsible of the differential movement between the metamorphic basement and the basin. This movement involves a gradual uplift of the ranges (e.g. Sierra Nevada) that is reflected in the landscape by a strong incision of the river network. This situation determines the occurrence of landslides, mostly in the bottom of the slopes where the river incision is stronger. Moreover, the generation of these landslides can be favoured by the seismic activity related to these active faults.

The main active faults having the most potential hazard in the Granada Basin are (Fig. 2-8): Ventas de Zafarraya, Granada, Padul, Santa Fe, Atarfe, Belicena-Alhendín, Pinos Puente, Dílar and Obéilar-Pinos Puente, among others (Sanz de Galdeano et al., 2003). Many of those faults can potentially generate earthquakes with magnitudes greater than M_w 6.0. Due to the large number of active faults in this area, only the faults with the greatest seismic potential have been discussed: Ventas de Zafarraya, Granada, Padul, Santa Fe and Atarfe faults (Fig. 2-8).

2.4.2.1. Ventas de Zafarraya Fault

The Ventas de Zafarraya Fault (FVZ) is located north of the Tejeda Range (Fig. 2-2 and 2-8) cutting the boundary between the External and Internal Betic Zones. The trace of the fault is about 20 km long with a main WNW-ESE trend, but can be divided into two E-W sections separated by a NW-SE central section (Reicherter et al., 2003). The striae of the fault plane indicate a main normal kinematics with a superimposed right-lateral strike-slip component. This fault is one of the few cases with seismic activity in the historical period at the Central Betic Cordillera. The rupture of this fault has been related to the occurrence of the 1884 Arenas del Rey earthquake with a maximum intensity of X (Munoz and Udías, 1981; Reicherter et al., 2003). This earthquake seriously damaged several villages in the region (Arenas del Rey, Zafarraya, Ventas de Zafarraya and Alhama de Granada, among many others). In addition, it triggered significant slope instabilities, such as the Güevéjar landslide (Jiménez Pintor, 2006; Jiménez Pintor and Azor, 2006), landslides and rock avalanches in Alhama de Granada and Albuñuelas towns and some liquefaction phenomena (IGME and Diputación de Granada, 2007).

A potential earthquake with a maximum moment magnitude of M_w 6.9 has been estimated (Sanz de Galdeano et al., 2003) based on the maximum length of the trace of the fault (23 km) and its slip rate (0.125 mm/year). The presence of colluvial deposits with preserved soils near the fault indicates that there was several seismic events during the Holocene. From palaeoseismic studies the average return period for this fault has been estimated in 2,000 years (Reicherter, 2001; Reichert et al., 2003).

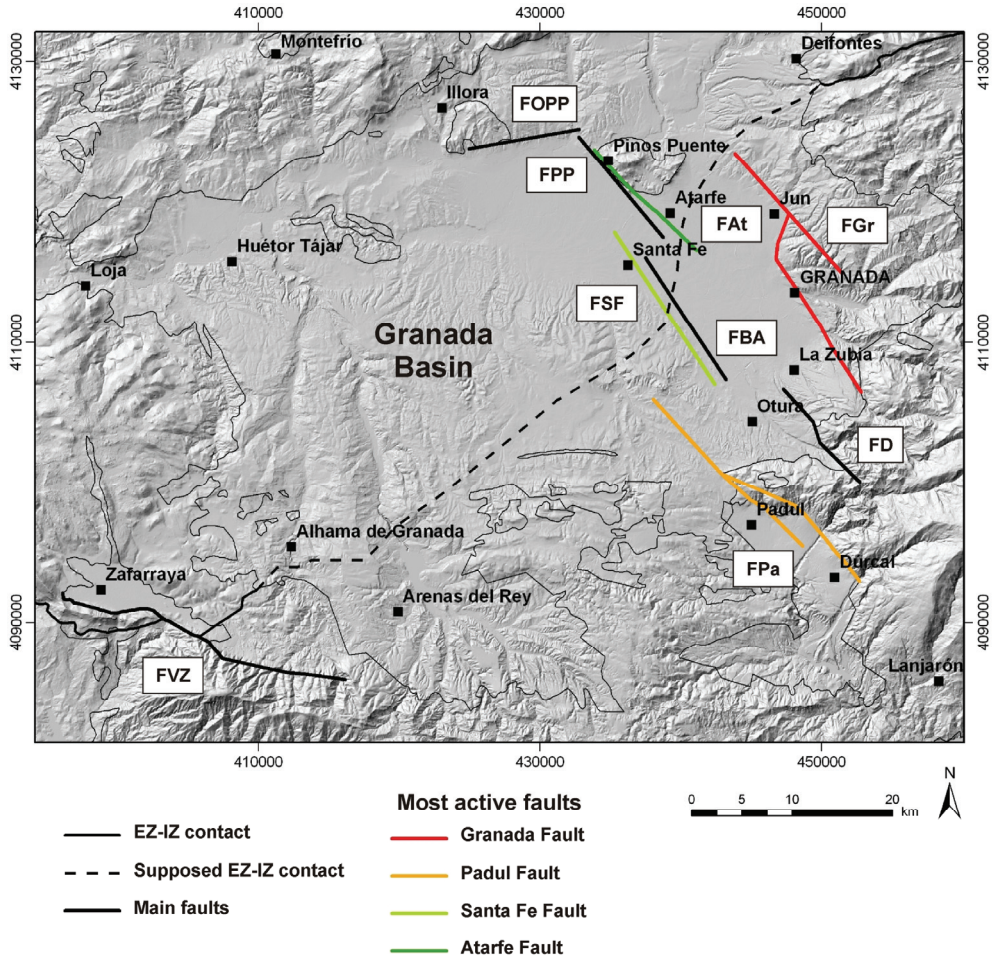

Figure 2-8. Shaded relief map of the Granada Basin showing major faults location. FGr: Granada Fault, FPa Padul Fault, FSF: Santa Fe Fault, FAt: Atarfe Fault, FVZ: Ventas de Zafarraya Fault, FOPPA: Obéilar-Pinos Puente Fault, FPP: Pinos Puente Fault, FBA: Belicena-Alhendín Fault, FD: Dílar Fault. The External Zones-Internal Zones contact (EZ-IZ) is also shown.

2.4.2.2. Granada Fault

The trace of the Granada Fault (Fig. 2-8) is about 23 km long with a main NW-SE trend, but in its central part presents a N-S segment. The El Fargue-Jun Fault has

been considered in this work as a segment of the Granada Fault (Sanz de Galdeano et al., 2003). This normal fault is located very close to the Granada City. For this reason the rupture of this fault is a critical issue that should be considered in any seismic hazard study developed in the Granada Basin area

The recent activity of the Granada Fault has been found in Pleistocene deposits where there are clearly significant movements of the fault (300-500 m). However, it is one of the most active faults in the Granada Basin because it has one of the highest slip rates, with values above 0.35 mm/year (Sanz de Galdeano et al., 2003). This fault seems to be associated to moderate to high seismicity during the historical period, such as the 1431 Atarfe earthquake (I_{MSK}=VIII-IX), which produced damage to the towers and walls of the Alhambra Palace, and the 1526 Granada earthquake with I_{MSK}=VIII (López Casado et al., 2001; Feriche and Botari, 2002; Azañón et al., 2004).

A maximum moment magnitude of an earthquake related to the rupture of the Granada Fault has been estimated at M_w 6.6 based on the surface length of the fault trace (23 km) and the slip rate (0.38 mm/year). The average recurrence period of this maximum earthquake is estimated in 3,000-4,000 years (Peláez Montilla et al., 2001; Sanz de Galdeano et al., 2003).

2.4.2.3. Padul Fault

The Padul Fault is about 20 km long with an approximately NNW-SSE trend (Fig. 2-8), presenting normal kinematics. The Padul-Dúrcal Fault has been considered as a segment of the Padul Fault that is displaced by other small WSW-ENE fault (Alfaro et al., 2001a, 2001b; Sanz de Galdeano et al., 2003). Padul Fault represents the boundary between Sierra Nevada Range and the endorheic Padul Depression. Geomorphologic and tectonic evidences indicate that the Padul Fault is active: deformed Holocene alluvial fans, triangular facets, fault scarps, strong incision of the drainage network, etc. A slip rate of 0.35 mm/year has been estimated for the Padul Fault from the study of displaced Plio-Pleistocene sediments (Alfaro et al., 2001a; Peláez Montilla et al., 2001; Sanz de Galdeano et al., 2003).

The seismic activity during the instrumental period in the Padul area is characterized by the occurrence of small-magnitude earthquakes. However, there is geological evidence of moderate to high-magnitude earthquakes during the Late Pleistocene and Holocene (Alfaro et al., 2001a, 2001b). The surroundings of the Padul Fault are also the epicentral area of very deep earthquakes (h~640 km). Five of these deep events have occurred in 1954, 1973, 1990, 1993 and 2010 (Buforn et al., 1991; 2004). The 1954 earthquake had a magnitude of 7.0, while the 1973 and 1990 shocks had a magnitude about 4.8. The 1993 earthquake had a lower magnitude (M_w=4.4) and the 2010 event had M_w of 6.2. However, these deep earthquakes seem to be related to a different origin without relation with the Padul Fault (Buforn et al., 1991).

The maximum moment magnitude of an earthquake related to a rupture of the Padul Fault is M_w 6.6 (Sanz de Galdeano et al., 2003). This magnitude has been estimated considering a total length of about 20 km and an average slip rate of 0.35 mm/year. The recurrence period of this event have been estimated in 7,000-10,000 years (Peláez Montilla et al., 2001; Sanz de Galdeano et al., 2003).

2.4.2.4. Santa Fe Fault

The main trace of the Santa Fe Fault is about 13 km long with a NW-SE trend (Peláez Montilla et al., 2001; Sanz de Galdeano, 2001a; Sanz de Galdeano et al., 2003). It is a conjugate normal fault of the Granada Fault that defines the western edge of the Vega of Granada, formed by of Upper Pleistocene- Holocene sediments.

This fault is associated with significant moderate earthquakes, mainly recorded in the historical period: Pinos Puente 1806 (I_{MSK}=VIII) and Santa Fe 1911 (I_{MSK}=VIII) earthquakes (López Casado et al., 2001; Feriche and Botari, 2002).

A maximum moment magnitude of an earthquake related to the rupture of the Santa Fe Fault has been estimated at M_w=6.5 according to the maximum length of surface fault trace (13 km) and its slip rate (0.20 mm/year). The average recurrence period of this maximum event is estimated in more than 7,000 years (Peláez Montilla et al., 2001; Sanz de Galdeano et al., 2003).

2.4.2.5. Atarfe Fault

The trace of the Atarfe Fault is about 10 km long with a main NW-SE trend, which defines the western edge of the Sierra Elvira (Peláez Montilla et al., 2001, Sanz de Galdeano, 2001a; Sanz de Galdeano et al., 2003).This fault has associated a relevant moderate seismicity. During the instrumental period, the Albolote 1956 earthquake stands out with a magnitude M_w=4.9 and I_{MSK}=VIII (López Casado et al., 2001; Feriche and Botari, 2002). This was the last earthquake that caused significant damage and deaths in Spain. Main affected populations were Atarfe, Albolote, Santa Fe and Granada. This earthquake also triggered rock falls in the Sierra Elvira and landslides close to Granada City (IGME and Diputación de Granada, 2007). A maximum magnitude of M_w=6.5 has been estimated for an earthquake related to the rupture of the Atarfe Fault, according to the maximum length of surface fault trace (about 10 km) and its slip rate (0.15 mm/year). The average recurrence period of this event is estimated in more than 7,000 years (Peláez Montilla et al., 2001, Sanz de Galdeano et al., 2003).

PART TWO

- **3. Methodology**
  - 3.1. Lithological groups
  - 3.2. Shear strength parameters
  - 3.3. Slope maps
  - 3.4. Safety factor
  - 3.5. Newmark's method
  - 3.6. Newmark displacement base on empirical relationships
  - 3.7. Interpretation of Newmark displacement values
  - 3.8. Seismic scenarios
  - 3.9. Site effects
  - 3.10. Probability of slope failure

3

Methodology

In this Thesis, I have implemented a comprehensive methodology for assessing earthquake-triggered slope instabilities at different scales. This method has been applied at regional and site scales following different approaches. At regional scale, a set of critical acceleration and Newmark displacement maps have been produced following an infinite-slope limit equilibrium model by means of a geographic information system (ArcGIS 9.3., ESRI, 2008). This regional approach concern mainly with the spatial distribution of the triggered slope instabilities considering different input seismic scenarios (probabilistic, pseudo-probabilistic and deterministic). For the site scale, back-analyses of specific slope-instability cases triggered by known earthquakes have been performed by means of a 2D slope stability analysis software (Slide, Rocscience Inc., 2003). This program is used for estimating safety factors and critical acceleration values for circular and non-circular failure surfaces based on different limit equilibrium methods (e.g. Bishop, Janbu and Morgenstern-Price). In this sense, this site approach allows for identifying the determinant parameters in the stability of a particular slope considering the occurrence of an actual earthquake.

The computation flow followed to achieve safety factor, critical acceleration, Newmark displacement and, eventually, probability of slope failure can be summarized in the following main steps (Fig. 3-1):

Step 1) Estimation of the static safety factor:

a) A lithological group classification is arranged based on digital geologic maps and general geotechnical behaviour of the lithologies (section 3.1.).

b) Representative specific weight, cohesion and friction angle values extracted from a compilation of shear strength parameters are assigned to each lithology (section 3.2.).

c) A slope map is derived from a digital elevation model (DEM) of the study area (section 3.3.).

d) The static safety factor is estimated combining the geotechnical properties (specific weight, cohesion and friction angle) and slope angle value by means of different limit equilibrium methods (section 3.4.).

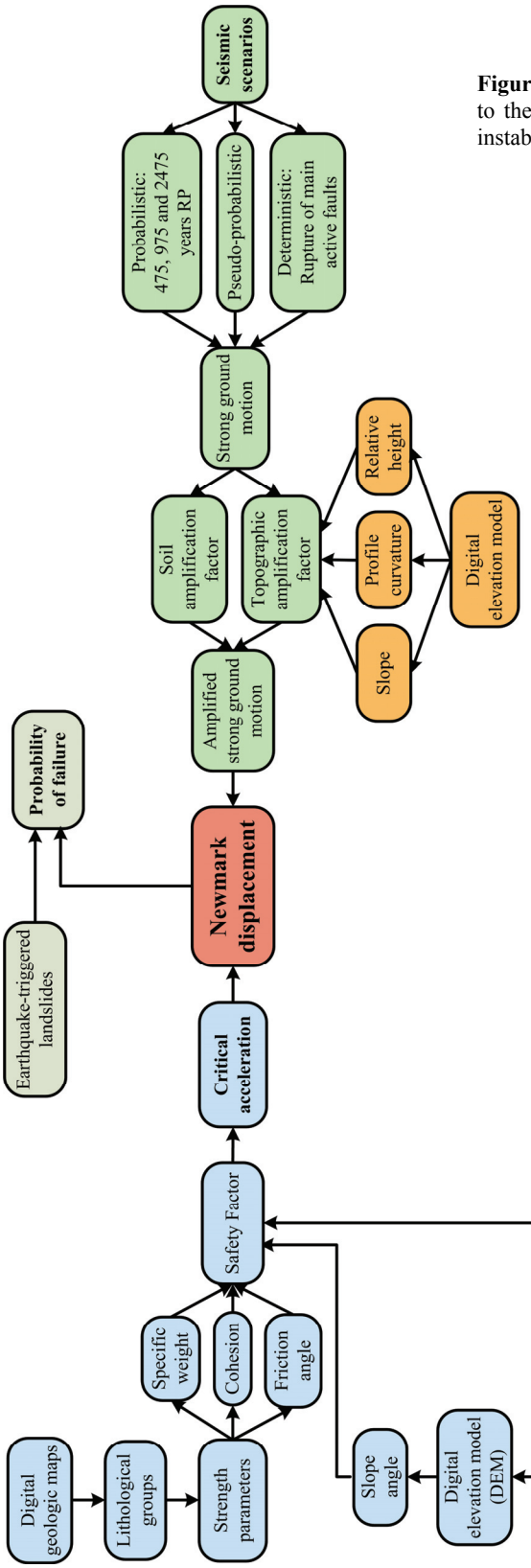

Figure 3-1. Overview of the proposed methodology to the assessment of the earthquake-triggered slope instabilities.

Step 2) Calculation of the critical acceleration:

The critical acceleration is calculated combining the static safety factor and geometrical features based on Newmark's method (section 3.5.).

Step 3) Estimation of Newmark displacement:

Characteristic parameters of strong ground-motion (e.g. Peak Ground Acceleration, PGA) are obtained from each of the considered seismic scenarios (section 3.8.). The strong ground-motion is usually determined on rock, so soil and topographic amplification effects have been considered (section 3.9.). Finally, the Newmark displacement is estimated comparing the critical acceleration with the amplified strong ground motion (section 3.6.).

Step 4) Estimating the probability of slope failure:

The probability of failure of slope instabilities during future earthquakes can be estimated comparing quantitatively the resulting Newmark displacement values and the location of actual slope instabilities triggered by a particular earthquake (section 3.10.).

3.1. Lithological classification

3.1.1. Regional scale

Due to the geological complexity that characterizes the Betic Cordillera, it becomes necessary to perform a simplified lithological map. Different lithological groups have been derived from 1:50,000 scale digital geological maps published by the Institute of Geology and Mines of Spain (IGME). In the Eastern Betic Cordillera, a geological map of the Murcia Region at 1:200,000 scale (ITGE, 1994) has been also used. In the Central Betic Cordillera, a 1:400,000 scale geological map of the Andalusian Autonomous Community (ENADIMSA, 1985) was also considered. The different lithological groups have also been grouped into three main sets (hard rock, soft rock and soils) considering general shear strength and behaviour as concerns to slope stability described in previous works (MOP, 1971; ITGE, 1992; ITGE, 1995; IGME, 2000; IGME and Diputación de Granada, 2007).

In general, the term "hard rock" refers to a rocky substratum that comprises very strong and highly consistent materials. These materials sometimes can develop a superficial weathering bed or a Quaternary covering whose thickness ranges between 2 and 4 m (ITGE, 1992). The main geotechnical characteristics are the rejection (N=R) in the standard penetration test (SPT) and very high values of uniaxial compressive strength. "Soft rock" makes reference to a firm and compact sedimentary material which often shows a soil or superficial weathering layer with less than 2-4 m thick (ITGE, 1992). Its general geotechnical characteristics are defined by variable

SPT values, mostly with N>40 and even N=R. The term "soil" usually refers to a loose, unconsolidated or poorly cemented sedimentary material. In these case, average SPT values are low with N=25, but can be very low (N=5-7) when the clay fraction is predominant (ITGE, 1992). In general, the uniaxial compressive strength for these materials is low or very low.

The following section describes the different lithological groups indicating their regional distribution.

a) Hard rocks:

- Micaschists, quartzites and gneisses (group 1): in general, this group comprises Paleozoic-Triassic metamorphic rocks belonging to the Internal Zones of the Betic Cordillera. In the Central Betic Cordillera are located in Sierra Nevada, Filabres and Contraviesa ranges, while in the Eastern Betic Cordillera are in Torrecilla, Estancias, Almenara ranges and north Puerto Lumbreras and Águilas.

- Phyllites and quartzites (group 2): this group is also constituted by Paleozoic-Triassic metamorphic rocks belonging to the Internal Zones of the Betic Cordillera but with a different grain size. In the Central Betic Cordillera are mainly located in the borders of Sierra Nevada and Contraviesa ranges surrounding the previous lithological group. In the Eastern Betic Cordillera are northwest of Puerto Lumbreras and south of Torrecilla Range.

- Limestones, dolostones and marbles (group 3): this group includes the Triassic-Jurassic carbonate lithologies, for which the presence of some soft levels does not alter the massive character of the rock. This group appears in large areas limiting the previous lithological group, standing out the Gador, Almijara, Arana and Sierra Elvira ranges in the Central Betic Cordillera, and Espuña, Ponce and others small ranges located north of Lorca Basin in the Eastern Betic Cordillera.

- Calcareous sandstones, argillaceous limestones and marls (group 4): this group represents a set of Upper Cretaceous-Tortonian limestones and marls quite massive, but less than the previous group. The largest outcrops in the Eastern Betic Cordillera are located northwest Espuña Range and in the Tercia Range, while in the Central Betic Cordillera are located in the borders of Granada Basin, mainly in its meridional edge.

- Volcanic rocks (group 5): this group comprises different Upper Miocene-Pliocene volcanic rocks (andesites, dacites, lamproites, verites and jumillites). These materials only outcrops in the Eastern Betic Cordillera between Mazarrón and Campo de Cartagena.

b) Soft rocks:

- Argillites, marls, sandstones and gypsums (group 6): in this group are included all the Triassic saline materials, either belonging to the Internal Zones or External Zones. The outcrops located northwards to Zarcilla de Ramos in the Eastern Betic Cordillera and Gádor and Arana ranges in the Central Betic Cordillera are the most remarkable.

- Marls and argillaceous limestones (group 7): this group comprises Upper Jurassic-Lower Cretaceous marls and argillaceous limestones. These materials are located mainly northwest of the Ponce Range and in the Arana Range in the Eastern and Central Betic Cordillera, respectively.

- Conglomerates, sandstones and argillites (group 8): this group is a set of detrital rocks whose degree of compaction allow for considering them as soft rocks. In general, these materials are alluvial fan deposits of Upper Paleogene-Neogene age and form part of the infilling of the Granada and Lorca basins.

- Gypsums and marls (group 9): this group includes the Messinian gypsums and Tortonian white marls that mostly compose the fillings of the Lorca, Granada and Guadix-Baza basins.

c) Soils:

- Gravels, sands, silts and clays (group 10): This group comprises detrital materials that can be found in a wide area mainly related to Quaternary sedimentary deposits (glacis, piedmont, alluvial fans, deltas and flood plains). These materials are part of the infilling of the north of Lorca Basin and Guadalentín Depression in the Eastern Betic Cordillera, and the Granada, Guadix-Baza and Padul basins in the Central Betic Cordillera.

3.1.2. Site scale

For site-specific studies of slope instabilities, the mapped lithologies in the 1:50,000 scale geological maps have been firstly considered. In some cases, detailed geological maps of the slope instability have been performed during field surveys in order to obtain a more accurate lithological classification and to identify the specific lithologies related to the slope failure.

3.2. Shear strength parameters

3.2.1. Regional scale

To perform a regional geotechnical characterization, average values of specific weight, cohesion and friction angle were assigned to each lithological unit (Table 3-1). These shear strength parameters were obtained from a compilation of typical ranges of

values derived from geotechnical bibliography and available geotechnical tests (see Appendix A1 for further information).

Previous studies on seismically-induced slope instabilities concluded that instabilities are controlled by pre-existing fractures in most rock-type lithologies (Keefer, 1984; Harp and Noble, 1993; Harp and Wilson, 1995; Keefer, 2002). They also indicated that the most important factor in determining the susceptibility to earthquake-induced rock failure is the aperture of the discontinuities. That is, the more open the fractures within a rock mass, the more easily failures can occur. Therefore, the shear strength parameters for rock matrix are not a determinant factor in the stability of rocky slopes. For this reason, cohesion and friction angle values for rock-type lithological groups mostly correspond to rock-discontinuities. Nevertheless, in relatively homogeneous materials, such as soils, the failure can occur through the intact material as well for pre-existing discontinuities.

Table 3-1. Typical values of shear strength parameters based on geotechnical bibliography and available geotechnical tests (cf. Appendix A1).

Group	Specific weight (t/m^3)					Cohesion (t/m^2)					Friction angle (º)				
	Min.	*Max.*	*n*	$\bar{x}$	σ	*Min.*	*Max.*	*n*	$\bar{x}$	σ	*Min.*	*Max.*	*n*	$\bar{x}$	σ
1	2.1	3.0	43	2.7	0.2	0.3	8.5	6	4.2	3.3	20	38	16	29	4
2	1.8	2.7	16	2.5	0.2	0.1	6.8	7	2.0	2.8	15	34	18	28	5
3	2.2	2.9	26	2.5	0.2	0.8	12.5	5	5.3	5.5	14	46	18	30	9
4	2.1	2.6	6	2.4	0.2	0.9	9.0	6	3.1	3.0	10	40	18	28	10
5	2.3	2.8	7	2.6	0.2	22	52	3	35.2	15.3	29	40	7	34	4
6	1.4	2.6	10	2.1	0.3	3.5	13.0	5	7.6	4.1	18	34	12	26	4
7	1.6	2.7	7	2.1	0.4	0.5	13	3	4.8	7.1	19	41	7	30	9
8	1.8	2.6	9	2.2	0.2	0.5	1.8	3	1.1	0.6	18	40	16	33	6
9	1.8	2.7	12	2.2	0.2	1.5	13.0	5	6.7	4.8	18	35	6	29	6
10	1.6	2.6	43	2.0	0.2	0.5	6.5	9	3.2	1.9	11	42	40	28	7

These shear strength parameters should be used as a first approach because actual values will likely vary from site to site, for a given rock type, and may vary slightly across a single site. For this reason, a sensibility analysis of these parameters has been done for each study area. The aim of this analysis is to obtain the specific weight, cohesion and friction angle values that provide the stability condition of the slopes (safety factor greater than 1.0). Finally, the values thus obtained have been used in the forthcoming calculation of the safety factor.

3.2.2. Site scale

In the case of site-specific studies, some in-situ and geotechnical tests have been performed in order to obtain the shear strength parameters of the materials related to the slope instability. The shear strength of joints in rock-type materials has been estimated based on the Barton-Bandis failure criterion (Barton and Choubey, 1977; Barton and Bandis, 1990). The Joint wall Compressive Strength (JCS) has been estimated using different Schmidt hammer rebound-JCS empirical equations

developed for a wide number of rock types (cf. Aydin and Basu, 2005). The N-type Schmidt hammer rebound (R_N) was obtained following the most recent procedure suggested by Aydin (2009). In some cases, L-type Schmidt hammer rebound has been estimated by means of an empirical relationship proposed by Aydin and Basu (2005). The data obtained during the field surveys and the different Schmidt hammer rebound-JCS correlations used in this thesis can be found in Appendix A2.

Another relevant parameter used in the Barton-Bandis failure criterion is the Joint Roughness Coefficient (JRC). Several methods have been proposed for evaluating this parameter. The most common procedure is to compare visually standard roughness profiles of 10 cm (Barton and Choubey, 1977), but this method is only valid for small-scale laboratory specimens and it has a great degree of subjectivity (Fig. 3-2). An alternative method for larger profile length is the measurement of the surface roughness amplitude from a straight edge (Bandis, 1980). However, this method has some limitations because the maximum asperity amplitude is measured in millimetres (Fig. 3-2). In actual field conditions where the length of the surface is large, JRC must be estimated for the full-scale surface.

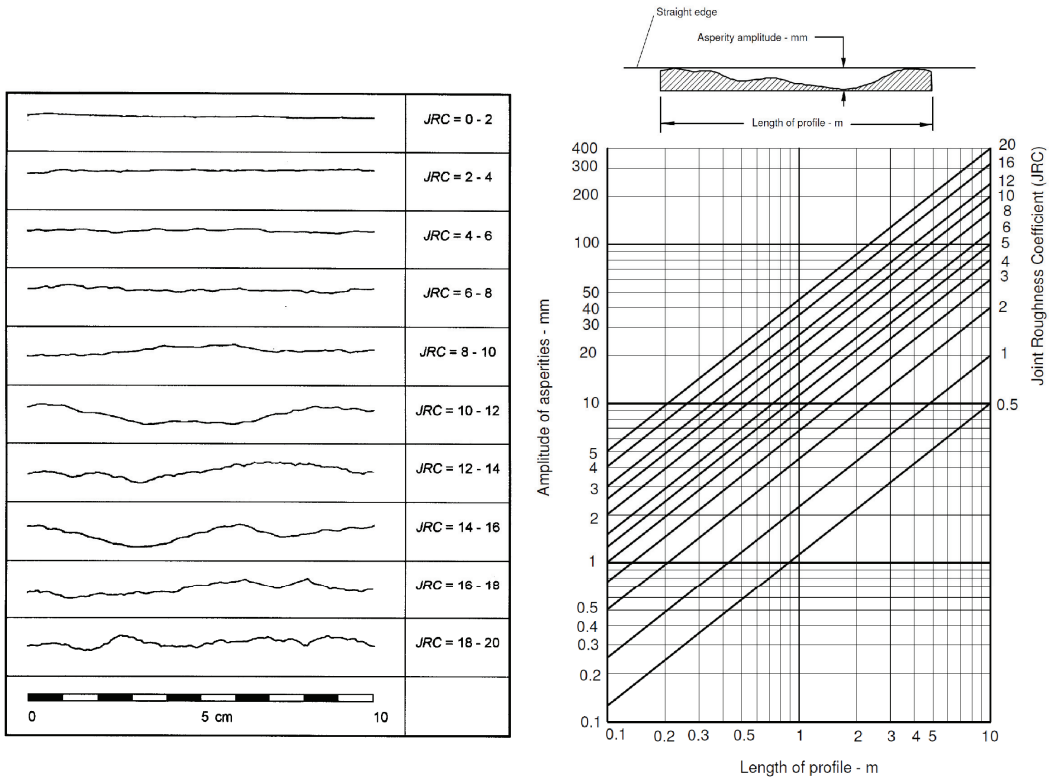

Figure 3-2. Most common methods for estimating JRC values. Left: From standard roughness profiles of 10 cm long (after Barton and Choubey, 1977). Right: From measurements of surface roughness amplitude from a straight edge (Bandis, 1980).

In this thesis, I make use of a published mathematical formula to estimate JRC value from high-resolution joint surface profiles (Tse and Cruden, 1979). These authors developed an empirical correlation based on the root-mean-square (RMS) of the local surface slope of a profile. More recently, Yang et al. (2001) improved this relation with a correlation coefficient of R=0.99326:

$JRC = 32.69 + 32.98 \log Z_2$

where

$$Z_2 = \sqrt{\frac{\sum_{i}^{N-1}(z_i - z_{i+1})^2}{(N-1)\Delta s^2}}$$

and N is the number of discrete measurements of the amplitude of the roughness in the profile, Δs is the constant distance between two adjacent amplitude readings, z_i is the height of the profile measured relative to a reference line and Z_2 is the root mean square of the first derivative of the profile. An average JRC was obtained considering a range of measure of 10 cm in order to compare with the standard roughness profiles of Barton and Choubey (1977). Finally, the JRC value was corrected taking into account the scale effect by means of the expression proposed by Barton and Bandis (1990):

$$JRC_N = JRC_0 \left(\frac{L_N}{L_0} \right)^{-0.02 JRC_0}$$

where L is the length of the joint surface and the suffixes N and 0 refer to the in situ block size and 10 cm laboratory-scale samples, respectively.

For soil-type materials, soil samples were taken from the failure surface related to the earthquake-triggered slope-instability cases, and the following laboratory tests were performed: unsaturated and saturated unit weight determination (AENOR, 1994a), specific gravity determination (AENOR, 1994b), Atterberg limits determination (AENOR, 1993, 1994c), engineering classification of soils (ASTM, 2000), direct shear test of soils under unconsolidated undrained (UU) and consolidated drained (CD) conditions (AENOR, 1998). The results of these laboratory tests can be found in Appendix A3.

3.3. Slope maps

In general, slope instabilities occur in areas with steep slopes, but significant movements can also take place in areas of gentle slope depending on lithology, hydrologic conditions and external factors (e.g. intensity level of the ground shaking).

The present-day topography of the Betic Cordillera can be described as a succession of mountain ranges and basins dissected by main rivers, which incised both the ranges and the basins. Some of these ranges represent the highest reliefs of the Iberian Peninsula (e.g. Sierra Nevada Range) and, hence, steep slopes can be frequently found. The major depressions are the Lorca and Granada basins that have a very flat relief, except in some areas where river incision is stronger.

3.3.1. Regional scale

Slope maps of the Lorca and Granada basins and Sierra Nevada Range areas have been derived from digital elevation models (DEMs) with a 10 x 10 m pixel size (Fig. 3-3) applying the spatial analysis tools implemented in the GIS (ArcGIS 9.3.). These DEMs were obtained from digital topographic maps of the Murcia Region developed by the Spanish Geographic Institute (IGN, Instituto Geográfico Nacional) and from the digital terrain model of the Andalusian Region published by the Junta de Andalucía.

Three main slopes categories have been distinguished concerning its potential susceptibility (ITGE, 1995; IGME and Diputación de Granada, 2007):

- Very low slopes: they correspond to flat or very gentle slopes (< 5º). These areas can be considered stable. Therefore, to boost the GIS calculations, these slopes were not considered in the safety factor calculation.

- Low slopes: slopes between 5º and 25º, which are located in the areas of ridged reliefs and in plains placed among moderate reliefs. These areas present low magnitude landslides (e.g. rock falls and landslides) with a low susceptibility.

- Moderate slopes: slopes between 25º and 35º corresponding to hills, gullied reliefs, low mountains and the lower edges of the highest ranges. In this case, rock falls and landslides can occur depending on lithology.

- Steep slopes: slopes greater than 35º, which are located in the highest ranges. Significant slope instabilities can occur with a high susceptibility.

Table 3-2 shows the relationship between slope and the most common slope instabilities that can occur and lthe ithological groups of the study area. The potential susceptibility of these slope instabilities is also shown (ITGE, 1995; IGME and Diputación de Granada, 2007). Considering these data, slopes instabilities might occur in general on slopes greater than 25º. Therefore, the slope map can be considered as a first approximation to the potential areas where slope instabilities can take place (Fig. 3-3). However, this heuristic approach is quite subjective and incomplete because the triggering factor of the instability is not considered.

Table 3-2. Relationship between slope, type of slope instability and potential susceptibility for each of the lithologic groups defined in the Lorca and Granada basins and Sierra Nevada Range (modified from ITGE, 1995; IGME and Diputación de Granada, 2007).

	LITHOLOGY	SLOPE (º)	SLOPE INSTABITY	SUSCEPTIBILITY
HARD ROCKS	Micaschists, quartzites and gneisses	> 35	Landslides and rock falls	Moderate
		25 - 35		Moderate-High
	Phyllites and quartzites	> 35	Landslides and rock falls	Moderate-High
	Limestones, dolostones and marbles	> 35	Rock falls and landslides	High
		25 - 35		Low
	Calcareous sandstones, argillaceous limestones and marls	> 35	Landslides and rock falls	Moderate
		25 - 35		Low
		< 25		
	Volcanic rocks	> 35	Rock falls	Moderate
SOFT ROCKS	Argillites, marls, sandstones and gypsums	25 - 35	Landslides	High
		< 25		Low
	Marls and argillaceous limestones	> 35	Landslides and rock falls	Moderate
		25 - 35	Landslides	Low
	Conglomerates, sandstones and argillites	25 - 35	Rock falls	Moderate
		< 25		Low
	Gypsums and marls	25 - 35	Rock falls	High
		< 25		Low
SOILS	Gravels, sands, silts and clays	25 - 35	Rock falls	Low
		< 25		

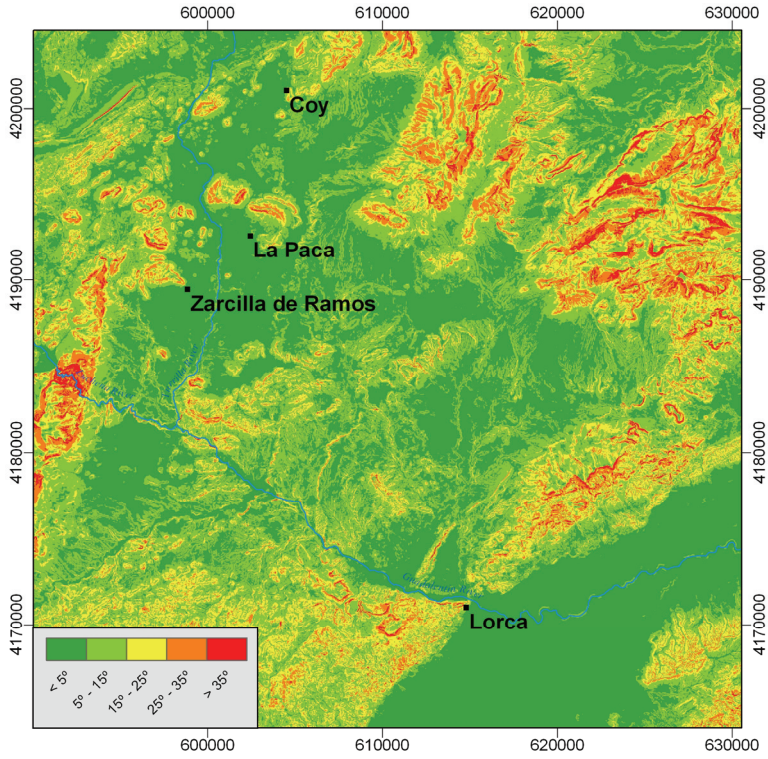

Figure 3-3. Example of a slope map corresponding to the Lorca Basin area. The slopes greater than 25º are shown in orange and red colours.

3.3.2. Site scale

Some specific areas have been studied at a sub-regional and site scales. In these cases, high-resolution DEMs have been derived using a terrestrial laser scanner of great coverage (1000-1500 m). These DEMs have been also used to obtain the high-resolution joint profiles required to estimate the JRC value (see section 3.2.2.). In order to avoid repetition, this issue is described with more detail in Chapter 6 (pages 109-110).

3.4. Safety factor

In general, the stability of a slope in aseismic conditions is expressed by its safety factor (SF) which is the relationship between the forces opposed to the failure of the slope and the forces that favour the rupture and movement of the slope. Therefore, if the SF is greater than 1.0, the slope is in static equilibrium and it is stable. If the SF is less than 1.0, the slope is unstable and displacement occurs. If the SF is equal to 1.0, the slope is in a critical state and it is metastable. In this last condition, either a small increase of the forces that favour the failure of the slope or a decrease of the forces opposed to the rupture of the slope produces a permanent displacement of the slope.

3.4.1. Regional scale

At regional scale, an infinite-slope limit equilibrium model following the Mohr-Coulomb criterion has been used (Graham, 1984). This model is originally only applicable to planar slip surfaces parallel to the slope (e.g. translational slides). However, the infinite-slope model has been widely used in previous works (see section 1.2.) as a reasonable good approach to evaluate the stability of non-planar failure surfaces (e.g. rotational slides). Moreover, it is the only model suitable for calculating slope stability on a pixel basis, and is therefore very suitable to be used in a GIS based on raster data. More complex limit-equilibrium models considering circular and non-circular slip surfaces can be used by means of cross sections. Nevertheless, the development of a safety factor map in a wide area required many cross sections and its implementation in a GIS is rather complicated and time-consuming.

According to Newmark (1965), the use of the infinite-slope model to estimate the stability of slopes during an earthquake requires undrained shear strength parameters. The behaviour of the materials of the slope is undrained since the excess pore pressure induced by the dynamic deformation cannot be dissipated during the short duration of the ground motion. However, cohesion and friction angles measured in undrained test can produce reasonably conservative results (Wilson and Keefer, 1985). Moreover, in slope materials with a similar behaviour under drained or undrained conditions, the drained or effective shear strength parameters can be used if the drained ones are not available. Nevertheless, according to Jibson et al. (2000), the

safety factor assuming the infinite-slope model can be estimated by means of the following equation:

$$SF = \frac{c'}{\gamma t \sin \alpha} + \frac{\tan \phi'}{\tan \alpha} - \frac{m \gamma_w \tan \phi'}{\gamma \tan \alpha}$$

where *c'* is the effective cohesion, ϕ' is the effective friction angle, α is the slope angle, γ is the specific weight of slope material, γ_w is the specific weight of water, *t* is the normal depth of the failure surface and *m* is the degree of saturation of the failure surface. In this equation, the first term corresponds to the cohesive component, the second one to the frictional component and the third term to the strength reduction due to pore pressure. In order to facilitate forthcoming calculations, the obtained safety factor maps only take into account safety factors between 1.0 and 4.0. This is because a value of SF=4.0 is assumed to be related to extremely stable slopes under natural conditions.

3.4.2. Site scale

The safety factor of specific slope-instability cases has been estimated by means of a 2D slope stability analysis software (Slide 5.0., Rocscience Inc., 2003). This program allow for performing either deterministic or probabilistic analyses considering circular and non-circular failure surfaces based on widely used limit equilibrium methods (e.g. Bishop, Janbu and Morgenstern-Price). It also allows for accounting different failure criteria (e.g. Mohr-Coulomb or Barton-Bandis) depending on the available input shear strength parameters.

The simplified Janbu method (Janbu, 1973) has been used in the slope instabilities developed in rock (e.g. rock slides) because it is the only limit equilibrium method that considers a non-circular failure surface and also satisfies the force equilibrium by not considering shear forces between slices. However, Morgenstern-Price method (Morgenstern and Price, 1965) has been used for slope failures developed in soil materials because considers both normal and shear interslice forces and satisfies both force and moment equilibrium. In addition, this method is valid for circular and non-circular slip surfaces.

3.5. Newmark's method

3.5.1. Critical acceleration

To consider seismic (or dynamic) conditions in slope-stability analyses, it is required to incorporate the effect of seismic waves passing throughout the slope. The Newmark's sliding rigid-block method (Newmark, 1965) simplifies slope instability as a frictional rigid block sliding on an inclined planar surface. This rigid block is subjected to the same seismic accelerations as the actual slope instability. Therefore,

when the sum of the static and dynamic forces exceeds the shear strength of the sliding surface, the safety factor is reduced to 1.0 and the block displaces. The critical acceleration can then be defined as the minimum seismic acceleration to overcome shear resistance and initiate the displacement of the rigid block –i.e., trigger the landslide. For this reason, the critical acceleration is the most significant parameter that has to be firstly estimated. According to Newmark (1965), the critical acceleration parallel to the slope is determined by the safety factor and the thrust angle by means of:

$$a_c = (SF - 1)\, g \sin \alpha$$

where a_c is the critical acceleration (in acceleration of the gravity units, 1g = 9.81 m/s^2), g is the acceleration of the gravity, SF is the static safety factor and α is the thrust angle. Assuming an infinite-slope model, the thrust angle is equal to the slope angle. However, when the safety factor is estimated by means of other limit equilibrium models considering rotational movement, α is the angle between the vertical and a line segment connecting the centre of gravity of the landslide mass and the midpoint of the slip circle (Newmark, 1965). In this sense, the Newmark's model is a simplified approach to a rapid estimate of the critical acceleration for both plane and circular sliding surfaces (e.g. translational slides and rotational slumps).

The previous equation to obtain the critical acceleration was developed assuming a_c inclined and parallel to the slope. Newmark (1965) indicated that a_c was taken inclined rather than horizontal in order to be conservative an also to consider the vertical component of the acceleration in same way. Nevertheless, the horizontal critical acceleration can be estimated with the following equation (Newmark, 1965):

$$a_c = (SF - 1)\, g \tan \alpha$$

The critical acceleration is an expression of slope capacity to resist the seismic vibration, so it is the most appropriate parameter to express the susceptibility of slopes to develop earthquake-triggered instabilities (Wilson and Keefer, 1985; Jibson et al., 2000). In this sense, mapping critical acceleration can be considered a suitable approach for identifying the most susceptible areas where slope instabilities might take place during the occurrence of an earthquake. Nevertheless, the common assumptions and limitations involved in Newmark's method need to be pointed (Newmark, 1965; Jibson, 1993):

1) The sliding mass is assumed to be a rigid-plastic body and so the mass does not deform internally.
2) No permanent displacements are allowed for accelerations below the critical acceleration.
3) Plastic deformations on the sliding surface are allowed when the critical acceleration is exceeded.

4) The static and dynamic strength parameters of the slope material are assumed equal and stationary.

5) The effects of dynamic pore pressure are neglected. In general, this statement is valid for overconsolidated clays and very dense or dry sands.

6) The critical acceleration is not strain dependent and thus remains constant throughout the analysis.

7) The upslope resistance to sliding is considered infinite thus upslope displacement is not allowed.

3.5.2. Newmark displacement

Newmark displacement is derived from the critical acceleration value and a real accelerogram corresponding to a representative earthquake. If the acceleration is less than the critical acceleration value, there is no displacement of the sliding block, whereas if it is greater than the critical acceleration, the displacement of the block occurs (Fig. 3-4 A). In the time intervals where the earthquake acceleration exceeds the critical acceleration, the speed of the sliding block can be calculated by integration of the acceleration over time (Fig. 3-4 B). The permanent displacement (i.e. Newmark displacement) is obtained then by integrating the velocity of the block as a function of time (Fig. 3-4 C).

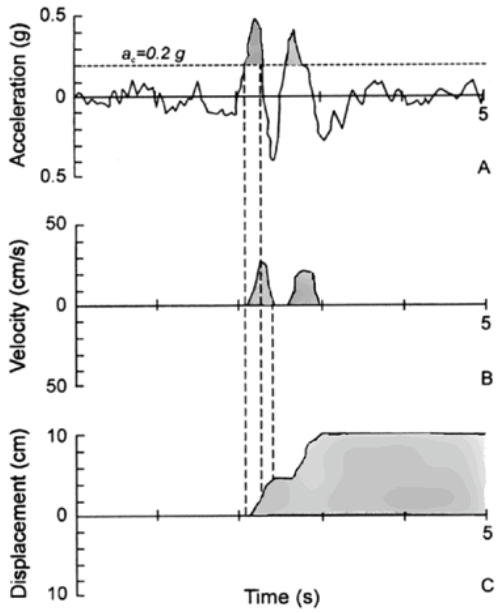

Figure 3-4. Double-integration approach to calculate the Newmark displacement from a real accelerogram (modified from Wilson and Keefer, 1983). A: Earthquake acceleration-time history

considering a critical acceleration of 0.2g. B: Velocity of landslide block versus time. C: Displacement of landslide block versus time.

Despite its relative simplicity, the calculation of Newmark displacement from a specific accelerogram has some limitations, particularly in regional scale applications. The main problem is that the number of accelerometers available in a region is usually low for this purpose and they are distributed in a wide area. For this reason, Newmark displacements calculated in these locations are too far between each other to be considered in a regional analysis. Moreover, in specific studies of earthquake-triggered landslides it is very infrequent to have an accelerometer located at the same site of the slope instability at the time of the earthquake. Therefore, a common procedure for solving such a problem is to estimate the Newmark displacement by means of empirical relationships.

3.6. Newmark displacement based on empirical relationships

The empirical estimation of Newmark displacement is done using regression equations based on basic earthquake parameters (magnitude and epicentral distance) and/or simple strong ground motion parameters (e.g. peak ground acceleration and Arias intensity). A comparison among the most recently published regression equations for Newmark displacement (Romeo, 2000; Jibson, 2007) has been performed in order to select the empirical relationship that provides the best results and to determine the ground motion parameter that is going to be used in the further calculations.

3.6.1. Estimation of Newmark displacement (D_N) from the critical acceleration ratio (a_c/PGA):

Ambraseys and Menu (1988) proposed a regression equation to estimate Newmark displacement as a function of the critical acceleration ratio based on the analysis of 50 strong ground motion records from 11 earthquakes in the magnitude range of 6.6 to 7.3:

$$\log D_N = 0.90 + \log\left[\left(1 - \frac{a_c}{PGA}\right)^{2.53}\left(\frac{a_c}{PGA}\right)^{-1.09}\right] \pm 0.30$$

where D_N is the Newmark displacement (in centimetres), a_c is the critical acceleration (in gravity acceleration units) and PGA is the peak ground acceleration (in gravity units). The last term is the standard deviation of the model.

More recently, Jibson (2007) provided a review of most available regression models, and also presented a newly updated equation on D_N from the critical acceleration ratio:

$$\log D_N = 0.215 + \log\left[\left(1-\frac{a_c}{PGA}\right)^{2.341}\left(\frac{a_c}{PGA}\right)^{-1.438}\right] \pm 0.510$$

Equation [6] from Jibson (2007)

This equation has a high level of statistical significance (R^2=84%, σ=0.51) and provided a good fit of the data because it was derived from a selected database of 875 records from worldwide earthquakes with a wide range of magnitudes from M_w 5.3 to 7.6. Moreover, its functional form matches very well the characteristic sigmoid-shape of the dataset cloud. Coherently, it draws displacements approaching to infinity and zero for a_c/PGA ratios close to 0 and 1, respectively.

3.6.2. Estimation of Newmark displacement (D_N) from Arias intensity (I_a):

Arias intensity (Arias, 1970) is a measure of the energy content of seismic shaking. It is defined as the time-integral of the square of the ground acceleration:

$$I_a = \frac{\pi}{2g}\int [a(t)]^2\, dt$$

where I_a is the Arias intensity (in m/s), g is the acceleration due to gravity (in m/s^2) and $a(t)$ is the seismic acceleration versus time (in m/s^2). Wilson and Keefer (1985) demonstrate that the Arias intensity is a reliable parameter to describe earthquake shaking necessary to trigger landslides. Arias intensity (I_a) can be alternatively estimated from peak ground acceleration (PGA) by means of the equation suggested by Romeo (2000) using Italian earthquakes, which shows a good statistical correlation (R^2=83%):

$$I_a = 0.0004\ PGA^{1.668}$$

a) Using the critical acceleration (a_c):

Jibson et al. (2000) developed a regression equation on D_N from critical acceleration with 555 records of strong ground motions of 13 worldwide earthquakes:

$$\log D_N = 1.521\, I_a - 1.1993\ \log a_c - 1.546 \pm 0.375$$

Equation [5] from Jibson (2007)

However, the seismic data used to develop this equation included many more values for lower a_c values than for higher ones. This resulted in a model that is well constrained at lower critical acceleration values but that progressively fits less well for higher values. For this reason, Jibson (2007) updated the regression equation

considering 875 worldwide records resulting in a more consistent Newmark displacement prediction across a wider range of possible input critical acceleration values:

$$\log D_N = 2.401 I_a - 3.481 \log a_c - 3.230 \pm 0.656$$

Equation [9] from Jibson (2007)

b) Using the critical acceleration ratio (a_c/PGA):

The peak ground acceleration can be also included in these equations in terms of the critical acceleration ratio *(a_c/PGA)*. Romeo (2000) developed a regression equation of this type from 190 accelerograms corresponding to 17 Italian earthquakes with magnitudes between 4.5 and 6.8.

$$\log D_N = 0.607 \log I_a - 3.719 \log\left(\frac{a_c}{PGA}\right) + 0.852 \pm 0.365$$

Equation [12] from Romeo (2000)

A similar regression equation was developed by Jibson (2007) but considering the worldwide database of 875 records with magnitudes of M_w 5.3 to 7.6:

$$\log D_N = 0.561 \log I_a - 3.833 \log\left(\frac{a_c}{PGA}\right) - 1.174 \pm 0.616$$

Equation [10] from Jibson (2007)

3.6.3. Estimation of Newmark displacement (D_N) from moment magnitude (M_w) and critical acceleration ratio (a_c/PGA):

Jibson (2007) also developed a regression model that takes into account earthquake moment magnitude and the critical acceleration ratio. This equation should be only applicable across the magnitude range of the data set (5.3 to 7.6):

$$\log D_N = -2.710 + \log\left[\left(1 - \frac{a_c}{PGA}\right)^{2.335}\left(\frac{a_c}{PGA}\right)^{-1.478}\right] \pm 0.424 M_w \pm 0.454$$

Equation [7] from Jibson (2007)

3.6.4. Estimation of Newmark displacement (D_N) based on a seismic attenuation law:

Romeo (2000) used the attenuation functional form of the attenuation law developed by Sabbeta and Pugliese (1996), which was the best attenuation relationship that fitted the Italian strong ground motion data. In this sense, he proposed a regression equation to estimate Newmark displacement as a function of earthquake magnitude (M) and epicentral distance (RE):

$$\log D_N = -1.281 + 0.648\,M - 0.934\,\log\left(\sqrt{RE^2 + 3.5^2}\right) - 3.699\left(\frac{a_c}{PGA}\right) \pm 0.418$$

Equation [16] from Romeo (2000)

3.6.5. Comparison between the different regression equations

The comparison between the different regression equations cited above have been done considering a hypothetical seismic scenario with M_w=5.0 at an epicentral distance of 0 km (Fig. 3-5). Applying the ground motion prediction equation of Sabetta and Pugliese (1996), the PGA is 0.19g and the estimated Arias intensity by means of the equation suggested by Romeo (2000) is I_a=0.25 m/s.

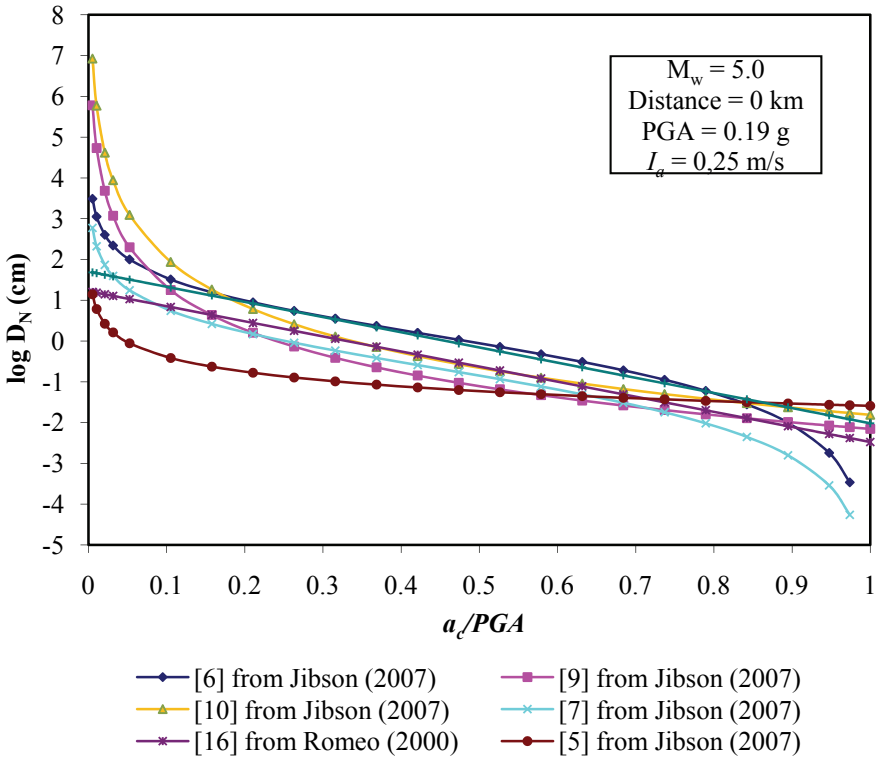

Figure 3-5. Comparison among different regression equations developed to estimate Newmark displacement from peak ground acceleration (PGA), Arias Intensity (I_a) and the critical acceleration ratio.

The regression equation [6] from Jibson (2007) has been selected in this work as the best approach to estimate Newmark displacement. This equation is based on the critical acceleration ratio (a_c/PGA), so it is the most convenient considering that the main input ground motion parameter used in this thesis will be the PGA (see section 3.8.). In addition, this equation was derived from many seismic records with magnitudes similar to those considered in this thesis. It also presents a relatively high statistical correlation (R^2=84%) showing the best results, particularly in the usual range of critical acceleration ratio from 0.2 to 0.8.

3.7. Interpretation of Newmark displacement values

Newmark displacement values obtained at regional scale should not be considered a precise measure of co-seismic slope displacement, but rather as an index of potential instability. In fact, the actual Newmark displacement that effectively triggers a landslide strongly depends on site-specific variables, particularly in the way deformation is accommodated. Slope materials that display a brittle behaviour (e.g. rocks) should have a lower critical displacement than lithologies which due to its ductility can accommodate larger deformations prior to sliding (e.g. soils s.l.).

Several authors have estimated different threshold values of Newmark displacement corresponding to specific cases of slope instabilities triggered by earthquakes. Wilson and Keefer (1983, 1985) used a Newmark displacement of 2 cm as a critical value to trigger rock falls and of 10 cm to induce coherent landslides in southern California. Wieczorek et al. (1985) considered a value of 5 cm as a critical Newmark displacement required to cause the failure of translational slides, rock slides and slumps in San Mateo County, California. Jibson and Keefer (1993) used a range of 5 to 10 cm as the critical Newmark displacement to produce coherent rotational slides in the Mississippi Valley. Detailed analysis of landslides triggered by the 1994 Northridge earthquake (California) performed by Jibson et al. (2000) showed that most landslides occurred in areas with Newmark displacement of 5 to 15 cm, but some landslides can also be found with lower displacements between 1 to 5 cm. Romeo (2000) suggested that failures occurring in rocky slopes (disrupted falls and slides) can be related to critical Newmark displacement of 5 cm, while a critical displacement of 10 cm can be assumed for flows and slides occurring in cohesive soils. More recently, Capalongo et al. (2003) found a critical value of 2 cm to failures developed in carbonates and of 10 cm for flysch materials.

According to the lower bounds found by these authors, Newmark displacements greater than 5 cm could potentially imply the occurrence of coherent-type landslides (e.g. landslides and earth flows), whereas values greater than 2 cm could trigger disrupted-type landslides (e.g. rock falls, rock and debris slides). However, the critical displacement related to the occurrence of disrupted-type landslides seems not to be well defined. In this Ph.D. Thesis, some well-known earthquake-triggered rock slides

have been studied in detail in order to propose a more accurate Newmark displacement threshold for disrupted-type landslides.

In areas where only a few well-documented earthquake-triggered slope instabilities are available (e.g. Betic Cordillera), the obtained regionally Newmark displacement maps can be compared to the actual inventory of slope instabilities in order to identify the areas where seismicity could contribute to reactivate old slope instabilities or to generate new ones, as well as for indentifying the involved landslide typology.

3.8. Seismic scenarios

Three different concepts of seismic scenarios have been considered: probabilistic, pseudo-probabilistic and deterministic. The first ones are useful as provide an overall view of the seismic hazard associated to a standard level of probability, usually in accordance to building design provisions. On the opposite, deterministic seismic scenarios represent a particular situation associated to the occurrence of specific conditions, usually very infrequent, but possible. These types of seismic scenarios are ideal for detailed risk evaluation, civil protection plans, as well as for engineering design of critical structures. Finally, the term pseudo-probabilistic is used here to refer to deterministic seismic scenarios based on the conclusions drawn from a probabilistic approach.

3.8.1. Probabilistic seismic scenarios

The probabilistic seismic scenarios were derived from published seismic hazard maps in terms of peak ground acceleration (PGA) on rock. In these maps, each value of PGA has associated an annual probability of exceedance, or a return period that is defined as the inverse of that probability. Contrary to what might be expected, the return period does not indicate the average time interval between two earthquakes, but the period in years that is expected to exceed the value of PGA with a given probability. In contrast to other seismic scenarios, probabilistic seismic hazard maps consider the effects of all the earthquakes that might occur in a site and takes into account the recurrence laws of these earthquakes.

Probabilistic seismic scenarios considered in this Thesis are based on several seismic hazard maps in terms of peak ground acceleration (PGA) on rock corresponding to 475-, 975- and 2475-year return periods –which are equivalent to a probability of exceedance of 10%, 5% and 2% in 50 years, respectively. This information has been taken from recent probabilistic seismic hazard analyses of the Murcia and Andalusian Autonomous Regions in the frame of major projects on seismic risk (Benito et al., 2006, 2010). Some examples of probabilistic seismic scenarios can be found in Figure 3-6.

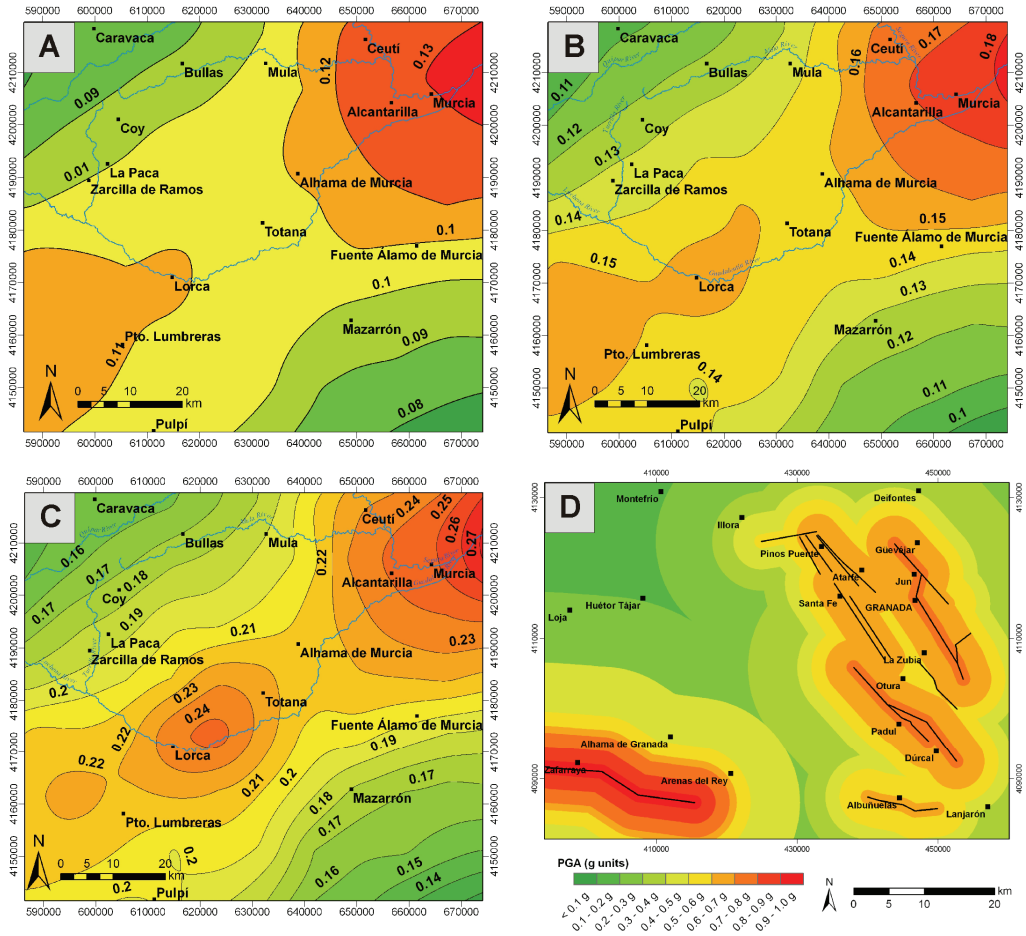

Figure 3-6. Seismic hazard maps in terms of Peak Gound Acceleration (PGA, g units). A: Probabilistic scenario for a 475-year RP for Lorca Basin area. B: Probabilistic scenario for a 975-year RP for Lorca Basin area. C: Probabilistic scenario for a 2475-year RP for Lorca Basin area. D: Deterministic scenario considering the rupture of the main active faults in Granada Basin.

3.8.2. Deterministic seismic scenarios

A deterministic seismic scenario assumes the worst hypothesis, which is the occurrence of a maximum earthquake without considering its probability. The general procedure to develop the deterministic seismic scenarios can be summarized in the following steps:

1) Identification of the seismic sources or active faults located in the study area, as well as its area of influence (see section 2.3.).

2) Definition of the maximum potential earthquake that can be generated for each seismic source or active fault (see section 2.3.). In the particular case that seismicity can be defined as homogeneous in the study area, a pseudo-probabilistic

seismic scenario can be defined. In such scenario, the occurrence of the maximum potential earthquake can be considered to the whole study area.

3) Estimation of the strong ground motion related to the maximum earthquake corresponding to specific seismic sources or to the total area. Strong ground motions have been obtained using an empirical Ground Motion Prediction Equation and considering different epicentral distances from the source (see following section 3.8.2.1.). In the case of a pseudo-probabilistic approach, the estimation of the ground motion to the total area has been performed considering an epicentral distance equal to zero. In this sense, these seismic scenarios show the maximum PGA values expected at a site.

4) Development of the final deterministic hazard seismic map in terms of PGA on rock integrating the estimated strong ground motions by means of a GIS (Fig 3-6 D).

3.8.2.1. Ground Motion Prediction Equations

In order to estimate the acceleration produced by seismic shaking on the ground it is necessary to make use of Ground Motion Prediction Equations (GMPEs). Only few studies devoted to this issue have been produced to date specifically for Spanish earthquakes (e.g., Martín et al., 1996; Cabañas et al., 1999; Cantavella et al., 2004). This is because the Spanish Strong Motion Network started operating in the 1980s (cf. Carreño et al., 1999), and so the available data set comprises very few earthquakes with magnitudes between 4.5 and 5.1 which are not representative for deriving statistically representative strong ground motion models. Therefore, different GMPEs for the Mediterranean zone which correlate magnitude and distance have been compiled from the literature to obtain an average PGA value from a specific earthquake (see Appendix A4).

A selection from these GMPEs has been done following three main criteria: (1) that they are derived from statistically-significant data sets which comprise wide magnitude and distance ranges; (2) that they are widely used in European countries located in a similar seismotectonic context (the European-African plate boundary) and (3) the magnitude scale is in terms of moment magnitude (M_w). The GMPEs finally selected to estimate the average PGA values are the following (Fig. 3-7): Skarlatoudis et al. (2003), Ambraseys et al. (2005), Akkar and Bommer (2007) and Bindi et al. (2009).

3.9. Site effects

It is well known today the influence of site effects on the amplitude, duration and frequency content in seismic strong ground motion (cf. Kramer, 1996). In fact, the intensity of the seismic shaking in a slope depends on the rigidity of the sedimentary materials located above the bedrock (soil amplification), and also the local topography (topographic amplification). As the GMPEs selected in the previous section are in

terms of PGA on rock conditions and no consideration is paid to the topographic factor, it is then necessary to account for both soil and topographic amplification phenomena in the calculations.

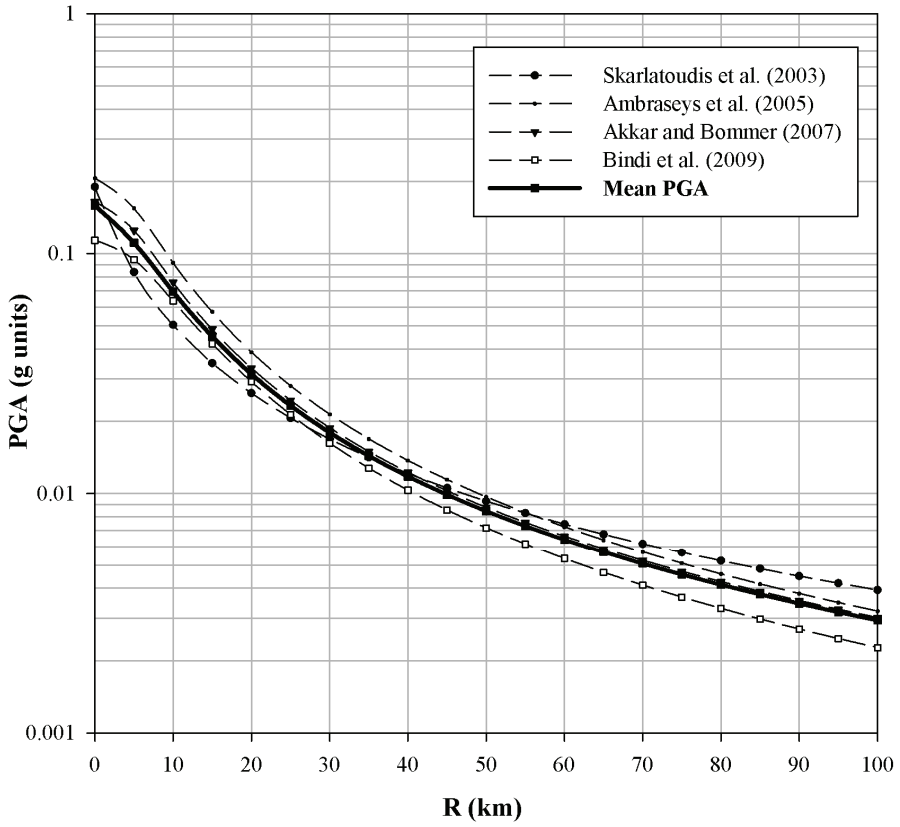

Figure 3-7. Example of mean PGA related to a M_w 5.0 earthquake derived from selected Ground Motion Prediction Equations for the Mediterranean zone (see text for more explanation).

3.9.1. Soil amplification factor

The soil amplification of the ground motion refers to the increase in the intensity of shaking due to local geological conditions, such as the presence of soft rocks and soils. The amplification of these soft sediments is related to the trapping of seismic waves due to the seismic impedance contrast between sediments and the underlying bedrock. In general, soil amplification effects are related to a significant increase of the damage caused by earthquakes in the infrastructures located on soft soils. The estimation of seismic ground motion in engineering practice starts from considering ground motion on hard rock –usually at bedrock depth and, from it, adding the influence of local geological conditions up to the surface.

In this Ph.D. Thesis, the soil amplification effect has been taken into account assigning a multiplying factor to each of the lithological groups previously defined in the study area (Table 3-3). These factors have been adopted after a comparative analysis with those proposed in several previous works on the subject (Benito et al., 2006; Tsige and García-Flórez, 2006; Navarro et al., 2009; Benito et al., 2010) (see Appendix A5). These works were carried out on the frame of two major projects on seismic risk in the south and southeast of Spain (RISMUR and SISMOSAN projects). The results of these projects have been the base for the official Emergency Plan of Seismic Risk of Andalusian Autonomous and Murcia Regions and represent the best quality data available for the study area. In this works different geotechnical classifications of the geological units have been developed based on the average shear-wave velocity in the upper 30 m (v_S^{30}) of the materials. The v_S^{30} values were assigned to each lithological group taking into account the values proposed empirically by Borcherdt (1994) and NEHRP (2003) provisions.

Table 3-3. Soil amplification factors for each lithological group located in the Granada and Lorca basins and Sierra Nevada Range. v_S^{30}: shear-wave velocity in the upper 30 m (in metres per second). SAF: Soil amplification factor.

Group	Lithology	v_S^{30} (m/s)	SAF
1	Schists, quartzites and gneisses	> 1500	1.0
2	Phyllites and quartzites	800-1500	1.0
3	Limestones, dolostones and marbles	800-1500	1.0
4	Calcareous sandstones, argillaceous limestones and marls	350-750	1.0
5	Volcanic rocks	> 1500	1.0
6	Argillites, marls, sandstones and gypsums	250-350	1.8
7	Marls and argillaceous limestones	350-450	1.2
8	Conglomerates, sandstones and argillites	250-350	1.8
9	Gypsums and marls	350-450	1.2
10	Gravels, sands, silts and clays	130-250	2.0

3.9.2. Topographic amplification factor

The seismic amplification due to topography occurs when seismic waves entering the base of a topographic ridge are partially reflected back into the rock mass and diffracted along the free surface. Thus, seismic waves are progressively focused upwards and the constructive interference of their reflections and diffractions increases towards the ridge crest, giving rise to enhanced ground accelerations on topographic highs (Geli et al., 1988; Pedersen et al. 1994). For this reason, the topographic amplification becomes a very important factor for assessing the stability of slopes located in mountainous regions (ITGE, 1992; Harp and Jibson, 2002; Sepúlveda et al., 2005a, 2005b; Murphy, 2006), such as many ranges located in the Betic Cordillera (e.g. Sierra Nevada Range).

However, the topographic amplification effects are not sufficiently understood and there are insufficient data to establish reliable empirical relationships. For this

reason, the topographic amplification is usually neglected in earthquake-triggered landslide assessment. Nevertheless, there are few official seismic codes that provide a first order approximation to take into account the topographic effects. One example is the guide for microzonation seismic studies by the French Association for Earthquake Engineering (AFPS, 1995), which provides topographic amplification factors (1.0 to 1.4) derived from representative topographic profiles in mountainous areas. However, the implementation of this procedure in a GIS is rather complicated and time-consuming. On the other hand, in the Appendix A of Eurocode-8 (CEN, 2004) topographic amplification factors are suggested to be applied when the slopes belong to two-dimensional topographic irregularities, such as long ridges and cliffs with height greater than about 30 m. This seismic code also suggests that for average slope angles less than 15° the topography effects may be neglected. For greater angles, the following guidelines are applicable:

"a) Isolated cliffs and slopes: a topographic amplification factor greater than 1.2 should be used for sites near the top edge.

b) Ridges with crest width significantly less than the base width: a topographic amplification factor greater than 1.4 should be used near the top of the slopes for average slope angles greater than 30°, and a topographic amplification factor greater than 1.2 for smaller slope angles.

c) Presence of a looser surface layer of more than 5 m thick: the smallest topographic amplification factor in a) and b) should be increased by at least 20 %.

d) Spatial variation of amplification factor: the topographic amplification factor may be assumed to decrease as a linear function of height above the base of the cliff or ridge, and to become unity at the base.

In general, topographic amplification also decreases rapidly with depth within the ridge. Therefore, topographic effects to be considered in stability analyses are largest and mostly superficial along ridge crests, but will be much smaller on deep-seated landslides with failure surface passing near the base. In the latter case, if the pseudostatic method of analysis is used, the topographic effects may be neglected" (sic. CEN, 2004).

In conclusion, Eurocode-8 provides a relevant simplification to the problem of topographic amplification. For this reason, I have developed in this thesis an original GIS tool to estimate the topographic amplification effect based on terrain geometry variables and Eurocode-8 provisions.

This tool first computes the slope and curvature maps from a digital elevation model (DEM) using the spatial analyst algorithms implemented in ArcGIS 9.3. The curvature represents the second derivative of the DEM surface or the slope of the slope. The curvature can be calculated in the direction of the maximum slope (profile curvature) or perpendicular to the direction of the maximum slope (planar curvature). In this GIS application, the profile curvature has been used. In the resulting curvature

map, a negative value indicates that the surface is convex at that pixel, while a positive value indicates that the surface is concave at that pixel. A value of zero indicates that the surface is flat. The convex areas are related to ridges while the concave areas are related to depressions. Then, the GIS tool extracts from the curvature map the ridges considering only the convex areas. Subsequently the relative height of the ridges is computed and then compared with the slope map. Eventually, the topographic amplification factor is assigned to each pixel according to the following possible cases:

1) Slopes lower than 15º or ridges with a relative height of less than 30 m: amplification factor equal to 1.0 (i.e. no topographic amplification).
2) Slopes between 15º and 30º and a relative height greater than 30 m: amplification factor equal to 1.2.
3) Slopes steeper than 30º and a relative height greater than 30 m: amplification factor equal to 1.4.

3.10. Probability of slope failure

The methodology proposed in this thesis is also useful to obtain the probability of failure of slope instabilities during future earthquakes. To do this, the predicted Newmark displacement must be quantitatively correlated with an actual inventory of slope instabilities triggered by a particular earthquake. However, this procedure requires a detailed investigation of an earthquake large enough to trigger many well-documented landslides. Jibson et al. (2000) conducted the best-documented study of this type following the 1994 Northridge earthquake (California). They compared the mapped distribution of earthquake-triggered landslides (Harp and Jibson, 1996) to Newmark displacements estimated at a regional scale to obtain the probability of failure as a function of Newmark displacement (Fig. 3-8):

$$P(f) = 0.335[1 - \exp(-0.048 D_N^{1.565})]$$

where $P(f)$ is the estimated probability of slope failure and D_N is the Newmark displacement in centimetres.

Although this equation is only valid for the specific geologic and seismic conditions of southern California, it has been used to estimate grossly the probability of slope failure in other similar areas (Jibson and Michael, 2009). Nevertheless, this regression equation has been regarded as inappropriate to be used in the study area considered in this thesis because both geologic and seismic conditions differ significantly from those of California. In addition, the current number of well-known earthquake-triggered slope instabilities is unfortunately not sufficient to develop successfully a new probability of failure equation for the study area.

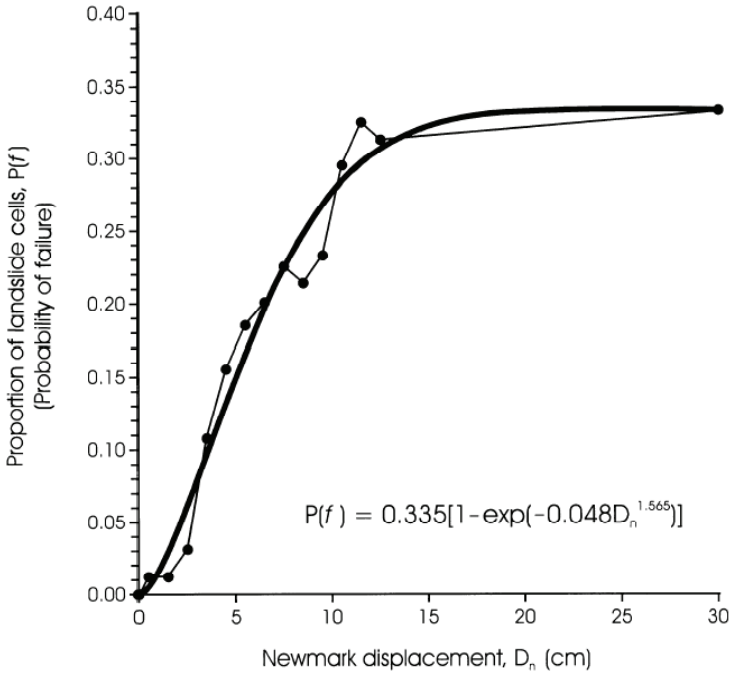

Figure 3-8. Probability of failure as a function of Newmark displacement (from Jibson et al., 2000).

PART THREE

- **4. Regional hazard assessment of earthquake-triggered slope instabilities considering site effects and seismic scenarios: Application to the Lorca Basin (Eastern Betic Cordillera, SE Spain)**

- **5. Regional hazard assessment of seismically-induced slope instabilities in Sierra Nevada Range (Betic Cordillera, South Spain) simulating the occurrence of a maximum magnitude earthquake related to the Padul Fault**

- **6. Applicability of Newmark's method at regional, sub-regional and site scales: seismically-induced SW Bullas and La Paca rock-slide cases (Murcia, SE Spain)**

- **7. Constraining pre-instrumental earthquake parameters from slope stability back-analysis: Paleoseismic reconstruction of the Güevéjar landslide during the 1st November 1755 Lisbon and 25th December 1884 Arenas del Rey earthquakes**

- **8. Effectiveness of deep drainage wells as a slope stabilization measure: The reactivation of the Diezma landslide (Southern Spain)**

4

Regional hazard assessment of earthquake-triggered slope instabilities considering site effects and seismic scenarios: Application to the Lorca Basin (Eastern Betic Cordillera, SE Spain)

M. J. Rodríguez-Peces [1], J. García-Mayordomo [2], J. M. Azañón [1,3] and A. Jabaloy [1]

[1] Departamento de Geodinámica, Universidad de Granada, Fuentenueva s/n, 18071 Granada, Spain.
[2] Instituto Geológico y Minero de España (IGME). C/La Calera, 1. 28760. Tres Cantos (Madrid), Spain.
[3] Instituto Andaluz de Ciencias de la Tierra (UGR-CSIC), Granada, Spain.

Soil Dynamics and Earthquake Engineering
Submitted 18 March 2010; under review 20 April 2010

ABSTRACT

We present a regional hazard assessment of earthquake-triggered slope instabilities based on considering the occurrence of specific seismic scenarios and taking into account soil and topographic amplification effects. The study area is the Lorca Basin, located in the Eastern Betic Cordillera, one of the most seismically active regions of Spain. We have followed the Newmark's sliding rigid-block methodology implemented in a geographic information system (GIS) with the aim of producing regional maps in terms of Newmark displacements for selected seismic scenarios. Strong ground-motion amplification site effects have been considered, particularly the topographic factor by means of designing a GIS tool based on terrain geometry features and Eurocode-8 provisions. Three different concepts of seismic scenarios have been considered: probabilistic, pseudo-probabilistic and deterministic. The obtained Newmark displacement maps are compared to the distribution of known slope instabilities in the area. Future seismically-induced slope instabilities in the Lorca Basin would be isolated disrupted-type landslides, mostly rock slides and rock falls. Only the occurrence of the deterministic scenario (M_w>6.7) seems capable of producing widespread slope instabilities and coherent landslides.

Keywords: Betic Cordillera, GIS, Landslides, Lorca Basin, Newmark, Rock falls, Soil amplification, Topographic amplification, Site effects.

4.1. Introduction

Slope instabilities are one of the most common and hazardous secondary effects of earthquake vibration. In fact, destruction and fatalities from earthquake-triggered landslides sometimes exceed damage directly related to strong shaking of buildings. Furthermore, triggered landslides are crucial in controlling the practicality of life-lines in the aftermath of the earthquake, and therefore in permitting a rapid response of emergency services.

The phenomenology of landslides triggered by earthquakes has been thoroughly studied by Keefer (1984, 2002) and Rodríguez et al. (1999). These authors concluded that the most common type of earthquake-triggered slope instabilities are rock falls, disrupted soil slides, and rock slides. These types of landslides can be triggered by earthquakes as small as magnitude M~4. Additionally, they found a positive correlation between the abundance of landslides and the area affected by them, with earthquake magnitude; although variations due to either specific geological and terrain conditions or seismic parameters are noted. In fact, seismically induced slope instabilities are strongly controlled by both the characteristics of strong ground-motion (magnitude and distance to the earthquake, soil and topographic amplification) and the deformational behaviour of the materials against seismic vibration (liquefaction, cyclic mobility, collapses).

The assessment of earthquake-triggered landslide hazard at a regional scale always implies important simplifications. Uncertainties in defining accurately strong ground-motion characteristics at a particular site, as well as in modelling the geotechnical parameters of the slope mass and its dynamic behaviour, make earthquake-triggered landslide assessment a very complex matter. The most common procedures followed in regional assessment deal with the well-known Newmark's sliding rigid-block method (Newmark, 1965) implemented in a geographic information system (GIS) (e.g. Miles and Ho, 1999; Jibson et al., 2000; Luzi et al., 2000; Romeo, 2000; Capolongo et al., 2002; Carro et al., 2003; among others). These works are mostly concerned with obtaining a probability function on Newmark displacement versus proportion of slope failures related to a specific earthquake and/or implementing the variability of input parameters, mainly geotechnical variables, into the computation of the critical acceleration. Less effort has been paid to incorporate the influence of site effects in seismic motion or to consider as seismic input specific scenarios of engineering significance.

This paper adds to the short list of works devoted to earthquake-triggered landslide hazard assessment in Spain (García-Mayordomo, 1999; Mulas et al., 2003; Delgado et al., 2006). It is the first one produced for the Lorca Basin, which is located in the Betic Cordillera, the most seismically active region of Spain. In this area, the occurrence of three consecutive seismic series (1999 Mula M_w=4.8, 2002 Bullas M_w=5.0, and 2005 La Paca M_w=4.8) have provoked significant building damage and considerable social warning –apart from few but significant rock slides and rock falls.

This situation instigated the launch of a major research project on seismic hazard and risk assessment (cf. García-Mayordomo et al., 2007; Gaspar-Escribano et al., 2008), which has produced very valuable information for proceeding with subsequent investigations. In this context, this paper represents the first step on a new project aimed at studying particular slope instability cases associated to specific earthquakes. Specifically, we mean to produce a regional picture of earthquake-triggered landslide hazard in the Lorca Basin following the Newmark method implemented in a GIS. In contrast to other studies of the same type, we have made a particular effort in considering as seismic input specific earthquake scenarios significant for civil protection and engineering purposes, as well as strong ground-motion site effects, namely soil and topographic amplification. We have finally obtained a set of Newmark displacement maps, which are compared to the distribution of known slope instabilities in the area. We conclude that future earthquake-triggered slope instabilities in the Lorca Basin would be disrupted landslides, mostly rock falls. Only the occurrence of a large but infrequent earthquake related to the activity of the main fault in the area could produce a widespread distribution of landslides and significant mass movements.

4.2. Regional Geology and Active Tectonics

The Lorca Basin is a Neogene intramontane depression located in the Eastern Betic Cordillera, in SE Spain (Murcia). Its west, south and east borders are sharp, formed by mountain ranges composed mainly by metamorphosed Palaeozoic and Mesozoic rocks, which form the so-called Internal Betic Zone (Fig. 4-1). These reliefs are the core of ENE-oriented anticlines, which gently folded and emerged the Lorca Basin during late Neogene (Montenat and Ott d'Estevou, 1999; Booth-Rea et al., 2002). The northern border is broader, and is formed by isolated reliefs formed mainly by limestone and dolomite rocks belonging to the Subbetic Domain of the External Betic Zone (García-Hernández et al., 1980).

The basin filling is composed of Neogene-Quaternary sedimentary rocks. Three principal facies associations are recognised, representing a transition from marine to continental conditions. The carbonate-dominated ramp association includes boundstones, grainstones, packstones and sandy calcarenites rich in marine fossils. The marginal-marine facies association includes conglomerates, sandstones and mixtures of calcarenites and sandstones. The continental deposits mainly consist of conglomerates with sandstones and siltstones. The sedimentary filling is more developed at the southern part of the basin, which is formed mainly of flat reliefs.

The most frequent type of slope instabilities in the Lorca Basin are rock falls and rock slides (Rodríguez-Peces, 2008). Although coherent landslides are also present, they are much less frequent. The spatial occurrence of rock falls and rock slides is clearly related to the mountain ranges that border the basin, as well as to isolated reliefs located inside the basin. The steep slopes and the strong tectonization are the main factors controlling the stability of the cliffs. Coherent landslides are

found mainly at the southern border of the basin, developed either in strongly weathered and tectonized metamorphic rocks or in uplifted Neogene sediments. Although less frequently, landslides also take place inside the basin favoured by steep gradients controlled by drainage incision.

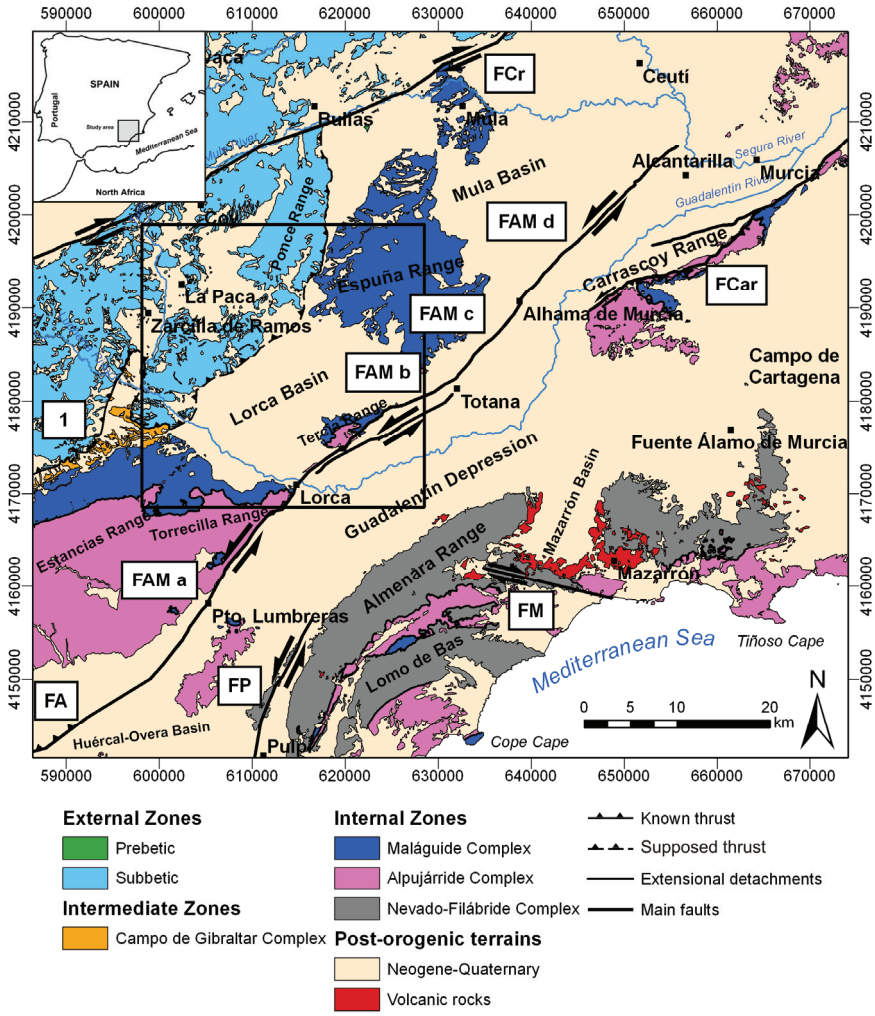

Figure 4-1. Geological map of part of the Eastern Betic Cordillera (SE Spain) showing the Lorca Basin and main faults in the study area. FCr: Crevillente Fault, FAM: Alhama de Murcia Fault (a: Puerto Lumbreras-Lorca, b: Lorca-Totana, c: Totana-Alhama and d: Alhama-Alcantarilla), FCar: Carrascoy Fault, FM: Moreras Fault, FP: Palomares Fault.

From a tectonic point of view, the Lorca Basin has been interpreted as a pull-apart basin (Montenat and Ott d'Estevou, 1999). Indeed, the basin is delimited at its NW and SE margins by long NE-SW trending strike-slip faults: Crevillente and Alhama de Murcia faults, respectively (Fig. 4-1); and by a system of normal faults both at the NE and SW margins. These fault systems had a significant influence on

Neogene basin sedimentation and were periodically active during the Miocene (Montenat and Ott d'Estevou, 1999). The Crevillente Fault is a large right-lateral strike-slip fault located at the northern part of the Lorca Basin (Fig. 4-1). Even though the Crevillente Fault was last tectonically active in the Lower-Medium Pleistocene, many authors have related the 1999 Mula earthquake (M_w=4.8) to the fault (Martínez-Díaz et al., 2002; Buforn et al., 2005; Sanz de Galdeano and Buforn, 2005). The Alhama de Murcia Fault has the highest seismic potential in the Betic Cordillera. This active left-lateral strike-slip fault has been responsible of earthquakes in historical times (Mezcua et al., 1984; Martínez-Díaz et al., 2001). Furthermore, palaeoseismological research based on trenching analysis has associated the occurrence of at least two to three M_w=6.5-7.0 earthquakes in the last 27,000 years to the activity of this fault (Masana et al., 2004). The main trace of the Alhama de Murcia Fault is divided into four segments from SW to NE (Fig. 4-1): the Puerto Lumbreras-Lorca, Lorca-Totana, Totana-Alhama de Murcia and Alhama de Murcia-Alcantarilla (Martínez-Díaz, 1998). The Puerto Lumbreras-Lorca and Lorca-Totana segments are the most tectonically active and their maximum earthquake recurrence has been estimated in less than 10,000 years (García-Mayordomo, 2005).

4.3. Seismicity and Triggered Landslides

The occurrence of earthquakes in the Lorca Basin and surroundings is known from historical times (Martínez Solares and Mezcua, 2002) (Fig. 4-2). The first reference dates to 1579 (Lorca, I_{MSK}=VII) and since then a number of earthquakes have been felt in the area, the most damaging one happening in 1674 (Lorca, I_{MSK}=VIII). Historical chronicles have been the subject of numerous studies aimed at evaluating macroseismic intensities according to the MSK scale, and recently to the EMS scale (cf. Martínez Solares and Mezcua, 2002). Nevertheless, these studies have been devoted mostly to evaluate building damage and casualties; less attention has been paid to analyse in detail environmental effects such as slope instabilities, even though it is known that these phenomena took place in some cases (López Marinas, 1978; Martínez Guevara, 1984).

Earthquake instrumental recording in the area starts around 1920 (Fig. 4-2). The most damaging earthquake in this period is the 1948 Cehegín earthquake (I_{MSK}=VIII, m_b=5.0). The report produced in the time by Rey Pastor (1949) mentions very briefly the occurrence of a couple of rock-fall phenomena in the epicentral area, although the earthquake was felt at intensities VII and VI in a very broad area. Apart from this earthquake, the instrumental catalogue of the area contains 15 earthquakes felt with MSK intensities between VI and VII. From the point of view of earthquake environmental effects, the most interesting ones are the 1999 Mula (M_w=4.8, I_{EMS}=VI), 2002 Bullas (M_w=5.0, I_{EMS}=VI) and 2005 La Paca (M_w=4.8, I_{EMS}=VII) earthquakes (Buforn et al., 2005; Murphy, 2005; Buforn et al., 2006; Benito et al., 2007). These earthquakes, in contrast to other studies, account for descriptions of specific cases of triggered rock falls and rock slides.

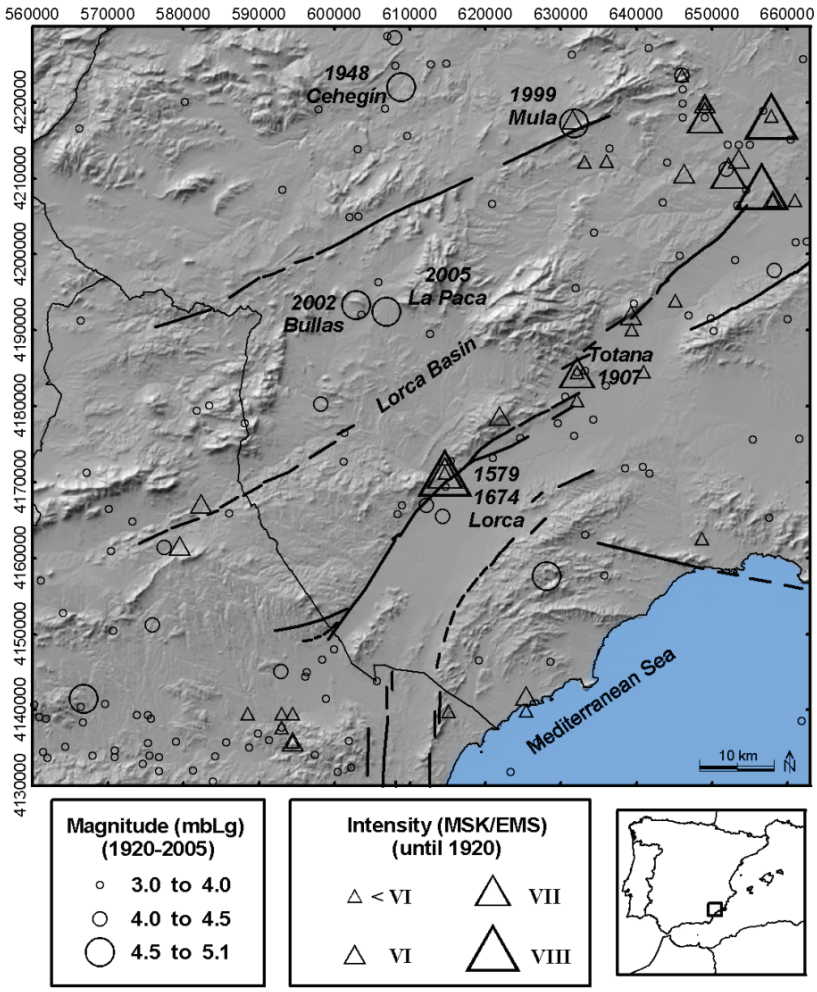

Figure 4-2. Distribution of historical and instrumental seismicity around the Lorca Basin (Murcia Region). Only main shocks are plotted. Earthquakes named in the figure are cited in the text.

The occurrence of earthquake-triggered slope instabilities in the area has to be more common than it can be thought based on the available descriptions. We attribute the scarceness of descriptions to a bias of the available information towards the evaluation of building damage in contrast to analysing effects occurred away from urban centres. According to the MSK and EMS intensity scales slope instabilities are common at intensity VI. The recently released ESI scale (Michetti et al., 2007), an intensity scale specifically devised to account for earthquake environmental effects, situates the initiation of slope instabilities at intensities as low as IV. Hence, it is very likely that a significant number of earthquakes in the Lorca Basin and surroundings have triggered slope instabilities. These instabilities would be mostly rock falls and rock slides as these are the commonest types in the area.

4.4. Methodology

Several methods have been proposed for evaluating co-seismic permanent slope displacements (cf. Kramer, 1996). Undoubtedly, the most popular one is that originally put forward by Newmark (1965) for earth dams, and later extended to natural slopes by Wilson and Keefer (1983). This method simplifies the slope instability as a rigid-block sliding on a planar surface, where static and dynamic strength parameters are assumed equal and stationary. Under these crucial assumptions, the calculation of the permanent displacement is a two-step procedure. First, the minimum seismic acceleration to overcome shear resistance and initiate the displacement of the block is calculated by:

$$a_c = (SF - 1)\, g \sin \alpha \qquad (1)$$

where a_c is the critical acceleration (in gravity units, 1g = 9.81 m/s^2), g is the gravity acceleration, SF is the static safety factor and α is the slope angle. Hence, the critical acceleration is an expression of slope capacity to resist seismic vibration and therefore, it can be regarded as an effective measure of the susceptibility to earthquake-induced slope instabilities.

Secondly, slope displacement is calculated considering an acceleration time history (accelerogram) representative of the expected strong ground motion at the site, and by double integrating the time intervals when the critical acceleration is overcome. Cumulative displacement calculated this way –i.e., the so-called Newmark displacement (D_N), provides a fairly estimation of the actual displacement, as it has been shown in both laboratory tests and field case studies (cf. Wilson and Keefer, 1983). Newmark displacement can also be approximate by using regression equations based on single strong ground motion parameters, such as Arias intensity (I_a) or Peak Ground Acceleration (PGA) (cf. Jibson, 2007).

Applying the Newmark method to regional hazard assessment implies computing equation (1) by means of a geographical information system (GIS) and processing geospatial information. The following sections deal with the construction of the critical acceleration map from the safety factor map and with the construction of Newmark displacement maps for selected seismic scenarios and accounting for site effects (Fig. 4-3).

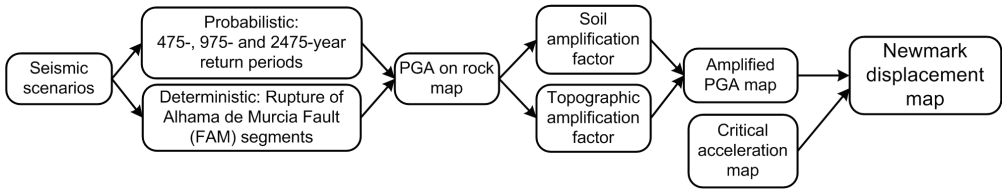

Figure 4-3. Flow diagram showing the method followed for obtaining Newmark displacement maps for each seismic scenario considered.

4.4.1. Calculation of safety factor and critical acceleration maps

To produce the critical acceleration map, we first need to estimate the static safety factor map. To do so, we arranged a lithological map from 1:50,000 digital geological maps published by the Institute of Geology and Mines of Spain (IGME). We have distinguished 11 lithological groups and grouped them into three main sets (hard rock, soft rock and soils) considering shear resistance and behaviour as concerns to slope stability (Fig. 4-4). Table 4-1 shows the adopted strength parameters for each group as well as the range of variation in each one. The limits of the range were set based on geotechnical bibliography and available geotechnical tests. For rock-type lithological groups, cohesion and friction angle correspond to rock-discontinuities. The final values adopted in the calculations were derived by iterating cohesion and friction angle until resulting safety factors were higher than 1.0 (cf. Jibson et al., 2000).

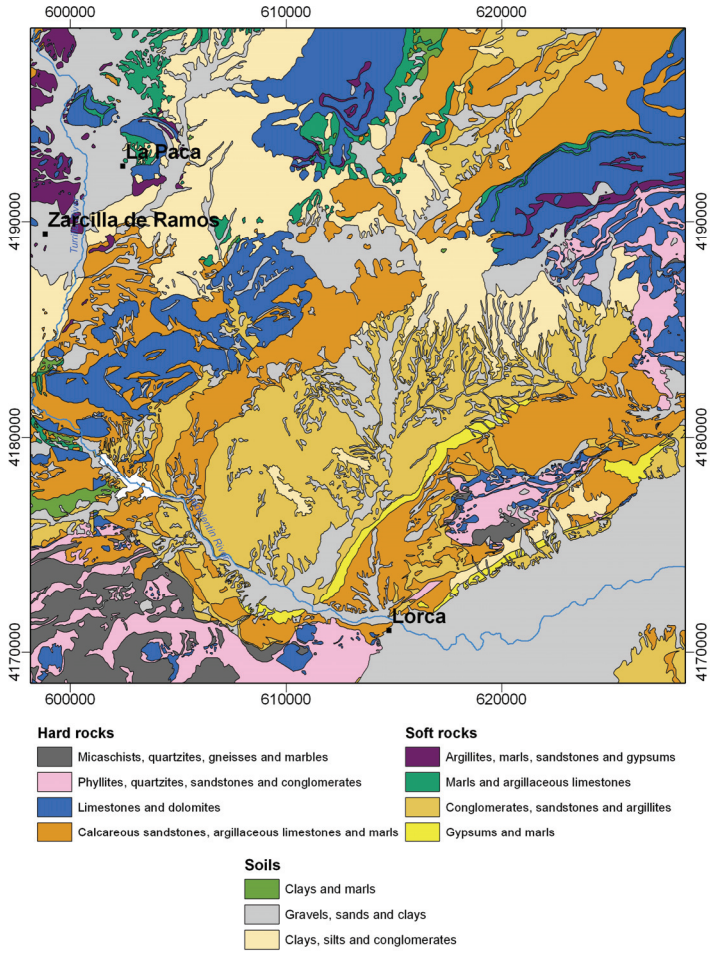

Figure 4-4. Lithological groups in the Lorca Basin. The map was built based on digital geological maps and geotechnical information. See text for further explanation.

Table 4-1. Lithological groups and strength parameters considered in the calculation of the safety factor map. Range of strength values is shown in brackets.

Lithological group	Specific weight (kN/m^3)	Cohesion (kN/m^2)	Friction angle (º)
Micaschists, quartzites, gneisses and marbles	**27** (25-29)	**46** (0-75)	**29** (25-33)
Phyllites, quartzites, sandstones and conglomerates	**25** (23-27)	**43** (0-48)	**28** (23-33)
Limestones and dolostones	**25** (23-27)	**45** (0-108)	**30** (21-39)
Calcareous sandstones, argillaceous limestones and marls	**24** (22-26)	**36** (0-61)	**28** (18-38)
Argillites, marls, sandstones and gypsums	**21** (18-24)	**25** (35-117)	**26** (22-30)
Marls and argillaceous limestones	**21** (17-25)	**29** (0-119)	**29** (21-39)
Conglomerates, sandstones and argillites	**22** (20-24)	**23** (4-16)	**33** (27-39)
Gypsums and marls	**22** (20-24)	**17** (0-115)	**28** (23-35)
Clays and marls	**19** (17-21)	**17** (0-78)	**18** (13-23)
Gravels, sands and clays	**20** (18-22)	**19** (0-32)	**32** (26-38)
Clays, silts and conglomerates	**19** (17-21)	**13** (22-58)	**23** (17-29)

The safety factor map (Fig. 4-5) is then calculated by computing the strength parameters maps with the slope map (pixel size: 10 x 10 m) and assuming a simple limit equilibrium model of an infinite slope following the Mohr-Coulomb criterion (Jibson et al., 2000):

$$SF = \frac{c'}{\gamma t \sin\alpha} + \frac{\tan\phi'}{\tan\alpha} - \frac{m\gamma_w \tan\phi'}{\gamma \tan\alpha} \qquad (2)$$

where c' is the effective cohesion, ϕ' is the effective friction angle, α is the slope angle, γ is the specific weight of slope material, γ_w is the specific weight of water, t is the normal thickness of the rupture surface and m is the degree of saturation of the slope. To this last respect, we have considered either saturated and dry conditions, and found that the former produces very unrealistic results, as the climate of the study area is arid and the water table is generally very deep (over 50 m) (ITGE, 1985). For the sake of simplicity, we only show here the results obtained in non-saturated conditions. On the other hand, the depth of the rupture surface has been set to three metres. This critical decision is supported on both field observations and computer testing. Firstly, slope instabilities in the Lorca Basin are generally small sized. In the case of rock slides and rock falls, the size of the blocks is usually in between 1 to 6 m long. Coherent landslides are small and shallow, the thickness of the weathering profile being usually in the first three meters. Secondly, considering a deeper rupture surface would increase the weight of the sliding block and so implied static safety factors far from stability (SF<1.0). In this circumstances, iterative tests showed that the stability condition (SF=1.0) was only reached when unrealistic strength parameters were assumed. In addition, the Newmark displacement maps obtained with these parameters were also unrealistic and against field observations.

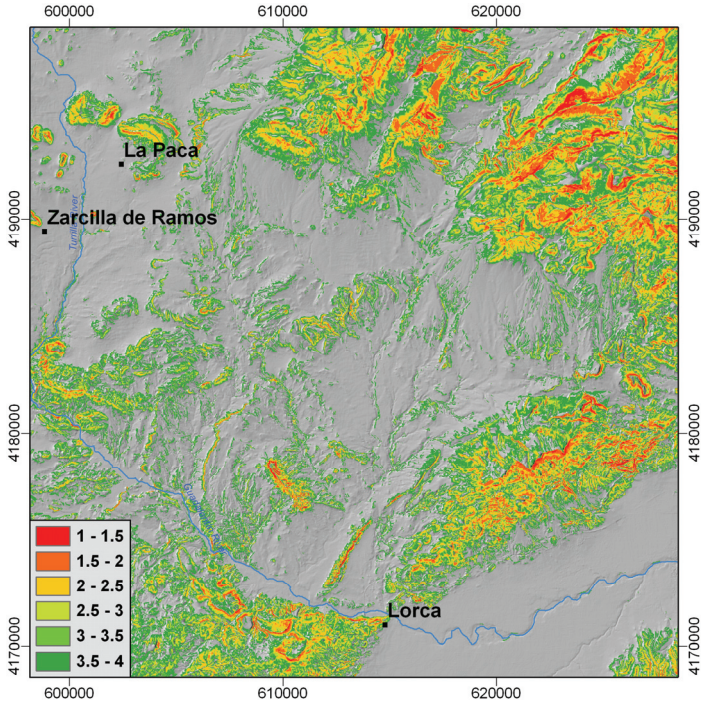

Figure 4-5. Map of static safety factors. Red colour areas indicate lower values. See text for details.

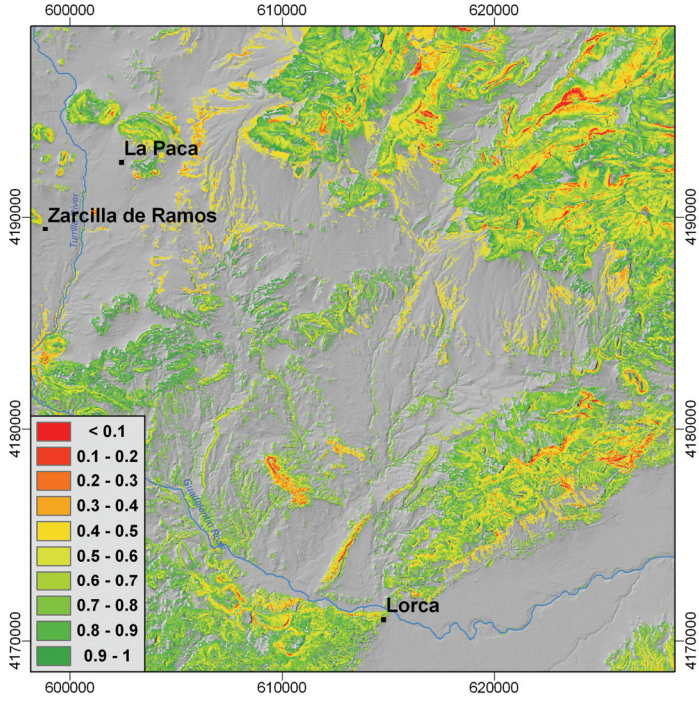

Figure 4-6. Map of critical acceleration (g units). Red colour areas are the most susceptible to earthquake triggering. See text for details.

Finally, we combined the static safety factor map with the slope map using equation (1) to produce the critical acceleration map (Fig. 4-6). This map is very useful to identify the most susceptible areas to seismic motion.

4.4.2. Computation of Newmark displacement maps

The computation of Newmark displacements (D_N) in regional hazard assessment is usually done making use of regression models based on basic earthquake parameters (magnitude and distance) and/or simple strong ground motion parameters. Jibson (2007) recently reviewed most of the available regression models, and also presented newly updated equations on D_N from: (a) critical acceleration ratio ($K=a_c/PGA$), (b) earthquake magnitude (M) and K, (c) Arias intensity (I_a) and a_c, and (d) I_a and K. The larger correlation coefficients (R^2) and lower standard deviations (σ) are attained by equations (a) and (b). In this work we have finally adopted equation (a) (Jibson, 2007):

$$\log D_N = 0.215 + \log\left[\left(1-\frac{a_c}{PGA}\right)^{2.341}\left(\frac{a_c}{PGA}\right)^{-1.438}\right] \qquad (3)$$

where D_N is the Newmark displacement (in centimetres), a_c is the critical acceleration (in gravity units) and PGA is the peak ground acceleration (in gravity units). The R^2 and σ values are 84% and 0.51, respectively. This equation was derived from a selected database of 875 records from earthquakes ranging from M_w 5.3 to 7.6. Its functional form is very similar to other equations that include the earthquake magnitude variable (e.g., Ambraseys and Srbulov, 1994). It also matches very well the characteristic sigmoid-shape of the dataset cloud. Coherently, it draws displacements approaching to infinity and cero for a_c/PGA ratios close to 0 and 1, respectively. Hence, Newmark displacement maps have been computed using this equation after PGA was corrected to account for soil and topographic amplification effects.

4.5. Seismic Scenarios

Three different concepts of seismic scenarios are considered in this work: probabilistic, pseudo-probabilistic and deterministic. The first ones are useful as provide an overall view of the seismic hazard associated to a standard level of probability, usually in accordance to building design provisions. On the opposite, deterministic seismic scenarios represent a particular situation associated to the occurrence of specific conditions, usually very infrequent, but possible. These types of seismic scenarios are ideal for detailed risk evaluation, civil protection plans, as well as for engineering design of critical structures. Finally, we use the term pseudo-probabilistic to refer to seismic scenarios based on the conclusions drawn from a probabilistic calculation.

Probabilistic seismic scenarios are based on three seismic hazard maps in terms of peak ground acceleration (PGA) on rock corresponding to 475-, 975- and 2475-year return periods –which are equivalent to a probability of exceedance of 10%, 5% and 2% in 50 years, respectively. This information has been taken from a recent probabilistic seismic hazard analysis of the Murcia Region in the frame of a major project on seismic risk, whose results have been the base for the official Civil Protection Emergency Plan of Murcia (Benito et al., 2006). This work represents currently the best estimation of seismic hazard in the area. The interested reader is referred to García-Mayordomo et al. (2007) for details on the calculations.

The pseudo-probabilistic seismic scenario is based on a hazard deaggregation analysis perfomed by Gaspar-Escribano et al. (2008) on the probabilistic results of García-Mayordomo et al. (2007) for the 475-year return period. Gaspar-Escribano et al. (2008) analysed three representative sites of the Murcia Region (Murcia, Lorca and Cartagena) and concluded that the most probable earthquake for such a return period and for PGA on rock is a M_w=4.0 to 5.5 at 0 to 10 km epicentral distance. In the present work we use this result to devise a conservative seismic scenario considering the hypothetically occurrence of a M_w=5.0 earthquake in every pixel covering the study area.

Deterministic scenarios are contrived based on the seismic potential of the main active faults located in the area, specifically the Alhama de Murcia Fault which is the most active structure in the area. The seismic hazard of this major fault has been modelled considering it divided in four segments of independent seismic behaviour, which follow a characteristic earthquake model (García-Mayordomo et al. 2007) (Fig. 4-1). The most active fault segments are the so-called Puerto Lumbreras-Lorca and Lorca-Totana; for each one García-Mayordomo (2005) estimates a maximum magnitude of M_w=6.8 and M_w=6.7 with a recurrence of 7,000 and 2,000 years, respectively. Following the deterministic method, we consider the occurrence of these earthquakes independently of its relatively long recurrence, which is the usual approach for defining extreme earthquakes in seismic hazard of critical structures. For the sake of simplicity, in this paper we present only the results derived from de Lorca-Totana scenario. Strong ground motion associated to this scenario is calculated using the Sabetta and Pugliese (1996) PGA on rock prediction equation and assuming that earthquake epicentres locate along the fault trace, which is virtually vertical (Fig. 4-7).

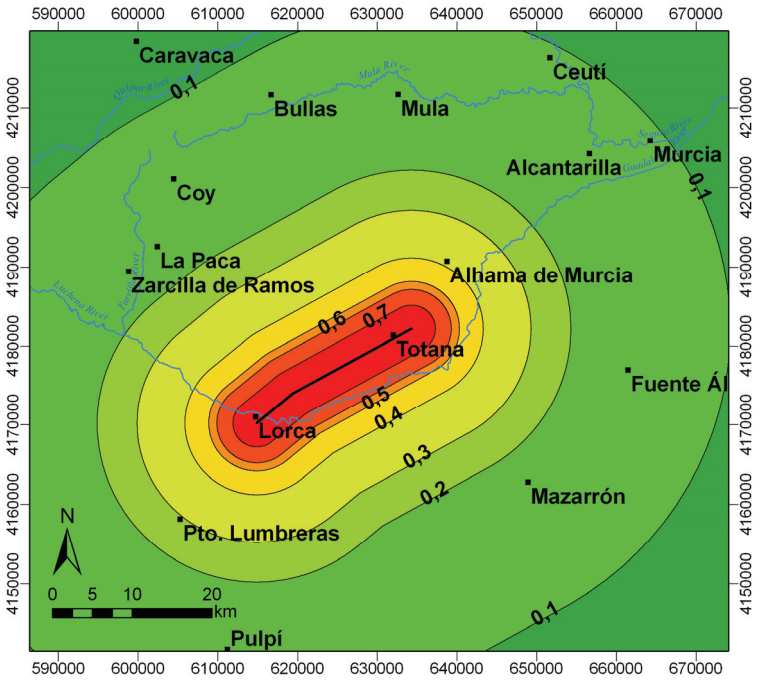

Figure 4-7. Map of Peak Ground Acceleration (PGA) on rock for the deterministic seismic scenario that considers the rupture of the Lorca-Totana segment of the Alhama de Murcia Fault (M_w=6.7) (g units).

4.6. Site Effects

It is well known today the importance of subsurface geology and topography on the amplitude, duration and frequency content of strong ground motion (cf. Kramer, 1996). Accounting for site effects in engineering practice starts from considering the ground motion on hard rock –usually at basement depth, and from it, the different effects affecting the seismic wave until it reaches the surface. Analysis at the site scale usually require the use of mathematical models and specific laboratory data, while for regional assessment important simplifications are made based on geological criteria and standard geotechnical data. Topographic effects are very often neglected in both site and regional scales, even though they are recognised as a crucial factor in seismic slope stability.

The seismic input represented by the scenarios explained above is always defined in terms of PGA on rock conditions. Hence, to compare to the critical acceleration in Newmark's method, in which the instability mass is supposed to be rigid, we precise the PGA on the surface after soil and topographic effects have been considered. The soil amplification effect has been taken into account assigning a multiplying factor to each of the lithological units defined previously (Fig. 4-8). These factors have been adopted from previous works in the subject (Benito et al, 2006; Tsige and García-Flórez, 2006), and represent the best quality data available at a regional scale for the Murcia Region. In these works, soil amplification factors were

assigned after matching the lithological groups of Murcia Region with the soil classes defined in NEHRP (2003) provisions.

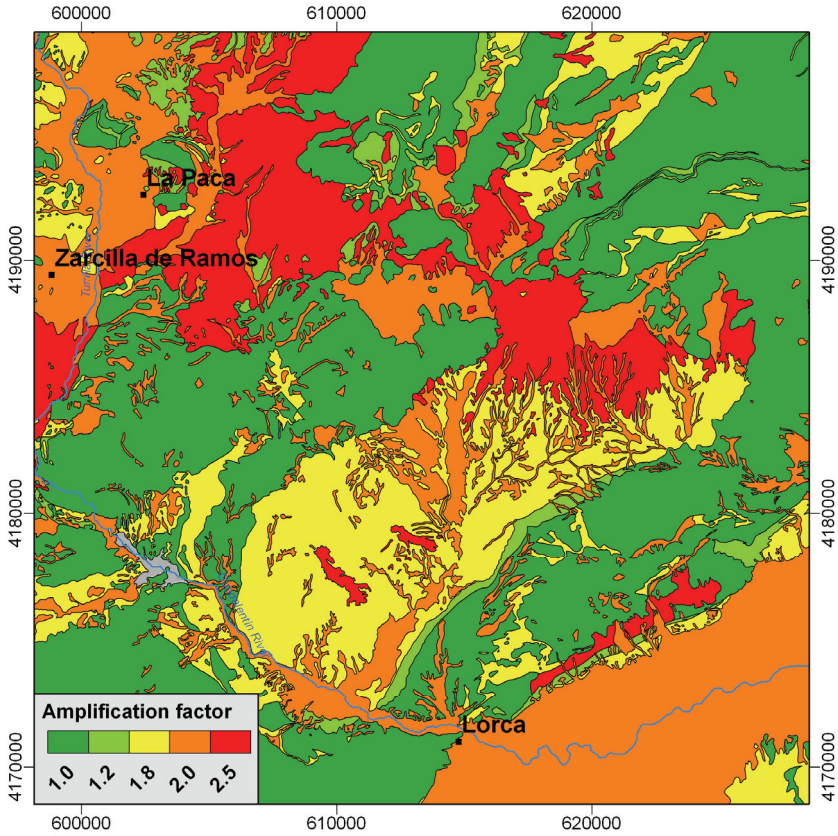

Figure 4-8. Map of soil amplification factors. Red colour areas show the highest values of seismic amplification. See text for further explanation.

The seismic amplification due to topography occurs when seismic waves entering the base of a topographic ridge are partially reflected back into the rock mass and diffracted along the free surface. Thus, seismic waves are progressively focused upwards and the constructive interference of their reflections and diffractions increases towards the ridge crest, giving rise to enhanced ground accelerations on topographic highs (Geli et al., 1988; Pedersen et al., 1994). For the case of slope stability, topographic amplification effects become a very important factor (Sepúlveda et al., 2005a, 2005b; Murphy, 2006). For this reason, an original GIS tool has been developed to estimate the topographic amplification effect based on terrain geometry features and Eurocode-8 provisions (CEN, 2004). This tool first computes the slope map and extracts ridge features from the digital elevation model. Subsequently, the relative height of the ridges is computed and then compared with the slope map. Eventually, the topographic amplification factor (TAF) is assigned to each pixel according to the following possible cases (Fig. 4-9): (a) Slopes lower than 15º or

ridges with relative height less than 30 m: TAF=1.0 (no topographic amplification), (b) Slopes between 15º and 30º and relative height greater than 30 m: TAF=1.2 and (c) Slopes steeper than 30º and relative height greater than 30 m: TAF=1.4.

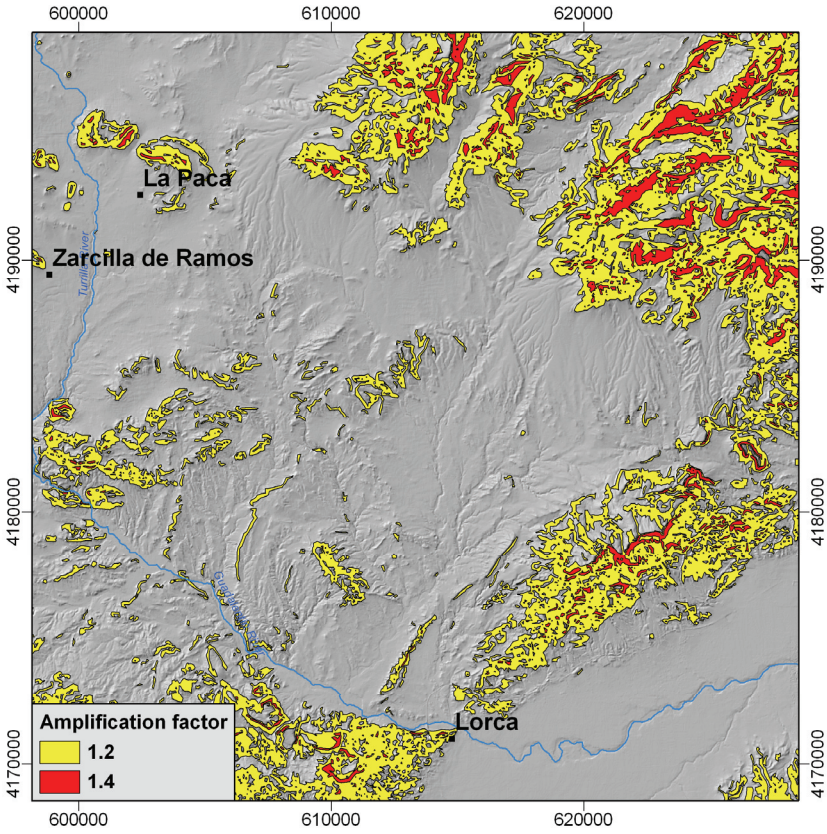

Figure 4-9. Map of topographic amplification factors showing in red colour the areas with the highest values of seismic amplification. See text for further details.

4.7. Results and Discussion

Newmark displacement maps for each seismic scenario are shown in figures 4-10 and 4-11. It is important to note that Newmark displacement values obtained in this work at a regional scale should not be considered as a precise measure of co-seismic slope displacement, but rather as an index of potential instability. The actual Newmark displacement that effectively triggers a landslide strongly depends on site-specific variables, particularly in the way the sliding mass accommodates the deformation. In a regional context, and for the sake of simplification, we consider that Newmark displacements greater than 5 cm could potentially imply the occurrence of coherent-type landslides (landslides s.s. and flows), whereas smaller values could suggest the occurrence of disrupted-type landslides (falls, disrupted slides and avalanches) (cf. Wilson and Keefer, 1983; Keefer, 1984; Romeo, 2000; Keefer, 2002).

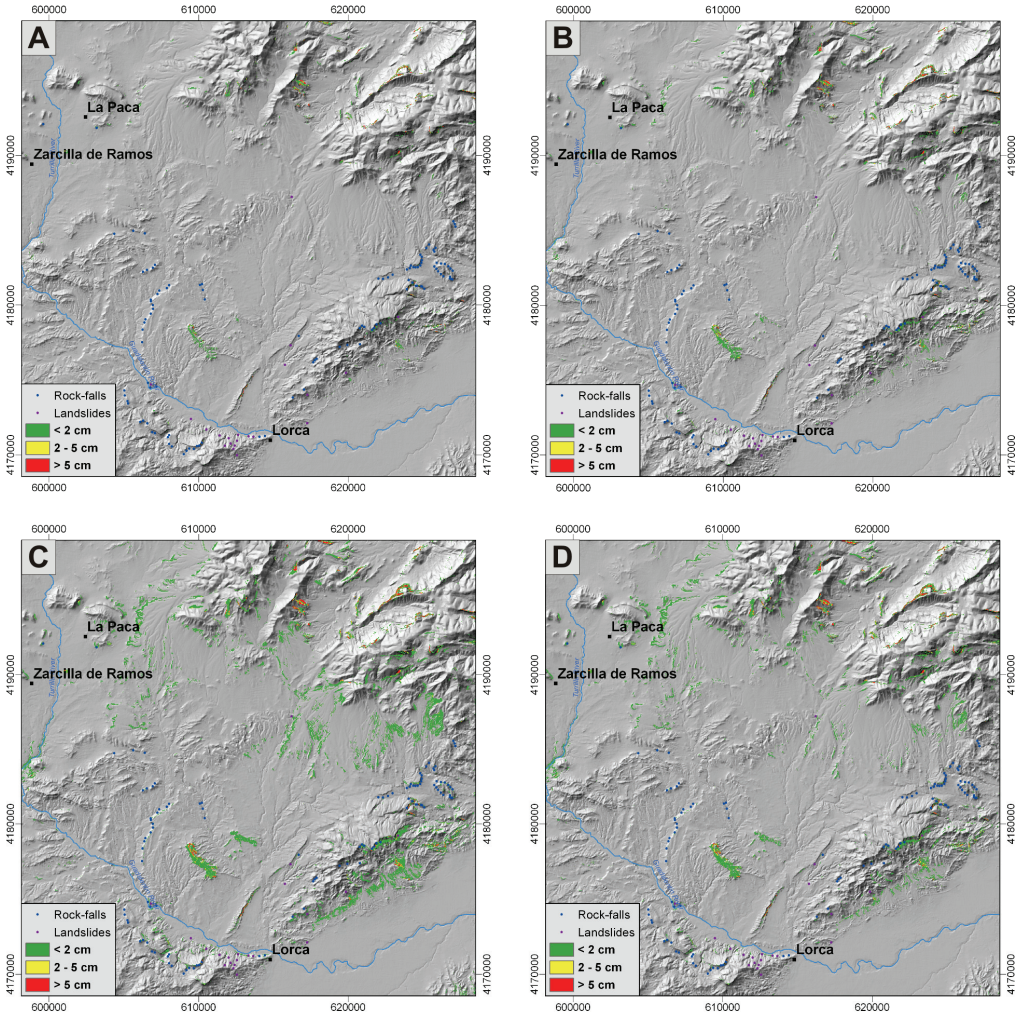

Figure 4-10. Newmark displacement maps for the probabilistic and pseudo-probabilistic seismic scenarios. A: 475-year return period. B: 975-year return period. C: 2475-year return period. D: Most probable earthquake for a 475-year return period (M_w=5.0, R_{epi}=0 km).

Newmark displacement maps for the 475- and 975-year return period probabilistic scenarios (Figures 4-10A and 4-10B) show small and scattered areas with Newmark displacement values mostly smaller than 2 cm. For the 2475-year return period these areas become wider and Newmark displacements greater than 5 cm are reached at few locations (Fig. 4-10C). Interestingly, the Newmark displacement map for the pseudo-probabilistic scenario –i.e., the most probable earthquake for a 475-year return period (M_w=5.0, R_{epi}=0 km) (Fig. 4-10D), shows very similar results to the 2475-year return period, although Newmark displacements are in general smaller.

The deterministic seismic scenario considering a complete rupture of the Lorca-Totana segment of the Alhama de Murcia Fault (Fig. 4-11), produce greater Newmark

displacements than the probabilistic scenarios, quite commonly greater than 2 cm and locally greater than 5 cm. Furthermore, they are distributed over a much wider area, especially near the fault trace. However, Newmark displacements at longer distances from the fault trace show similar results to both the 2475-year return period and the pseudo-probabilistic scenarios.

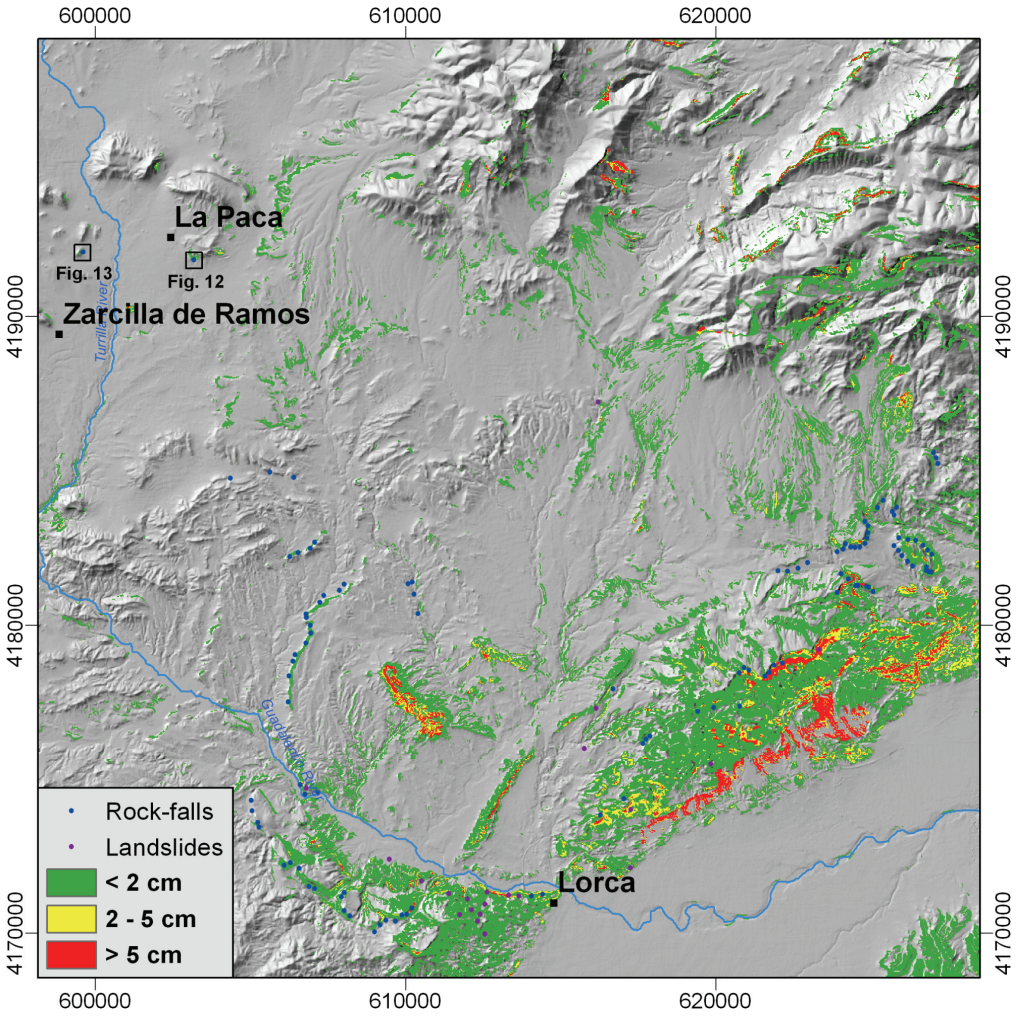

Figure 4-11. Newmark displacement map for the deterministic seismic scenario that considers the rupture of the Lorca-Totana segment of the Alhama de Murcia Fault (M_w=6.7).

Slope-instability sites previously identified in a number of studies (MOP, 1971; ITGE, 1995; Rodríguez-Peces, 2008) are also plotted in figures 4-10 and 4-11. The 475- and 975-year return period scenario maps show a very bad correlation, while the 2475-year return period and the pseudo-probabilistic scenarios fail to match the instability-sites located inside the Lorca Basin. Only the deterministic seismic scenario considering the rupture of the Alhama de Murcia Fault show a fair correlation with the

location of field instabilities (Fig. 4-11). The most frequent Newmark displacement value of the pixels where the site-cases are located is 2 cm, or even less. This fact matches coherently with the occurrence of disrupted landslides exhibiting brittle behaviour (rock falls, rock slides and avalanches), which are the most common slope instability in the region. Figures 4-10 and 4-11 also include the location of 2002 Bullas and 2005 La Paca earthquake-triggered rock slides (Fig. 4-12 and 4-13), located close to Zarcilla de Ramos and La Paca villages, respectively. All seismic scenarios predict Newmark displacements less than 2 cm for both locations – excluding the 475-year return period scenario, which predicts cero centimetres at La Paca site. These results support the idea that even very small Newmark displacements are potentially capable to produce disrupted landslides.

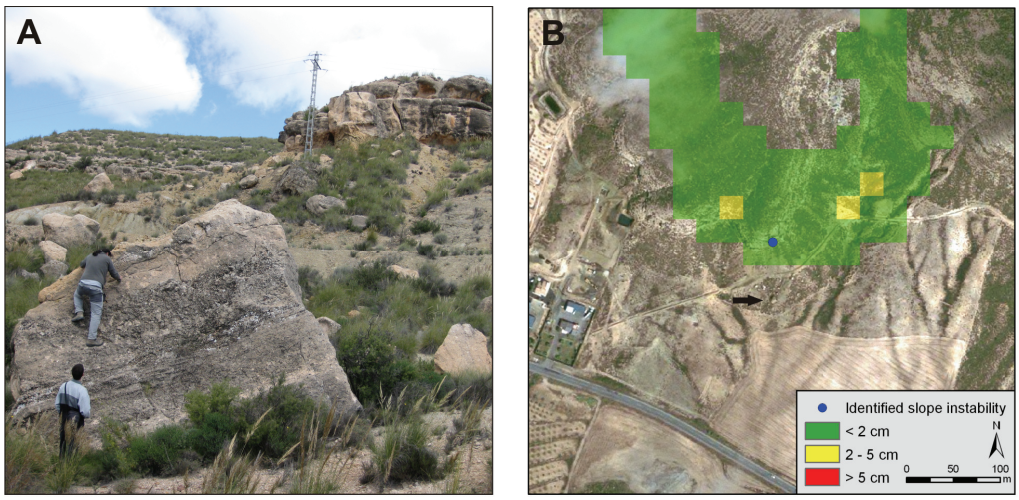

Figure 4-12. A: Rock slide and rock falls triggered by 2002 Bullas earthquake (M_w=5.0) in Pliocene-Quaternary conglomerates. B: Calculated Newmark displacements for this area are in general less than 2 cm but locally up to 5 cm. See figure 4-11 for site location.

In addition, it can be inferred that strong ground motion related to either the 475- or 975-year return period probability, would be incapable of producing significant coherent landslides but just disrupted ones. Even in the later case, these would be small and isolated cases. Effectively, the seismic series of 1999 Mula, 2002 Bullas or 2005 La Paca, which have earthquake magnitudes in the 4.5-5.0 range and, hence, similar to the most probable earthquake for a 475-year return period, produced very few and scattered rock slides and rock falls. On the contrary, deterministic scenarios considering the rupture of the Alhama de Murcia Fault show greater Newmark displacements (locally >5 cm) across larger areas, especially at reliefs next to the trace of the fault. Thus, we can infer that only the occurrence of a large earthquake (M_w=6.7-6.8) associated to the Alhama de Murcia Fault would be able to trigger coherent landslides –although just at few locations near the trace, while disrupted landslides would be widespread across the Lorca Basin.

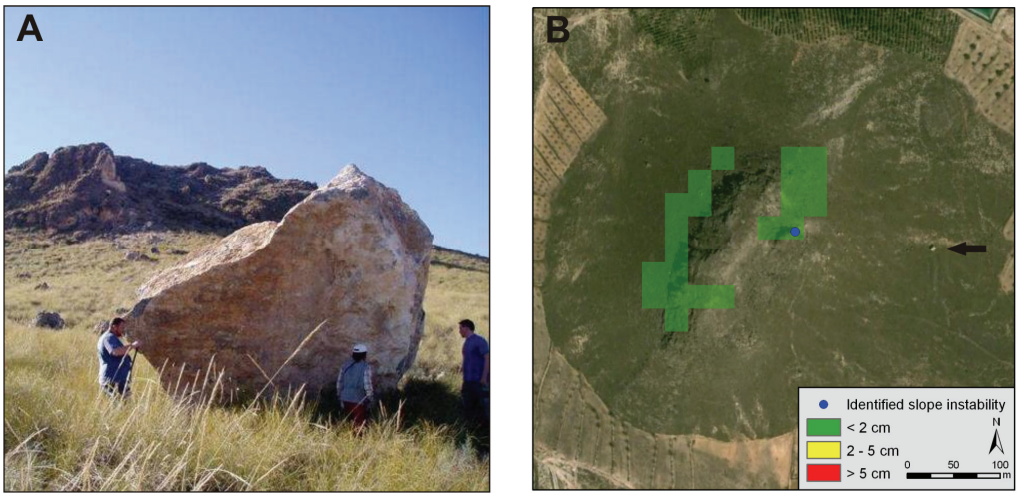

Figure 4-13. A: Rock slide triggered by 2005 La Paca earthquake (M_w=4.8) in Triassic dolostones. B: Calculated Newmark displacements for this area are less than 2 cm. See figure 4-11 for site location.

4.8. Conclusions

Earthquake-triggered landslide hazard in Lorca Basin has been analysed by means of computing Newmark displacement maps for specific seismic scenarios. These maps are useful to identify the areas with the highest hazard and also to infer the most likely type of slope instability that could be triggered in relation to a particular seismic scenario. In this sense, these maps offer a first order assessment on the possible interruption of life-lines (roads, electric lines, gas pipes) and, hence, they could be used to improve emergency plans in the aftermath of an event.

The occurrence of widespread slope instabilities across the Lorca Basin is only expected in the event of a low-frequency but powerful earthquake (M_w=6.7-6.8) related to the activity of the Alhama de Murcia Fault. Probabilistic scenarios for common return periods in seismic engineering (e.g., 475-, 975- and 2475-years), and even for the most probable earthquake for the 475-year return period (M_w=5.0, R_{epi}=0 km), appear able only to produce small and isolated cases of slope instabilities.

Earthquake-triggered landslide hazard in the Lorca Basin can be regarded as low. However, we have found that in many parts of the basin even very small Newmark displacements (less than 2 cm) could potentially trigger rock slides and rock falls. Actually, that is the case of the slope instabilities triggered by the latest seismic events of the region (1999 Mula, 2002 Bullas and 2005 La Paca). Forthcoming research is devoted to performing specific back-analysis at the 2002 Bullas and 2005 La Paca rock-slides sites (Rodríguez-Peces et al., 2009).

Acknowledgments

This study was supported by research projects CGL2008-03249/BTE, TOPOIBERIA CONSOLIDER-INGENIO2010 CSD2006-00041 from the Spanish Ministry of Science and Innovation and SISMILAD from Instituto Geológico y Minero de España (IGME).

5

Regional hazard assessment of seismically-induced slope instabilities in Sierra Nevada Range (Betic Cordillera, South Spain) simulating the occurrence of a maximum magnitude earthquake related to the Padul Fault

Martín Jesús Rodríguez-Peces [1], Julián García-Mayordomo [2], José Miguel Azañón [1,3], Antonio Jabaloy [1], Concepción Espinosa-Montes [1]

[1] Departamento de Geodinámica, Universidad de Granada, Fuentenueva s/n, 18071 Granada, Spain.
[2] Instituto Geológico y Minero de España (IGME). C/La Calera, 1. 28760. Tres Cantos (Madrid), Spain.
[3] Instituto Andaluz de Ciencias de la Tierra (UGR-CSIC), Granada, Spain.

Comptes Rendus Geoscience
Submitted 18 February 2010; revised 5 May 2010; under review 28 June 2010

ABSTRACT

A regional assessment of earthquake-triggered slope instabilities in the Sierra Nevada Range (Central Betic Cordillera, Southern Spain), one of the most seismically active regions of Spain, has been developed considering the occurrence of a specific deterministic seismic scenario: a maximum magnitude earthquake related to a complete rupture of one of the most active faults in the area, the Padul fault. First, a slope-instability inventory of the Sierra Nevada Range has been performed to identify the most common instability types in the area. Subsequently, the well-known Newmark's sliding rigid-block methodology implemented in a geographic information system (GIS) has been used to obtain the distribution of Newmark displacements in the area considering a M_w 6.6 earthquake related to the activity of the Padul Fault. This map is then compared to the distribution of the inventoried slope instabilities in order to identify the areas where seismicity could contribute to reactivate old slope instabilities or generate new ones, as well as to identify the involved landslide typology. The most likely seismically-induced slope instabilities in the Sierra Nevada Range would be landslides, rock falls and rock slides. These types of instabilities can be potentially triggered by a critical Newmark displacement of 2 cm or less.

Keywords: Betic Cordillera; Landslides; Newmark; Rock-falls; Soil amplification; Topographic amplification.

5.1. Introduction

Slope instabilities are one of the most common and hazardous secondary effects of earthquake vibration. In fact, destruction and fatalities from earthquake-triggered landslides sometimes exceed damage directly related to the strong shaking of buildings. Furthermore, triggered landslides are crucial in controlling the practicality of life-lines (roads, power lines) in the aftermath of an earthquake, and therefore in permitting a rapid response from the emergency services.

The most common procedures followed in earthquake-triggered hazard assessment at a regional scale deal with the well-known Newmark's sliding rigid-block method (Newmark, 1965) implemented in a geographic information system (GIS) (e.g. Jibson et al., 2000; Luzi et al., 2000; Romeo, 2000; Carro et al., 2003; among others). However, there are very few works devoted to this subject in Spain (García-Mayordomo, 1999; Mulas et al., 2003; Delgado et al., 2006; Rodríguez-Peces et al., 2008). A review of the main results of these studies can be found in García-Mayordomo et al. (2009).

The main aim of this paper is to develop a regional earthquake-triggered landslide hazard assessment in the Sierra Nevada Range, which is the most seismically active region of Spain. In this area important earthquakes (e.g. 1884 Arenas del Rey) have occurred triggering several slope instabilities. Due to space limitations, in this paper we only show the western part of the Sierra Nevada Range (Fig. 5-1). A slope-instability inventory of the study area has been built as the first step required for performing a proper landslide hazard assessment. This inventory allows the identification of the most common slope-instability types in the Sierra Nevada. An earthquake-triggered landslide hazard map in terms of Newmark displacements has been obtained simulating the occurrence of a maximum magnitude earthquake related to the Padul Fault and taking into account site effects (soil and topographic amplification). Finally, the Newmark displacement map has been compared to the distribution of the inventoried slope instabilities in order to identify the areas where the seismicity could contribute to reactivate old slope instabilities or generate new ones, as well as the involved landslide typology.

5.2. Geological setting

The Sierra Nevada Range is the highest relief in the Central Betic Cordillera (South Spain). The Sierra Nevada is composed mainly of metamorphosed Palaeozoic and Mesozoic rocks, which form the so-called Internal Betic Zone or Alborán Domain (Fig. 5-1). The Internal Zones are mainly constituted by three superposed metamorphic complexes separated by detachment faults: Nevado-Filábride, Alpujárride and Maláguide Complexes (Martínez-Martínez et al., 2002). The Sierra Nevada Range comprises the Nevado-Filábride and Alpujárride complexes. The Nevado-Filábride Complex is constituted mainly of micasquists and quartzites while the Alpujárride Complex is composed of metapelites and carbonate rocks. The Sierra

Nevada emerged in the Late Miocene, progressively isolating different intramontane basins (e.g. Granada and Guadix Basins).

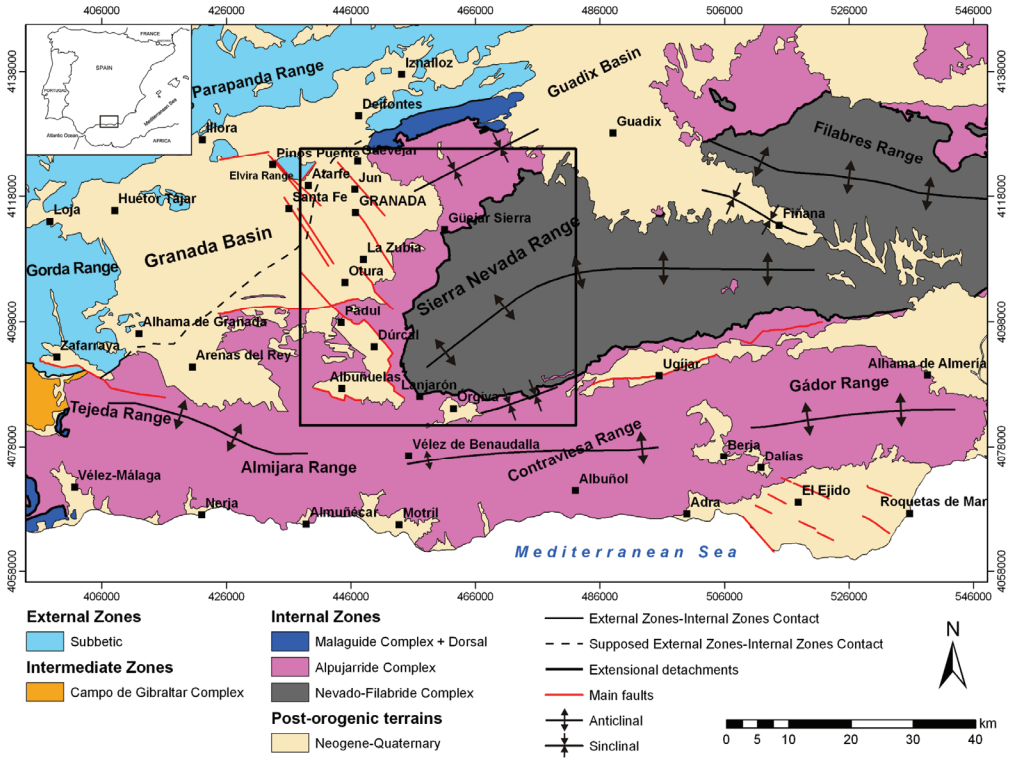

Figure 5-1. Geological map of Central Betic Cordillera (South Spain) showing the Granada Basin, Sierra Nevada Range and main active faults in the study area.

5.3. Landslides distribution

In this study, a slope-instability database was implemented based on previous studies (IGME and Diputación de Granada, 2007), the interpretation of aerial photographs and field surveys. Classification of landslides was made referring to internationally accepted terms (Varnes, 1978; Keefer, 1984; Cruden and Varnes, 1996). A total of 2444 slope instabilities were mapped in the study area covering 1959 km^2. The slope instabilities were found to affect 7.7% of the total study area with an average instability density of 1.25 instability/km^2. The inventory includes a total of 862 debris flows, 705 falls (rock falls and rock slides), 660 landslides (translational and rotational slides) and 217 earth flows. Hence, the most common slope instability types in the Sierra Nevada Range are debris flows, followed by rock falls and rock slides (Table 5-1). These are the most abundant types of earthquake-triggered slope instabilities worldwide (Keefer, 1984, 2000). These types of landslides are shallow with depths typically less than 3 m and can be triggered by earthquakes as small as M~4. For this reason, it is likely that some of the most common instability types of the

Sierra Nevada have been triggered by earthquakes. All the inventoried slope movements present non-permanent activity but some of them could have occasional seasonal reactivation.

Table 5-1. Distribution of slope-instability types related to total number of instability processes and affected area related to total study area.

	Count	%	Affected area (km^2)	% related to total area
Debris flows	862	35.5	100.10	5.1
Rock falls	705	28.8	9.95	0.5
Landslides	660	27.0	14.43	0.7
Earth flows	217	8.9	27.08	1.4
Total	2444	100	1959.13	7.7

The relation between areas affected by slope instabilities and some determining factors for the slope-stability condition has been analysed. In this paper, three main determinant factors are considered: lithology, slope angle and slope aspect. Lithology is related to the strength of the materials and their behaviour concerning slope stability. A lithological map was arranged using the 1:50 000 scale digital geological maps from the Institute of Geology and Mines of Spain (IGME). Debris flows are developed mainly in micaschists, rock falls in micaschists and marbles, landslides in micaschists, and earth flows in conglomerates, sandstones and argillites (Table 5-2). The micaschists and quartzites unit is the most unstable lithology in the Sierra Nevada Range, comprising 64 % of the inventoried slope instabilities. This fact is significant because this lithological unit is the most frequent in the Sierra Nevada Range. Slope angle has a great influence on the susceptibility of a slope to landsliding. For this reason, it is the most commonly determinant factor used in slope-stability assessment by GIS.

Table 5-2. Distribution of slope-instability typologies (percentages, %) related to each lithological group outcropping in the Sierra Nevada Range. 1: Micaschists, quartzites and gneisses; 2: Phyllites and quartzites; 3: Limestones, dolostones and marbles; 4: Calcareous sandstones, argillaceous limestones and marls; 5: Argillites, marls, sandstones and gypsums; 6: Marls and argillaceous limestones; 7: Conglomerates, sandstones and argillites; 8: Gypsums and marls; 9: Gravels, sands, silts and clays.

	Lithological group								
	1	2	3	4	5	6	7	8	9
Debris flows	63.7	8.7	10.6	0.8	2.9	1.4	6.3	0.4	5.1
Rock falls	79.4	3.2	13.3	0.0	3.9	0.0	0.0	0.0	0.1
Landslides	1.0	0.0	0.9	19.8	0.0	0.5	65.4	3.2	9.3
Earth flows	95.2	0.4	4.4	0.0	0.0	0.0	0.0	0.0	0.0
Total	64.3	6.0	8.7	2.4	2.2	1.0	10.4	0.6	4.3

Following Wasowski et al. (2002), a 20°-25° slope range seems to provide a separation between soil and rock failures, the latter generally occurring on slopes steeper than 35°. As regards failures on rocky slopes, Keefer (1984) reports a threshold of 35° for disrupted slides (e.g. rock falls and rock slides). In this work, we have used a 10 x 10 m pixel size digital elevation model (DEM) of the study area to derive a slope map. In general, slopes angles for the areas affected by slope instabilities in the Sierra Nevada range between 15º and 25º (Table 5-3). However, most common slope angles related to debris flows and falls are slightly greater (25º-35º). These ranges of slope angle comprise about 53% of the study area. The slope aspect can also influence landslide initiation. This factor is related to soil moisture and weathering, which are commonly greater on slopes oriented to the north, because of the lower insolation. However, inventoried slope instabilities do not show a preferred orientation (Table 5-4), so the slope aspect seems not to be a determinant factor regarding slope stability.

Table 5-3. Slope angle distribution (%) for each slope-instability typology.

	Slope angle (º)					
	0-5	5-15	15-25	25-35	35-45	>45
Debris flows	0.7	11.1	31.6	41.2	13.7	1.8
Falls	0.7	9.0	21.8	29.5	24.6	14.4
Landslides	1.5	16.9	33.6	23.4	23.4	1.2
Earth flows	7.6	47.2	30.5	10.7	3.3	0.6
Total	2.1	20.6	36.8	28.9	9.4	2.3

Table 5-4. Slope aspect distribution (%) for each slope-instability typology.

	Slope aspect				
	Flat	N	S	E	W
Debris flows	1.3	31.2	16.2	39.0	12.3
Falls	0.8	24.0	22.2	27.1	25.9
Landslides	1.2	21.0	27.7	23.7	26.5
Earth flows	3.7	26.5	28.3	15.6	25.8
Total	1.4	23.5	25.3	25.9	23.9

5.4. Seismic activity and earthquake-triggered landslides

The seismic activity is concentrated along the western and southern borders of the Sierra Nevada Range. These borders represent the contact with the Neogene-Quaternary sediments of the Granada Basin, which is the most seismically active area in Spain. Since the beginning of the instrumental record in the region in the 1920's, a large number of earthquakes have been recorded in the Granada Basin, although all of them of low to moderate magnitude (m_b<5.5) (De Miguel et al., 1989). The most important earthquakes to have occurred in the Granada Basin took place during the period between the XV and the XIX centuries (Vidal, 1986; López Casado et al., 2001; Feriche and Botari, 2002): 1431 Atarfe (I_{EMS}=IX), 1526 Granada (I_{EMS}=VIII), 1806 Pinos Puente (I_{EMS}=IX) and 1884 Arenas del Rey (I_{EMS}=X). Historical reports demonstrate that most of the landslide phenomena occurring on the Granada Basin are related to some of these major historical earthquakes (e.g. 1884 Arenas del Rey). Some examples of earthquake-induced slope instabilities are the Güevéjar landslide (Jiménez Pintor and Azor, 2006), rock falls and rock avalanches produced in Alhama de Granada and Albuñuelas villages and even some liquefaction phenomena (Muñoz

and Udías, 1981; IGME and Diputación de Granada, 2007). However, no evidence of seismically-induced slope instabilities have been documented in the Sierra Nevada Range. The occurrence of earthquake-triggered slope instabilities in the area has to be more common than previously thought based on the available descriptions. The scarceness of descriptions can be attributed to a bias of the available information towards the evaluation of building damage, rather than analysing the effects occurring away from populated areas.

From a seismotectonic point of view the Sierra Nevada Range is delimited at its western border by NW-SE faults (Fig. 5-1). Many of these faults show Quaternary activity and can potentially be seismic sources of earthquakes with magnitudes larger than M_w=6.0 (Sanz de Galdeano et al., 2003). Among the different NW-SE active normal faults, the Padul Fault (also known as the Padul-Nigüelas Fault) stands out because it is one of the closest to the Sierra Nevada. This fault is about 15 km long comprising two connected segments: Padul and Padul-Dúrcal (Sanz de Galdeano et al., 2003), which mainly dip towards the SW. The seismic activity during the instrumental period in the Padul area is characterized by the occurrence of small-magnitude earthquakes. However, there is geological evidence of moderate to large-magnitude earthquakes during the Quaternary (Alfaro et al., 2001). Hence the occurrence of moderate to high-magnitude earthquakes associated with this fault is likely in the future. The surroundings of the Padul Fault are also the epicentral area of very deep earthquakes (h~640 km), some of these having reached magnitudes larger than M_w 6.0 (Buforn et al., 1991; 2004). However, the origin of these deep earthquakes has no relation to the Padul Fault. Considering the Padul Fault as the most likely seismogenic source, the maximum magnitude of an earthquake related to a complete rupture of the fault is M_w 6.6 (Sanz de Galdeano et al., 2003). This magnitude has been estimated considering a total length of 15.2 km and an average slip rate of 0.35 mm/year over the last million years. The estimated return period of this event ranges 7000-10 000 years.

5.5. Hazard assessment of earthquake-triggered slope instabilities

5.5.1. Calculation of Safety Factor and Critical Acceleration Maps

The Newmark method simplifies the slope instability as a rigid-block sliding on a planar surface, where static and dynamic strength parameters are assumed equal and stationary. Under these crucial assumptions, the calculation of the displacement is a two-step procedure. First, the minimum seismic acceleration to overcome shear resistance and initiate the displacement of the slope is calculated by:

$$a_c = (SF - 1)\, g \sin \alpha \quad [1]$$

where a_c is the critical acceleration (in gravity units, 1g = 9.81 m/s^2), g is the gravity acceleration, SF is the static safety factor and α is the slope angle. Hence, the critical acceleration is an expression of slope capacity to resist seismic vibration and therefore, it can be regarded as an effective measure of the susceptibility to earthquake-induced slope instabilities. Secondly, slope displacement is calculated considering an acceleration time-history (accelerogram) representative of the expected seismic input at the site and a double integration of the time intervals where the critical acceleration is overcome. Cumulative displacement calculated this way –i.e., so-called *Newmark displacement (D_N)*, provides a fair estimation of the actual displacement, as it has been shown in both laboratory tests and field case studies (cf. Wilson and Keefer, 1983). However, Newmark displacement can be estimated at a regional scale by means of regression equations based on single strong ground motion parameters, such as the Arias intensity (I_a) or Peak Ground Acceleration (PGA) (cf. Jibson, 2007).

Estimation of the static safety factor map is a first step required to produce the critical acceleration map. The safety factor map (Fig. 5-2) was calculated using the equation (Jibson et al., 2000):

$$SF = \frac{c'}{\gamma t \sin \alpha} + \frac{\tan \phi'}{\tan \alpha} - \frac{m \gamma_w \tan \phi'}{\gamma \tan \alpha} \quad [2]$$

where c' is the effective cohesion, ϕ' is the effective friction angle, α is the slope angle, γ is the specific weight of slope material, γ_w is the specific weight of water, t is the normal depth of the failure surface and m is the degree of saturation of the failure surface. Average values of specific weight, cohesion and friction angle were assigned to each lithological unit. These shear strength parameters were obtained from geotechnical bibliography and available geotechnical tests (cf. Rodríguez-Peces, 2008). The range of the shear strength parameters was very wide, particularly the cohesion values. Average specific weight and friction angle values were assumed as representative at the working scale while cohesion has been fitted by iteration until all safety factors in the study area were higher than 1.0. Table 5-5 shows the adopted strength parameters values for the safety factor calculation.

Table 5-5. Lithological groups and strength parameters considered in the calculation of the safety factor map. Range of strength values are shown in brackets.

N	Lithological group	Specific weight (kN/m^3)	Cohesion (kN/m^2)	Friction angle (º)
1	Micaschists, quartzites and gneisses	27 (25-29)	46 (0-75)	29 (25-33)
2	Phyllites and quartzites	25 (23-27)	43 (0-48)	28 (23-33)
3	Limestones, dolostones and marbles	25 (23-27)	45 (0-108)	30 (21-39)
4	Calcareous sandstones, argillaceous limestones and marls	24 (22-26)	36 (0-61)	28 (18-38)
5	Argillites, marls, sandstones and gypsums	21 (18-24)	25 (35-117)	26 (22-30)
6	Marls and argillaceous limestones	21 (17-25)	29 (0-119)	29 (21-39)
7	Conglomerates, sandstones and argillites	22 (20-24)	23 (4-16)	33 (27-39)
8	Gypsums and marls	22 (20-24)	17 (0-115)	28 (23-35)
9	Gravels, sands, silts and clays	19 (17-21)	13 (22-58)	23 (17-29)

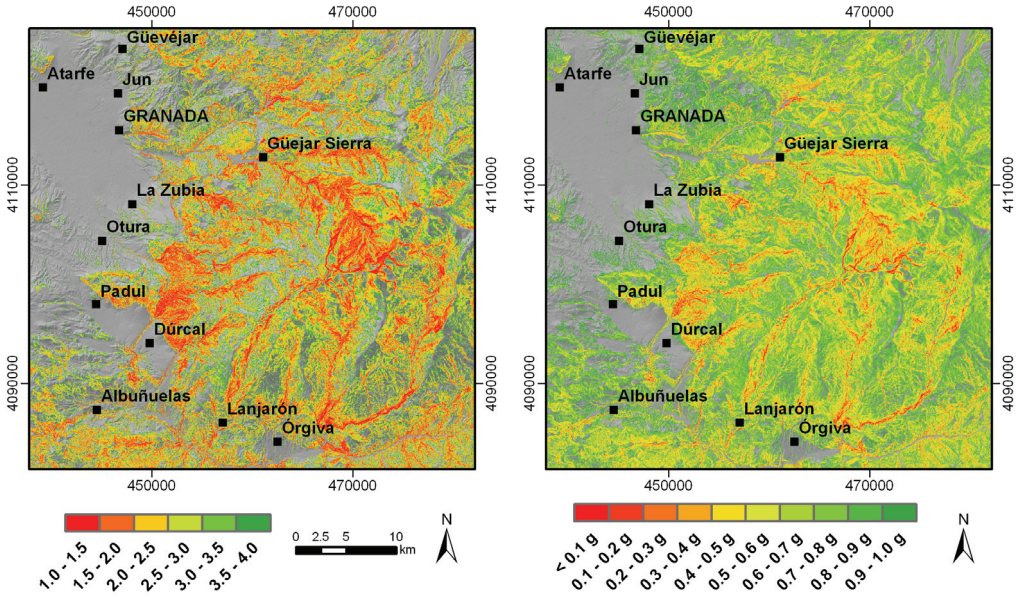

Figure 5-2. Maps of static safety factor (left) and critical acceleration (right). Red coloured areas show lowest values. See text for more details.

The failure surface has been considered to have null saturation because the climate of the study area is semi-arid, precipitation is low and the water table is usually deep (over 20 m) (IGME and Diputación de Granada, 2007). The depth of the failure surface has been set at three metres based on field observations. Most common slope instabilities in the Sierra Nevada Range (rock slides and rock falls) identified during the field surveys are generally small with a block size of between 1 to 6 m long. This 3 metre depth is also in agreement with the typical value proposed by

Keefer (1984, 2002) for shallow disrupted-type landslides (debris flows, rock falls and rock slides), which are the dominant typology in the Sierra Nevada. Furthermore, considering a deeper rupture surface would increase the weight of the sliding block and so implied safety factors are far from stable (SF<1.0) at the steepest slopes. In these circumstances, iterative tests showed that the stability condition (SF=1.0) was only reached when unrealistic strength parameters were assumed. Finally, the static safety factor map has been combined with the slope map using equation [1] to produce the critical acceleration map (Fig. 5-3). This map is very useful to identify the areas most susceptible to seismic motion.

5.5.2. Input seismic scenario

In this work, a deterministic seismic scenario has been considered based on the seismic potential of the Padul Fault. Strong ground motion related to the earthquake magnitude associated with a complete rupture of this fault has been calculated using different Ground Motion Prediction Equations (GMPEs) for the Mediterranean zone (Fig. 5-4). GMPEs have been selected from the literature in order to obtain an average PGA value as a function of magnitude and distance from the fault (Skarlatoudis et al., 2003; Ambraseys et al., 2005; Akkar and Bommer, 2007; Bindi et al., 2009). Three main criteria have been considered to select these GMPEs: (1) that they are derived from statistically-significant data sets; (2) that they are widely used in European countries in a similar seismotectonic context (the European-African plate boundary) and (3) the magnitude scale is in terms of M_w.

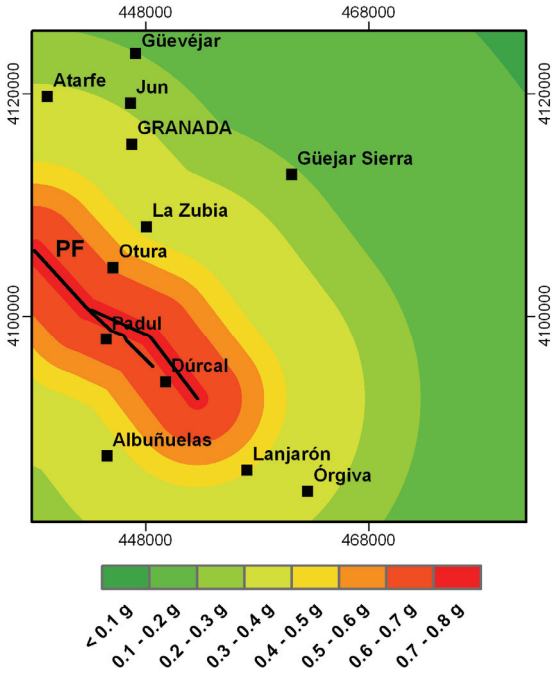

Figure 5-3. Map of Peak Ground Acceleration (PGA) on rock for deterministic seismic scenario that consider the complete rupture of the Padul Fault (PF).

The seismic input represented by the scenario explained above is defined in terms of PGA on rock conditions. Hence, the PGA on the surface after soil and topographic effects has been considered in order to compare to the critical acceleration. The soil amplification effect has been taken into account assigning a multiplying factor to each of the lithological units defined previously (Fig. 5-5). These factors have been adopted from previous works in the subject (Benito et al., 2010). A GIS tool has been developed to estimate the topographic amplification effect based on terrain geometry variables and Eurocode-8 provisions (CEN, 2004). This tool first computes the slope and curvature maps and extracts the ridges from the digital elevation model. Subsequently the relative height of the ridges is computed and then compared with the slope map. Finally, the topographic amplification factor (Fig. 5-6) is assigned to each pixel according to the following possible cases: (a) Slopes lower than 15º or ridges with a relative height of less than 30 m: amplification factor equal to 1.0 (no topographic amplification), (b) Slopes between 15º and 30º and a relative height greater than 30 m: amplification factor equal to 1.2 and (c) Slopes steeper than 30º and a relative height greater than 30 m: amplification factor equal to 1.4.

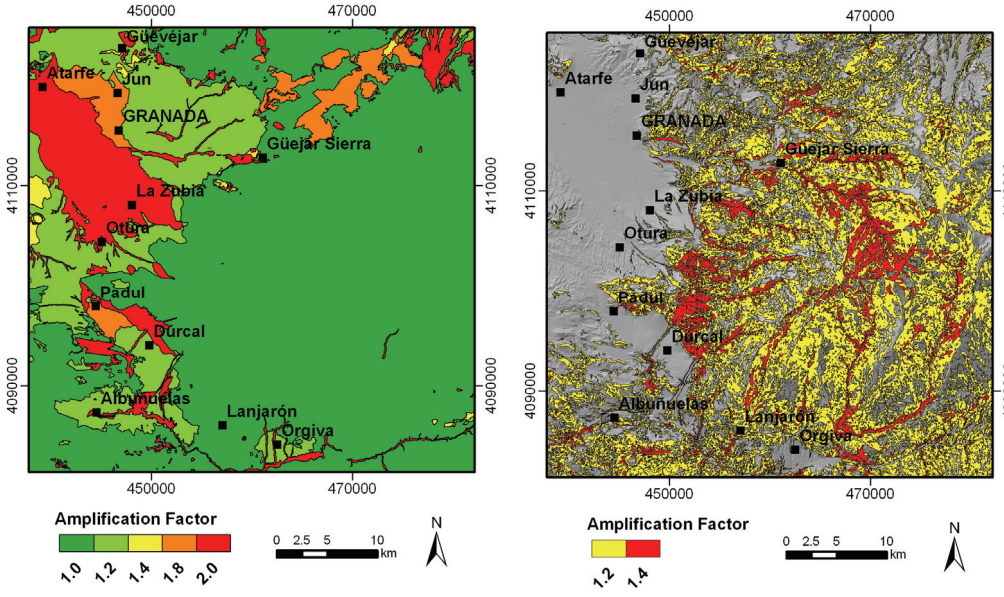

Figure 5-4. Maps of soil and topographic amplification factors (left and right, respectively). Red coloured areas show the highest values of seismic amplification. See text for further explanation.

5.5.3. Computation of Newmark displacement maps

The computation of Newmark displacements (D_N) in regional hazard assessments is usually done making use of regression models based on basic earthquake parameters (magnitude and distance) and/or simple strong ground motion parameters. In this work, we have adopted the equation (Jibson, 2007):

$$\log D_N = 0.215 + \log\left[\left(1 - \frac{a_c}{PGA}\right)^{2.341}\left(\frac{a_c}{PGA}\right)^{-1.438}\right] \quad [3]$$

where D_N is the Newmark displacement (in centimetres), a_c is the critical acceleration (in gravity units) and PGA is the peak ground acceleration (in gravity units). The R^2 and σ values are 84% and 0.51, respectively. This equation was derived from a selected database of 875 records from earthquakes ranging from M_w 5.3 to 7.6. Hence, Newmark displacement maps have been computed using this equation after PGA was corrected to account for soil and topographic amplification effects.

Newmark displacement values obtained in this work should not be considered a precise measure of co-seismic slope displacement, but rather as an index of potential instability. The actual Newmark displacement that effectively triggers a landslide strongly depends on site-specific variables, particularly in the way deformation is accommodated. In a regional context, different authors have estimated that Newmark displacements greater than 5-10 cm could potentially imply the occurrence of coherent-type landslides (landslides and earth flows), whereas smaller values could trigger disrupted-type landslides (rock falls, rock slides and debris flows) (cf. Wilson and Keefer, 1983; Keefer, 1984; Romeo, 2000; Keefer, 2002). In this work, a 5 cm value has been considered as the minimum Newmark displacement required to induce coherent-type landslides based on the lower bound proposed by these authors. However, it has been found in other mountainous areas of the Betic Cordillera that even very small Newmark displacements (less than 2 cm) could potentially trigger disrupted-type landslides (Rodríguez-Peces, 2008; Rodríguez-Peces et al., 2008, 2009).

5.6. Results and Discussion

A maximum magnitude earthquake related to the complete rupture of the Padul Fault would produce Newmark displacements quite frequently smaller than 2 cm and locally larger than 5 cm (Fig. 5-7). These Newmark displacements are distributed over wide areas, especially near the fault trace, while Newmark displacements at longer distances from the fault are more scattered. In general, areas showing Newmark displacements appear related to the strong incision of the rivers of the Sierra Nevada Range, which imply slopes with both low safety factor and critical acceleration values. Furthermore, the steep slopes contribute to a significant topographic amplification. The Newmark displacement map shows, in general, a fair correlation with the location of the slope instabilities previously identified in the Sierra Nevada (Fig. 5-7 and Table 5-6).

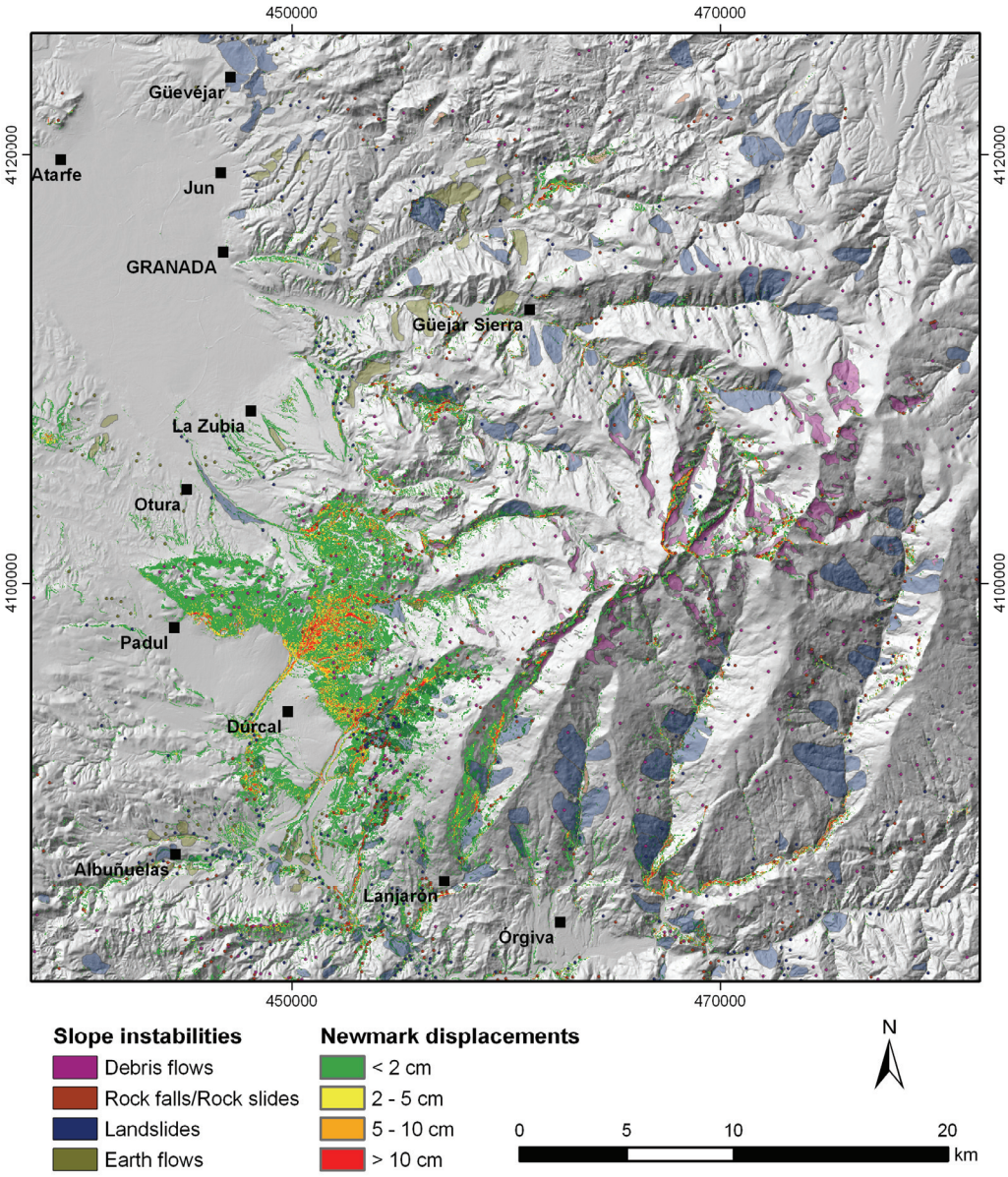

Figure 5-5. Newmark displacement map for deterministic seismic scenario that consider the complete rupture of the Padul Fault (M_w=6.6).

Table 5-6. Newmark displacements distribution (%) for each slope-instability typology.

	Newmark displacement (cm)			
	< 2	2-5	5-10	> 10
Debris flows	87.8	4.7	2.5	5.0
Falls	66.1	9.4	5.8	18.6
Landslides	86.2	5.8	2.7	5.2
Earth flows	91.4	5.4	1.8	1.5
Total	83.2	6.3	3.2	7.4

The percentage of the areas where the instabilities are located related to the total area with Newmark displacements is about 10%. This fact suggests that the seismicity could contribute to the reactivation of old slope instabilities, apart from causing the generation of new ones. The most frequent Newmark displacement value in these unstable areas is 2 cm, or even less. This low value agrees with the results obtained in other mountainous zones of the Betic Cordillera (Rodríguez-Peces, 2008; Rodríguez-Peces et al., 2008, 2009). However, Newmark displacements larger than 5 cm are also reached at some areas. Considering only the threshold values of Newmark displacement proposed by different authors (see section 5.3.), the occurrence of both disrupted and coherent slope instabilities might be possible. Landslides and falls (rock falls and rock slides) are the slope-instability types with the greatest concentration of Newmark displacements (64% and 20%, respectively), while earth flows show the lowest density of Newmark displacements (5%).

5.7. Conclusions

Earthquake-triggered landslide hazard of the Sierra Nevada Range has been analysed for the first time by means of computing a Newmark displacement map considering the rupture of the Padul Fault. This regional map is useful to identify areas with the highest hazard and also to infer the most common type of slope instability that could be triggered in relation to the occurrence of a great earthquake (M_w=6.6) close to the Sierra Nevada Range. In this sense, this map offers a first order assessment on the possible interruption of life-lines and, hence, they could be used to improve emergency plans in the aftermath of an event.

From the landslide inventory developed in the Sierra Nevada, the most common slope instability types are the debris flows, followed by the rock falls and rock slides. Most frequent slope angles related to these instabilities are between 25º and 35º, which comprise more than 50 % of the study area. However, we have noticed that the slope aspect is not a determinant factor. In addition, the most unstable lithological group in the study area is the micaschists and quartzites. This fact is significant because these lithologies are outcropping in practically the whole of the Sierra Nevada area.

Future seismically-induced slope instabilities in the Sierra Nevada Range would be mostly landslides, rock falls and rock slides. Moreover, the reactivation of a few number of old slope instabilities could be also possible. In general, these types of instabilities can be potentially triggered by small Newmark displacements (2 cm or less), which is in agreement with results obtained in other mountainous areas of the Betic Cordillera. However, earthquake-induced instabilities will be most likely related to areas with Newmark displacements larger than 5 cm.

Acknowledgments

This study was supported by research projects CGL2008-03249/BTE, TOPOIBERIA CONSOLIDER-INGENIO2010 CSD2006-00041 and FASE-GEO CGL2009-09726 from the Spanish Ministry of Science and Innovation and MMA083/2007 from the Spanish Ministry of Environment. We also thank recommendations of an anonymous reviewer that allowed us to significantly improve this article. Nicola Woollard is thanked for revising the English.

6

Applicability of Newmark's method at regional, sub-regional and site scales: seismically-induced SW Bullas and La Paca rock-slide cases (Murcia, SE Spain)

Martín Jesús Rodríguez-Peces [1], José Luis Pérez García [2], Julián García-Mayordomo [3], José Miguel Azañón [1, 4], Juan Miguel Insua-Arévalo [5] and Jorge Delgado García [2]

[1] Departamento de Geodinámica. Universidad de Granada, Campus Fuentenueva s/n. 18002. Granada.
[2] Departamento de Ingeniería Cartográfica, Geodésica y Fotogrametría. Universidad de Jaén, Campus de las Lagunillas, s/n. 23071. Jaén.
[3] Instituto Geológico y Minero de España (IGME). C/La Calera, 1. 28760. Tres Cantos (Madrid).
[4] Instituto Andaluz de Ciencias de la Tierra (Universidad de Granada-CSIC), Granada.
[5] Departamento de Geodinámica. Facultad de Ciencias Geológicas. Universidad Complutense de Madrid, 28040. Madrid.

Journal of Geotechnical and Geoenvironmental Engineering
Submitted 22 June 2010

ABSTRACT

In this paper the applicability of the Newmark's method at regional, sub-regional and site scales has been investigated at the Lorca Basin (Murcia). This basin is located in one of the most seismically active regions of Spain. This area is very interesting for studying earthquake-induced slope instabilities as there are well-known cases associated to specific earthquakes (e.g., 2002 SW Bullas and 2005 La Paca). For the regional and sub-regional scales, a geographic information system (GIS) have been used to develop an implementation of Newmark's sliding rigid block method. Soil and topographic amplification effects have been particularly considered. Subsequently, "Newmark displacement" maps for deterministic seismic scenarios have been produced. Some specific studies have been also performed using limit equilibrium methods to estimate the safety factor and the critical acceleration of some slope instabilities at a site scale. These instabilities were the rock slides related to recent seismic series at Lorca Basin: 2002 SW Bullas (M_w=5.0) and 2005 La Paca (M_w=4.8). Finally, the safety factor, critical acceleration and Newmark displacement values estimated at different scales have been compared to determine which scale is most suitable for the Newmark's method.

Keywords: GIS, Murcia, Newmark, Rock falls, Site effects, Topographic amplification

6.1. Introduction

Seismically-induced slope instabilities are one of the most hazardous secondary effects of earthquakes. They can cause damage to buildings and infrastructure and widespread loss of human life. In fact, damage and fatalities from triggered landslides and other ground failures has sometimes exceeded damage directly related to strong shaking and fault rupture during earthquakes (Keefer, 1984).

In 1965, the Civil Engineer Nathan M. Newmark developed a simple method to estimate the permanent displacement induced by earthquakes in earth dams (Newmark, 1965). Later, Wilson and Keefer (1983) developed a variation of Newmark's sliding rigid block method and applied it successfully to natural slopes. Nowadays, this method is very often applied in regional assessments of seismically-induced slope instabilities (e.g. Miles and Ho, 1999; Luzi et al., 2000; Romeo, 2000; Capalongo et al., 2002; Carro et al. 2003). However, few studies in Spain used this approach (e.g. García-Mayordomo, 1999; Mulas et al., 2003; Delgado et al., 2006; Rodríguez-Peces et al., 2008). A review of the main results of these studies can be found in García-Mayordomo et al. (2009).

The assessment of earthquake-triggered landslide hazard may be undertaken using both deterministic and probabilistic techniques. Deterministic methods are usually used to obtain a value of the expected displacement because they fix certain representative values for the input geotechnical and seismic parameters. Moreover, probabilistic methods have been developed because most of the data can be considered as random variables. For the study of seismically-induced slope instabilities, the seismic input data is fixed by the related earthquakes, so the most useful technique is the deterministic.

In this paper, the applicability of the Newmark's method to the study of seismically-induced slope instabilities has been investigated at regional, sub-regional and site scales. For the regional scale, an implementation of Newmark's sliding rigid block method using a GIS has been developed but also considering soil and topographic amplification effects. Subsequently, "Newmark displacement" maps have been produced for several different input seismic scenarios. These maps will allow identifying areas with the highest potential hazard as well as other interesting areas for future detailed studies. The selected study area is the Lorca Basin (Murcia, SE Spain) because it exhibits a high seismic activity, some of the most active faults in Spain are in the surroundings of the basin and there are well-known cases of disrupted slides, rock falls and rock slides associated to specific earthquakes (e.g., 1999 Mulas, 2002 SW Bullas, 2005 La Paca). For a sub-regional and site scales, the well known cases of SW Bullas and La Paca rock slides (Fig. 6-1) have been selected, which are associated to 2002 SW Bullas (M_w=5.0, I_{EMS}=V) and 2005 La Paca (M_w=4.8, I_{EMS}=VII) earthquakes, respectively (Benito et al., 2007; Gaspar Escribano and Benito, 2007). These earthquakes produced widespread damages at the villages of La Paca and Zarcilla de Ramos and a very important social concern. For the site scale, a back-

analysis of the SW Bullas and La Paca rock slides has been performed based on field and geotechnical data. The safety factor and the critical acceleration values were estimated using limit equilibrium methods. Finally, the results were compared with the previous GIS estimations to determine which scale is most suitable for the Newmark's method.

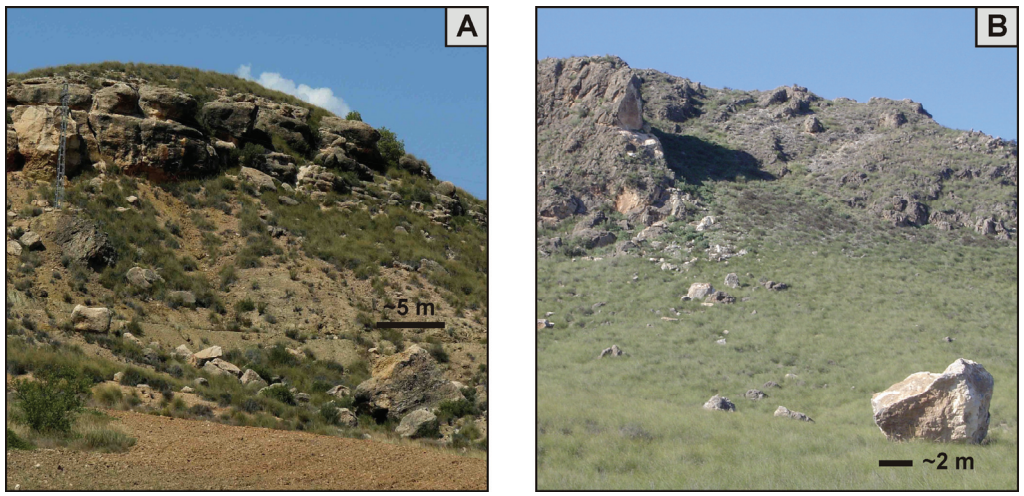

Figure 6-1. Earthquake-triggered slope instabilities at the Lorca Basin. A: Rock slide induced by 2002 SW Bullas earthquake (M_w=5.0). B: Rock slide induced by 2005 La Paca earthquake (M_w =4.8). The black lines show the size of the main fallen blocks.

6.2. Methodology

Several models have been proposed for evaluating co-seismic landslide displacements. The most popular is that proposed by Newmark (1965), where the slope instability acts as a rigid block sliding on an inclined surface. The Newmark's sliding rigid block method permits obtain the minimum horizontal seismic acceleration to overcome shear resistance and start the displacement of the rigid block, provided the static safety factor is known:

$$a_c = (SF - 1)\, g \sin \alpha \qquad (1)$$

where a_c is the critical acceleration (in gravity units, 1g=9.81 m/s^2), g is the acceleration of the gravity, SF is the static safety factor and α is the thrust angle. The critical acceleration is an expression of slope capacity to resist the seismic vibration. The safety factor was estimated at regional and sub-regional scale assuming the infinite slope model proposed by Jibson et al. (2000) following the Mohr-Coulomb criterion. In this limit equilibrium model, the thrust angle is equal to the slope angle. However, when the safety factor is estimated by means of other limit equilibrium models considering rotational movement, α is the angle between the vertical and a line segment connecting the centre of gravity of the landslide mass and the midpoint of the

slip circle (Newmark, 1965). Finally, to estimate the displacement of the slope induced by earthquakes –i.e., Newmark displacement (D_N), the Jibson (2007) regression equation have been used. This equation correlates the Newmark displacement with the critical acceleration and peak ground acceleration values:

$$\log D_N = 0.215 + \log\left[\left(1-\frac{a_c}{PGA}\right)^{2.341}\left(\frac{a_c}{PGA}\right)^{-1.438}\right] \quad (2)$$

where D_N is the Newmark displacement (in centimetres), a_c is the critical acceleration (in gravity acceleration units) and *PGA* is the peak ground acceleration (in gravity units). For further details of the implementation of the Newmark's method using a GIS, the reader is referred to Rodríguez-Peces (2008) and Rodríguez-Peces et al. (2008). The minimum value of Newmark displacement related to a slope failure can vary widely depending on the type of slope instability (e.g. rock fall, landslide), lithology and geometry of the slope. However, some authors found that the critical Newmark displacement value is 5 cm for landslides (Wieczorek et al., 1985; Jibson and Keefer, 1993). In the case of more brittle rupture mechanism (e.g. rock falls and rock slides), the critical Newmark displacement value is 2 cm (Rodríguez-Peces, 2008; Rodríguez-Peces et al., 2008).

Seismic input comprised two different deterministic scenarios: 1) the occurrence of M_w=5.0 2002 SW Bullas and M_w=4.8 2005 La Paca earthquakes (Benito et al., 2007; Gaspar Escribano and Benito, 2007); 2) the most probable earthquake for a 475-year return period (M_w=5.0) (Gaspar-Escribano et al., 2008). The average peak ground acceleration (PGA) on rock of each earthquake have been calculated as a function of the moment magnitude and epicentral distance using different Ground Motion Prediction Equations (GMPEs) for the Mediterranean zone (Skarlatoudis et al, 2003; Ambraseys et al, 2005; Akkar and Bommer, 2007; Bindi et al, 2010). The SW Bullas rock slide was located about 5 km from the epicentre of the 2002 SW Bullas earthquake (M_w=5.0). The PGA on rock estimated using this magnitude-epicentral distance pair is 0.11g (±0.03). The La Paca rock slide was located about 7 km from the epicentre of the 2005 La Paca earthquake (M_w=4.8). In this case, the average PGA on rock is 0.06g (±0.01). However, other authors found that PGA for a M_w=4.8 earthquake at an epicentral distance of 8 km for rock conditions ranges between 0.10g and 0.15g (Buforn et al., 2005). Additional estimations based on Gaspar-Escribano and Benito (2007) for an earthquake with M_w=4.8 are PGA on rock between 0.08g and 0.13g at an epicentral distance of 5 km and PGA on rock between 0.07g and 0.11g at an epicentral distance of 10 km. Therefore, the average PGA on rock estimated using these results is 0.08g (±0.02).

Since PGA is referred to rock conditions, it required to correct PGA values to allow for site effects –i.e. soil and topographic seismic amplification (Table 6-1). Soil amplification factors were adopted from the values derived in the RISMUR Project (Benito et al., 2006) which represents the best quality data available for Murcia

Region. This project developed a geotechnical classification of the geological units following Borcherdt (1994), NCSE-2002 (2002), NEHRP (2003) and Eurocode-8 (CEN, 2004) criteria. Moreover, the topographic amplification factor was particularly evaluated considering slope and relative height of ridges, following Eurocode-8 provisions (CEN, 2004). Then, the PGA on rock values was multiplied by both amplification factors. Considering these seismic amplification factors, the estimated PGA at the SW Bullas and La Paca rock-slide locations are 0.20g (±0.05) and 0.11g (±0.03), respectively.

6.2.1. Regional and sub-regional scales

To produce the critical acceleration maps, a lithological map have been firstly arranged using digital geological maps (Baena-Pérez, 1972; Kampschuur et al., 1972) from the Institute of Geology and Mines of Spain (IGME, Instituto Geológico y Minero de España). Three lithological groups have been distinguished in function of general shear resistance of the materials and their behaviour against slope instabilities (Table 6-1). Average values of specific weight, cohesion and friction angle have been assigned to each lithological unit. These shear strength parameters were derived from geotechnical bibliography and available geotechnical tests (cf. Rodríguez-Peces, 2008). Then, cohesion and friction angle values were estimated by iteration until all obtained safety factors were higher than one (stability conditions). Table 6-1 shows the shear strength parameters and seismic amplification factors considered in the forthcoming calculations.

Table 6-1. Lithological groups, shear strength parameter values considered in the estimation of safety factor at regional and sub-regional scale (initial range of values of the parameters is in brackets) and seismic amplification factors. γ: Unit weight; c: Cohesion; ϕ: Friction angle; SAF: Soil amplification factor; TAF: Topographic amplification factor.

Lithological group	γ (kN/m^3)	c (kPa)	ϕ (º)	SAF	TAF
Dolomites and limestones	25 (23-27)	46 (0-108)	30 (21-39)	1.0	1.2
Conglomerates, sandstones and argillites	22 (20-24)	31 (4-16)	33 (27-39)	1.8	1.0
Argillites, marls, sandstones and gypsums	21 (18-24)	36 (35-117)	26 (22-30)	1.8	1.0

The digital elevation model (DEM) used for SW Bullas and La Paca rock slides at regional scale has a 25 x 25 metres pixel size. This DEM was obtained from digital topographic maps of the Murcia Region developed by the Spanish Geographic Institute (IGN, Instituto Geográfico Nacional). At sub-regional scale, a high-resolution DEM corresponding to the SW Bullas and La Paca rock-slides locations have been used (Fig. 6-2). These DEMs were derived using a terrestrial laser scanner (OPTECH) of great coverage (1000-1500 m). The data capture was carried out at different places and from different points of view, so that the entire area was captured at a centimetric resolution (10 x 10 cm). All the individual scans have been integrated in a single local reference system, and later transfer them to the global reference system (UTM-30 ED50). Finally, the point cloud was edited manually using different filters to remove

vegetation and existing fallen blocks of rock. Thus, a DEM with a pixel size of 2.5 x 2.5 m was interpolated from this point cloud corresponding to the ground level.

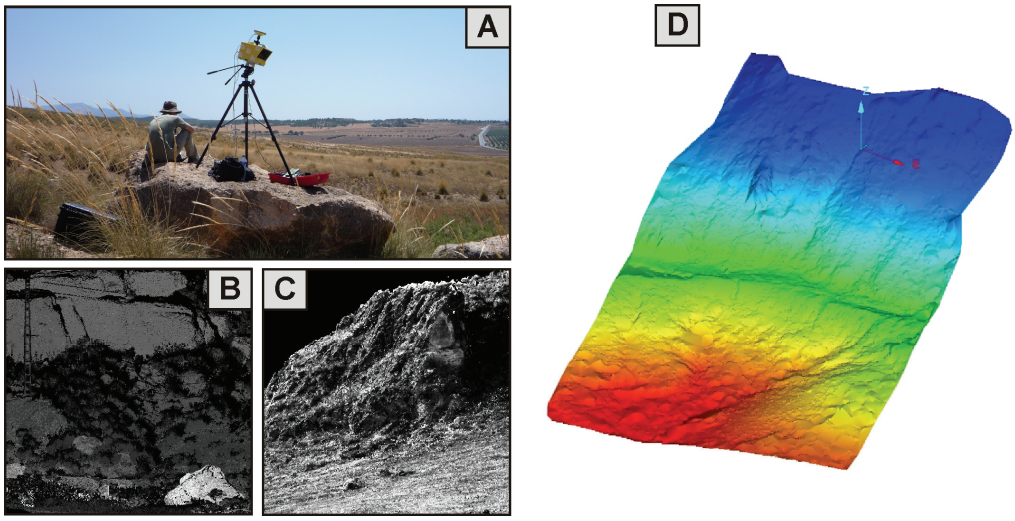

Figure 6-2. Preparation of the high-resolution digital elevation models using a terrestrial laser scanner. A: Scanning process. B: Point cloud for the 2002 SW Bullas rock-slide area. C: Point cloud for the 2005 La Paca rock-slide area. D: Interpolated high-resolution DEM for the 2002 SW Bullas rock-slide area.

6.2.2. Site scale

A back-analysis has been performed of both SW Bullas and La Paca rock slides to estimate the safety factor and critical acceleration values. 2D slope-stability analysis software (Slide, Rocscience Inc., 2003) has been used for this purpose. This program calculates safety factors for circular and non-circular slope failure surfaces based on a number of widely used limit equilibrium methods. We have decided to use the simplified Janbu method because it is the only limit equilibrium technique that estimate the safety factor values for non-circular failure surfaces and satisfy the force equilibrium by not considering shear forces between slides.

Several field surveys have been performed to obtain the geometry and the mechanical behaviour of materials related to both SW Bullas and La Paca rock slides. The slope profile was firstly derived from the high-resolution DEM (0.10 x 0.10 m) obtained of the terrestrial laser scanner survey cited above. This cross section represents the observed main path of the fallen rock blocks corresponding to each rock slide. In both cases, a non-circular slope failure surface has been set based on field data. In addition, different laser scanner captures of the main fallen blocks and the failure surface of both rock slides have been carried out at a millimetric resolution. The individual captures have been integrated and transferred to the global reference system using the same method explained at sub-regional scale (Fig. 6-3). From the resulting point clouds, a high-resolution DEM (1 x 1 mm) of the joint surface related to each rock slide has been extracted from the corresponding face of each rock block

and from the in situ failure surface. Subsequently, different joint surface profiles have been derived from each failure surface using as a reference for these profiles, the average plane of the surface.

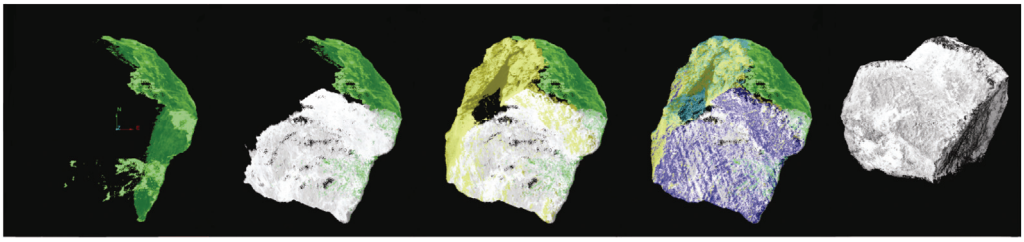

Figure 6-3. Getting the point cloud of the main fallen rock block of the 2005 La Paca rock slide by union of single laser scanner captures.

Some in-situ and geotechnical tests have been performed in order to obtain the shear strength parameters of the materials related to the failure surface. The Barton-Bandis failure criterion (Barton and Choubey, 1977; Barton and Bandis, 1990) was used for estimating of peak shear strength of joints in the rock-type materials. The Joint wall Compressive Strength (JCS) have been estimated using different Schmidt hammer rebound-JCS empirical equations developed for carbonate rocks (cf. Aydin and Basu, 2005). The N-type Schmidt hammer rebound (R_N) was obtained following the most recent procedure suggested by Aydin (2009). Several methods have been proposed for evaluating the Joint Roughness Coefficient (JRC) of a discontinuity. The most common procedure is compare visually standard roughness profiles of 10 cm (Barton and Choubey, 1977), but this method is only valid for small-scale laboratory specimens and it has a great degree of subjectivity. An alternative method for larger profile length is the measurement of the surface roughness amplitude from a straight edge (Bandis, 1980). However, this method has some limitations because the maximum asperity amplitude is measured in millimetres. In actual field conditions where the length of the surface is large, JRC must be estimated for the full-scale surface. This paper makes use of a published mathematical formula to estimate JRC value from the joint surface profiles derived from a high-resolution DEM. Tse and Cruden (1979) developed an empirical correlation based on the root-mean-square (RMS) of the local surface slope of a profile. Yang et al. (2001) improved this relation more recently with a correlation coefficient of R=0.99326:

$$JRC = 32.69 + 32.98 \log Z_2 \quad (3)$$

where

$$Z_2 = \sqrt{\frac{\sum_{i}^{N-1} \left(z_i - z_{i+1}\right)^2}{\left(N-1\right)\Delta s^2}}$$

and N is the number of discrete measurements of the amplitude of the roughness in the profile, Δs is the constant distance between two adjacent amplitude readings, z_i is the height of the profile measured relative to a reference line and Z_2 is the root mean square of the first derivative of the profile. An average JRC was obtained considering a range of measure of 10 cm in order to compare with the standard roughness profiles of Barton and Choubey (1977). Finally, the JRC value was corrected taking into account the scale effect by means of the expression proposed by Barton and Bandis (1990):

$$JRC_N = JRC_0 \left(\frac{L_N}{L_0} \right)^{-0.02\,JRC_0} \quad (4)$$

where L is the length of the surface and the suffixes N and 0 refer to the in situ block size and 10 cm laboratory-scale samples, respectively.

For the soil-type materials, some soil samples were taken from the failure surface and some laboratory test have been performed: unsaturated and saturated unit weight determination (AENOR, 1994a), specific gravity determination (AENOR, 1994b), Atterberg limits determination (AENOR, 1993, 1994c), engineering classification of soils (ASTM, 2000), direct shear test of soils under consolidated drained (CD) conditions (AENOR, 1998).

Finally, all the data was used together to perform the slope models corresponding to both rock slides. The critical acceleration was evaluated fitting the seismic acceleration value by iteration until the safety factor obtained was equal to one (stability condition). This value of seismic acceleration is a more accurate estimation of the critical acceleration at the rock-slides location. However, the critical acceleration related to a circular approximation of the failure surface was also obtained by means of the equation (1) and determining the thrust angle at both rock-slide cases. Then, the static safety factor prior to each earthquake was estimated removing the seismic acceleration value.

6.3. Results and discussion

6.3.1. Regional scale (25 x 25 m)

At SW Bullas rock-slide area at a 25 x 25 m pixel resolution the safety factor values are between 1.6 and 2.0 and the critical acceleration values are between 0.24g and 0.39g (Fig. 6-4). In the case of the La Paca rock-slide area, the safety factors are between 1.4 and 2.0 and the critical accelerations are between 0.22g and 0.50g (Fig. 6-5). In both cases, the most-likely source areas of the slope instabilities can be identified by showing the lowest values of safety factor and critical acceleration.

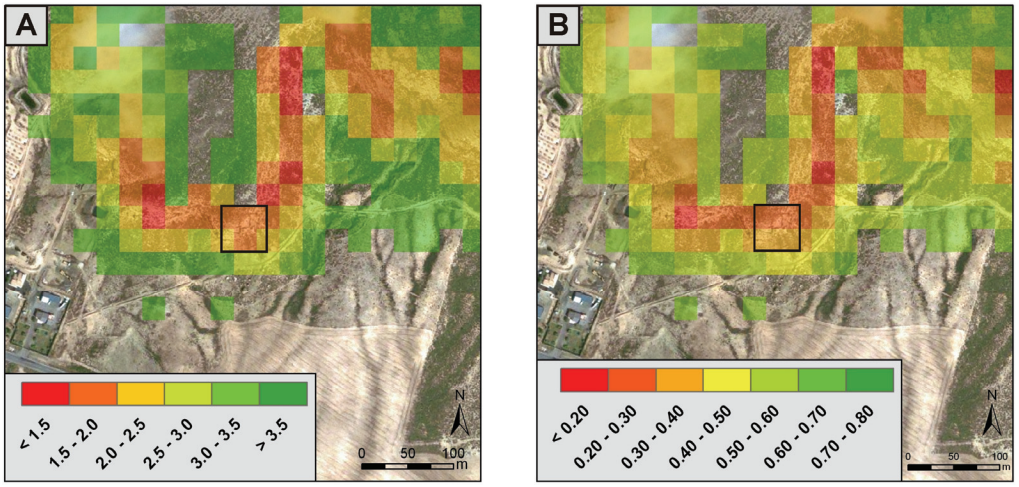

Figure 6-4. Safety factor (A) and critical acceleration (B) maps at SW Bullas rock-slide area at a 25 x 25 m pixel resolution (regional scale). The critical acceleration is given in gravity units (1g=9.81 m/s^2). The black square indicates SW Bullas rock-slide failure surface location.

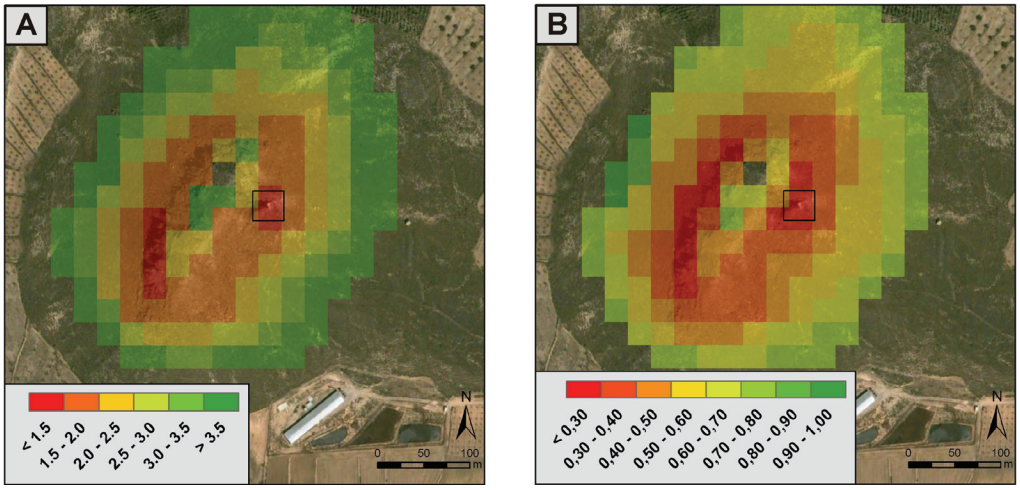

Figure 6-5. Safety factor (A) and critical acceleration (B) maps at La Paca rock-slide area at a 25x25 meters pixel resolution (regional scale). The critical acceleration is given in gravity units (1g=9.81 m/s^2). The black square indicates La Paca rock-slide failure surface location.

Estimated Newmark displacements at regional scale for the occurrence of the most probable earthquake for a 475-year return period (M_w=5.0) shows in both cases low values, mostly lower than 2 cm (Tables 6-2 and 6-3). However, the seismic scenarios for 2002 SW Bullas and 2005 La Paca earthquakes show Newmark displacements equal to zero. These results imply that these slopes did not move during these earthquakes. This is due to the obtained safety factor values in both cases are relatively high and so, the critical acceleration are relatively high too (Tables 6-2 and 6-3). Therefore, a regional map with a 25 x 25 m pixel size turns out to be unsuitable

for estimating Newmark displacement for the SW Bullas and La Paca rock slides. However, the safety factor and critical acceleration maps at a regional scale (Fig. 6-4 and 6-5) are very useful to identify preliminarily the areas with the greatest potential hazard, which can be studied in more detail later.

6.3.2. Sub-regional scale (2.5 x 2.5 m)

The safety factor values obtained at SW Bullas rock-slide site at a 2.5 x 2.5 m pixel resolution range from 1.0 to 1.9 and the critical acceleration values are between 0.02g and 0.40g (Fig. 6-6). At La Paca rock-slide site the safety factors are between 1.0 and 1.7 and the critical accelerations are between 0.03g and 0.45g (Fig. 6-7). At this scale, the safety factor and critical acceleration values are lower than at regional scale (Table 6-1). Moreover, in both rock-slide cases the safety factor values prior to each earthquake are very close to the condition of instability –i.e., SF<1.00. In contrast to the results at regional scale, the most-likely source areas of the slope instabilities, which show the lowest values of safety factor and critical acceleration, can be identified with greater accuracy (Fig. 6-6 and 6-7). In fact, the rupture areas of 2002 SW Bullas and 2005 La Paca rock slides can be accurately distinguished by means of the safety factor and critical acceleration maps at sub-regional scale.

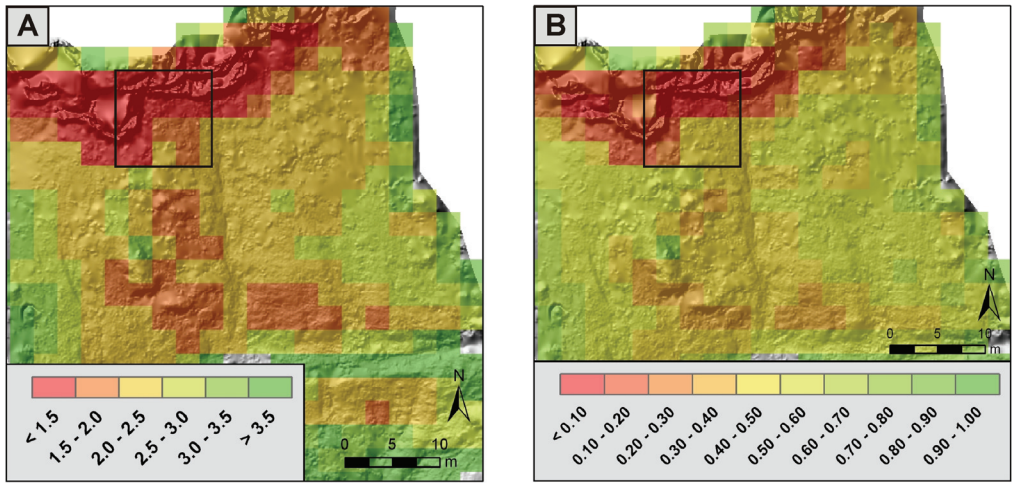

Figure 6-6. Safety factor (A) and critical acceleration (B) maps at SW Bullas rock-slide area at a 2.5 x 2.5 m pixel resolution (sub-regional scale). The critical acceleration is given in gravity units (1g=9.81 m/s^2). The black square indicates SW Bullas rock-slide failure surface location.

The occurrence of the most probable earthquake for a 475-year return period (M_w=5.0) show in both cases greater Newmark displacement values than at regional scale, which are mainly greater than 5 cm (Table 6-2 and 6-3). In this case, the seismic scenarios for 2002 SW Bullas and 2005 La Paca earthquakes show Newmark displacements at the rock-slides location equal to 4.7 cm and 13.6 cm, respectively (Table 6-2 and 6-3). These values are in agreement with the critical Newmark displacement of 5 cm suggested by others authors for the occurrence of coherent-type

landslides. However, the lower bounds of estimated Newmark displacement for the SW Bullas and La Paca rock slides (2 and 4 cm, respectively) are closer to the minimum value of 2 cm required to trigger disrupted-type slope instabilities.

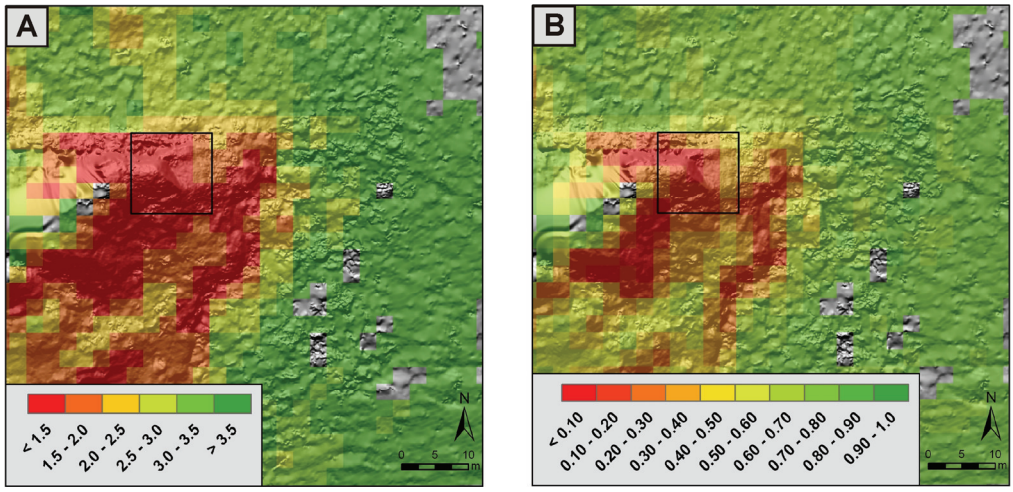

Figure 6-7. Safety factor (A) and critical acceleration (B) maps at La Paca rock-slide area at a 2.5 x 2.5 m pixel resolution (sub-regional scale). The critical acceleration is given in gravity units (1g=9.81 m/s^2). The black square indicates La Paca rock-slide failure surface location.

6.3.3. Site scale

6.3.3.1. 2002 SW Bullas rock slide

Two different materials have been recognized related to the failure surface corresponding to the SW Bullas rock slide: cemented conglomerates over a thick marls layer (Fig. 6-8). The conglomerate is composed by decimetric carbonate grains embedded in carbonate-rich cement, so its geotechnical behaviour is closer to that of a limestone. Assuming a unit weight of 24.68 kN/m3 (±2.27) and a mean Schmidt hammer rebound of r_N=51 (±2), the average Joint wall Compressive Strength (JCS) is 95 MN/m^2 (±39) and the residual friction angle is 30º (±3). The average JRC derived from the high-resolution profiles is 20 (±1) (Fig. 6-8). This numerical estimate agrees with a standard roughness profile with JRC of 18 to 20. Considering the total length of the joint profile (about 4 m), the corrected JRC is 4. For the Triassic marls located at the bottom of the rock block, the unit weight is 20.21 kN/m^3, the cohesion value is 33.35 kN/m^2 and a friction angle is 23.4º. This soil is classified as a low-plasticity clay (CL) since the liquid limit is 42.40% and the plastic index is 18.12%.

The estimated safety factor and critical acceleration values prior to the 2002 SW Bullas earthquake was 1.07 and 0.04g, respectively. These values are slightly lower than those obtained at the sub-regional scale (Table 6-2). The safety factor value is also nearby to the instability condition and it is within the range of estimated safety factors at sub-regional scale. A thrust angle of 47º and a critical acceleration of 0.05g

(±0.01) have been estimated assuming a circular approximation of the failure surface by means of equation (1). This critical acceleration is slightly greater than the value obtained using the Slide software (0.04g), which is a more accurate estimation because take into account the actual asperity and shape of the failure surface.

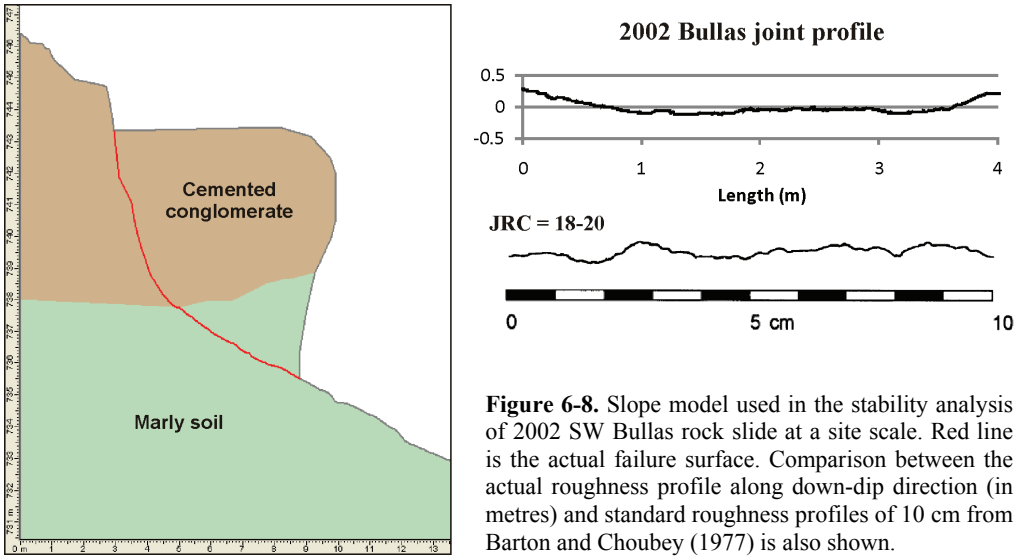

Figure 6-8. Slope model used in the stability analysis of 2002 SW Bullas rock slide at a site scale. Red line is the actual failure surface. Comparison between the actual roughness profile along down-dip direction (in metres) and standard roughness profiles of 10 cm from Barton and Choubey (1977) is also shown.

The average PGA value estimated considering the seismic scenario for 2002 SW Bullas earthquake was 0.20g. An unstable safety factor of 0.76 (±0.04) has been found implementing this acceleration to the slope model. A Newmark displacement of 10 cm was obtained at SW Bullas rock slide location combining the PGA and critical acceleration values by means of equation (2). This result is slightly greater than the Newmark displacement found at the sub-regional scale (about 5 cm) but it is within the range of estimated displacements at that scale (Table 6-2). Considering the lower bound of the estimates, a Newmark displacement of 3 cm has been found as a more accurate critical value required to the occurrence of this disrupted-type slope instability. Estimated Newmark displacement for the occurrence of the most probable earthquake for a 475-year return period (27 cm) was also greater than the value obtained at the sub-regional scale (Table 6-2).

Table 6-2. Comparison between static safety factor (SF), critical acceleration (a_c, gravity units) and Newmark displacement (D_N, cm) values estimated for regional, sub-regional and site scales to the SW Bullas rock-slide location.

Scale	Regional	Sub-regional	Site
SF	1.64 (±0.03)	1.12 (±0.07)	1.07 (±0.02)
a_c	0.25 (±0.01)	0.06 (±0.04)	0.04
D_N 2002 SW Bullas (M_w=5.0)	0.0	4.7 (1.5-15.3)	9.9 (3.0-31.9)
D_N 475-years RP (M_w=5.0)	0.1 (0-0.4)	12.8 (3.9-41.3)	26.8 (8.3-86.8)

6.3.3.2. 2005 La Paca rock slide

At La Paca rock slide (Fig. 6-9), the failure surface was developed in a rock-type material (Triassic dolomites). Assuming a unit weight of 26.50 kN/m3 (±2.03) and the obtained Schmidt hammer rebound of r_N=35 (±4), the average Joint wall Compressive Strength (JCS) is 43 MN/m^2 (±18) and the residual friction angle is 30º (±4). The average JRC derived from the high-resolution profiles is 17 (±5). This estimation is consistent with a JRC of 16 to 18 from the standard roughness profiles (Fig. 6-9). Considering the total length of the joint profile (about 14 m), the corrected JRC is 4.

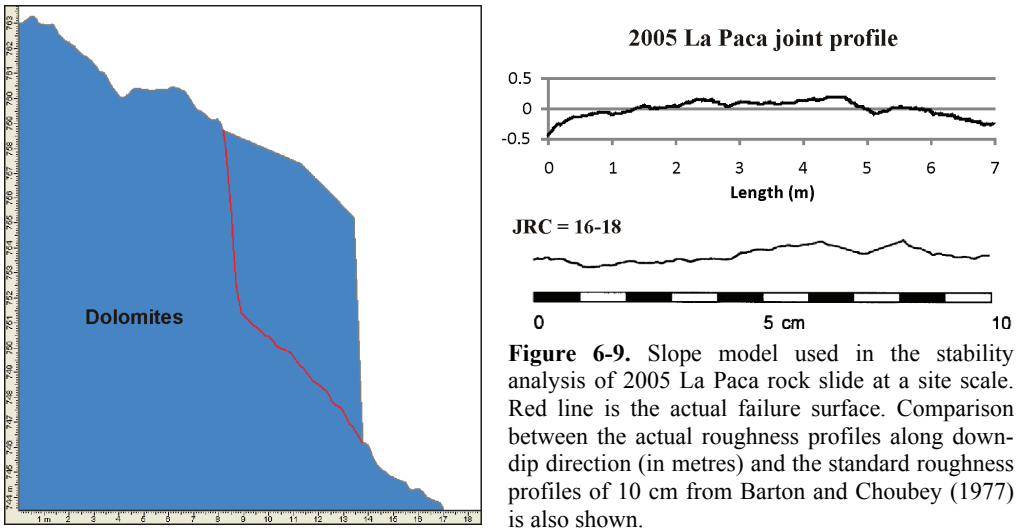

Figure 6-9. Slope model used in the stability analysis of 2005 La Paca rock slide at a site scale. Red line is the actual failure surface. Comparison between the actual roughness profiles along down-dip direction (in metres) and the standard roughness profiles of 10 cm from Barton and Choubey (1977) is also shown.

The estimated safety factor and critical acceleration values prior to the 2005 La Paca earthquake was 1.02 and 0.01g, respectively. These values are also similar to those obtained at the sub-regional scale (Table 6-3). In this case, the safety factor very close to the instability condition (SF<1.00) and are. Assuming a circular approximation of the failure surface, the estimated thrust angle is 69º and the critical acceleration is 0.02g (±0.01) which is slightly greater than the former result. As in the previous case, the former estimate of the critical acceleration using Slide is a more accurate value.

An unstable safety factor of 0.83 (±0.03) have been obtained applying the average PGA value corresponding to the 2005 La Paca earthquake (0.11g) to the slope. Considering this PGA and the critical acceleration derived above, the mean Newmark displacement at La Paca rock-slide location was about 40 cm. In this case, the critical Newmark displacement required to trigger the rock slide is 13 cm. These relative high displacement values are due to the safety factor prior to the earthquake was very low and so, the critical acceleration was very low too. Moreover, these results are slightly greater than the Newmark displacement obtained at the sub-regional scale but both values are the same order of magnitude (Table 6-3). Estimated

Newmark displacement for the occurrence of the most probable earthquake for a 475-year return period was also slightly greater than the value obtained at the sub-regional scale (Table 6-3).

Table 6-3. Comparison between static safety factor (SF), critical acceleration (a_c, g units) and Newmark displacement (D_N, cm) values estimated for regional, sub-regional and site scales to the La Paca rock-slide location.

Scale	Regional	Sub-regional	Site
SF	1.46 (±0.01)	1.05 (±0.05)	1.02 (±0.02)
a_c	0.25 (±0.002)	0.02 (±0.02)	0.01
D_N 2005 La Paca (M_w=4.8)	0.0	13.6 (4.2-43.8)	41.3 (12.8-133.5)
D_N 475-years RP (M_w=5.0)	0.4 (0.1-1.2)	56.5 (17.4-182.7)	171.8 (53.1-555.8)

6.4. Conclusions

In this paper, it has been proved that the estimated Newmark displacements at a sub-regional scale are in good agreement with those obtained in detailed studies at a site scale. Moreover, the fact that the estimated safety factor and critical acceleration values at both scales are very similar justifies the shear strength parameters and limit equilibrium method used at regional and sub-regional scales.

In addition, the results for the regional scale are strongly influenced by the grid size of the digital elevation model and the dimensions of the slope instability. For the 2002 SW Bullas and 2005 La Paca cases, the 25 x 25 m pixel size is larger than the rock-slides dimensions resulting in values of safety factor and critical acceleration greater than those obtained at sub-regional and site scales. These values are so high that the calculated Newmark displacements are equal to zero for both 2002 SW Bullas and 2005 La Paca rock slides. However, the regional scale maps are still useful to show the areas with the highest potential hazard which which can be interesting for future particular studies.

A critical Newmark displacement value of 3 cm has been obtained from the detailed studies at a site scale. This value can be considered as a minimum threshold to trigger disrupted-type slope instabilities similar than SW Bullas and La Paca rock slides. These earthquake-triggered slope failures seem to be related to sites with safety factors close to instability condition and, hence, low critical acceleration values.

The estimated PGA and Newmark displacement values would be much more accurate if representative accelerograms to each earthquake at the rock-slide locations were available that which is not currently possible for these slope instability cases. Finally, these results should be contrasted with the study of more cases of seismically-induced slope instabilities.

Acknowledgments

This study was supported by research projects CGL2008-03249/BTE, TOPOIBERIA CONSOLIDER-INGENIO2010 CSD2006-00041 and FASE-GEO CGL2009-09726 from the Spanish Ministry of Science and Innovation and MMA083/2007 from the Spanish Ministry of Environment.

7

Constraining pre-instrumental earthquake parameters from slope stability back-analysis: Paleoseismic reconstruction of the Güevéjar landslide during the 1st November 1755 Lisbon and 25th December 1884 Arenas del Rey earthquakes

Martín J. Rodríguez-Peces [1], Julián García-Mayordomo [2], José M. Azañón [1,3], Juan M. Insua Arévalo [4], Juan Jiménez Pintor [5]

[1] Departamento de Geodinámica. Universidad de Granada, C/Fuentenueva, s/n. 18002-Granada. Spain.
[2] Instituto Geológico y Minero de España. Área de Investigación en Peligrosidad y Riesgos Geológicos. C/La Calera, 1 (Tres Cantos). 28760-Madrid. Spain.
[3] Instituto Andaluz de Ciencias de la Tierra (UGR-CSIC), C/Fuentenueva, s/n. 18002-Granada, Spain.
[4] Departamento de Geodinámica. Universidad Complutense de Madrid. Ciudad Universitaria, s/n. 28040-Madrid, Spain.
[5] Departamento de Urbanismo. Consejería de Vivienda y Ordenación del Territorio de la Junta de Andalucía. Delegación Provincial de Málaga. Plaza de San Juan de la Cruz, s/n. 29071 -Málaga. Spain.

Quaternary International (Special Issue on Palaeoseismology)
Submitted 15 May 2010. Accepted 22 June 2010.

ABSTRACT

Slope stability back-analysis performed in landslides known to have been triggered by an earthquake can provide additional constraints on the size and location of pre-instrumental seismic events. In this paper we reconstruct the pre-earthquake conditions of a major landslide located in the Granada Basin –the Güevéjar landslide, which was triggered twice by the 1755 Lisbon and 1884 Arenas del Rey earthquakes. For each case the minimum seismic acceleration needed to trigger the instability has been calculated, and from this datum the most likely magnitude and epicentral location has been inferred for each event. Our results suggest that the moment magnitude of the 1755 Lisbon earthquake was at least 8.5 and that it was located as far as 580 km from the landslide, so confirming the epicentral location proposed by Martínez Solares and Mezcua (2004). For the 1884 Arenas del Rey earthquake we conclude that its moment magnitude was at least 6.5 and that it was located in the first 55 km around Güevéjar. These results support the Ventas de Zafarra Fault as the seismogenic source of the event. Apart from these two major events, other significant historical earthquakes occurred in the Granada Basin are also analysed in the paper. It is confirmed that none of them were able to reactivate the landslide, particularly for the 1806 Pinos Puente earthquake. The Güevéjar landslide is stable at present-day conditions but it could be reactivated by an earthquake as small as M_w=4.7 if it takes place right at site.

Keywords: Granada Basin; Güevéjar; Historical earthquake; Landslide; Newmark; Paleoseismicity

7.1. Introduction

In countries of moderate seismic activity and long history, like Spain, a key element in the evaluation of seismic hazard is the identification of earthquakes occurred before the deployment of seismic networks –i.e., the so-called historical earthquakes. In order to account for these earthquakes in hazard calculations it is crucial to estimate their size and epicentral location. The standard way to estimate these parameters is by the evaluation of building damage described in the chronicles available at that age and across the region. However, the analysis of the effects produced by seismic shaking in the ground can be an additional useful source of data for estimating the size and location of historical earthquakes. Particularly, earthquake-triggered landslides have been studied either from regional or case-specific approaches. Keefer (1984, 1994, 2002) studied the phenomenology of earthquake-triggered landslides world-wide, and found minimum earthquake magnitudes and intensities that have triggered landslides of different types. He also proposed a number of empirical relationships between the area and total volume affected by landslides with earthquake magnitude, and maximum distance from earthquake epicentre to landslide with magnitude. However, these correlations have to be used with caution and as a first order approximation as they do not account for important variables controlling the stability of the landslide, such as specific geological/geotechnical conditions or the occurrence of ground motion amplification effects. A more elaborated approach to study seismically-induced landslides consists in applying slope-stability methods to particular cases (Jibson, 1996). In these studies the stability of the landslide prior to the earthquake is back-analyzed in order to estimate the minimum ground acceleration that triggered the instability, and from that estimation, information regarding to the size and location of historical earthquakes can be inferred.

In this work, we focus on the case study of the Güevéjar landslide, located in the Granada Basin, southern Spain. It is well documented that this major landslide was triggered twice, firstly by the 1st November 1755 Lisbon earthquake and 129 years later by the 25th December 1884 Arenas del Rey event. For both cases, we have performed a reconstruction of the landslide conditions prior to the earthquakes based on contemporaneous written descriptions, field data, and geotechnical investigations. We have then analysed the stability of the slope considering ground shaking in order to find the failure surface that better matches field data. From this failure surface, we have estimated the safety factor of the slope prior to the earthquake and from it the minimum acceleration that triggered the landslide. Based on that acceleration value and making use of ground motion prediction equations, we analyse which are the most likely values of magnitude and distance to epicentre of the earthquakes. Apart from those two major events, we have also studied the stability of the landslide in relation to other significant historical earthquakes occurred in the Granada Basin. Finally, we have analysed the conditions for a future reactivation of the Güevéjar landslide due to an earthquake.

7.2. Regional Geology and Seismicity

The Güevéjar landslide is located 10 km north of the City of Granada, at the eastern border of the Granada Basin (South Spain), which is a Neogene-Quaternary intermontane depression located in the central part of the Betic Cordillera (Fig. 7-1). The basement of the Granada Basin is formed by metamorphic rocks belonging to the Alboran Domain (Dorsal, Maláguide and Alpujárride Complexes) in the southeastern border, and by Jurassic and Cretaceous carbonate sedimentary rocks belonging to the Subbetic Domain of the South Iberian Domain (García-Hernández et al., 1980) in the northwestern border. The sedimentary infilling of the Granada Basin is up to 2 km thick (Rodríguez-Fernández and Sanz de Galdeano, 2006). The oldest sediments in the basin are conglomerates, calcarenites and marls deposited in marine environments in the Lower Tortonian. During the uppermost Tortonian-lowermost Messinian the depositional environment changed to continental conditions with sedimentation of conglomerates, lutites and sandstones deposited in relation to rivers and alluvial fans that drained the surrounding mountain ranges. The central part of the basin was evaporated and filled with gypsum and halite. On top of this sequence were deposited Messinian to lower Pliocene lacustrine marls and limestones and fine-siliciclastic sandstones of the Turolian mammal stage. These lacustrine sediments also include marls with lignitic layers and gastropod-rich limestones (Bandel et al., 2000). The Pliocene to Pleistocene is represented by piedmont and glacis formed by thick deposits of conglomerates and sands, locally intercalated by clays and travertines (Fernández et al., 1996).

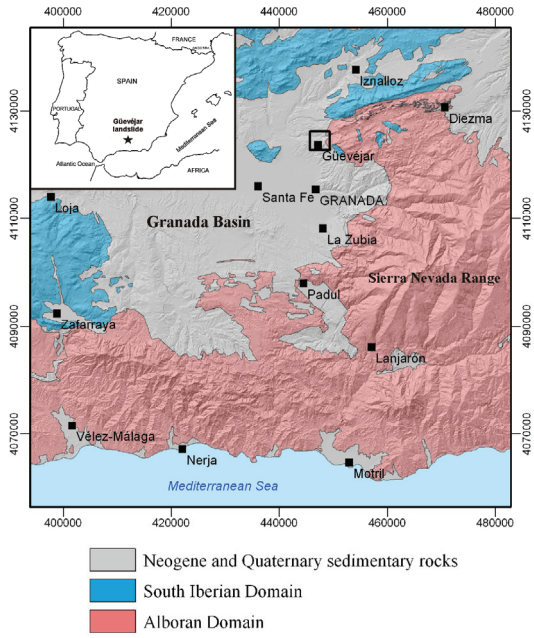

Figure 7-1. Simplified geological sketch of the central part of the Betic Cordillera (South Spain). The location of the Güevéjar landslide is marked with a rectangle.

From a seismotectonic point of view the Granada Basin is delimited by E-W faults along the southern boundary (e.g. Ventas de Zafarraya Fault) and NW-SE faults at its western and eastern margins (e.g. Granada, Santa Fe and Atarfe faults). Many of those faults show Quaternary activity and can potentially generate earthquakes with magnitudes greater than M_w=6.0 (Sanz de Galdeano et al., 2003). In fact, the Granada Basin is the most seismically active area in Spain. The most important earthquakes ocurred in the Granada Basin (Table 7-1) have taken place during the period between the XV and the XIX centuries (Vidal, 1986; López Casado et al., 2001; Feriche and Botari, 2002): 1431 Granada (I_{EMS}=IX), 1526 Granada (I_{EMS}=VIII), 1806 Pinos Puente (I_{EMS}=IX) and 1884 Arenas del Rey (I_{EMS}=X). During the XX century the Betic region has experienced a moderate seismic activity with some slightly destructive earthquakes, such as the 1910 Adra earthquake with a magnitude of M_w=6.1 (Stich et al., 2003). Since the beginning of the instrumental record in the region in 1920's, a large number of earthquakes have been recorded in the Granada Basin, although all of them of low magnitude (m_b<5.5) (De Miguel et al., 1989). The last significant seismic events occurred in the Granada Basin are the Albolote 1956 and Jayena 1984 earthquakes with magnitude M_w=4.9 and M_w=5.0 (Vidal, 1986; Morales et al., 1996), respectively.

Table 7-1. Main historical earthquakes with an epicentral intensity greater than I_{EMS}=VII felt at the Güevéjar landslide location.. I_0: epicentral intensity; M_w: moment magnitude (in bold are the M_w extracted from specific studies); R_{ep}: epicentral distance to Güevéjar landslide (km); $I_{Güevéjar}$: local intensity at Güevéjar landslide location; *: intesity values extracted from macroseismic maps; PGA: peak ground acceleration (g units); AF: amplification factor (see text for more details).

Location	Date	Lon.	Lat.	I_0	M_w	SD	R_{ep}	$I_{Güevéjar}$	Mean PGA	PGA_{rock}	AF
Atarfe	1431/04/24	-3.74	37.24	IX	**6.7**	**0.5**	13.9	VII-IX	0.263	0.168 (±0.035)	1.6
Granada	1526/07/04	-3.57	37.18	VIII	5.4	0.4	8.6	VII-VIII	0.177	0.108 (±0.016)	1.6
Lisbon	1755/11/01	-10	36.5	XII	**8.5**	**0.3**	580	VI*	0.092	0.047 (±0.022)	2.0
Granada	1778/11/13	-3.6	37.2	VII	4.9	0.4	6.7	VI-VII	0.098	0.087 (±0.025)	1.1
Atarfe	1801/06/20	-3.68	37.22	VII	4.9	0.4	9.4	V-VI	0.073	0.067 (±0.017)	1.1
Pinos Puente	1806/10/27	-3.7	37.2	IX	6.0	0.3	15.5	VII-VIII	0.231	0.100 (±0.008)	2.3
Granada	1822/07/29	-3.6	37.2	VII	4.9	0.4	6.7	VI-VII	0.098	0.087 (±0.025)	1.1
Granada	1826/05/15	-3.6	37.2	VII	4.9	0.4	6.7	VI-VII	0.098	0.087 (±0.025)	1.1
Güéjar	1863//04/17	-3.6	37.12	VII	4.9	0.4	6.7	VI-VII	0.098	0.087 (±0.025)	1.1
Arenas del Rey	1884/12/25	-3.98	36.95	X	**6.5**	**0.3**	50	VII*	0.149	0.043 (±0.005)	3.4
Adra	1910/06/16	-3.08	36.58	VIII	**6.7**	**0.4**	88	VI*	0.082	0.029 (±0.004)	2.9
Santa Fe	1911/05/31	-3.7	37.2	VIII	5.4	0.4	14.3	V-VI*	0.069	0.068 (±0.008)	1.0
Atarfe	1918/04/28	-3.68	37.22	VII	4.9	0.4	9.8	V-VI	0.071	0.064 (±0.016)	1.1
Arenas del Rey	1954/01/08	-3.88	36.9	VIII	**5.2**	**0.4**	44.8	III-IV	0.014	0.011 (±0.003)	1.3
Albolote	1956/04/19	-3.69	37.19	VIII	**4.9**	**0.3**	13.6	VI-VII*	0.124	0.046 (±0.010)	2.7
Otura	1964/09/09	-3.62	37.09	VII	**4.3**	-	19.5	IV-V	0.032	0.011 (±0.001)	2.8

7.3. The Güevéjar landslide

7.3.1. Local geology and geotechnical investigations

The Güevéjar landslide extends between the Güevéjar and Nívar villages, northwest of the "Cerro del Castillejo" (Fig. 7-2). The sediments outcropping in the landslide area are from bottom to top: a) lignite-bearing marls (upper Turolian); b) clays, silts and conglomerates (Pliocene); c) marls and oncolitic limestones (Pleistocene); d) travertines (Pleistocene). The materials affected by the landslide are mainly the lignite-bearing marls and the clays, silts and conglomerates. The lignite-bearing marls are gray-green color and include abundant organic matter beds with black clays and lignite. The clays, silts and conglomerates are reddish detrital sediments related to distal facies of alluvial fan deposits. The contact between these two soils is aproximately horizontal and is located at about 890 m above sea level. The thickness of the displaced materials and the position of the main failure surfaces have been determined based on field surveys and previous works (Sanz Pérez, 1992; Jiménez Pintor, 2006; Jiménez Pintor and Azor, 2006).

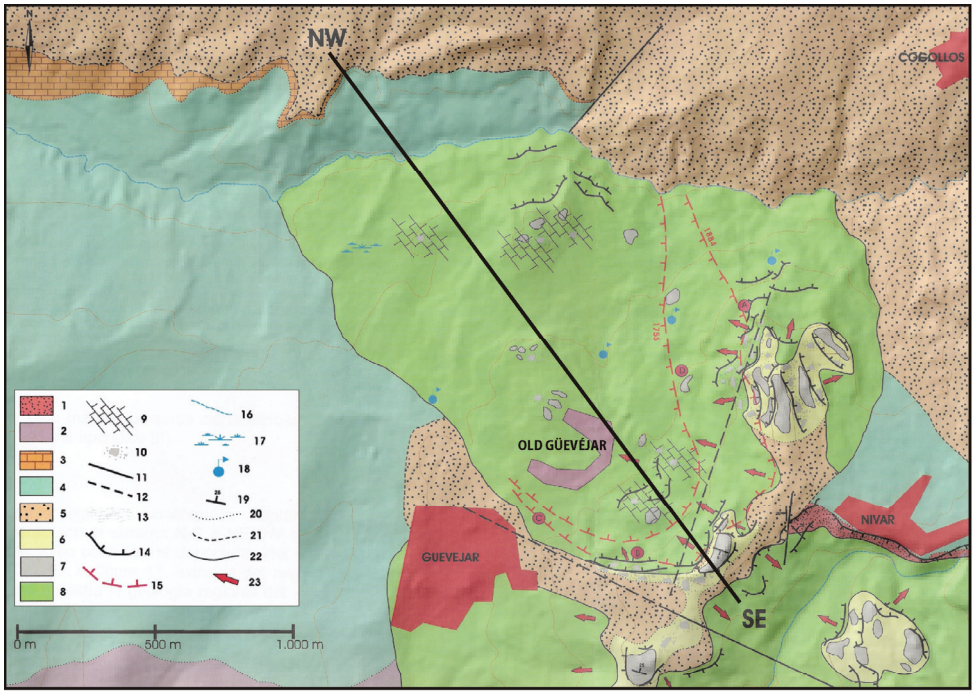

1: Grey marls, silts and sands; 2: Gypsums and marls; 3:Limestones and argillaceous limestones with gasteropods; 4: Lignite-bearing marls; 5: Clays, silts and conglomerates; 6: Marls and oncolitic limestones; 7: Travertines; 8: Landslide deposits; 9: Landslide deposits with prevalence of limestones and argillaceous limestones with gasteropods; 10: Limestone sliding blocks. 11: Fault; 12: Supposed fault; 13: Joints; 14: Scarps; 15: Main scarps during 1755 and 1884 earthquakes; 16: Bermejo river; 17: Endorreic areas; 18: Springs; 19: Strike and dip; 20: Normal contact; 21:Discordant contact; 22: Landslide limits; 23: Landslide movement direction.

Figure 7-2. Detailed geological map of the Güevéjar landslide and sorrrounding area (modified from Jiménez Pintor and Azor, 2006).

The mechanical behaviour of the materials that composed the Güevéjar landslide has been determined through a number of laboratory tests on samples taken from the landslide area: unsaturated and saturated unit weight determination (AENOR, 1994a), specific gravity determination (AENOR, 1994b), Atterberg limits determination (AENOR, 1993, 1994c), engineering classification of soils (ASTM, 2000), direct shear test of soils under unconsolidated undrained (UU) and consolidated drained (CD) conditions (AENOR, 1998). We have also performed some in situ tests using N-type Schmidt hammer and determining the Joint Roughness Coefficient (JRC) to estimate the shear strength parameters of the travertines. Table 7-2 shows the main representative geotechnical properties obtained from these tests. Within the slope, we have found that the potential sliding surface was developed inside the lignite-bearing marls and the clays, silts and conglomerates. These are high and low plasticity soils, respectively (Table 7-2). The shear strength parameters obtained for these materials are similar to the values derived for similar low- and high-plasticity Neogene marly and silty soils in the Granada Basin (El Amrani Paaza et al., 1998, 2000; Azañón et al., 2009). These authors obtained residual friction angles for the high-plasticity soils resulting in values between 6º and 12º which are slightly lesser than our results. In the case of the low-plasticity soils, the average friction angle is between 17º and 31º which is a range of values coherent with our results. However, the estimated cohesion values in both cases are lesser than our estimations with values ranging from 3 to 11 kPa for the low-plasticity soils and from 8 to 26 kPa for the high-plasticity soils.

Table 7-2. Summary of geotechnical data of materials in the Güevéjar landslide. γ, Unsaturated unit weight; γ_{sat}, Saturated unit weight; γ_{solid}, Unit weight of the solid particles; LL, Liquid Limit; PI, Plasticity Index; c, Cohesion; ϕ, Residual friction angle.

Material	γ (kN/m^3)	γ_{sat} (kN/m^3)	γ_{solid} (kN/m^3)	LL (%)	PI (%)	c (kPa)	ϕ (º)	USCS class
Travertines	24.39	25.18	27.00	-	-	4	29	Rock
Marls and oncolitic limestones	14.90	18.22	24.08	-	-	0	41	SM
Clays, silts and conglomerates	18.75	21.14	28.10	36.75	16.04	51.69	22	CL
Lignite-bearing marls	20.70	20.89	23.86	51.20	25.67	43.33	15	CH
Landslide deposits	19.80	21.31	26.18	33.10	13.44	27.38	25	CL

7.3.2. Earthquake-triggering history of the landslide

Following the historical chronicles, the Güevejar lanslide was first triggered by the 1755 Lisbon earthquake and was reactivated 129 years later by the 1884 Arenas del Rey earthquake. The old Güevéjar village, which was located on the landslide mass, was destroyed by the landslide movement in both events but it was reconstructed in 1887 at its current location outside the landslide body. Despite there are no written evidences of the occurrence of landsliding before the 1755 earthquake, it is possible that the Güevéjar landslide was developed in an old landslide. During the period between the 1755 Lisbon and 1884 Arenas del Rey earthquakes, the landslide

seems to be stable despite some relevant earthquakes have occurred (e.g. 1806 Pinos Puente eathquake).

7.3.2.1. 1st November 1755 Lisbon Earthquake

The 1st November 1755 Lisbon earthquake is one of the largest earthquakes known to have happened in the world with an estimated maximum intensity (EMS-98) of XI-XII (Martínez Solares and López Arroyo, 2004). It caused a huge impact at that time, as it produced several thousand victims in Portugal, Spain and North Africa, as well as high economic losses. One of the most significant effects of this earthquake was a strong tsunami which swept the Atlantic coast of the Iberian Peninsula and North Africa. The 1755 Lisbon earthquake also caused some hydrogeological and slope failure effects (Martínez Solares and López Arroyo, 2004). The hydrogeological effects were a raise of the water level of wells and changes or temporary interruption of the springs flows. The slope failure effects observed were minor cracks, small rock falls, landslides and some liquefaction phenomena. The only known evidence of a landslide took place in the village of Güevéjar (Granada, south Spain). According to the ESI-2007 Macroseismic Scale (Michetti et al., 2007) based only on environmental effects, we have estimated a maximum intensity of I_{ESI}=XI-XII for the 1755 Lisbon earthquake, which is coherent with the intensity assigned to this earthquake using the European Macroseismic Scale (Table 7-1).

The epicentral location of the 1755 Lisbon earthquake has been widely discussed and proposed sources are located over a large area at SW of Cape San Vicente (cf. Reid, 1914; Machado, 1966; Johnston, 1996; Baptista et al., 1998; Martínez Solares and Mezcua, 2002; Martínez Solares and López Arroyo, 2004; Gutscher et al., 2006; Grandin et al., 2007; Barkan et al., 2009). Considering all the different locations (Fig. 7-3), the epicentral distance to the Güevéjar landslide ranges from 460 to 725 km.

The estimated magnitude is also heavily debated by different authors ranging from 8.5 to 9.0. Johnston (1996) proposed M_w 8.7 (±0.4) with the epicentre located about 690 km from the Güevéjar landslide based on isoseismal lines calibrated with the macroseismic field of the 28 February 1969 earthquake. More recently, Martínez Solares and López Arroyo (2004) use the methodology used by Johnston (1996) together with a more accurate intensity map (Fig. 7-3) and a different approach to extrapolate offshore isoseismal areas, leading to the value of M_w 8.5 (±0.3) at an epicentral distance from the Güevéjar landslide of about 580 km. However, Mezcua et al. (2004) performed a reevaluation of historical earthquakes in Spain and proposed a value of M_w 8.7 (-0.3,+0.2) at an epicentral distance to the Güevéjar landslide of 725 km.

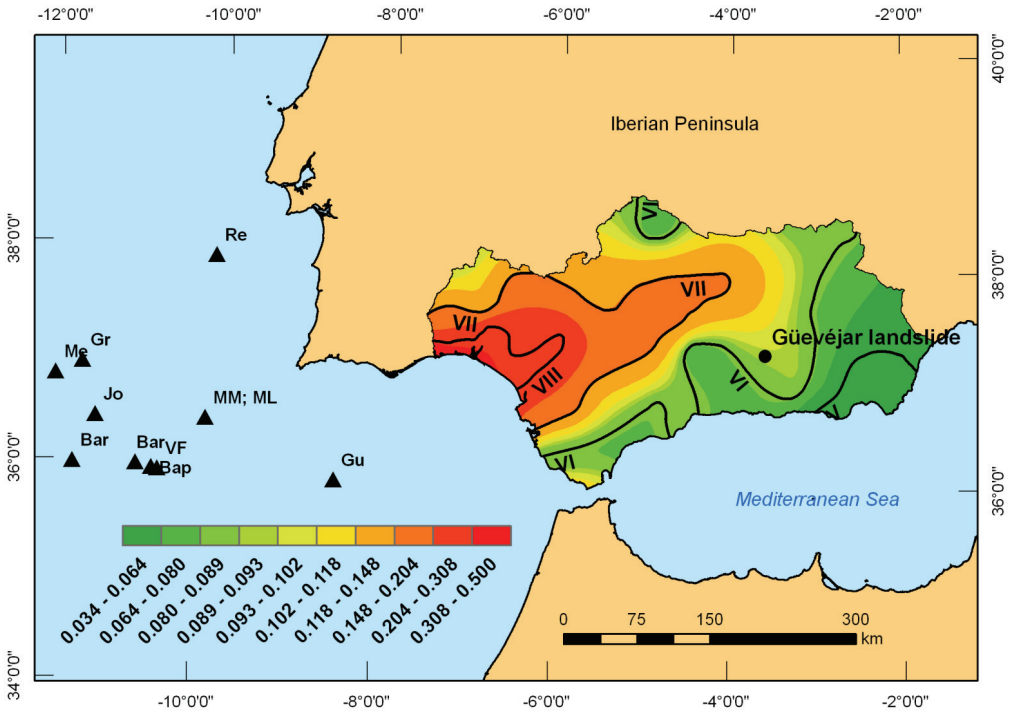

Figure 7-3. Peak Ground Acceleration (g units) isolines corresponding to the 1755 Lisbon earthquake at the Andalusian Autonomus Community (S Spain). The black lines are the isoseismal of the macroseismic intensity map of the 1755 Lisbon earthquake (modified from Martínez Solares and López Arroyo, 2004). The triangles are the different epicentres proposed by diferent authors. Re: Reid (1914), Jo: Johnston (1992), Bap: Baptista et al. (1998), MM: Martínez Solares and Mezcua (2002), ML: Martínez Solares and López Arroyo (2004), Gu: Gutscher et al. (2006), Gr: Grandin et al. (2007), Bar: Barkan et al. (2009).

7.3.2.2. 25th December 1884 Arenas del Rey Earthquake

The 25th December 1884 Arenas del Rey earthquake was the last large one felt in the Iberian Peninsula with a epicentral intensity (EMS-98) of X (Muñoz and Udías, 1981), causing widespread material and personal damage in villages around the Granada and Málaga provinces (South Spain). For this earthquake there are a lot of detailed historical data, especially in the reports of the three main commissions established for its study: Spanish, French and Italian. Moreover, there are more recent studies which complete the information with additional historical records, field observations and environmental effects (Muñoz and Udías, 1981). Drawings and photographs of the damage are also available. This information was used by Vidal (1986) to obtain a more accurate isoseismal map at the epicentral area (Fig. 7-4). The high density of sites with macroseismic data allows a good definition of the isoseismal lines.

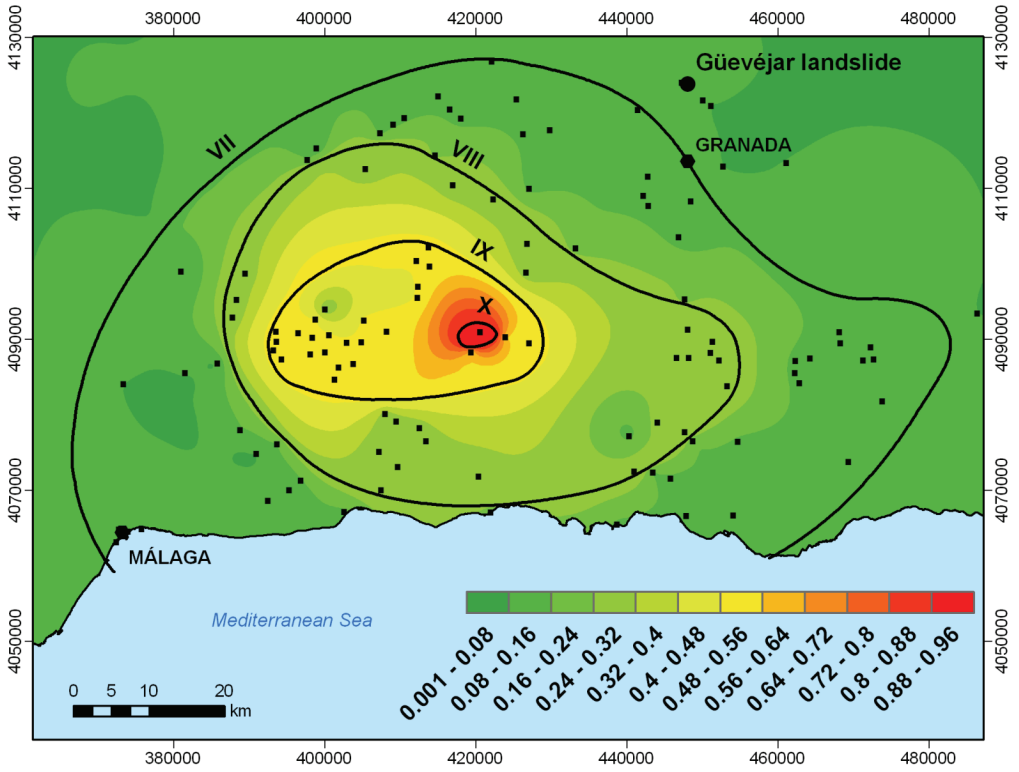

Figure 7-4. Peak Ground Acceleration (g units) isolines corresponding to the 1884 Arenas del Rey earthquake (S Spain). The black lines are the isoseismal of the macroseismic intensity map of the 1884 Arenas del Rey earthquake (modified from Vidal, 1986).

The 1884 Arenas del Rey earthquake seriously damaged several towns in the Granada Basin (Arenas del Rey, Zafarraya, Ventas de Zafarraya and Alhama de Granada, among many others). In addition, it caused a lot of hydrogeological and slope failure effects. The hydrogeological effects comprise the increase of the water level of wells and changes of the springs flows. The slope failure effects observed were important slope instabilities, such as the Güevéjar landslide, rock falls and rock avalanches produced in Alhama de Granada and Albuñuelas towns, and some liquefaction phenomena (Muñoz and Udías, 1981; IGME and Diputación de Granada, 2007). According to ESI-2007 Macroseismic Scale, the epicentral intensity of 1884 Arenas del Rey can be quoted as much as I_{ESI}=X which is coherent with the intensity assigned to this earthquake using the European Macroseismic Scale (Table 7-1).

The earthquake epicentre was located southwest of the Granada Basin at about 41 to 55 km from Güevéjar landslide, close to the Arenas del Rey village (Taramelli and Mercalli, 1886; Udías and Muñoz, 1979; Muñoz and Udías, 1981; Martínez Solares and Mezcua, 2002; Mezcua et al., 2004). The estimated magnitudes for this event range between 6.5 to 6.8 (Muñoz and Udías, 1981; Martínez Solares and Mezcua, 2002). Recent paleoseismological studies concluded that the 1884 earthquake

was related to the rupture of the Ventas de Zafarraya Fault and have a magnitude of M_w 6.5 (±0.3) (Reicherter et al., 2003). More recently, the reevaluation of historical earthquakes performed by Mezcua et al. (2004) proposed a value of M_w 6.5 (-0.3,+0.2).

7.3.3. Geomorphological features of the landslide

The geometry of the Güevéjar landslide during the 1755 Lisbon and 1884 Arenas del Rey earthquakes is described in Table 7-3, following the nomenclature for landslides suggested by IAEG Commission on landslides (1990). The average depth of the failure surface during the 1775 Lisbon earthquake was approximately 38 m and the surface area was 1,420,904 m^2. The mean volume of the 1755 landslide material may then be roughly estimated at 54 hm^3. In the case of the 1884 Arenas del Rey earthquake, the average depth of the failure surface was approximately 40 m and the surface area was 1,755,704 m^2. The estimated mean volume of the 1884 landslide was 70 hm^3. The volume of landslides can also be estimated by means of empirical equations relating the landslide volume to geometrical features of landslides, mainly the landslide area. Recently, Guzzeti et al. (2009) have developed an area-volume empirical relationship from a worldwide catalogue of landslides. These authors consider that the relationship is largely geometrical, and not influenced significantly by geomorphological or mechanical properties of the failed soils or rocks, or the landslide types. For this reason, this area-volume relationship have been used to obtain an additional estimate of the Güevéjar landslide volume during the 1755 and 1884 earthquakes. The obtained mean volumes are 62 hm^3 (55-70 hm^3) and 84 hm^3 (74-95 hm^3) for the 1755 and 1884 landslides, respectively. These mean values are slightly larger than the ones estimated above, but the minimum volumes are the same order of magnitude.

Table 7-3. Main geomorphological parameters of the Güevéjar landslide during the 1755 Lisbon and 1884 Arenas del Rey earthquakes.

	1755	**1884**
Total length	L = 1600 m	L = 1750 m
Length of the displaced mass	L_d = 1596 m	L_d = 1625 m
Length of the rupture surface	L_r = 1350 m	L_r = 1525 m
Width of the displaced mass	W_d = 1230 m	W_d = 1315 m
Width of the rupture mass	W_r = 680 m	W_r = 938 m
Depth of the displaced mass	D_d = 58 m	D_d = 82 m
Depth of the rupture surface	D_r = 58 m	D_r = 65 m
Total height (the height from the crown to the tip of toe)	ΔH = 217 m	ΔH = 227 m
Perimeter	P = 4943 m	P = 5468 m
Total area	A = 1 420 904 m^2	A = 1 755 704 m^2

7.4. Stability back-analysis and estimation of earthquake parameters

The fact that the Güevéjar landslide moved during the 1755 Lisbon and 1884 Arenas del Rey earthquakes let us to perform a slope stability back-analysis in order to estimate parameters related to the size and location of these earthquakes. In addition, other significant earthquakes ocurred in the Granada Basin, which did not move the landslide, can also be useful to provide additional indications about its seismic characteristics, particularly on the local intensity felt (e.g., 1806 Pinos Puente earthquake). The main aim of the stability back-analysis is to estimate the static safety factor (SF) of the slope prior to the ocurrence of the earthquake, and from this SF value obtain the minimum seismic acceleration required to trigger the landslide. Then, the minimum magnitude and epicentral location of historical earthquakes can be estimated using this critical acceleration value together with ground motion predictive equations (GMPEs).

7.4.1. Stability back-analysis

The first step to perform the stability back-analysis was the reconstruction of the topography of the slope before the earthquakes based on a 10 x 10 m grid-size digital elevation model (DEM) of the Güevéjar landslide area. Pre-1755 topography was reconstructed subtracting the contour lines of the total landslide area and interpolating a new DEM by means of a geografic information system (GIS). We have considered that the pre-1884 topography is similar to the pre-1755 topography at the scale of the model and the results will not be affected too much. This assumption agrees with the historical observation that the Güevéjar landslide had a small total displacement (about 4 m) during the 1755 Lisbon earthquake (Table 7-3). The longitudinal profiles of the landslide corresponding to the 1755, 1884 and present-day situation have been derived from these new topographic maps (Fig. 7-5, 7-7 and 7-9). The geotechnical model of these slopes has been performed based on the results of the geotechnical investigations carried out on the materials that composed the Güevéjar landslide. Residual shear strength parameters have been used in all the slope models. From a hydrogeological point of view, a shallow water table have been fitted in all the slope models because of the written evidence of increases in the water level of wells and springs flows during the occurrence of 1755 and 1884 earthquakes. This assumption is also in agreement with the present-day situation, with a very shallow water table (3-4 m depth) and several springs in the central part of the landslide (Jiménez Pintor, 2006; Jiménez Pintor and Azor, 2006).

In order to consider in the stability analysis the ground motion related to the ocurrence of each earthquake at the Güevéjar landslide location, the peak ground acceleration (PGA) was estimated from macroseismic intensity values. In the case of historical earthquakes, the macroseismic intensity is the only known seismic parameter which could be used to estimate the PGA. The intensity values at the Güevéjar landslide location have been extracted for the avalaible isoseismal maps

corresponding to the historical earthquakes. For some earthquakes, it does not exist enough data to make a macroseismic map but the epicentral intensity values are well known. In these cases, the intensity values at the Güevéjar landslide location have been estimated using the intensity attenuation laws proposed by López Casado et al. (2000) for the Iberian Peninsula. These authors considered a very high attenuation for the Granada Basin. A few studies deal with the relationships between intensity and PGA values and the majority has been published for the western USA (Neuman, 1954; Gutenberg and Richter, 1956; Trifunac and Brady, 1975; Murphy and O'Brien, 1977; Wald et al., 1999; Boatwright et al., 2001). In Italy, relationships between the macroseismic data and PGA records have been proposed among others by Margottini et al. (1992), Panza et al. (1997) and by Faccioli and Cauzzi (2006). In Spain, the correlation equation is in the Spanish Building Code (NCSE-02, 2002), but it is an adaptation of a foreign relationship (Medvedev and Sponheuer, 1969). For this reason, the average values of PGA corresponding to the ocurrence of the historical earthquakes have been estimated using the Margottini et al. (1992) relationship:

$$\log PGA = -2.634 + 0.258 \cdot I$$

where *PGA* values are in acceleration of gravity units (1g=9.81 m/s^2) and the local intensity (*I*) is in the EMS-98 intensity scale. This equation has been developed using the accelerometer and intensity databases of Italy which has a similar seismotectonic context (the European-African plate boundary) and type of buildings than to Spain. The dataset consisted of 56 records derived from nine Italian earthquakes that occurred between 1980 and 1990. The correlation coefficient for this equation is R=0.70 and the standar deviation is σ=0.21. In addition, the PGA values predicted by the Margottini et al. (1992) relationship are similar to the PGA values estimated from the I-PGA relationship for the Mediterranean zone:

$$\log PGA = -2.757 + 0.277 \cdot I$$

This correlation has been obtained by regression analysis of the average values drawn from a number of relationships published in the literature (Medvedev and Sponheuer, 1969; Ambraseys, 1974; Murphy and O'Brien, 1977; Chiaruttini and Siro, 1981; Margottini et al., 1992; Theodulidis ans Papazachos, 1992; Decanini et al., 1995; Koliopoulos et al., 1998; NCSE-02, 2002; Faccioli and Cauzzi, 2006; Tselentis and Danciu, 2008).

The geometry and location of the failure surfaces corresponding to the 1755, 1884 and present-day Güevéjar landslide were fixed by means of different control points and analysing the slope surface geometry (Fig. 7-5, 7-7 and 7-9). For each case, the main scarp and toe location have been set from the field observations and previous studies (Sanz Pérez, 1992; Jiménez Pintor, 2006; Jiménez Pintor and Azor, 2006). The possible slip surfaces which fit the location of these control points were obtained using a 2D slope stability software (Slide, Rocscience Inc., 2003) and the Morgenstern-Price limit equilibrium method. The most likely failure surface was selected considering that

the landslide must be stable before the earthquake and unstable after the earthquake. Hence, the safety factors after each earthquake have been estimated applying the horizontal PGA values obtained using the Margottini et al. (1992) relationship. The static safety factor previous to each earthquake have been obtained removing the seismic acceleration. Then, the minimum seismic acceleration required for overcoming the shear resistance and initiating the displacement of the landslide is calculated by the equation (Newmark, 1965):

$$a_c = (SF - 1)\, g \sin \alpha$$

where a_c is the critical seismic acceleration (in gravity units, 1g=9.81 m/s^2), g is the gravity acceleration, SF is the static safety factor and α is the thrust angle. For rotational movement, Newmark (1965) showed that the thrust angle is the angle between the vertical and a line segment connecting the centre of gravity of the landslide mass and the centre of the slip circle.

7.4.2. Estimation of earthquake parameters

The most likely minimum magnitude and epicentral distance from Güevéjar landslide of potential earthquakes which PGA could be able to overcome the critical acceleration value –i.e. to trigger the landslide, have been obtained using different Ground Motion Prediction Equations (GMPEs). There are few studies that provide GMPEs for Spain (e.g., Martín et al., 1996; Cabañas et al., 1999; Cantavella et al., 2004). This is because the Spanish Strong Motion Network started operating in the 1980s (cf. Carreño et al., 1999). The available data set comprises very few earthquakes with magnitudes between 4.5 and 5.1 which are not representative for deriving strong motion regression models. Therefore, different GMPEs for the Mediterranean zone which correlate magnitude and distance have been selected from the literature to obtain an average PGA value from each earthquake at the Güevéjar landslide location (Table 7-1). Three main criteria have been considered to select these GMPEs: (1) that they are derived from statistically-significant data sets which comprise wide magnitude and distance ranges; (2) that they are widely used in European countries located in a similar seismotectonic context (the European-African plate boundary) and (3) the magnitude scale is in terms of M_w.

We have estimated the moment magnitude (M_w) of the main historical earthquakes which have been felt at the Güevéjar landslide location with an epicentral intensity larger than I_{EMS}=VII (Table 7-1). First, we have assumed M_w values provided by specific studies whenever available (e.g., Mezcua et al., 2004). For the rest, a mean M_w value have been estimated using different epicentral intensity to M_w relationships for Spain (Karnik, 1971; Rueda and Mezcua, 2001). For some cases where the magnitude m_b is known, the M_w was estimated using m_b to seismic moment (M_0) Nuttli (1985) relationships, and then M_0 to M_w through Hanks and Kanamori (1979) equation. Finally, the expression of Rueda and Mezcua (2002) for the Iberian Peninsula was used to convert m_{bLg} to M_w.

The average PGA values estimated using the selected GMPEs (Skarlatoudis et al., 2003; Ambraseys et al., 2005; Akkar and Bommer, 2007; Bindi et al., 2009) have been calculated based on rock conditions and not considering site effects (soil and topographical amplification). The seismic amplification at Güevéjar landslide for each earthquake have been estimated comparing the PGA values estimated using the macroseismic data, which include the site effects, with the PGA on rock values (Table 7-1).

7.5. Constraints on historical earthquakes based on the paleoseismic reconstruction of the Güevejar landslide

7.5.1. 1st November 1755 Lisbon Earthquake

The intensity values have been adopted from the most recent isoseismal map of the 1755 Lisbon earthquake provided by Martínez Solares and López Arroyo (2004). For this reason, we have also used the values of magnitude and epicentre location estimated by these authors (Table 7-1). The 1755 Lisbon earthquake was felt in Güevéjar with a intensity I_{EMS}=VI. According with this intensity value, an average horizontal PGA value of 0.092g has been estimated at the Güevéjar landslide location. Considering this PGA value, the safety factor under saturated condition was close to one (SF=0.92) (Fig. 7-5). This result is coherent with the historical observation that the 1755 landslide did not have much displacement (about 4 m). Removing the seismic acceleration effect, the static safety factor previous to the earthquake was 1.42. Hence, the Güevéjar landslide was stable before the 1755 Lisbon earthquake considering both saturated and unsaturated conditions. We have obtained a thrust angle of 12º and a critical acceleration under saturated condition of 0.087g.

The most likely magnitude-distance pairs of potential earthquakes which have been able to overcome the critical acceleration value for the 1755 Güevéjar landslide have been obtained using the GMPEs. First, the epicentral distances to Güevéjar landslide which could trigger the landslide was estimated considering the magnitude range proposed by different authors (M_w=8.2-8.9). Secondly, the minimum magnitude required to trigger the landslide corresponding to the epicentre location proposed by different authors have been evaluated. On the first estimation, the epicentral distances to Güevéjar landslide range between 300 and 2040 km. The only distance which matches with the possible epicentral locations is 580 km and is related to a M_w of 8.5 (Fig. 7-6). On the second calculation, the minimum magnitudes obtained considering different epicentral distances range between 8.4 and 8.6 but the most frequent value is M_w 8.5.

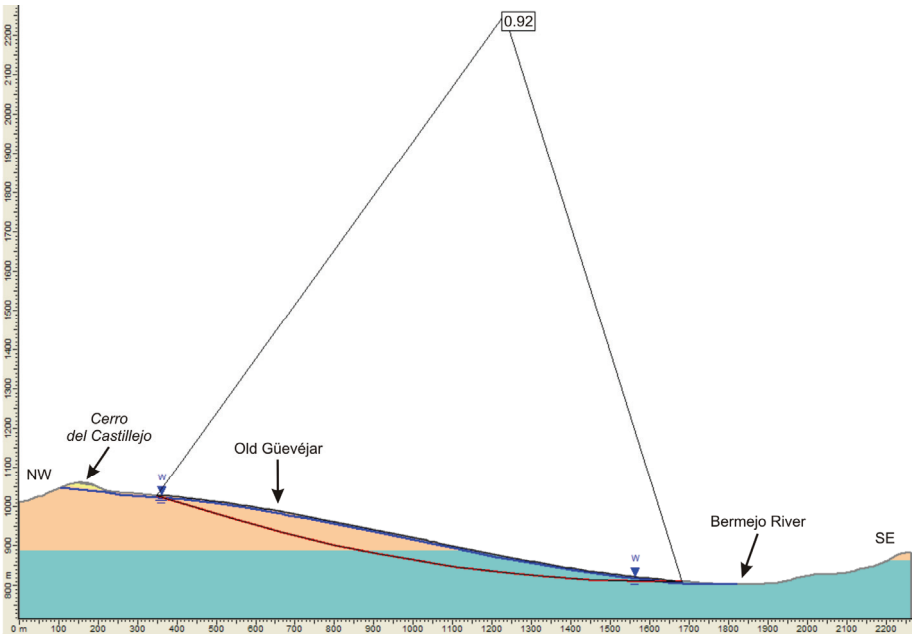

Figure 7-5. Cross-section and limit-equilibrium analysis of the Güevéjar landslide under saturated conditions during the 1755 Lisbon earthquake. Obtained safety factor is shown.

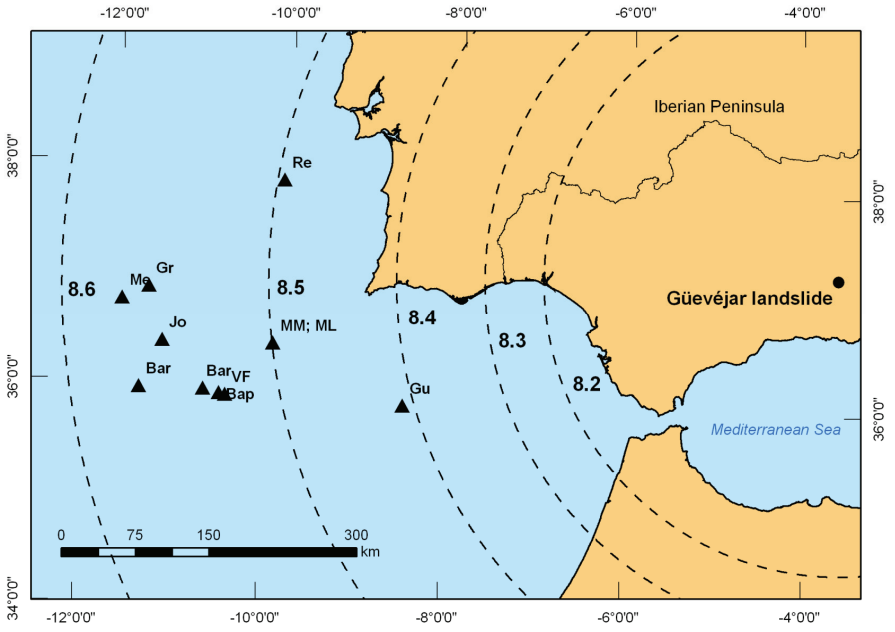

Figure 7-6. Comparison between the most likely moment magnitude and minimum epicentral distance pairs of potential earthquakes which could triggered the 1755 Güevéjar landslide and the epicentral location of the 1755 Lisbon earthquake proposed by different authors. Re: Reid (1914), Jo: Johnston (1992), Bap: Baptista et al. (1998), MM: Martínez Solares and Mezcua (2002), ML: Martínez Solares and López Arroyo (2004), Gu: Gutscher et al. (2006), Gr: Grandin et al. (2007), Bar: Barkan et al. (2009).

The estimated M_w 8.5 at 580 km from Güevéjar landslide agrees with the average values proposed by Martínez Solares and López Arroyo (2004). Therefore, we suggest that the epicentre of the 1775 Lisbon earthquake was located at the coordinates proposed by these authors (Table 7-1). The estimated magnitude values above must be interpreted as minimum ones which could triggered the landslide. Then, the magnitude of the 1775 Lisbon earthquake must be larger than M_w 8.5.

7.5.2. 25th December 1884 Arenas del Rey Earthquake

The 1884 Arenas del Rey earthquake was felt in Güevéjar with a intensity I_{EMS}=VII based on both Muñoz and Udías (1981) and Vidal (1986) isoseismal maps. An equivalent horizontal PGA value of 0.149g has been estimated at the Güevéjar landslide location (Table 7-1). Considering this PGA value, the safety factor under saturated condition was lower than the 1755 case (SF=0.79) (Fig. 7-7). This result is coherent with the fact that the 1884 landslide mass had more displacement. Removing the seismic acceleration, the static safety factor prior to the earthquake was 1.54. Hence, the landslide was also stable under aseismic and saturated conditions. The thrust angle obtained is 14º and the critical acceleration under saturated condition is 0.130g.

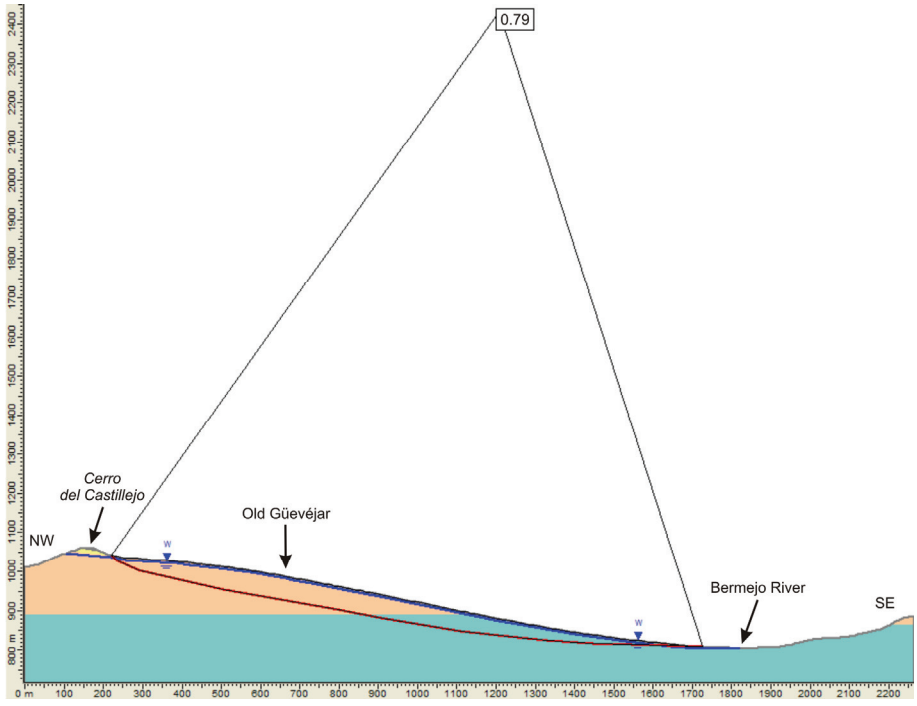

Figure 7-7. Cross-section and limit-equilibrium analysis of the Güevéjar landslide under saturated conditions during the 1884 Arenas del Rey earthquake. Obtained safety factor is shown.

The most likely magnitude-distance pairs of potential earthquakes which have been able to overcome the critical acceleration value for the 1884 Güevéjar landslide have been obtained using the different GMPEs (Table 7-4). Wells and Coppersmith (1994) relationships have been also used to estimate the length and width of the potential faults which could be related to the 1884 earthquake. The estimated epicentral distances to Güevéjar landslide corresponding to the possible magnitude range proposed by different authors (M_w=6.2-6.8) are between 43 and 72 km.

In this case, there is no match between the epicentral distance to Güevéjar landslide and the possible 1884 earthquake epicentral locations proposed by different authors (Fig. 7-8). However, the 1884 Arenas del Rey earthquake was probably related to the rupture of the Ventas de Zafarraya Fault (Reicherter at al., 2003). This normal fault is located around 55 km (50-60 km) from the Güevéjar landslide with a length of approximately 22 km (Fig. 7-8). The focal depth of the 1884 earthquake was between 10 and 20 km (Muñoz and Udías, 1981). Combining these data, we have found that the location of the Ventas de Zafarraya Fault matches with a magnitude of M_w 6.5 at an epicentral distance to Güevéjar landslide of 55 km (Table 7-4). Hence, we could confirm that the 1884 Arenas del Rey earthquake was likely related to the rupture of the Ventas de Zafarraya Fault with a minimum magnitude of M_w 6.5.

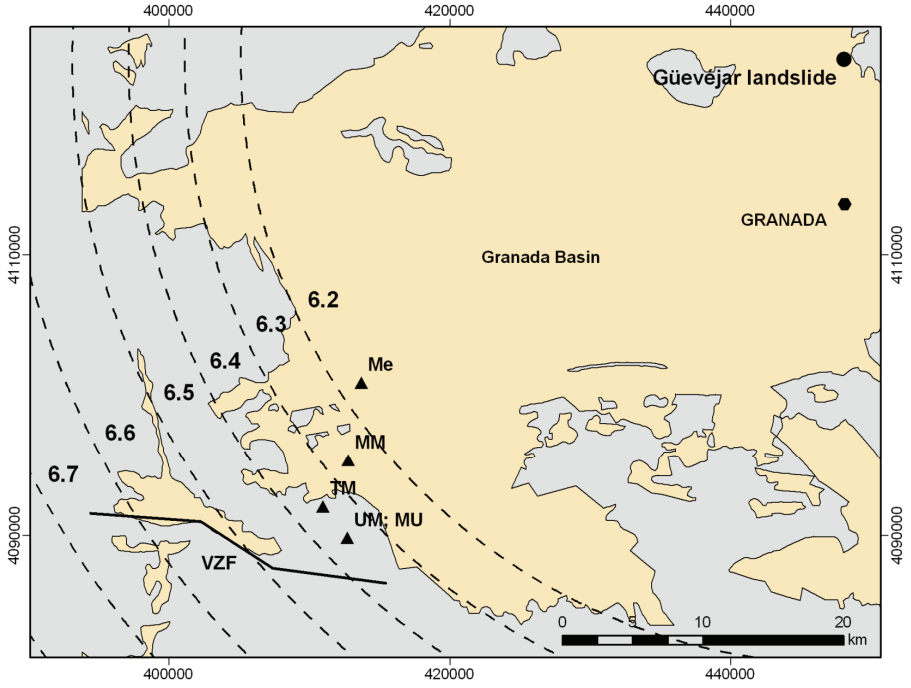

Figure 7-8. Comparison between the most likely moment magnitude and minimum epicentral distance pairs of potential earthquakes which could triggered the 1884 Güevéjar landslide and the epicentral location of the 1884 Arenas del Rey earthquake proposed by different authors. TM: Taramelli and Mercalli (1885), UM: Udías and Muñoz (1979), MU: Muñoz and Udías (1981), MM: Martínez Solares and Mezcua (2002), Me: Mezcua et al. (2004). VZF: Ventas de Zafarraya Fault.

Table 7-4. Most likely magnitude-distance pairs of potential earthquakes which could triggered the 1884 Güevéjar landslide. M_w: moment magnitude; R_{ep}: epicentral distance to Güevéjar landslide (km); SRL: surface rupture length (km); DRW: downdip rupture width (km).

M_w	R_{ep}	SRL	DRW
6.2	43	12.3 (±6.2)	10.7 (±3.0)
6.3	47	13.8 (±6.9)	11.6 (±3.3)
6.4	51	15.5 (±7.8)	12.6 (±3.5)
6.5	55	17.4 (±8.7)	13.7 (±3.8)
6.6	60	19.5 (±9.8)	14.8 (±4.1)
6.7	66	21.9 (±11.0)	16.0 (±4.5)
6.8	72	24.5 (±12.3)	17.4 (±4.9)

7.5.3. Other main historical earthquakes

Despite the only known triggering earthquakes were the 1755 Lisbon and 1884 Arenas del Rey earthquakes, the possible effects of other historical events on the stability of the Güevéjar landslide can help to verify the macroseismic data, which it is known that might be overestimated in some cases. The main historical earthquakes with an epicentral intensity greater than I_{EMS}=VII (Table 7-1) felt at the Güevéjar landslide location have been analysed. In most cases, the average PGA values estimated using the Intensity-PGA relationship are smaller than the critical accelerations obtained after the 1755 and 1884 earthquakes. In this situation, the safety factors remain stables and the reactivation of the Güevéjar landslide is not possible. This is in agreement with the fact that there is no historical evidence of this event occurred. Nevertheless, in the particular case of the 1806 Pinos Puente earthquake, the estimated PGA was 0.231g (Table 7-1). This value of PGA overcomes the critical acceleration value of 0.087g obtained after the 1755 Lisbon earthquake. In this situation, the safety factor is very unstable (SF=0.61) and the reactivation of the Güevéjar landslide is possible. One possible explanation is that the ground was not saturated during the 1806 Pinos Puente earthquake. Assuming this condition, a greater safety factor (SF=0.93) have been obtained but it still remains unstable. However, considering an intensity of I_{EMS}=VI at the Güevéjar landslide location, the estimated PGA is 0.080g and the safety factor under saturated condition is unstable (SF=0.91) but close to one. Considering dry conditions, the safety factor is stable (SF=1.42). In the second case the reactivation of the landslide is not possible. Assuming the second hypothesis, an epicentral intensity of VIII have been estimated by means of the intensity attenuation law proposed by López Casado et al. (2000) for the Granada Basin. For this reason, we suggest that the epicentral intensity of the 1806 Pinos Puente earthquake (I_0=IX) would be overestimated and a new value of I_0=VIII is proposed.

7.5.4. Constraints on the future reactivation of the Güevejar landslide

The future possible reactivation of the Güevéjar landslide have been evaluated considering the present-day topography and the 1884 failure surface. This is because there is no reactivation due to seismic activity since the 1884 Arenas del Rey earthquake (Fig. 7-9). The static safety factor obtained under saturated and unsaturated conditions are SF=2.66 and SF=4.00, respectively. Therefore, the present-day Güevéjar landslide is very stable in both dry and saturated conditions. However, ocurrence of small secondary landslides in the toe of the landslide seems possible. These slope instabilities are not further analyzed in this work. The thrust angle obtained is 8º and the critical acceleration under saturated conditions is 0.178g which is equivalent to a critical intensity of I_{EMS}=VII-VIII. This value is similar to the intensity grade caused by 1884 Arenas del Rey earthquake at Güevéjar landslide location. Since 1884 to date, no earthquakes with local intensity larger than VII have been felt at Güevéjar landslide location (Table 7-1), and so that they could not overcome the estimated critical intensity and acceleration values cited above. For this reason, we suggest that the Güevéjar landslide has not been reactivated by seismicity since the 1884 Arenas del Rey earthquake.

The likely magnitude-distance pairs of possible earthquakes which might reactivate the present-day Güevéjar landslide have been obtained using the different GMPEs. The maximum epicentral distance from Güevéjar landslide have been estimated considering moment magnitudes between 4.7 and 6.9 (Table 7-5). Wells and Coppersmith (1994) relationships have been also used to estimate the length and width of the potential faults which might reactivate the Güevéjar landslide (Table 7-6). The magnitudes values must be considered as the minimum ones, so the ocurrence of an earthquake with larger magnitude than estimated for each magnitude-distance pair might also reactivate the Güevéjar landslide (Fig. 7-10).

Table 7-5. Most likely magnitude-distance pairs of potential earthquakes which might overcome the critical acceleration at present-day Güevéjar landslide considering saturated conditions. M_w: moment magnitude; R_{ep}: epicentral distance to Güevéjar landslide (km); SRL: surface rupture length (km); DRW: downdip rupture width (km).

M_w	R_{ep}	SRL	DRW
4.7	1	-	-
4.9	6.5	-	-
5.2	9	3.9 (±2.0)	4.8 (±1.3)
5.6	13	6.2 (±3.1)	6.6 (±1.9)
6.0	17.5	9.8 (±4.9)	9.1 (±2.6)
6.5	25	17.4 (±8.7)	13.7 (±3.8)
6.6	26.5	19.5 (±9.8)	14.8 (±4.1)
6.7	28.5	21.9 (±11.0)	16.0 (±4.5)
6.9	33	27.5 (±13.8)	18.8 (±5.3)

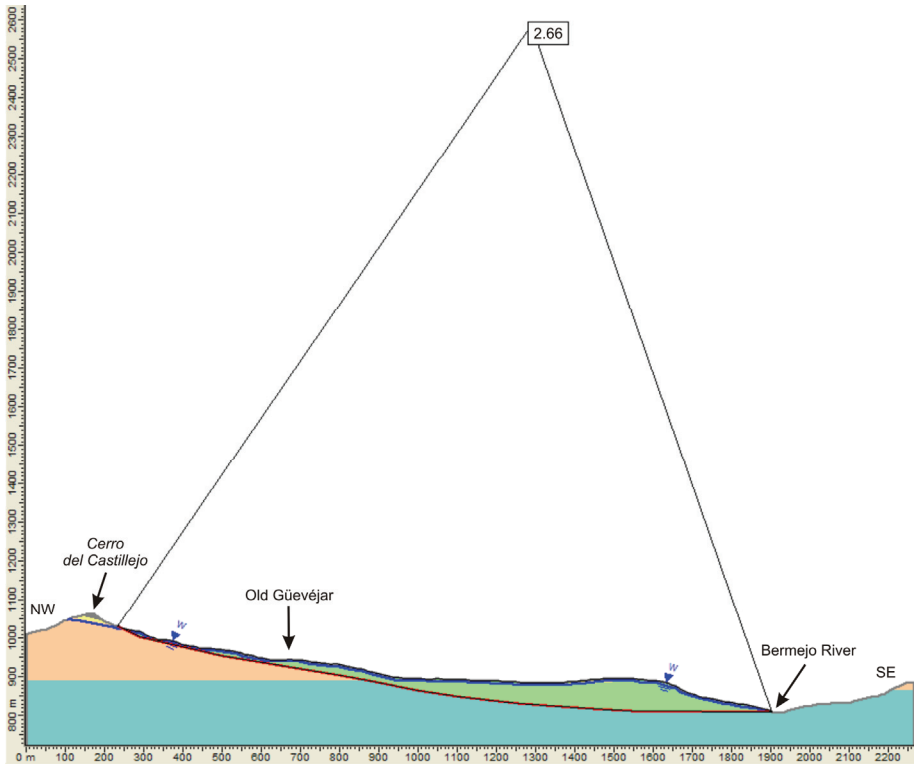

Figure 7-9. Cross-section and limit-equilibrium analysis of the present-day Güevéjar landslide under saturated conditions. Obtained static safety factor is also shown.

Table 7-6. Main active faults in the Granada Basin which might reactivate the Güevejar landslide and expected PGA for each one.*: moment magnitude values estimated by Sanz de Galdeano et al. (2003) considering the length and slip rate of the faults. R_{ep}: epicentral distance to Güevéjar landslide (km).

Fault	Maximum Length	Maximum M_w*	R_{ep}	PGA $_{rock}$	Expected PGA
Ventas de Zafarraya	22	6.9	55	0.055 (±0.008)	0.120 (±0.015)
Granada	17	6.6	10	0.202 (±0.043)	0.363 (±0.057)
Santa Fe	13	6.5	16	0.139 (±0.019)	0.261 (±0.009)
Atarfe	10	6.5	12	0.169 (±0.027)	0.321 (±0.024)

From these magnitude-distance pairs, the earthquakes with magnitudes greater than M_w=6.5 and a epicentral distance from Güevéjar landslide smaller than 25 km could most likely be associated with the rupture of one of the active faults in the Granada Basin. Based on the seismic hazard study developed by Sanz de Galdeano et al. (2003) for the main active faults in the Granada Basin, the faults with the major seismic potencial have been selected (Fig. 7-10) as the possible sources of the Güevejar landslide reactivation (Table 7-6). Each fault have been modelled considering the maximum surface fault length and following a characteristic

earthquake model (García-Mayordomo et al. 2007). The PGA associated to a complete rupture of these faults was calculated using different GMPEs for the Mediterranen zone and assuming earthquake epicentres locate along the fault traces, as fault planes are virtually vertical.

The PGA values have been estimated based on rock conditions and not considering site effects (soil and topographical amplication). For this reason, PGA on rock was multiplied by a seismic amplification factor to take into account site effects. A mean amplification factor of 1.9 (±0.3) have been obtained at the Güevéjar landslide location considering the values estimated from the historical earthquakes (Table 7-1). This factor is also coherent with the mean value of 2.0 (±0.4) obtained as result of comparing the soil classifications and amplification factors proposed by different Spanish and international codes: NCSE-2002 (2002), NEHRP (2003), Eurocode-8 (CEN, 2004) and SISMOSAN project (Benito et al., 2010).

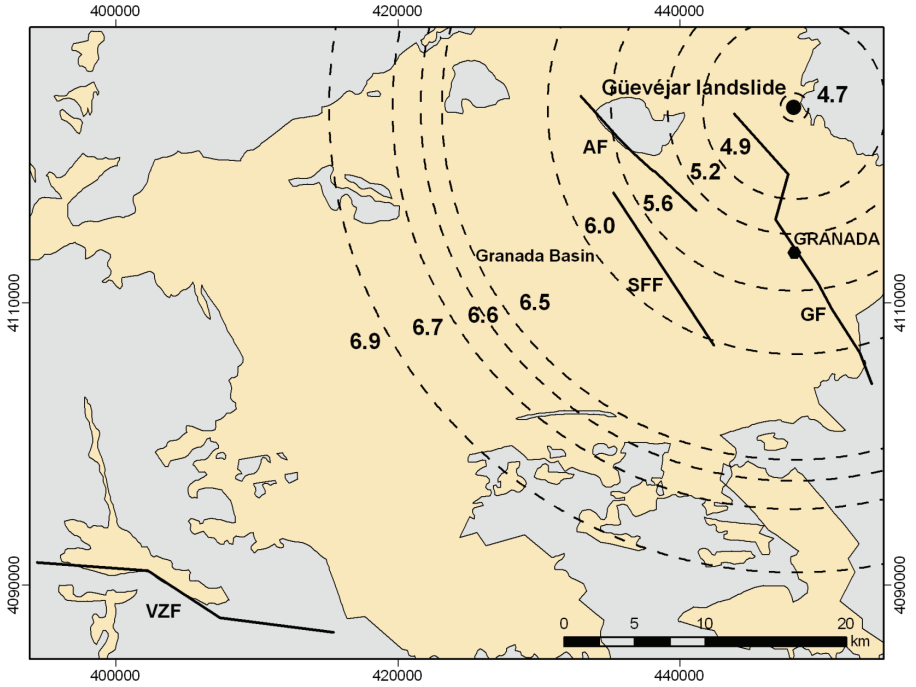

Figure 7-10. Most likely moment magnitude-epicentral distance pairs of potential earthquakes which might reactivate the present-day Güevéjar landslide and location of the main active faults with the major seismic potencial in the Granada Basin. VZF: Ventas de Zafarraya Fault, GF: Granada Fault, AF: Atarfe Fault, SSF: Santa Fe Fault.

The reactivation of the Güevéjar landslide is possible under dry conditions with the ocurrence of a great earthquake related to the complete rupture of the Granada and Atarfe faults (SF=0.76 and SF=0.84, respectively). In addition, it is also possible the landslide reactivation under saturated conditions with the complete rupture of the Santa Fe Fault (SF=0.64). By contrast, the Ventas de Zafarraya Fault will not be able

to reactivate again the Güevéjar landslide (SF=1.11). This fact is also shown clearly in the figure 7-10 since the Ventas de Zafarraya Fault is located further away from the maximum distance corresponding to an earthquake with moment magnitude of 6.9.

7.6. Discussion and conclusion

A new methodology has been developed to reassess the moment magnitude and epicentral location of historical earthquakes by means of the study of singular earthquake-triggered landslides. The slope back-analyses of the Güevéjar landslide using limit equilibrium methods have been found as an useful tool to improve the reliability of historical earthquake parameters and also to evaluate the potential hazard of future earthquake-triggered landslides in a seismically active region. Nevertheless, the results of the proposed methodology to reassess the moment magnitude and epicentral location of historical earthquakes comprise a range of errors and uncertainties, because the estimation methods are based on a variety of empirical data and theoretical assumptions. The first significant source of uncertainties is related to the shaking intensity values, both the epicentral as the local intensity felt in the Güevéjar landslide location. However, the abundant historical documentation and the high density of sites with macroseismic data allows a good definition of the epicentral and local intensity felt in the Güevéjar landslide corresponding to the 1755 and 1884 earthquakes. In addition, epicentral intensity values estimated using the recent ESI-2007 Macroseismic Scale are coherent with the intensity assigned to this earthquakes using the European Macroseismic Scale. In some cases, the intensity felt at the Güevéjar landslide was estimated using the López Casado et al. (2000) intensity attenuation law. However, this represents a good estimate of intensity for Iberian Peninsula because these authors reduced the modeling and statistical uncertainties selecting an attenuation equation which fit properly the data and also developed a good regionalization of the data. The second and most significant source of uncertainties is related to the Intensity-PGA empirical relationships. The maximum and minimum values of PGA predicted using the Margottini et al. (1992) equation comprise a wide range. However, the average PGA value could be considered a fairly estimate because it is coherent with the PGA obtained by means of the I-PGA relationship performed for the Mediterranean zone. Finally, the third source of uncertainties corresponds to the PGA values estimated by means of different ground motion prediction equations (GMPEs). These estimations would be improve when a proper relationship for Spain will be developed.

For the 1755 Lisbon earthquake our results agree with a minimum M_w 8.5 and an epicentral distance from the Güevéjar landslide of 580 km, and for the 1884 Arenas del Rey earthquake with a minimum M_w 6.5 and an epicentral distance from the Güevéjar landslide of 55 km. In the case of the 1806 Pinos Puente earthquake we have found that its epicentral intensity (I_{EMS}=IX) was probably overestimated and a new value of I_{EMS}=VIII is proposed. The moment magnitude and epicentral location obtained for the 1755 Lisbon and 1884 Arenas del Rey earthquakes has been

compared with the estimations performed by means of the Keefer (1994, 2002) empirical relationships and other authors estimations.

A comparison between our results and the estimations resulting from the use of Keefer (1994, 2002) empirical relationships highlights the fact that such correlations provide first order approximation. A M_w of 8.8 has been obtained for the 1755 earthquake by means of the magnitude-maximum distance correlation. This value was estimated considering a epicentral distance to the Güevéjar landslide of 460 km, which it is the only distance in the range of applicability of the relationship. This estimation of magnitude must be considered as a lower-bound value, so it might be slightly overestimated considering the range of magnitudes (M_w=8.6-8.8) corresponding to this epicentre location (Gutscher et al., 2006). In addition, a M_w of 7.1 has been obtained by means of the magnitude-total volume correlation considering the volume estimated for the 1755 landslide (see section 3.3.). This value is out of range of the possible magnitudes estimated by others authors for the 1755 Lisbon earthquake (M_w=8.2-8.9). In this case of the 1884 Arenas del Rey earthquake, a M_w range of 6.0-6.1 has been obtained considering the different epicentral distance to the Güevéjar landslide and the maximum distance-magnitude correlation. These minimum magnitudes are slightly smaller than the lower bound value estimated by other authors (M_w=6.2). Assuming the estimated volume for the 1884 landslide (see section 3.3.), a M_w of 7.2 have been obtained by means of the magnitude-total volume correlation. Similar to the 1755 case, this value is out of range of the possible magnitudes estimated by others authors for the 1884 earthquake.

Our results for the 1755 Lisbon earthquake agrees with the estimations proposed by Martínez Solares and López Arroyo (2004). The minimum magnitud of M_w of 8.5 is coherent with the average magnitude estimated for these authors. In addition, the epicentre location of the 1775 Lisbon earthquake proposed by Martínez Solares and López Arroyo (2004) are in agreement with the epicentral distance from the Güevéjar landslide that we have estimated (580 km). For the case of the 1884 Arenas del Rey earthquake, our estimation of a lower bound magnitude of M_w 6.5 agrees with the average moment magnitude proposed by others authors (Muñoz and Udías, 1981; Reicherter et al., 2003; Mezcua et al., 2004). Moreover, the epicentral distance from the Güevéjar landslide of 55 km confirms the Reicherter et al. (2003) proposal that the rupture of the Ventas de Zafarraya Fault was related to the 1884 Arenas del Rey earthquake.

Finally, the Güevéjar landslide is stable at present-day conditions even if a complete saturation of the slope is considered. The reactivation of the Güevéjar landslide is expected in case of moderate seismic events similar to the last ones occurred in the Granada Basin with M_w=4.7-5.6 (e.g. 1956 Albolote earthquake) but located at a epicentral distances between 1 to 13 km. In the case of a large earthquake (M_w=6.5-6.9) the longer requiered epicentral distance is 25 to 33 km. This earthquake could most likely be associated with one of the active faults in the Granada Basin, which can potentially generate earthquakes with magnitudes larger than M_w=6.5.

Hence, the active faults which could reactivate the Güevéjar landslide are the Granada, Atarfe and Santa Fe faults.

Acknowledgements

This study was supported by research project TOPOIBERIA CONSOLIDER-INGENIO2010 CSD2006-00041 of Spanish Ministry of Science and Innovation, research project MMA083/2007 of Spanish Ministry of Environment and research projects CGL2008-03249/BTE and FASE-GEO CGL2009-09726 of Spanish Ministry of Science and Innovation. We thank Mercedes Feriche from the Andalusian Geophysics Institute (Instituto Andaluz de Geofísica).

8

Effectiveness of deep drainage wells as a slope stabilization measure: The reactivation of the Diezma landslide (Southern Spain)

Martín Jesús Rodríguez-Peces [1], José Miguel Azañón [1,2], Julián García-Mayordomo [3], Emilia Troncoso [1,2]

[1] Departamento de Geodinámica, Universidad de Granada, Campus Fuentenueva s/n, 18071 Granada, Spain.
[2] Instituto Andaluz de Ciencias de la Tierra (UGR-CSIC), Granada, Spain.
[3] Instituto Geológico y Minero de España (IGME). C/La Calera, 1. 28760. Tres Cantos (Madrid), Spain.

Bulletin of Engineering Geology and the Environment
Submitted 24 June 2010.

ABSTRACT

In this paper, the effectiveness of slope stabilization measures, particularly deep drainage wells, have been analysed. A complete failure analysis of a complex landslide located in Southern Spain (the Diezma landslide) has been performed using detailed geotechnical, geophysical and geological data. The triggering factors were a shallow water table and the reduction of the shear strength parameters of the high-plasticity clay levels to residual values. The 2010 landslide reactivation was related to a bad performance of the first line of deep drainage wells. The second and third line of wells and the anchored piles barrier seem to work effectively by stopping the landslide from reaching the toe of the slope. However, the reactivation of the Diezma landslide is expected if all the drainage wells fail following a period of heavy rain, or in the case that an earthquake occurs close to the site.

Keywords: Betic Cordillera; Drainage wells; Landslides; Diezma; A-92 motorway; Newmark.

8.1. Introduction

A large number of landslides occur quite often during rainy seasons primarily owing to the development of substantial pore water pressure in a slope mass. Rain-induced failures are the most common to cause landslides. Different measures for controlling the occurrence of landslides are usually designed based on empirical criteria. There is a need to develop suitable models to examine the effectiveness of different stabilising techniques to be adopted or proposed. To prevent the occurrence of landslides, trench and wells are widely used for draining out water from the soil in order to reduce the pore water pressure and restore the stability of the hill slope. In marly and clayey soils, these drainage works are considered high yield solutions. However, the effectiveness of these stabilization measures cannot be validated over time by direct or indirect observations.

In this paper, the effectiveness of the stabilization measures, particularly deep drainage wells, have been analysed in a complex landslide affecting a motorway in SE Spain. A complete failure evolution of this instability, named as the Diezma landslide, has been performed considering different steps: 1) The slope before and after the A-92 motorway construction; 2) The slope during the 2001 Diezma landslide; 3) The slope after the stabilisation measures; 4) The slope at the 2010 reactivation; 5) Possible future reactivation. In all cases, the mechanism of slope failure was identified using detailed geotechnical, geophysical and geological data. The water and seismic activity are the main controlling factors required to trigger the landslide, but the water seems to be the most relevant. For this reason, the accurate performance of deep drainage wells is a major concern for the stability of this type of landslide through time.

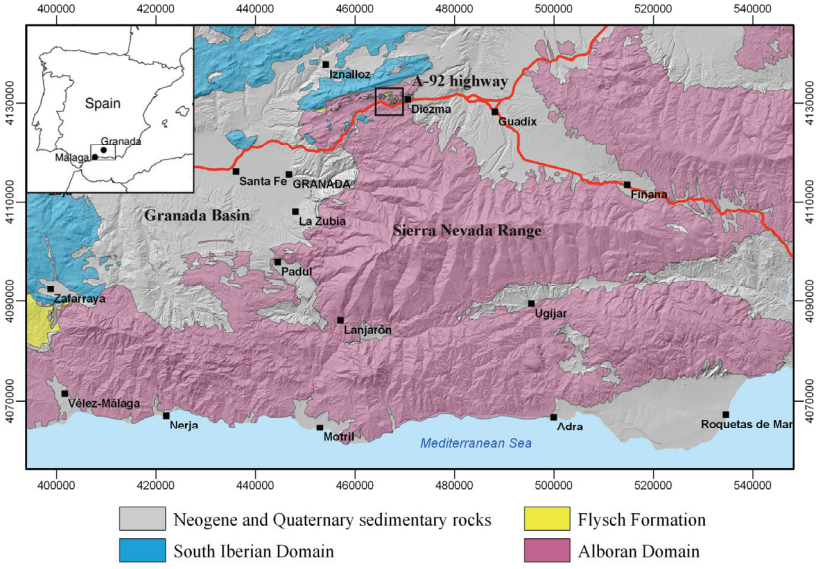

Figure 8-1. Simplified geological sketch of the central part of the Betic Cordillera (South Spain). The location of the Diezma landslide is marked with a rectangle.

8.2. Diezma landslide description

The Diezma landslide is located in the north of the Sierra Nevada Range (Betic Cordillera, Southern Spain), close to the village of Diezma (Fig. 8-1). The landslide mass comprise high- to moderate-plasticity clays, silts and marls containing embedded limestone and dolostone blocks. These lithologies were part of a Flysch-type formation, which represents a turbiditic sequence of Cretaceous-Lower Miocene age (Bourgois et al. 1974). This Flysch formation shows a chaotic appearance because it was intensively deformed during the Alpine orogeny. In the Diezma area, the Flysch formation is structurally superposed over rocks belonging to the Alboran Domain. These rocks are shales, phyllites, sandstones and conglomerates of the Malaguide Complex. The South Iberian Domain is made up of Upper Jurassic limestones and dolostones belonging to the Subbetic Zone, which thrust onto the Malaguide Complex (Alboran Domain). These carbonate rocks outcrop just to the north of the Diezma landslide constituting an unconfined karstic aquifer that drains an abundance of water to the south, very close to the head of the landslide. Moreover, there are some significant springs located at the contact surface between the carbonate rocks and the low-permeability soils related to the slide. Therefore, the water table is commonly shallow after a period of heavy rains.

The Diezma landslide took place on 18 March 2001 following a period with a high rate of precipitation. It produced significant damage on the Sevilla-Almería motorway (A-92) which was closed for several days because its cut-face completely collapsed (Fig. 8-2). The stabilization of the Diezma landslide began immediately after it took place. The stabilization works were performed by means of the smoothing of the topography, surface drainage systems, deep drainage wells and the construction of a barrier of anchored piles (Oteo, 2001, 2003). However, the Diezma landslide was partially reactivated because of the heavy rainfalls recorded during the winter of December 2009-February 2010.

The Diezma landslide is a complex movement that covers an area of 7.76 ha, with a maximum length of 510 m and maximum width of 205 m (Fig. 8-3). The landslide volume is approximately 1.2 hm^3, with an average thickness of 20 m. From field observations, the landslide body can be divided into three different parts: the head, the intermediate and the toe zones. The head area is located very close to the old Granada-Almería road (CN-342) where several metre-scale scarps were observed. The main scarp corresponding to the 2010 reactivation of the Diezma landslide is located approximately 50 metres to the north of this road which partially collapsed (Fig. 8-3). The intermediate part of the landslide is related to the occurrence of lateral spreading and some secondary scarps that produce some ponds and bulges with tension cracks at the crests (Azañón et al. 2009). In addition, many decimetre-scale lateral cracks with the same trend as the mass movement have damaged the intermediate road built during the slope restoration works. At the toe sector, the thickness of mass movement is greater in the central area (about 30 m) and the main cracks are opened obliquely to the direction of the slide. These cracks can be interpreted as the scarp related to the

first failure surface of the slope. The lower half of the toe corresponds to the accumulation zone of an earth flow that partially covered the A-92 motorway. All observed scarps at the three zones described above are related to rotational landslides developed successively in the clay-rich soils from the Flysch formation. These low-permeability soils have also favoured the development of ponds at the head and intermediate zones of the landslide.

Figure 8-2. Panoramic view of the toe of the Diezma landslide during the 2001 collapse over the A-92 motorway, which was closed for several days.

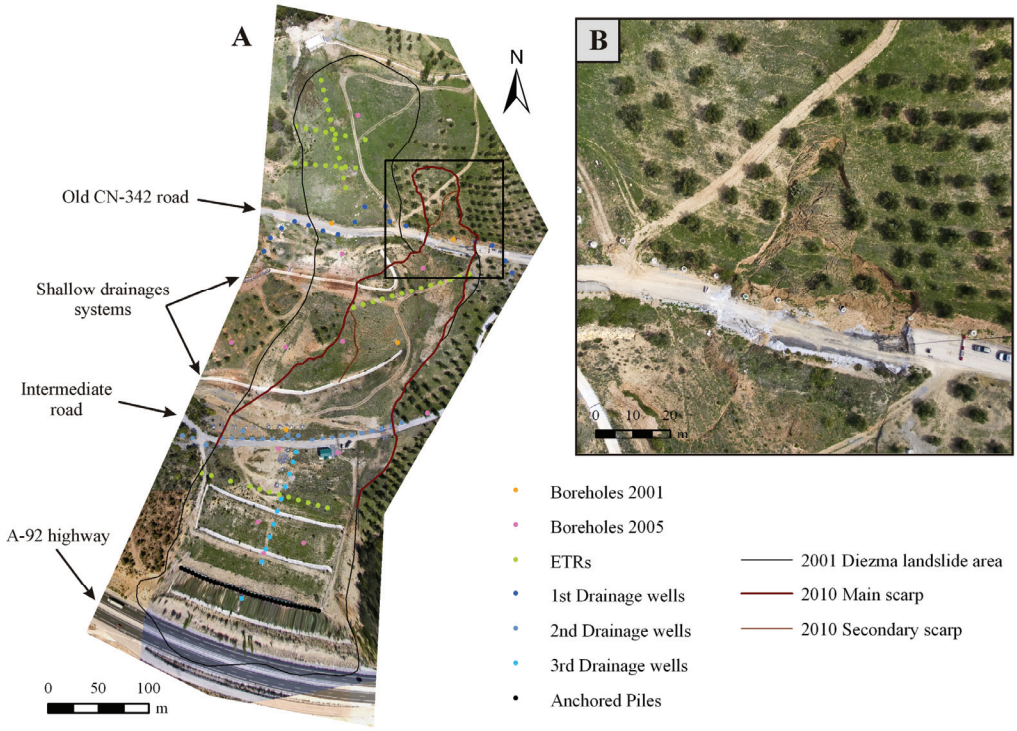

Figure 8-3. A. Map of the Diezma landslide showing the geotechnical and geophysical investigations and the location of the slope stabilization measures. The photograph used for depicting the different parts of the landslide is a vertical aerial view taken after the 2010 landslide reactivation. B. Detailed view of the 2010 main scarp at the head of the landslide.

8.3. Geotechnical investigations

At the Diezma landslide area, three different lithological units can be distinguished which are from bottom to top: a) bedrock, constituted by dark grey shales and phyllites with conglomerates and greywackes of the Malaguide Complex (Alboran Domain); b) a thick layer of a green smectite-rich clay; c) chaotic landslide debris, mainly composed of reddish and yellowish clays with sandstone and dolostone blocks. The main failure surface of the landslide has been found using available borehole and geophysical data (Azañón et al. 2006, 2009) completed with field observations. The geophysical data correspond to transversal and longitudinal electrical resistivity tomography (ERT) cross-sections (Fig. 8-3) which have allowed us to infer the shape of the contact between the landslide body and the bedrock. The thickness of the landmass deposit, as derived from the resistivity contrasts observed in the ERTs, varies from less than 10 m to 30 m. The geophysical data were compared with the data from the boreholes, which have been equipped with an inclinometer and extensometer device, in order to verify the depth of the slide surface. This critical surface is related to an oversaturated smectite-rich layer, which is the boundary between the debris units and high-plasticity clayey soils. In addition, several inclinometer surveys confirmed the existence of at least three sliding surfaces along the slope (Azañón et al. 2006). The main shear strength parameters corresponding to the lithological units described above (Table 8-1) have been obtained from direct shear tests under consolidated drained (CD) conditions on unweathered samples extracted from the boreholes in the landslide. These parameters have been used in the forthcoming Diezma landslide back-analysis.

Table 8-1. Summary of the main geotechnical properties of the lithological units found in the Diezma landslide. The range of the parameters is in brackets. γ, Unsaturated unit weight; γ_{sat}, Saturated unit weight; c_p, Peak cohesion; Φ_p, Peak friction angle; c_r, Residual cohesion; Φ_r, Residual friction angle.

Lithological unit	γ (kN/m^3)	γ_{sat} (kN/m^3)	c_p (kPa)	Φ_p (º)	c_r (kPa)	Φ_r (º)
Landslide debris	18.19 (±0.91)	20.60	5.4 (±3.2)	31 (±4)	0.6 (±0.5)	11 (±3)
Smectite-rich clay	15.24 (±0.49)	17.66	1.3 (±0.7)	21 (±4)	0.4 (±0.3)	8 (±1)
Bedrock (shales)	25.02	25.51	49.1	35	-	-

8.4. Reconstruction of the Diezma landslide

The back-analyses of the Diezma landslide have been made using 2D slope stability software (Slide, Rocscience Inc. 2003). This program calculates safety factors (SF) for circular and non-circular slope failure surfaces based on a number of widely used limit equilibrium methods. In this work we have used the Morgenstern-Price method because it is the most appropriate for slope ruptures developed in soils and is also valid for circular and non-circular failure surfaces. In general, to evaluate the stability of a slope the Slide program calculates a significant number of possible circular slip surfaces in order to find the location of the most critical one that has the

minimum safety factor value. In this work the location of the main failure surface in depth is constrained based on combining data from boreholes, geophysical surveys and field observations, and circular ruptures computed by the program are only used to complete the rupture surface at the head and toe zones.

8.4.1. The Diezma landslide before the A-92 motorway construction

Before the construction of the A-92 motorway, the Diezma landslide was stable. In fact, the results of the slope stability analysis performed for this situation draw high safety factors either when considering peak or residual shear strength values, and a deep water table (2.43 and 1.15, respectively). The slope remains stable even when considering a situation after a period of heavy rains with a shallow water table as deep as 3 m. In this case the minimum safety factor for peak shear strength conditions is still very high (SF=2.23) while for residual shear strength values it gets close to the instability condition (SF=1.09).

8.4.2. The Diezma landslide after the A-92 motorway construction

The construction of the A-92 motorway in 1993 substantially modified the geometry of the natural slope at the toe. The projected talus had a 3H:2V profile including one intermediate berm (Fig. 8-4). Even after this significant modification of the topography, the slope remained stable. The safety factor for peak shear strength parameters and a deep water table (18-20 m) is still very high (SF=2.12) compared to the one found in the previous section. Similarly, the minimum safety factor found when considering residual shear strength values is still over one (SF=1.05), stable although closer to the instability condition (Fig. 8-4). This situation fits very well with the occurrence of a small and shallow landslide that took place in May 2000 at the toe of the slope, which represented the first sign of instability of the Diezma landslide area after the A-92 motorway construction.

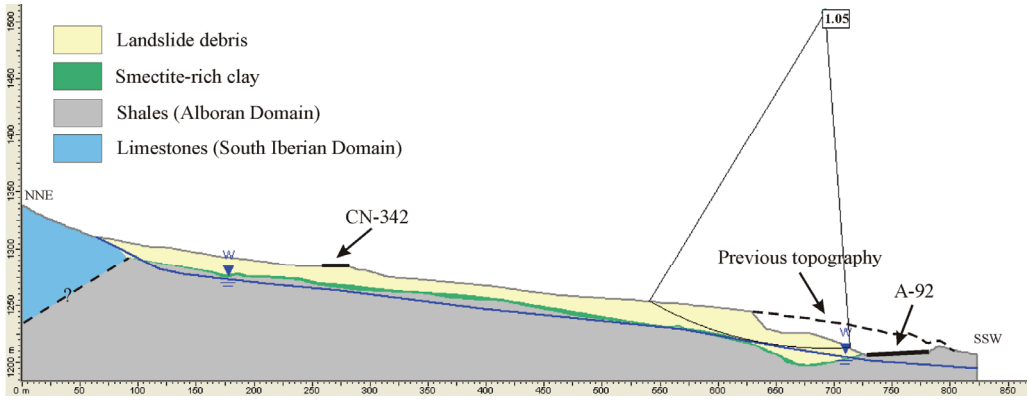

Figure 8-4. Longitudinal cross-section of the Diezma landslide after the construction of the A-92 motorway considering a deep water table (blue line) and residual shear strength parameters.

8.4.3. The Diezma landslide during the 2001 collapse

The complete failure of the Diezma landslide is composed of three consecutive movements. The first one took place on 18 March 2001 following a period of heavy rainfall, which is clear was the main triggering factor. The landslide covered the toe of the slope, which collapsed onto the A-92 motorway changing the topography and the water table location (Fig. 8-5). A safety factor as low as 0.53 is calculated for these conditions, with residual shear strength values and a shallow water table. A few days later, a second broader movement took place. In this case, the main scarp was developed towards the intermediate part of the slope (Fig. 8-5). The safety factor obtained for this situation is 0.66. Shortly after, the third and last movement took place. This landslide comprised practically the whole slope, with the main scarp developed very close to the old CN-342 road, which was damaged (Fig. 8-5). The safety factor obtained for this mass movement is 0.69, similar to the previous case.

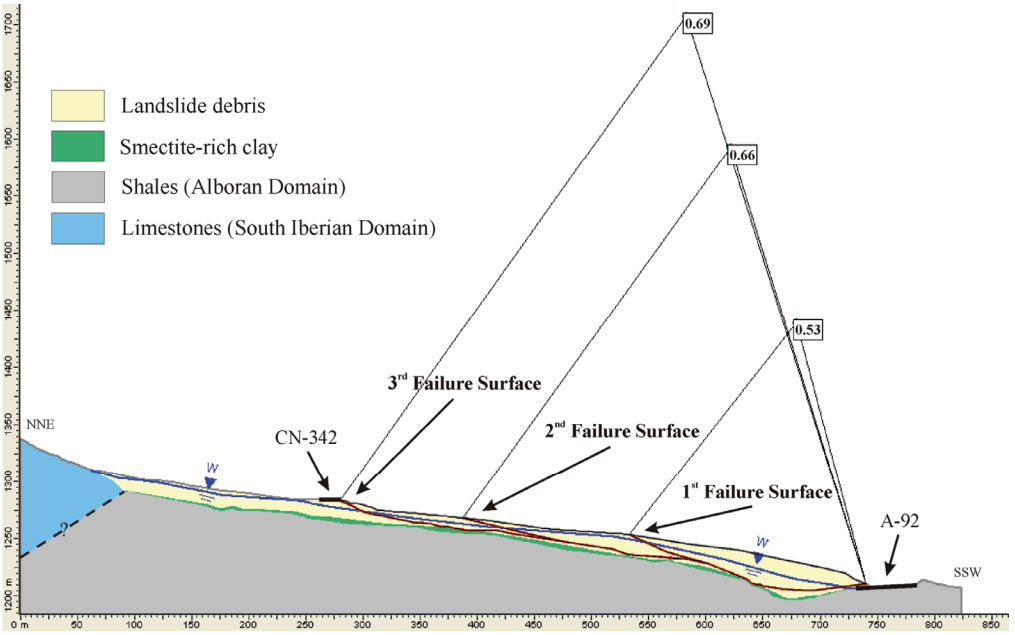

Figure 8-5. Longitudinal cross-section of the Diezma landslide after the A-92 motorway construction considering a shallow water table (blue line) and residual shear strength parameters. Red lines show the different failure surfaces.

8.4.4. The Diezma landslide after the restoration works

The stabilization works carried out on the Diezma landslide consisted of four lines of surface drainage systems (trenches), three lines of deep drainage wells and the construction of a barrier of anchored piles and a retaining wall at the toe of the slope (Oteo, 2001, 2003) (Fig. 8-3). The deep drainage wells are interconnected by means of sub-horizontal drainages that evacuate the water outside the landslide body. The first

line of wells was planned for capturing the water from the carbonate aquifer located few metres above. The other two lines of wells were designed to ensure that the water table was deep (20 m or lower) and parallel to the ground surface along the axis of the landslide. For this situation, and assuming a perfect performance of the drainage systems –which means that the water table should remain always deep, a safety factor of 1.44 is calculated. However, during field surveys in 2005 it was observed that the water table was very shallow at the head area of the Diezma landslide, showing that the drainage systems were not working properly in this zone (Azañón et al. 2006). In addition, some new cracks were found in the old CN-342 road evidencing that the landslide was still active. This fact seems to be related to the bad performance of the first line of wells. Nevertheless, when considering the piezometric levels recorded during the field surveys in 2005 a safety factor of 1.40 is calculated.

8.4.5. 2010 reactivation of the Diezma landslide

The reactivation of the Diezma landslide took place following the heavy rainfalls recorded during the winter December 2009-February 2010. The main scarp was developed over the old CN-342 road, which collapsed and moved downhill. The first line of drainage wells located close to this road and the first shallow drainage system were broken and moved by the landslide (Fig. 8-6). The landslide did not reach the A-92 motorway thanks to the correct performance of the retaining wall of anchored piles. Actually, the minimum safety factor that can be calculated when considering a movement of the whole slope is 1.13. The toe of the reactivated landslide was found at the intermediate area of the slope affecting the intermediate road and the second line of deep drainage wells (Fig. 8-7). The safety factor calculated considering this constraint is 0.97.

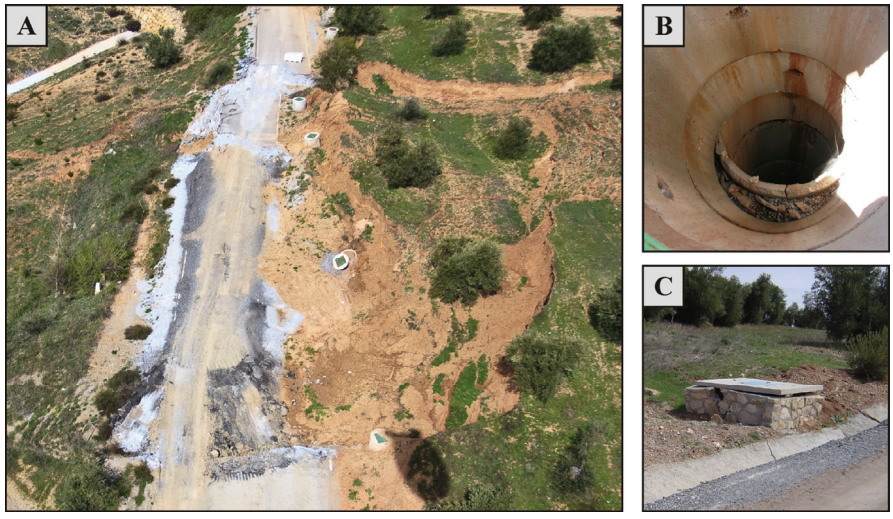

Figure 8-6. A. Aerial view of the first line of deep drainage wells and the old CN-342 road which were collapsed and moved during the 2010 landslide reactivation. B. Broken well of the first line of drainage wells. C. A damaged well of the second line of drainage wells.

8.4.6. Possible future reactivation of the Diezma landslide

The future stability of the Diezma landslide is controlled by the correct performance of the drainage systems after periods of heavy rain. Considering a total failure of the three lines of drainage wells a safety factor of 0.81 is calculated for a landslide implicating the whole slope. In this critical situation, it appears that the anchored piles would no longer be effective and the mass movement could reach the A-92 motorway once again.

Apart from heavy rains, another important triggering mechanism in landslide reactivation is seismicity. The Diezma landslide is located in the central Betic Cordillera, close to the Granada Basin, which is the most seismically active area in Spain. A number of significant earthquakes have taken place in this area since historical times and so earthquake loads must be considered in engineering design according to official seismic provisions (NCSE-02 2002) and, particularly in slope stability analyses (Rodríguez-Peces 2008). Considering 2010 failure conditions the minimum seismic acceleration required for overcoming the shear resistance and initiating the displacement of the landslide can be calculated by (Newmark 1965):

$$a_c = (SF - 1)\ \mathrm{g} \sin \alpha$$

where a_c is the critical acceleration (in gravity units, 1g=9.81 m/s^2), g is the gravity acceleration, SF is the static safety factor and α is the angle between the vertical and a line connecting the centre of gravity of the landslide mass and the centre of the slip circle. The critical acceleration estimated for the Diezma landslide is 0.02g, which is a fairly low value. The most likely magnitude-distance pairs of potential earthquakes whose horizontal peak ground acceleration could exceed the critical acceleration have been obtained using a number of ground motion prediction equations selected from specialised literature (Skarlatoudis et al. 2003, Ambraseys et al. 2005, Akkar and Bommer 2007, Bindi et al. 2009) (Table 8-2). The reactivation of the Diezma landslide can be triggered by the occurrence of an earthquake as small as M_w=4.0-5.0 –which are relatively frequent in the area (Morales et al. 1996, López-Casado et al. 2001), provided that it takes places in the vicinity of the landslide (R<25 km).

Table 8-2. Most likely magnitude-distance pairs of potential earthquakes which might exceed the critical acceleration at present-day Diezma landslide. M_w: moment magnitude; R_{ep}: epicentral distance to Diezma landslide (km).

M_w	4.0	4.5	5.0	5.5	6.0	6.5
R_{ep}	≤ 10	≤ 15	≤ 25	≤ 40	≤ 60	≤ 100

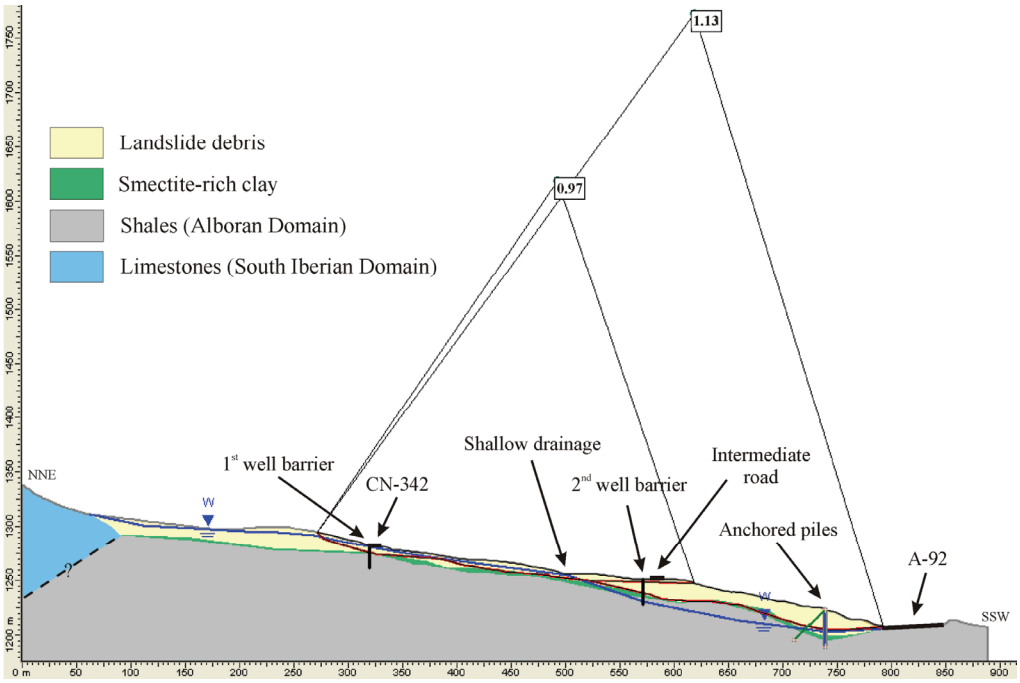

Figure 8-7. Longitudinal cross-section of the Diezma landslide after the 2010 reactivation considering a shallow water table (blue line) at the head zone and residual shear strength parameters. Red lines show the different failure surfaces.

8.5. Discussion and Conclusions

The typical Mediterranean rainfall regime of Southern Spain is a major factor controlling the triggering of landslides, especially in areas where high-plasticity expansive soils appear in relation to clayey and marly sedimentary formations. Slope stabilization measures typically comprise drainage systems like trenches and wells. An inappropriate design and/or maintenance of the drainage systems can lead to a reduction in the effectiveness of reducing pore water pressure and favour the instability of the slope.

In this work, we have reconstructed the history of the Diezma landslide through time, in particular looking at the role played by the drainage systems deployed in the slope in relation to heavy rain periods. It has been shown that the first signs of instability started after the modification of the topography at the toe of the slope produced by the construction of the A-92 motorway in 1993. Before this situation the slope was stable even when considering residual shear strength parameters and a shallow water table. Nevertheless, it was 8 years after the construction of the motorway in 2001 when, coinciding with a period of heavy rains, the Diezma landslide moved significantly. The increase in pore water pressure due to a shallow water table was recognised as the main triggering factor, so the design of stabilization measures included a drainage system formed by four trenches and three lines of deep

drainage wells. The Diezma landslide remained stable for 9 years until 2010 when it was reactivated again coinciding with a period of high rate precipitation. The main cause of the reactivation was the bad performance of the first line of deep drainage wells, which are known to have been working inadequately since at least 2005 because of a small movement of the landslide at the head zone. Fortunately, the 2010 landslide reactivation did not reach the motorway because of the anchored wall of piles emplaced at the toe of the slope constructed during the stability works in 2001.

Nevertheless, it has been shown that the landslide could be reactivated in the future and reaches the motorway, if a total failure of the drainage system is assumed after a heavy rain period. This situation can be expected if the broken drainage systems of the first and second lines of wells are not rebuilt and properly maintained on a regular basis. Moreover, the reactivation of the landslide could also take place if a low magnitude earthquake (4.0-5.0) occurs near the landslide area.

Acknowledgments

This study was supported by research projects CGL2008-03249/BTE, TOPOIBERIA CONSOLIDER-INGENIO2010 CSD2006-00041 and FASEGEO (CGL2009-09726) from the Spanish Ministry of Science and Innovation, MMA083/2007 from the Spanish Ministry of Environment. N. Woollard is thanked for reviewing the English.

PART FOUR

- **9. Conclusions/Conclusiones**
- **10. Future research perspectives**

9

Conclusions

This chapter summarizes briefly the main results obtained in this Ph.D. Thesis, focussed on the development, testing and application of a new methodology for assessing earthquake-triggered slope instabilities at different scales in the South of Iberian Peninsula. First, the findings obtained from the regional application of the proposed methodology using a GIS are presented, followed by the results found after testing the applicability of the methodology at different scales. Finally, the results obtained from detailed studies of specific known seismically-induced slope instabilities at a site scale are presented.

9.1. Development of a comprehensive methodology to evaluate potential earthquake-triggered slope instabilities

The earthquake-triggered landslide phenomenon has been analysed by means of the implementation of a comprehensive methodology that can be applied successfully in seismically active regions at different scales.

The first step of the proposed methodology involves the calculation of the safety factor in order to obtain the critical acceleration and, eventually, the Newmark displacement. The estimation of the safety factor is a critical issue that comprises a range of limitations and uncertainties due to the natural variability of the geotechnical parameters and the limit equilibrium methods considered in the computation. This fact is particularly significant at regional scales where an unique value, taken from a compilation of general geotechnical parameters, is assigned to a whole lithological group and a simple infinite-slope limit equilibrium method is considered. In this sense, the parameters have to be assumed as sufficiently representative for the study area. However, in this Ph.D. Thesis it has been evidenced that the results at a site scale using the data obtained in detailed studies are very similar to those derived at a sub-regional scale. This fact supports the simplification assumed in assigning shear strength parameters and the limit equilibrium method used at a regional scale.

In contrast to previous works on the subject, the methodology proposed in this Thesis considers for the first time specific seismic scenarios significant for civil protection and engineering purposes (probabilistic, pseudo-probabilistic and deterministic). In the particular case of the deterministic scenarios, the seismic hazard related to the rupture of the major active faults in the area has been estimated in terms of peak ground acceleration (PGA). PGA values have been obtained using a number of ground motion prediction equations (GMPEs) derived for the Mediterranean region,

as to date there is still not available a specific statistically reliable GMPE for southern Spain. In this sense, the estimated PGA values comprise a certain degree of epistemic uncertainty, apart from the aleatory variability inherent to ground motion prediction.

When considering a specific seismic scenario as an input in the calculations, the proposed methodology takes into account the occurrence of ground motion amplification phenomena (site effects) related to both soil conditions and topographic features. Soil amplification has been considered on the base of previous studies and different soil classifications contained in seismic codes. On the other hand, the topographic amplification –a factor usually neglected in previous works, is taken into account by means of an original and simple tool developed in this Ph.D. Thesis using a geographical information system. In mountainous areas such as the ones studied here, it has been shown that the topographic amplification is a significant factor for the slope stability during an earthquake.

The methodology has also been tested and applied in several slope instabilities cases in the South of Spain, particularly in the Lorca and Granada basins and the Sierra Nevada Range. The resulting Newmark displacement maps have been shown very useful for identifying the areas with the highest susceptibility and hazard, as well as for inferring the most likely type of slope instability that could be triggered in relation to a particular seismic scenario. These maps represent a first order assessment that can be used later for detailed risk evaluation, emergency plans and engineering design of critical structures.

In addition, the methodology proposed in the Ph.D. Thesis can be also applied successfully at a site scale in detailed slope-stability analyses. This approach has been shown here to be very useful in a variety of applications such as the identification of determinant parameters in the stability of significant earthquake-triggered landslides, the reassessment of magnitude and epicentre location of pre-instrumental earthquakes, the estimation of the most likely seismic sources for landslide reactivation, as well as in testing the efficiency of slope stabilisation measures at present-day landslides.

9.2. Regional assessment of earthquake-triggered slope instabilities in Lorca and Granada basins and Sierra Nevada Range

Seismically-induced landslide hazard in the Lorca Basin and Sierra Nevada Range can be considered as low according to the results obtained considering the probabilistic seismic scenarios. However, considering the results from the deterministic scenarios the occurrence of widespread slope instabilities across these areas is expected related to a low-frequency but powerful earthquake (M_w>6.6) corresponding to the activity of a main fault takes place.

In the Lorca Basin, the Newmark displacement values calculated at the sites of the earthquake-triggered Bullas and La Paca rock slides are always less than 2 cm independently of the seismic scenario considered. This small Newmark displacement

threshold can also be found in many other parts of the Lorca Basin, so it is likely that similar earthquake-triggered rock slides and rock falls could occur in these areas in the future.

In the particular case of Sierra Nevada Range, where the distribution of earthquake-induced slope instabilities in the past is unknown, the most common slope instability types are debris flows, rock falls and rock slides. These instabilities are mainly related to micaschists and quartzite, which are the most common lithologies in the Sierra Nevada Range. Therefore, it can be assumed that future seismically-induced slope instabilities in this area will be of such typologies. The critical Newmark displacements related to these types of instabilities are around 2 cm, similarly to what was found in the Lorca Basin.

Finally, it has also been evidenced that the seismic reactivation of a few number of old slope instabilities in the Lorca Basin and Sierra Nevada Range might be also possible.

As a general conclusion, the regional assessment of earthquake-triggered landslide has allowed to identify disrupted-type slides as the most likely seismically-induced slope instability in the Lorca Basin and Sierra Nevada Range. These instabilities seem to be related to a threshold Newmark displacement of 2 cm or even smaller.

9.3. Applicability of the methodology at different scales (regional, sub-regional and site)

It has been evidenced in this Ph.D. Thesis that the evaluation at a regional scale of earthquake-triggered landslides can provide wrong estimates of the Newmark displacements. This was the case of the well-known seismically-induced Bullas and La Paca rock slides, where the estimated Newmark displacements at regional scale were at both sites equal to zero. However, the results at a sub-regional scale seem to be in good agreement with those obtained from detailed studies of these slides at a site scale.

Results obtained from the regional scale are strongly influenced by the size of the grid of the digital elevation model and in relation to the dimensions of the slope instability. In this sense, a regional map with a pixel size much bigger than the slope instability provides values of safety factor and critical acceleration larger than those obtained using a better resolution digital elevation model.

The simplifications and uncertainties assumed at regional and sub-regional scales can be admitted considering that the safety factor, critical acceleration and even Newmark displacement values estimated at both sub-regional and site scales are very similar. Therefore, this situation justifies the infinite-slope limit equilibrium method and the shear strength parameters applied at regional scale. Hence, the regional scale

maps are useful as a first order approximation to detect the areas with the highest susceptibility and hazard that can be interesting for developing future specific studies at a larger scale.

A critical Newmark displacement value of 3 cm has been obtained from the detailed studies performed at site scale. This value can be considered as a minimum threshold to trigger disrupted-type slope instabilities similar to the Bullas and La Paca rock slides. These earthquake-triggered instabilities seem to be related to slopes with safety factors close to the instability condition and, hence, to low critical acceleration values.

9.4. Application of the methodology to assess pre-instrumental earthquake parameters

A new methodology has been developed to improve the reliability of historical earthquakes parameters by studying in detail singular earthquake-triggered landslides. In particular, the implementation of the Newmark's method in the slope back-analyses of the Güevéjar landslide has been found as an useful tool to reassess the magnitude and epicentral location of historical earthquakes.

A minimum M_w 8.5 and an epicentral distance from the Güevéjar landslide of 580 km have been estimated for the 1755 Lisbon earthquake. This result agrees with the average magnitude and epicentral location proposed by Martínez Solares and López Arroyo (2004).

For the case of the 1884 Arenas del Rey earthquake, the minimum magnitude and the epicentral distance from the Güevéjar landslide have been estimated in M_w 6.5 and 55 km, respectively. The estimated magnitude value is in agreement with the average moment magnitude proposed by others authors (Muñoz and Udías, 1981; Reicherter et al., 2003; Mezcua et al., 2004). In addition, the obtained epicentral distance value is consistent with the Ventas de Zafarraya Fault as the causative fault of the 1884 Arenas del Rey earthquake.

In the particular case of the 1806 Pinos Puente earthquake it has been found that its epicentral intensity (I_{EMS}=IX) was probably overestimated and a new value of I_{EMS}=VIII is then proposed.

A comparison between the obtained magnitude and epicentral distance values and the estimates resulting from the use of empirical relationships highlights the fact that such correlations provide unreliable results. However, the methodology proposed in this Ph.D. Thesis provides more accurate results.

9.5. Evaluation of potential seismic reactivation of landslides

The methodology developed in the Ph.D. Thesis can also be used successfully to consider the potential seismic reactivation of present-day slope instabilities. This approach provides minimum magnitudes at different epicentral distances that are required to overcome the critical acceleration value and thus to trigger the instability.

From the slope stability analysis of the Güevéjar landslide, it has been found that its reactivation is expected in the case that a moderate seismic event (M_w=4.7-5.6) located close to the landslide (epicentral distance between 1 to 13 km) takes place. In the case of a large earthquake (M_w=6.5-6.9), the longest possible epicentral distance is 25 to 33 km. This powerful earthquake would be very likely generated by some of the active faults of the Granada Basin (Granada, Atarfe and Santa Fe faults).

9.6. Testing the efficiency of slope stabilisation measures

The Diezma landslide has been reactivated several times since at least 1993, when the A-92 motorway was constructed. The reactivations occurred coinciding with periods of heavy rains, so the main triggering factor was the increase in pore water pressure. In fact, the last movement took place in 2010 following a period of high rate precipitation. The main cause of this reactivation was the bad performance of some of the slope stabilisation measures previously built, in particular the deep drainage wells. Nevertheless, it has been found that the Diezma landslide might be also reactivated in the future if a low magnitude earthquake (M_w=4.0-5.0) occurs close to it. Hence, in order to analyse properly the efficiency of the slope stabilisation measures planned to be deployed in the future, it is recommended to perform a slope-stability analysis considering the dynamic input related to this seismic event.

9

Conclusiones

En este capítulo se resume brevemente los principales resultados obtenidos en esta Tesis Doctoral, en la que se desarrolla, se pone a prueba y se aplica una nueva metodología para evaluar las potenciales inestabilidades de ladera producidas por efecto sísmico a diferentes escalas en el sur de la Península Ibérica. En primer lugar, se presentan los resultados a escala regional obtenidos de la aplicación de la metodología propuesta mediante el uso de un SIG, seguidos de los resultados encontrados al poner a prueba la aplicabilidad de la metodología a diferentes escalas. Finalmente, se exponen los resultados obtenidos a escala local a través de estudios de detalle de algunas inestabilidades de ladera que han sido generadas por terremotos.

9.1. Desarrollo de una metodología integral para evaluar potenciales inestabilidades de ladera provocadas por terremotos

El fenómeno de las inestabilidades de ladera provocadas por terremotos ha sido analizado mediante el desarrollo de una metodología integral que puede ser aplicada con éxito en regiones sísmicamente activas considerando diferentes escalas.

El primer paso de la metodología propuesta es el cálculo del factor de seguridad con el fin de obtener la aceleración crítica y, posteriormente, el desplazamiento de Newmark. El cálculo del factor de seguridad es un problema crítico que comprende una serie de limitaciones e incertidumbres debido a la variabilidad natural de los parámetros geotécnicos y a los métodos de equilibrio límite empleados en los cálculos. Este hecho es especialmente significativo a escalas regionales donde un único valor, tomado de una recopilación de parámetros geotécnicos generales, se le asigna a un grupo litológico entero y se aplica un método simple de equilibrio de límite de talud infinito. En este sentido, los parámetros han de ser asumidos como suficientemente representativos para el área de estudio. Sin embargo, en esta Tesis Doctoral se ha demostrado que los resultados a una escala local empleando los datos obtenidos en estudios de detalle son muy similares a los obtenidos a una escala sub-regional. Este hecho justifica la simplificación asumida en los parámetros de resistencia al corte y el método de equilibrio límite empleado a escala regional.

A diferencia de los trabajos previos en el tema, la metodología propuesta en esta Tesis considera por primera vez escenarios sísmicos concretos de importancia para la protección civil y los propósitos de la ingeniería (probabilista, pseudo-probabilista y determinista). En el caso particular de los escenarios deterministas, la peligrosidad sísmica relacionada con la rotura de las principales fallas activas en el área de estudio

se ha estimado en términos de aceleración sísmica máxima (PGA). Los valores de PGA se han obtenido empleando varias ecuaciones de predicción del movimiento del terreno (GMPEs) desarrolladas para la región mediterránea, ya que en la actualidad todavía no existe una GMPE que sea estadísticamente aceptable para el caso concreto del sureste de España. En este sentido, los valores de PGA estimados comprenden un cierto grado de incertidumbre epistémica, a parte de la variabilidad aleatoria inherente a la predicción del movimiento del terreno.

Al considerar un escenario sísmico concreto como parámetro de entrada en los cálculos, la metodología propuesta tiene en cuenta los fenómenos de amplificación del movimiento del terreno (efectos de sitio) que pueden ocurrir en relación con las condiciones del suelo y con las características topográficas. La amplificación del suelo se ha considerado sobre la base de estudios previos y las distintas clasificaciones del suelo contenidas en los códigos sísmicos. Por otra parte, la amplificación topográfica, un factor que no es considerado habitualmente en trabajos anteriores, se tiene en cuenta a través de una original y sencilla herramienta desarrollada en esta Tesis Doctoral utilizando un sistema de información geográfica. En zonas montañosas, como las que se estudian en este trabajo, se ha demostrado que la amplificación topográfica es un factor importante para la estabilidad de las laderas durante un terremoto.

La metodología también ha sido puesta a prueba y aplicada en varias casos de inestabilidades de ladera en el sur de España, en particular en las cuencas de Lorca y de Granada y en Sierra Nevada. Los mapas de desplazamiento de Newmark resultantes son muy útiles para identificar las áreas con una mayor susceptibilidad y peligrosidad, así como para inferir el tipo más probable de inestabilidad de ladera que podría desencadenarse en relación con un escenario sísmico concreto. Estos mapas ofrecen una evaluación de primer orden que puede ser utilizada posteriormente para una evaluación detallada de riesgos, en planes de emergencia y en el diseño de infraestructuras de vital importancia.

Además, la metodología propuesta en esta Tesis Doctoral puede ser también aplicada con éxito a escala local en análisis detallados de estabilidad de laderas. Este enfoque tiene varias aplicaciones tales como la identificación de los parámetros determinantes en la estabilidad de importantes inestabilidades de ladera provocados por terremotos, la reevaluación de la magnitud y la localización epicentral de terremotos pre-instrumentales, la obtención de las fuentes sísmicas más probables para la reactivación de deslizamientos, así como la comprobación de la eficacia de medidas de estabilización de laderas en deslizamientos actuales.

9.2. Evaluación regional de inestabilidades de ladera producidas por terremotos en las cuencas de Lorca y de Granada y en Sierra Nevada.

La peligrosidad de inestabilidades de ladera inducidas por eventos sísmicos en las cuencas de Lorca y de Granada y en Sierra Nevada se puede calificar como baja de

acuerdo con los resultados obtenidos al considerar los escenarios sísmicos probabilistas. Sin embargo, si se consideran los resultados obtenidos a partir de los escenarios deterministas, es de esperar que se produzcan inestabilidades de ladera en estas zonas de manera generalizada si tiene lugar un gran terremoto (M_w>6.6) en relación con la actividad de una de las fallas principales.

En la Cuenca de Lorca, los valores de desplazamiento de Newmark calculados para los desprendimientos rocosos inducidos por terremotos de Bullas y La Paca son siempre menores de 2 cm, independientemente del escenario sísmico considerando. Este valor tan bajo de desplazamiento de Newmark crítico también puede ser encontrado en muchas otras zonas de la Cuenca de Lorca, por lo que es probable que similares desprendimientos de rocas provocados por eventos sísmicos pudieran ocurrir en estas áreas en el futuro.

En el caso particular de Sierra Nevada, donde la distribución de inestabilidades de ladera inducidas por terremotos en el pasado es desconocida, las tipologías de inestabilidades de ladera más frecuentes son flujos de derrubios, desprendimientos y deslizamientos rocosos. Estas inestabilidades se relacionan principalmente con micaesquistos y cuarcitas que son las litologías más comunes en Sierra Nevada. Por lo tanto, se puede asumir que las futuras inestabilidades de ladera desencadenadas por terremotos en esta área serán de ese tipo. De manera parecida a los resultados obtenidos en la Cuenca de Lorca, los desplazamientos de Newmark críticos relacionados con este tipo de inestabilidades son de unos 2 cm.

Finalmente, se ha observado que la reactivación sísmica de un reducido número de antiguas inestabilidades de ladera también podría ser posible en la Cuenca de Lorca y Sierra Nevada.

Como conclusión general, la evaluación regional ha permitido identificar las inestabilidades de tipo disgregado como las inestabilidades de ladera provocadas por terremotos más probables en la Cuenca de Lorca y Sierra Nevada. Estas inestabilidades parecen estar relacionadas con un desplazamiento de Newmark mínimo de 2 cm o incluso más pequeño.

9.3. Aplicabilidad de la metodología a diferentes escalas (regional, sub-regional y local)

En esta Tesis Doctoral se ha demostrado que la evaluación a escala regional de inestabilidades de ladera causadas por terremotos puede resultar en estimaciones no satisfactorias de los desplazamientos de Newmark. Este ha sido el caso de los desprendimientos rocosos inducidos por terremotos de Bullas y La Paca, donde los desplazamientos de Newmark calculados a escala regional fueron en ambos casos iguales a cero. Sin embargo, los resultados a escala sub-regional parecen estar de acuerdo con los obtenidos a escala local mediante estudios detallados de estos desprendimientos.

Los resultados de la escala regional están fuertemente influenciados por el tamaño de píxel del modelo digital de elevaciones y por las dimensiones de la inestabilidad de ladera. En este sentido, un mapa regional con un tamaño de píxel mucho mayor que la inestabilidad de ladera proporciona unos valores de factor de seguridad y aceleración crítica mayores que los obtenidos con un modelo digital de elevaciones con mayor resolución.

Las simplificaciones e incertidumbres asumidas a escala regional y sub-regional pueden ser admisibles teniendo en cuenta que el factor de seguridad, la aceleración crítica e incluso los valores de desplazamiento de Newmark estimados a escala sub-regional y local son muy similares. Por tanto, esta circunstancia justifica el método de equilibrio límite de talud infinito y los parámetros de resistencia al corte empleados a escala regional. Por consiguiente, los mapas a escala regional son útiles como una aproximación de primer orden para distinguir las zonas con mayor susceptibilidad y peligrosidad que pueden ser interesantes para el desarrollo de futuros estudios a una escala mayor.

Se ha obtenido un valor de desplazamiento de Newmark crítico de 3 cm a partir de los estudios detallados desarrollados a escala local. Este valor puede ser considerado como un umbral mínimo para provocar inestabilidades de ladera de tipo disgregado, similares a los desprendimientos rocosos de Bullas y La Paca. Estas inestabilidades de ladera causadas por terremotos parecen estar relacionadas con laderas con factores de seguridad próximos a la condición de inestabilidad y, por consiguiente, con bajos valores de aceleración crítica.

9.4. Aplicación de la metodología para evaluar parámetros de terremotos pre-instrumentales

Una nueva metodología ha sido desarrollada para mejorar la fiabilidad de los parámetros de terremotos históricos mediante del estudio de inestabilidades de ladera inducidas por terremotos. En particular, la incorporación del método de Newmark en el análisis retrospectivo de la estabilidad del deslizamiento de Güevéjar se ha revelado como una herramienta útil para reevaluar la magnitud y la localización epicentral de los terremotos históricos.

Se ha estimado una magnitud mínima de M_w 8.5 y una distancia epicentral desde el deslizamiento de Güevéjar de 580 km para el terremoto de Lisboa de 1755. Este resultado está de acuerdo con la magnitud media y localización epicentral propuestas por Martínez Solares y López Arroyo (2004).

Para el caso del terremoto de Arenas del Rey de 1884, se ha estimado la magnitud mínima y la distancia epicentral desde el deslizamiento de Güevéjar en M_w 6.5 y 55 km, respectivamente. La magnitud estimada coincide con la magnitud momento media propuesta por otros autores (Muñoz y Udías, 1981; Reicherter et al.,

2003; Mezcua et al., 2004). Además, la distancia epicentral obtenida es coherente con el hecho de que la rotura de la Falla de Ventas de Zafarraya fuera la causante del terremoto de Arenas del Rey de 1884.

En el caso particular del terremoto de Pinos Puente de 1806 se ha comprobado que su intensidad epicentral (I_{EMS}=IX) fue probablemente sobrestimada, por lo que un nuevo valor de I_{EMS}=VIII ha sido propuesto.

La comparación entre la magnitud y la distancia epicentral obtenidos y las estimaciones resultantes del uso de relaciones empíricas destaca el hecho de que dichas correlaciones proporcionan resultados poco fiables. Sin embargo, la metodología propuesta en esta Tesis Doctoral proporciona resultados más precisos.

9.5. Evaluación de la posible reactivación de inestabilidades de ladera por efecto sísmico

La metodología desarrollada en esta Tesis Doctoral también puede ser utilizada con éxito para considerar la posible reactivación sísmica de inestabilidades de ladera actuales. Este enfoque proporciona las magnitudes mínimas a diferentes distancias epicentrales que se requieren para superar el valor de aceleración crítica y, por lo tanto, para desencadenar la inestabilidad.

A partir del análisis de estabilidad del deslizamiento de Güevéjar, se ha encontrado que su reactivación es esperable en caso de que un evento sísmico moderado (M_w=4.7-5.6) se produjera cerca del deslizamiento (distancias epicentrales entre 1 a 13 km). En el caso de un gran terremoto (M_w=6.5-6.9), la distancia epicentral más alejada requerida es de 25 a 33 km. Este potente terremoto podría ser generado muy probablemente por alguna de las fallas activas presentes en la Cuenca de Granada (fallas de Granada, Atarfe y Santa Fe).

9.6. Comprobación de la eficacia de medidas de estabilizaciones en deslizamientos

El deslizamiento de Diezma se ha reactivado en varias ocasiones por lo menos desde 1993, cuando la autopista A-92 fue construida. Las reactivaciones se produjeron coincidiendo con períodos de lluvias intensas, por lo que el principal factor desencadenante fue el aumento de la presión del agua intersticial. De hecho, el último movimiento tuvo lugar en 2010 tras un período de abundantes precipitaciones. La principal causa de esta reactivación fue el mal funcionamiento de algunas de las medidas de estabilización construidas previamente, en particular los pozos de drenaje profundos. Sin embargo, se ha comprobado que el deslizamiento de Diezma también podría ser reactivado en el futuro si un terremoto de baja magnitud (M_w=4.0-5.0) se produce en las cercanías del mismo. Por lo tanto, con el fin de analizar adecuadamente la eficacia de las medidas de estabilización de laderas que se planeen desplegar en el futuro, es recomendable realizar un análisis de la estabilidad de laderas considerando la acción dinámica relacionada con este evento sísmico.

10

Future research perspectives

Although slope instabilities are one of the most frequent induced phenomena described in the chronicles of earthquakes either in the instrumental or historical periods, very few cases are currently known in Spain to be associated uniquely to specific earthquakes. This fact determines the appearance of two main lines of research. The first one is the study of instabilities clearly associated to recent seismic activity and therefore with well-constrained earthquakes; and a second one: the study of instabilities presumably associated to pre-instrumental earthquakes or even to paleoseismic events.

The first line of research comprehends a detailed study of recent earthquake-triggered slope instabilities, such as the 2002 Bullas and 2005 La Paca rock slides which are a good example of the disrupted-type instabilities that can occur in the South of Spain. The second line of research would include, first, the study of the chronicles of major earthquakes in the area and the identification and location of the slope instabilities associated to them. In certain cases, it would be important to date the instability using different dating techniques (e.g. cosmogenic methods, lichenometry, dendrochronology,…). In the case of old instrumental earthquakes, the study would be preceded by an analysis of the uncertainty related to the location and magnitude of the earthquake. In the case of historical earthquakes, the study would be conducted retrospectively in order to estimate the size of the historical event in terms of both ground-motion and magnitude. A significant example of a major slope instability induced by historical earthquakes is the Güevéjar landslide, which is also a representative model of the coherent-type instabilities that might occur in the South of Spain. Finally, having identified the most important cases of earthquake-triggered slope instabilities, a specific detailed study would follow.

The strong ground-motion parameters (e.g. PGA) and Newmark displacement values estimated in this Ph.D. Thesis would be much more reliable if representative accelerograms for each of the analyzed earthquake-scenarios were available at each of the slope-instability sites, an issue that is currently being explored. If the magnitude of the main earthquake were known with precision, as well as its location and distance to the slope, it would be possible to obtain a representative accelerogram at the slope-instability site. This acceleration time-history could be derived by means of real accelerograms recorded in similar earthquakes using the European Ground Motion Database or by developing synthetic accelerograms derived from specific earthquake parameters. Using these accelerograms, the real Newmark displacement associated to the rupture of the selected slope instabilities could be calculated and then compared to

the Newmark displacement estimated by means of empirical relationships following the approach described in this Ph.D. Thesis in order to check the validity of the use of these empirical equations in the Betic Cordillera.

The assessment of earthquake-triggered slope instabilities would also be improved by using Finite Element Analysis codes (e.g. Plaxis, Gefdyn). These programs are useful to perform a 2D or even a 3D simulation of the geotechnical behaviour of rocks and soils using different advanced constitutive models, including the widely used Mohr-Coloumb model. The main advantage of this procedure is that an accelerogram can be implemented into the model. The results of this dynamic analysis are mainly in terms of stress and deformation (i.e. displacements). In addition, site effects (soil and topographic amplification) can be evaluated through the slope model, so it is possible to obtain an amplified accelerogram at any point of the finite element mesh. Therefore, the Newmark displacement could be estimated at different points of interest.

Finally, the results of all the investigations described above would produce a database that would relate Newmark displacements with different types of slope instabilities and to geotechnical and geometrical constraints. Using these data, probability distributions of slope failure associated to particular levels of Newmark displacement could be constructed. Based on these distributions, the assessment of earthquake-triggered slope instabilities in the study area could be then done in terms of probability of slope failure. In this second evaluation the same seismic scenarios used in this Ph.D. Thesis could be considered or, instead, the probability distribution of slope rupture could be implemented directly into the seismic hazard integral.

APPENDIXES

- **A1. Shear strength parameters database**
- **A2. Empirical relationships between Schmidt hammer rebound and Join Compressive Strength (JCS)**
- **A3. Laboratory test on soils samples**
- **A4. European Ground Motions Prediction Equations**
- **A5. Soil amplification factors**
- **A6. Intensity-PGA relationships for the Mediterranean zone**

Appendix A1: Shear strength parameters database

Hough (1957)

Soil	Friction angle (º)
Low plasticity silt (loose)	26 - 30
Low plasticity silt (medium dense)	28 - 32
Low plasticity silt (dense)	30 - 34
Uniform fine to medium sand (loose)	26 - 30
Uniform fine to medium sand (medium dense)	30 - 34
Uniform fine to medium sand (dense)	32 - 36
Well-graded sand (loose)	30 - 34
Well-graded sand (medium dense)	34 - 40
Well-graded sand (dense)	38 - 46
Sand and gravel (loose)	32 - 36
Sand and gravel (medium dense)	36 - 42
Sand and gravel (dense)	40 - 48

Clark (1966)

Average density of sedimentary rocks (g/cm^3)		
Sandstone	2.32	1.61 - 2.76
Shale	2.42	1.77 - 2.45
Limestone	2.54	1.93 - 2.90
Dolomite	2.70	2.36 - 2.90

Stagg and Zienkiewicz (1968)

Rock	Cohesion (kp/cm^2)	Friction angle (º)
Limestone	175 - 232	37 - 58
Sandstone	112 - 290	48 - 50

Jiménez-Salas and Justo-Alpañés (1975)

TIPO DE ROCA	c' kp/cm²	φ' grados
Andesita	280	—
Anhidrita	94	42
Antracita	100	16-22
Arenisca	42- 420	48-50
	100	59
	140	38
Arenisca de grano muy fino (*siltstone*)	50	—
Basalto	300- 420	50-48
Caliza	35- 350	37-58
	140- 350	58-35
Caliza de Solenhofen ...	780	24
Caliza margosa	10- 60	30-40
Carbón poco hecho	10- 30	35-26
Creta	0- 2,4	24-46
	(media 0,5)	(media 38)
Cuarcita	960	54
Diabasa	900-1.300	50-40
Diorita	140	—
Dolomía	520-1.600	17-37
Esquisto	20- 140	54-27
Esquisto arcilloso (*shale*)	80- 580	22-43
Gabro	350	35
Gneiss	175- 210	43
Granito	100- 480	58-51
	220	58
Granito alterado	13- 1	62-41
Grauwacka	60- 110	50-45
Mármol	210- 350	34
Mortero de cemento y arena (1:2) ...	45	34,3
Piedra de cieno (*mudstone*) meteorizada	0- 0,07	19-27
Pizarra	40- 330	36-48
Porfido	< 200	51,2
Toba	7	—

TIPO DE ROCA	TIPO DE SUPERFICIE	SECA				SATURADA			
		PICO		RESIDUAL		PICO		RESIDUAL	
		c' t/m²	φ' grados	c'_r t/m²	φ'_r grados	c' t/m²	φ' grados	c'_r t/m²	φ'_r grados
Arenisca	Plano de sedimentación	0	34-45	0	27-34	0	37-39	—	>25
Arenisca	Diaclasa	≃0	31-43			0	39-40		
Arenisca de grano muy fino (*siltstone*)	Diaclasa	—	28-30	—	—	—	—	—	—
Basalto	Diaclasa	0	47	—	—	0	47	—	—
Caliza	Diaclasa	—	>45	—	33-37	—	—	—	—
Caliza metamórfica	Superficie de sedimentación	3,8	49	0	49	1,5	42	—	—
Caliza oolítica	Diaclasa	0	44	—	27-41	—	—	—	—
Contacto entre arena ($\phi' = 37,5°$) y esquisto cuarzo sericítico muy meteorizado, duro, de Venezuela	Plano de esquistosidad	—	—	—	—	0	31	—	—
Contacto entre arenisca y arcilla esquistosa (*clay shale*).	Plano de sedimentación	1,2 (*)	33,5 (*)	—	—	0,5 (**)	35 (**)	—	—
Conglomerado	—	—	—	—	35-38,7	—	—	—	—
Creta	Planos de sedimentación o diaclasas	0- 0,7	40-41	—	—	0-1,3	34-41	—	—
Cuarcita	Diaclasa	0	41-44	—	—	0	37	0	24
Diabasa (Evdokimov y Sapegin, 1964)	Diaclasas de 0,5 a 1,5 mm rellenas con clorita	24-74 44	31-43 31	—	—	— 37	— 51	—	—
Idem pero con deformación tangencial máxima de 10 milímetros	—	17-41	39-24	—	—	—	—	—	—
Idem pero con deformación tangencial máxima de 5 milímetros	—	15-36	33-23	—	—	—	—	—	—
Idem pero con deformación tangencial máxima de 2 milímetros	—	9-32	27-19	—	—	—	—	—	—
Dolerita	Diaclasas	0	52	—	—	0	37	—	—
Esquisto	Plano de esquistosidad	13,3	41	4	39,8	—	—	—	—
Esquisto arcilloso (*shale*)	Diaclasa	0	37	—	—	—	27	—	—
Esquisto cretoso	Diaclasa	0	29-38	—	—	—	—	—	—
Esquisto cuarzo - sericítico, muy meteorizado, duro, de Venezuela	Plano de esquistosidad	>40,7	>51,5	—	—	38	>33	—	—
Esquisto grafitoso, descompuesto, de Venezuela	Plano de esquistosidad	—	—	—	—	<2,5	>57	—	—
Esquisto sericítico descompuesto, de Venezuela	Plano de esquistosidad	—	>45,8	—	—	<2,1	>34	—	—
Filita	Plano de esquistosidad	0- 1,3	40-42	—	—	0	32	—	—
Gabro	Diaclasa	0	47	—	—	0	48	—	—
Gneiss	Plano de esquistosidad	7	49	0	35-49	0	44	—	>31
Grauwacka	Diaclasa	—	>38	—	—	—	—	—	—
Mármol	—	—	—	—	32	—	—	—	—
Monzonita con cuarzo	—	—	—	—	32	—	—	—	—
Piedra de cieno (*mudstone*) meteorizada	—	—	—	—	—	—	—	0	17,5-19
Pizarra	Plano de esquistosidad	0	32	—	—	0	26	—	—
Pizarra sericítica	Plano de esquistosidad	—	>15,5	—	—	—	—	—	—
Roca de silicato cálcico	Plano de sedimentación	—	48	—	—	—	—	—	—
	Diaclasa	—	47	—	—	—	—	—	—

Barton and Choubey (1977)

Rock type	Moisture condition	Basic friction angle ϕ_b	Reference
A. Sedimentary Rocks			
Sandstone	Dry	26—35	Patton, 1966
Sandstone	Wet	25—33	Patton, 1966
Sandstone	Wet	29	Ripley & Lee, 1962
Sandstone	Dry	31—33	Krsmanović, 1967
Sandstone	Dry	32—34	Coulson, 1972
Sandstone	Wet	31—34	Coulson, 1972
Sandstone	Wet	33	Richards, 1975
Shale	Wet	27	Ripley & Lee, 1962
Siltstone	Wet	31	Ripley & Lee, 1962
Siltstone	Dry	31—33	Coulson, 1972
Siltstone	Wet	27—31	Coulson, 1972
Conglomerate	Dry	35	Krsmanović, 1967
Chalk	Wet	30	Hutchinson, 1972
Limestone	Dry	31—37	Coulson, 1972
Limestone	Wet	27—35	Coulson, 1972
B. Igneous Rocks			
Basalt	Dry	35—38	Coulson, 1972
Basalt	Wet	31—36	Coulson, 1972
Fine-grained granite	Dry	31—35	Coulson, 1972
Fine-grained granite	Wet	29—31	Coulson, 1972
Coarse-grained granite	Dry	31—35	Coulson, 1972
Coarse-grained granite	Wet	31—33	Coulson, 1972
Porphyry	Dry	31	Barton, 1971b
Porphyry	Wet	31	Barton, 1971b
Dolerite	Dry	36	Richards, 1975
Dolerite	Wet	32	Richards, 1975
C. Metamorphic Rocks			
Amphibolite	Dry	32	Wallace et al., 1970
Gneiss	Dry	26—29	Coulson, 1972
Gneiss	Wet	23—26	Coulson, 1972
Slate	Dry	25—30	Barton, 1971b
Slate	Dry	30	Richards, 1975
Slate	Wet	21	Richards, 1975

Hoek and Bray (1981)

			Density γ		Friction angle ϕ			Cohesion c	
Type		Material	Kg/m³	Lb/ft³	Material	Degs.	Material	Kg/m²	Lb/ft²
COHESIONLESS	Sand	Dry coarse sand	1440	90	Compacted, well graded, uniform	40-45			
		Dry fine sand	1600	100					
		Wet sand	1840	115	Uniform, coarse, medium fine or silty sand	35-40			
		Very wet sand	1920	120					
					Loose, well graded sand	35-40			
					Fine dry sand	30-35			
	Gravel	Common mixed	1760	110	Common mixed	35-45			
		River gravel	2240	140	Shingle	40			
		Loose Shingle	1840	115	Sandy compact	40-45			
		Sandy gravel	1920	120	Sandy loose	35-40			
	Waste rock	Granite	1600-2000	100-125	Crushed or broken rock	35-45			
		Basalt and dolerite	1760-2240	110-140	Broken chalk	35-45			
		Limestone and sandstone	1280-1920	80-120	Broken shale	30-35			
		Chalk	1000-1280	62-80					
		Shale	1600-2000	100-125					
COHESIVE	Clay	Dry clay	1760	110	Dry boulder clay	30	Very stiff boulder clay	17600	3600
		Damp, drained clay	1840	115	Damp, drained boulder clay	40	Hard shaley clay	14600	3000
		Wet clay	1920	120	Stiff clay	10-20	Stiff clay	9800	2000
		Sandy loam	1600	100	Soft clay	5-7	Firm clay	4900	1000
		Marl	1760	110	Clay gouge	10-20	Soft clay	2400	500
		Gravelly clay	2000	125	Calcite shear zone material	20-27			
					Shale fault material	14-22			
	Overburden	Top soil	1360	85					
		Dry soil	1440	90	Overburden soil	30-35	Overburden soil	490-4900	100-1000
		Moist soil	1600	100					
		Wet soil	1680	105					
	Rock mass	Granite	2614	164	Granite	30-50	Hard rock mass (granite, porphyry etc)	9800-30000	2000-6400
		Quartzite	2614	164	Quartzite	30-45			
		Sandstone	1950	122	Sandstone	30-45	Sandstone or limestone mass	4900-14600	1000-3000
		Limestone	3169	180	Limestone	30-50			
		Porphyry	2580	160	Porphyry	30-40	Shale or soft rock mass	2400-9800	500-2000
		Shale	2400	150	Shale	27-45			
		Chalk	1760	110	Chalk	30-40			

Rodríguez Ortiz et al. (1986)

TIPO DE SUELO	GRANULOMETRIA		LIMITES DE ATTERBERG (Fracción < 0,04 mm)			PESO ESPECIFICO		HDAD. NATURAL	PROCTOR NORMAL		DEFORMABILIDAD (2)		RESISTENCIA AL CORTE			PERM.
											$E_s = E_o \left(\frac{\sigma}{\sigma_{at}}\right)^{\alpha}$		φ'	c'	φ'_r	K
	mm	mm	w_L	w_P	I_P	γ	γ_{sum}	w	D. seca	w_{PN}	E_s kp/cm²	α	(°)	t/m²		m/s
	%	%	%	%	%	t/m³	t/m³	%	t/m³	%						
Grava	<5	<60	—	—	—	1,60 1,90	0,95 1,05	5 2	1,70 1,90	8 5	400 900	0,60 0,40	34 42	— —	32 35	2.10^{-1} 1.10^{-2}
Grava arenosa con pocos finos	<5	<60	—	—	—	2,10 2,30	1,15 1,35	7 3	2,00 2,25	7 4	400 1100	0,70 0,50	35 45	— —	32 35	1.10^{-2} 1.10^{-6}
Grava arenosa con finos limosos o arcillosos que no alteran la estructura granular	8 15	<60	20 45	16 25	4 25	2,10 2,40	1,15 1,45	9 3	2,10 2,35	7 3	400 1200	0,70 0,50	35 43	1 0	32 35	1.10^{-5} 1.10^{-8}
Mezcla de gravas y arenas envueltas por finos	20 40	<60	20 50	16 25	4 30	2,00 2,25	1,05 1,30	13 5	1,90 2,20	10 5	150 400	0,90 0,70	28 35	3 0,5	22 30	1.10^{-8} 1.10^{-11}
Arena uniforme a) Fina	<5	100	—	—	—	1,60 1,90	0,95 1,10	22 8	1,60 1,75	15 10	150 300	0,75 0,60	32 40	— —	30 32	2.10^{-4} 1.10^{-5}
Arena uniforme b) Gruesa	<5	100	—	—	—	1,60 1,90	0,95 1,10	16 6	1,60 1,75	13 8	250 700	0,70 0,55	34 42	— —	30 34	5.10^{-3} 2.10^{-4}
Arena bien graduada y arena con grava	<5	60	—	—	—	1,80 2,10	1,00 1,20	11 5	1,90 2,15	10 6	200 600	0,70 0,55	33 41	— —	32 34	5.10^{-4} 2.10^{-5}
Arena con finos que no alteran la estructura granular	8 15	>60	20 45	16 25	4 25	1,90 2,25	1,05 1,30	15 4	2,00 2,20	13 7	150 500	0,80 0,65	32 40	1 0	30 32	1.10^{-5} 1.10^{-7}
Arena con finos que alteran la estructura granular	20 40	>60	20 50	16 30	4 30	1,80 2,15	0,90 1,10	20 8	1,70 2,00	18 12	50 250	0,90 0,75	25 32	5 1	22 30	1.10^{-7} 1.10^{-10}
Limo poco plástico	>50	>80	25 35	20 28	4 11	1,75 2,10	0,95 1,10	28 15	1,60 1,80	22 15	40 110	0,80 0,60	28 35	2 0,5	25 30	1.10^{-5} 1.10^{-8}
Limo de plasticidad media a alta	>80	>100	35 50	22 25	7 20	1,70 2,00	0,85 1,05	35 20	1,55 1,75	23 16	30 70	0,90 0,70	25 33	3 1	22 29	2.10^{-6} 1.10^{-9}
Arcilla de baja plasticidad	>80	100	25 35	15 22	7 16	1,90 2,20	0,95 1,20	28 14	1,65 1,85	20 14	20 50	1,00 0,90	24 32	6 1,5	20 28	1.10^{-7} 2.10^{-9}
Arcilla de plasticidad media	>90	100	40 50	18 25	16 28	1,80 2,10	0,85 1,10	38 18	1,55 1,75	23 17	10 30	1,00 0,95	20 30	8 2	10 20	5.10^{-8} 1.10^{-10}
Arcilla de alta plasticidad	100	100	60 85	20 35	33 55	1,65 2,00	0,70 1,00	55 20	1,45 1,65	27 20	6 20	1,00 1,00	17 27	10 3	6 15	1.10^{-9} 1.10^{-11}
Limo o arcilla orgánicos	>80	100	45 70	30 45	10 30	1,55 1,90	0,55 0,90	60 30	1,45 1,70	27 18	5 20	1,00 0,85	20 26	7 2	15 22	1.10^{-9} 1.10^{-11}
Turba	—	—	—	—	—	1,04 1,30	0,04 0,30	800 100	—	—	3 8	1,00 1,00	25 30	1,5 0,5	—	1.10^{-5} 1.10^{-8}
Fango	—	—	100 250	30 80	50 170	1,25 1,60	0,25 0,60	200 50	—	—	4 15	1,00 0,90	22 28	2 0,5	—	1.10^{-7} 1.10^{-9}

(1) Según el Grundbau-Taschenbuch, 3.ª ed. 1.ª Parte, 1980.
(2) $\sigma_{at} = 0{,}1$ kp/cm²

CLASE DE SUELO	PESO ESPECIFICO		VALORES DE CALCULO			COEFICIENTE DE COMPRESIBILIDAD
			Resistencia final		Resistencia inicial	
	Emergido γ t/m^3	*Sumergido* γ_{sum} t/m^3	*Angulo de rozamiento (grados)* ϕ'	*Cohesión* c' t/m^2	*Resistencia al corte sin drenaje* c_u t/m^2	E_s t/m^2
Suelos no cohesivos						
— Arena suelta, redondeada	1,8	1,0	30	—	—	2.000- 5.000
— Arena suelta, angulosa	1,8	1,0	32,5	—	—	4.000- 8.000
— Arena semidensa redondeada	1,9	1,1	32,5	—	—	5.000-10.000
— Arena semidensa angulosa	1,9	1,1	35	—	—	8.000-15.000
— Grava sin arena	1,6	1,0	37,5	—	—	10.000-20.000
— Grava gruesa, angulosa	1,8	1,1	40	—	—	15.000-30.000
Suelos cohesivos	(Valores empíricos para muestras inalteradas de la zona Norte alemana)					
— Arcilla semidura	1,9	0,9	25	2,5	5 -10	500- 1.000
— Arcilla difícil de moldear, dura	1,8	0,8	20	2	2,5- 5	250- 500
— Arcilla moldeable, blanda	1,7	0,7	17,5	1	1 - 2,5	100- 250
— Marga glacial, sólida	2,2	1,2	30	2,5	20 -70	3.000-10.000
— Arcilla arenolimosa media	2,1	1,1	27,5	1	5 -10	500- 2.000
— Arcilla arenolimosa blanda	1,9	0,9	27,5	—	1 - 2,5	400- 800
— Limo	1,8	0,8	27,5	—	1 - 5	300- 1.000
— Sedimento ligeramente arcilloso, orgánico, blando	1,7	0,7	20	1	1 - 2,5	200- 500
— Sedimento muy arcilloso, fuertemente orgánico, blando	1,4	0,4	14	1,5	1 - 2	50- 300
— Turba	1,1	0,1	15	0,5	—	40- 100
— Turba moderadamente preconsolidada	1,3	0,3	15	1	—	80- 200

PARAMETROS GEOTECNICOS NORMALIZADOS DE SUELOS ARENOSOS (INDEPENDIENTEMENTE DE SU ORIGEN, ANTIGUEDAD Y HUMEDAD)

TIPO	PARAMETRO	VALORES CARACTERISTICOS PARA UN INDICE DE POROS e, DE			
		0,45	*0,55*	*0,65*	*0,75*
Arenas con grava	c	0,02	0,01	—	—
	φ	43	40	38	—
	E	500	400	300	—
Arenas medias	c	0,03	0,02	0,01	—
	φ	40	38	35	—
	E	500	400	300	—
Arenas finas	c	0,06	0,04	0,02	—
	φ	38	36	32	28
	E	480	380	280	180
Arenas limosas	c	0,08	0,06	0,04	0,02
	φ	36	34	30	26
	E	390	230	180	110

PARAMETROS GEOTECNICOS NORMALIZADOS DE SEDIMENTOS ARCILLOSOS CUATERNARIOS

TIPO	$I_L = \frac{w - w_p}{w_L - w_p}$	PARAMETRO	VALORES CARACTERISTICOS PARA UN INDICE DE POROS e. DE						
			0,45	*0,55*	*0,65*	*0,75*	*0,85*	*0,95*	*1,05*
Arenoso	$0 \le I_L \le 0,25$	c^H	0,15	0,11	0,08	—	—	—	—
		φ^H	30	29	27	—	—	—	—
	$0,25 < I_L \le 0,75$	c^H	0,13	0,09	0,06	0,03	—	—	—
		φ^H	28	26	24	21	—	—	—
Limoso	$0 \le I_L \le 0,25$	c^H	0,47	0,37	0,31	0,25	0,22	0,19	—
		φ^H	26	25	24	23	22	20	—
	$0,25 < I_L \le 0,5$	c^H	0,39	0,34	0,28	0,23	0,18	0,15	—
		φ^N	24	23	22	21	19	17	—
	$0,5 < I_L \le 0,75$	c^H	—	—	0,25	0,20	0,16	0,14	0,12
		φ^H	—	—	19	18	16	14	12
Arcilloso	$0 \le I_L \le 0,25$	c^H	—	0,81	0,68	0,54	0,47	0,41	0,36
		φ^N	—	21	20	19	18	16	14
	$0,25 < I_L \le 0,5$	c^H	—	—	0,57	0,50	0,43	0,37	0,32
		φ^N	—	—	18	17	16	14	11
	$0,5 < I_L \le 0,75$	c^H	—	—	0,45	0,41	0,36	0,33	0,29
		φ^H	—	—	15	14	12	10	7

Dobrin and Savit (1988)

Average density of metamorphic rocks (g/cm^3)		
Gneiss, Chester, Vermont	2.69	2.66 - 2.73
Granitic gneiss	2.61	2.59 - 2.63
Gneiss, Grenville	2.84	2.70 - 3.06
Gneiss with oligoclase	2.67	-
Micaschist with quartz	2.82	2.70 - 2.96
Schist with muscovite and biotite	2.76	-
Schist with staurolite and garnet	2.76	-
Schist with chlorite and sericite	2.82	2.73 - 3.03
Slate	2.81	2.72 - 2.84

Corominas (1989)

Rock	ϕ° (intact rock)	ϕ° (discontinuity)	ϕ° (ultimate)	c (massive rock) kN m^{-2}
Andesite	45	31–35	28–30	
Basalt	48–50	47		
Chalk		35–41		
Diorite	53–55			
Granite	50–64		31–33	100–300
Greywacke	45–50			
Limestone	30–60		33–37	50–150
Monzonite	48–65		28–32	
Porphyry		40	30–34	100–300
Quartzite	64	44	26–34	
Sandstone	45–50	27–38	25–34	50–150
Schist	26–70			
Shale	45–64	37	27–32	25–100
Siltstone	50	43		
Slate	45–60		25–34	

Infilling material	ϕ° (approximate)
Remolded clay gouge	10–20
Calcitic shear zone material	20–27
Shale fault material	14–22
Hard rock Breccia	22–30
Compacted hard rock aggregate	40
Hard rock fill	38

Franklin and Dusseault (1989)

Rock	Cohesion (kPa)	Friction angle (º)
Crystalline limestone	0	42 - 49
Porous limestone	0	32 - 48
Chalk	0	30 - 41
Sandstone	0	24 - 35
Quartzite	0	23 - 44
Clay Shale	0	22 - 37
Schist	0	32 - 40

Koloski et al. (1989)

Soil	Cohesion (MPa)	Friction angle (º)
Alluvial - high energy (GW, GP, GM)	0	30 - 35
Alluvial - low energy (ML, SM, SP, SW)	0 - 0.024	15 - 30
Eolian - dune sand (SP)	0	30 - 35
Eolian - loess (ML, SM)	0.024 - 0.048	20 - 30
Glacial - till (SM, ML)	0.048 - 0.192	35 - 45
Glacial - outwash (GW, GP, SW, SP, SM)	0 - 0.048	30 - 40
Glacial - glaciolacustrine (ML, SM, SP)	0 - 0.144	15 - 35

Giani (1992)

Rock	Cohesion (kPa)	Friction angle (º)
Limestone	0	40 - 42
Sandstone	0	34 - 36
Dolomite	0	30 - 38
Schist	0	21 - 36
Gypsum	0	34 - 35
Quartzite	0	38 - 40
Gneiss	0	39 - 41

Terzaghi et al. (1996)

Description	Porosity, n (%)	Void ratio (e)	Water content, w (%)	Density (Mg/m^3)		Unit Weight (kN/m^3)	
				ρ_d	ρ_{sat}	γ_d	γ_{sat}
1. Uniform sand, loose	46	0.85	32	1.43	1.89	14.0	18.5
2. Uniform sand, dense	34	0.51	19	1.75	2.09	17.2	20.5
3. Mixed-grained sand, loose	40	0.67	25	1.59	1.99	15.6	19.5
4. Mixed-grained sand, dense	30	0.43	16	1.86	2.16	18.2	21.2
5. Glacial till, very mixed-grained	20	0.25	9	2.12	2.32	20.8	22.7
6. Soft glacial clay	55	1.2	45		1.77	12.0	17.4
7. Stiff glacial clay	37	0.6	22		2.07	16.7	20.3
8. Soft slightly organic clay	66	1.9	70		1.58	9.1	15.5
9. Soft very organic clay	75	3.0	110		1.43	6.7	14.4
10. Soft bentonite	84	5.2	194		1.27	4.2	12.5

w = water content when saturated, in percent of dry weight.
ρ_d = density in dry state.
ρ_{sat} = density in saturated state.
γ_d = unit weight in dry state.
γ_{sat} = unit weight in saturated state.

El Amrani Paaza et al. (1998)

Geotechnical properties of the lower Neogene marls

Neogene marls	LL (%)	PI (%)	V_B (g 100 g^{-1})	DI (%)	$\delta h/H$ (%)	ϕ (°)	c (kPa cm^{-2})	q_u (kPa cm^{-2})	C_s (cm^2 kPa^{-1})	C_c (cm^2 kPa^{-1})	$CaCO_3$ (%)	SO_4^- (%)	C_2 (%)
Number of sample	41	41	41	41	41	10	10	41	14	14	41	10	41
Range	30–80	5–40	0.4–3.2	0–27	1–25	4–15	3–23	7–100	8–20	6–16.5	0–15	0–4	0–60
Average	52	23	2.2	5	10	9	10.3	39	10.4	11	5	2	20
Typical deviation	13	11	1.2	9	6	4	5.9	26	3.5	3.9	3.3	1.6	11
Variationcoefficient	25	47	54	180	59	44	57	68	34	35	67	80	54

LL, Liquid limit; PI, plasticity index; V_B, blue valor; DI, dispersion index; $\delta h/H$, swelling ratio; ϕ, friction angle; c, drained cohesion; q_u, uniaxial compressive strength; C_s, swelling index; C_c, compression index; $CaCO_3$, Calcium carbonate content; SO_4 , sulphate content; C_2, Clay fraction.

Geotechnical properties of the upper Neogene marls

Neogene marls	LL (%)	PI (%)	V_B (g 100 g^{-1})	DI (%)	$\delta h/H$ (%)	ϕ (°)	c (kPa cm^{-2})	q_u (kPa cm^{-2})	C_s (cm^2 kPa^{-1})	C_c (cm^2 kPa^{-1})	$CaCO_3$ (%)	SO_4^- (%)	C_2 (%)
Number of sample	130	130	130	130	130	10	10	130	14	14	130	11	130
Range	16–52	1–19	0.1–1.4	0–100	1–11	13–22	0–20	12–129	1–7.5	17–24	2–86	0–16	3–58
Average	27	10.6	0.5	23	1.24	18	5.3	49	4	20	24	3	18
Typical deviation	5	4	0.26	32	1.6	3	6	23	2	2.4	16	4	12
Variationcoefficient	19	39	52	140	76	17	107	47	50	12	67	133	68

LL, Liquid limit; PI, plasticity index; V_B, blue valor; DI, dispersion index; $\delta h/H$, swelling ratio; ϕ, friction angle; c, drained cohesion; q_u, uniaxial compressive strength; C_s, swelling index; C_c, compression index; $CaCO_3$, calcium carbonate content; SO_4^-, sulphate content; C_2, Clay fraction.

El Amrani Paaza et al (2000)

Average values of residual shear strength, effective residual cohesion and effective residual friction obtained for soils of the Granada Basin and the Guadix Basin

		Residual shear strength	Effective residual cohesion	Effective residual friction
High plasticity soils of the	φ'_r min.	$\tau'_r = 35 + 0.14\sigma'_n$	$c'_r = 35$ kPa	$\varphi'_r = 8°$
Granada Basin (Group 1)	φ'_r max.	$\tau'_r = 5 + 0.2\sigma'_n$	$c'_r = 5$ kPa	$\varphi'_r = 11°$
Low plasticity soils of the	φ'_r min.	$\tau'_r = 5.7 + 0.35\sigma'_n$	$c'_r = 5.7$ kPa	$\varphi'_r = 19°$
Granada basin (Group 2)	φ'_r max.	$\tau'_r = 13 + 0.57\sigma'_n$	$c'_r = 13$ kPa	$\varphi'_r = 30°$
Fill of Fco. Abellán dam		$\tau'_r = 7.3 + 0{,}325\sigma'_n$	$c'_r = 7.3$ kPa	$\varphi'_r = 18°$
Fill of Portillo dam		$\tau'_r = 9.7 + 0.37\sigma'_n$	$c'_r = 9.7$ kPa	$\varphi'_r = 20°$

Keystone Retaining Wall Systems (2000)

Wall Backfill Classification	Common Description	UNSC Classification	ϕ range	γ range (moist)	Comments
Good	Sand, Gravel, Stone	GW, GP, GM GC, SW, SP	32° - 36°	100 - 135 pcf	Poor grading lowers weight (ie: #57 stone)
Moderate	Silty Sands Clayey Sands	SM, SC	28° - 32°	110 - 130 pcf	Moisture Sensitive
Difficult	Silts, Low Plastic Clays	ML, CL, OL	25° - 30°	110 - 125 pcf	PI < 20 LL < 40
Bad	High Plastic Silts & Clays, organics	CH, MH OH, PT	0° - 25°	50 - 110 pcf	PI > 20 LL > 40

Hoek (2000)

Rock	Description	Peak c' (MPa)	Peak ϕ^o	Residual c' (MPa)	Residual ϕ^o
Basalt	Clayey basaltic breccia, wide variation from clay to basalt content	0.24	42		
Bentonite	Bentonite seam in chalk	0.015	7.5		
	Thin layers	0.09-0.12	12-17		
	Triaxial tests	0.06-0.1	9-13		
Bentonitic shale	Triaxial tests	0-0.27	8.5-29		
	Direct shear tests			0.03	8.5
Clays	Over-consolidated, slips, joints and minor shears	0-0.18	12-18.5	0-0.003	10.5-16
Clay shale	Triaxial tests	0.06	32		
	Stratification surfaces			0	19-25
Coal measure rocks	Clay mylonite seams, 10 to 25 mm	0.012	16	0	11-11.5
Dolomite	Altered shale bed, ± 150 mm thick	0.04	1(5)	0.02	17
Diorite, granodiorite and porphyry	Clay gouge (2% clay, PI = 17%)	0	26.5		
Granite	Clay filled faults	0-0.1	24-45		
	Sandy loam fault filling	0.05	40		
	Tectonic shear zone, schistose and broken granites, disintegrated rock and gouge	0.24	42		
Greywacke	1-2 mm clay in bedding planes			0	21
Limestone	6 mm clay layer			0	13
	10-20 mm clay fillings	0.1	13-14		
	<1 mm clay filling	0.05-0.2	17-21		
Limestone, marl and lignites	Interbedded lignite layers	0.08	38		
	Lignite/marl contact	0.1	10		
Limestone	Marlaceous joints, 20 mm thick	0	25	0	15-24
Lignite	Layer between lignite and clay	0.014-.03	15-17.5		
Montmorillonite Bentonite clay	80 mm seams of bentonite (mont-morillonite) clay in chalk	0.36 0.016-.02	14 7.5-11.5	0.08	11
Schists, quartzites and siliceous schists	100-15- mm thick clay filling	0.03-0.08	32		
	Stratification with thin clay	0.61-0.74	41		
	Stratification with thick clay	0.38	31		
Slates	Finely laminated and altered	0.05	33		
Quartz / kaolin / pyrolusite	Remoulded triaxial tests	0.042-.09	36-38		

Vazquez Carretero (2001)

Valores medios de las propiedades geotécnicas de los estratos del suelo de Murcia

PROPIEDAD \ ESTRATO	1	1a	2	2'	2a	2a'	3	3'	4
CONTENIDO EN CARBONATOS (%)	29,66	-	30,53	32,19	30,77	-	30,78	-	-
CONTENIDO EN MATERIA ORGÁNICA (%)	4,35	-	2	1,76	-	-	-	-	-
CONTENIDO EN SULFATOS (% concentración ión SO_3)	-	-	0,03	0,04	-	0,03	0,03	-	0,05
% que pasa por TAMIZ 200	99	-	89,81	87,05	77,9	67,38	37,65	55	9,54
% que pasa por TAMIZ 40	99,5	-	99,34	97,88	99,1	96,33	92,72	94,33	25,75
COHESIÓN CONSOLIDADA SIN DRENAJE, c_u (kPa)	-	-	-	20	-	-	-	-	-
ÁNGULO DE ROZAMIENTO INTERNO CONSOLIDADO SIN DRENAJE, ϕ_{cu} (°)	-	26	-	-	-	-	-	-	-
COHESIÓN CON DRENAJE, c' (kPa)	-	-	38	20	-	-	14	-	-
ÁNGULO DE ROZAMIENTO INTERNO CON DRENAJE, ϕ' (°)	-	-	22	26	-	-	32	-	>35
COEFICIENTE DE CONSOLIDACION, c_v (cm^2/s)	-	-	-	$3,55x10^{-4}$	-	-	-	-	-
HUMEDAD por encima del N.F., w (%)	29,66	-	21,6	26,07	-	20,18	17	20	-
HUMEDAD por debajo del N.F., w (%)	-	-	25,74	25,26	25,5	25,31	20,62	-	8,08
LIMITE LIQUIDO, w_L (%)	46,3	-	38,14	35,27	32,23	31,83	29,58	25,5	22,8
LIMITE PLASTICO, w_P (%)	22,06	-	18,98	18,92	13,93	16,08	19,72	17	14,05
ÍNDICE DE PLASTICIDAD, I_P (%)	24,24	-	18,5	16,35	18,3	15,74	9,86	8,5	8,75
INDICE DE COMPRESIÓN, Cc	-	-	0,17	0,16	0,13	0,15	0,14	-	-
INDICE DE HINCHAMIENTO, Cs	-	-	0,02	0,019	0,033	0,009	0,014	-	-
INDICE DE POROS, e	-	-	0,7	0,76	0,69	0,65	0,72	-	-
MÓDULO EDOMÉTRICO, E_{oed} (kPa)	-	-	5.874	7.843	12.200	<4600	9609	-	-
PERMEABILIDAD, k (cm/s)			$1,65x10^{-6}$	$5,15x10^{-6}$			$6,24x10^{-6}$		
PESO ESPECÍFICO APARENTE, γ (kN/m^3)	-	-	19,7	20	-	20,5	20,7	-	-
PESO ESPECÍFICO SATURADO, γ_{sat} (kN/m^3)	-	-	20,1	20,5	20	20,3	20,3	-	-

1: Rellenos antrópicos y tierra vegetal
1a: Fangos bajo la cota del fondo del río Segura
2: Arcillas
2': Arcillas limosas y arenosas
2a: Limos arcillosos con algo de arena fina
2a': Limos arcillosos muy blandos y saturados
3: Arenas, arenas finas limosas y arenas con algo de grava fina e indicios de limo
3': Arenas finas, flojas y saturadas, correspondientes a la terraza baja del río Segura
4: Gravas arenosas

González de Vallejo et al. (2002)

Roca	Peso específico (g/cm^3)	Porosidad (%)
Andesita	2,2-2,35	10-15
Anfibolita	2,9-3,0	—
Arenisca	2,3-2,6	5-25 (16,0)
Basalto	2,7-2,9	0,1-2
Caliza	2,3-2,6	5-20 (11,0)
Carbón	1,0-2,0	10
Cuarcita	2,6-2,7	0,1-0,5
Creta	1,7-2,3	30
Diabasa	2,9	0,1
Diorita	2,7-2,85	—
Dolomía	2,5-2,6	0,5-10
Esquisto	2,5-2,8	3
Gabro	3,0-3,1	0,1-0,2
Gneiss	2,7-3,0	0,5-1,5
Granito	2,6-2,7	0,5-1,5 (0,9)
Grauvaca	2,8	3
Mármol	2,6-2,8	0,3-2 (0,6)
Lutita	2,2-2,6	2-15
Pizarra	2,5-2,7	0,1-1
Riolita	2,4-2,6	4-6
Sal	2,1-2,2	5
Toba	1,9-2,3	14-40
Yeso	2,3	5

Entre paréntesis algunos valores medios de porosidad eficaz.
Datos seleccionados a partir de Goodman (1989), Rahn (1986), Walthan (1999), Farmer (1968).

Roca	Cohesión c (kp/cm^2)	Ángulo de fricción básico ϕ_b (grados)
Andesita	280	45
Arenisca	80-350	30-50
Basalto	200-600	48-55
Caliza	50-400	35-50
Caliza margosa	10-60	30
Cuarcita	250-700	40-55
Diabasa	900-1.200	40-50
Diorita	150	50-55
Dolomía	220-600	25-35
Esquisto	250	25-30*
	20-150*	20-30*
Gabro	300	35
Gneiss	150-400	30-40
Granito	150-500	45-58
Grauvaca	60-100	45-50
Mármol	150-350	35-45
Lutita	30-350	40-60
		15-25*
Pizarra	100-500	40-55
	< 100*	15-30*
Toba	7	—
Yeso	—	30

(*) En superficies de laminación o esquistosidad.
Datos seleccionados a partir de Walthan (1999), Rahn (1986), Goodman (1989), Farmer (1968), Jiménez Salas y Justo Alpañés (1975).

Lamas et al. (2002)

Carbonate marls (32 samples)	Specific Gravity	Cohesion (kPa)	Friction angle (º)
Range	2.52 - 2.75	1.0 - 4.6	15.5 - 35.0
Mean	2.68 ± 0.05	1.9 ± 0.9	24.8 ± 3.9

Mayne et al. (2002)

Rock Type	Unit Weight Range (kN/m^3)
Shale	20 - 25
Sandstone	18 - 26
Limestone	19 - 27
Schist	23 - 28
Gneiss	23 - 29
Granite	25 - 29
Basalt	20 - 30

Smoltczyk (2002)

	a	b	c					
	Soil designation	Group symbol after DIN 18196	Grading		Uniformity coefficient C_U	*Atterberg* limits of particles < 0.4 mm		
			< 0.06 mm %	< 2.0 mm %		w_L %	w_P %	I_P %
1	Gravel, uniform	GE	< 5	< 60	2 5	·	–	·
2	Gravel sandy, with small amount of fines	GW, GI	< 5	< 60	10 100	–	–	–
3	Gravel, sandy, with silt or clay admixture not dividing skeleton	GU, GT	8 15	< 60	30 300	20 45	16 25	4 25
4	Gravel, sandy soil with fines dividing skeleton	GU, GT	20 40	< 60	100 1000	20 50	16 25	4 30
5	Sand uniform a) fine sand	SE	< 5	100	1,2 3	–	–	–
	b) coarse sand	SE	< 5	100	1,2 3	–	–	–
6	Sand, well graded and sand, gravelly	SW, SI	< 5	> 60	6 15	–	–	–
7	Sand with fines not dividing skeleton	SU, ST	8 15	> 60	10 50	20 45	16 25	4 25
8	Sand with fines dividing skeleton	SU, ST	20 40	> 60 > 70	30 500	20 50	16 30	4 30
9	Silt of low plasticity	UL	> 50	> 80	5 50	25 35	21 28	4 11
10	Silt of intermediate or high plasticity	UM, UA	> 80	100	5 50	35 60	22 25	7 25
11	Clay of low plasticity	TL	> 80	100	6 20	25 35	15 22	7 16
12	Clay of intermediate plasticity	TM	> 90	100	5 40	40 50	18 25	16 28
13	Clay of high plasticity	TA	100	100	5 40	60 85	20 35	33 55
14	Silt or clay, organic	OU, OT	> 80	100	5 30	45 70	30 45	10 30
15	Peat	HN, HZ	·	·	–	·	·	–
16	Mud	F	–	–	–	100 250	30 80	50 170

d			e		f		g	h			i
Unit weight			Proctor-values		Compressibility of normally consolidated soils			Shear strength parameters			Coefficient of permeability
γ	γ'	w	ϱ_{opt}	w_{opt}	$E_{oed} = v_e \cdot \sigma_{at}\left(\frac{\sigma}{\sigma_{at}}\right)^{w_e}$			φ'	$\frac{c'}{\sigma'_{vc}}$	φ'_r	k
kN/m³	kN/m³	%	t/m³		v_e	w_e	Δu	Grad		Grad	m/s
16.0	9.5	4	1.70	8	400	0.6	0	34	–	32	2.10^{-1}
19.0	10.5	1	1.90	5	900	0.4		42	–	35	1.10^{-2}
21.0	11.5	6	2.00	7	400	0.7	0	35	–	32	1.10^{-2}
23.0	13.5	3	2.25	4	1100	0.5		45	–	35	1.10^{-6}
21.0	11.5	9	2.10	7	400	0.7	0	35	0.01	32	1.10^{-5}
24.0	14.5	3	2.35	4	1200	0.5	+	43	0	35	1.10^{-8}
20.0	10.5	13	1.90	10	150	0.9	++	28	0.02	22	1.10^{-7}
22.5	13.0	6	2.20	5	400	0.7		35	0.008	30	1.10^{-11}
16.0	9.5	22	1.60	15	150	0.75	0	32	–	30	1.10^{-4}
19.0	11.0	8	1.75	10	300	0.60		40	–	32	2.10^{-5}
16.0	9.5	16	1.60	13	250	0.70	0	34	–	30	1.10^{-3}
19.0	11.0	6	1.75	8	700	0.55		42	–	34	5.10^{-4}
18.0	10.0	12	1.90	10	200	0.70	0	33	–	32	5.10^{-4}
21.0	12.0	5	2.15	6	600	0.55		41	–	34	2.10^{-5}
19.0	10.5	15	2.00	11	150	0.80	+	32	0.01	30	2.10^{-5}
22.5	13.0	4	2.20	7	500	0.65		40	0	32	5.10^{-7}
18.0	9.0	20	1.70	19	50	0.90	++	25	0.03	22	2.10^{-6}
21.5	11.0	8	2.00	12	250	0.75		32	0.01	30	1.10^{-9}
17.5	9.5	28	1.60	22	40	0.80	+	28	0.01	25	1.10^{-5}
21.0	11.0	15	1.80	15	110	0.60		35	0.003	30	1.10^{-7}
17.0	8.5	35	1.55	24	30	0.90	++	25	0.02	22	2.10^{-6}
20.0	10.5	20	1.75	18	70	0.70		33	0.007	29	1.10^{-9}
19.0	9.5	28	1.65	20	20	1.00	++	24	0.04	20	1.10^{-7}
22.0	12.0	14	1.85	15	50	0.90		32	0.015	28	2.10^{-9}
18.0	8.5	38	1.55	23	10	1.00	++	20	0.06	10	5.10^{-8}
21.0	11.0	18	1.75	17	30	0.95		28	0.02	20	1.10^{-10}
16.5	7.0	55	1.45	27	6	1.00	+++	12	0.10	6	1.10^{-9}
20.0	10.0	20	1.65	20	20	1.00		20	0.03	15	1.10^{-12}
15.5	5.5	60	1.45	27	5	1.00	+++	18	0.05	15	1.10^{-9}
18.5	8.5	26	1.70	18	20	0.90		26	0.02	22	2.10^{-11}
10.4	0.4	800	–	–	3	1.00	++	24	0.025		1.10^{-5}
12.5	2.5	80			8	1.00		30	0.008		1.10^{-8}
12.5	2.5	160	–	–	4	1.00	+++	18	0.025		1.10^{-7}
16.0	6.0	50			10	0.90		26	0.008		1.10^{-9}

Waltham (2002)

Rock type	Unit weight (kN m^{-3})	Porosity (%)	Dry UCS range (MPa)	Dry UCS mean (MPa)	Saturated UCS (MPa)	Modulus of elasticity (GPa)	Tensile strength (MPa)	Shear strength (MPa)	Friction angle (φ°)
Granite	27	1	50–135	200		75	15	35	55
Basalt	29	2	100–350	250		90	15	40	50
Greywacke – Ordovician	26	3	100–200	180	160	60	15	30	45
Sandstone – Carboniferous	22	12	40–100	70	50	30	5	15	45
Sandstone – Triassic	19	25	5–40	20	10	4	1	4	40
Limestone – Carboniferous	26	3	50–150	100	90	60	10	30	35
Limestone – Jurassic	23	15	15–70	25	15	15	2	5	35
Chalk – Cretaceous	18	30	5–30	15	5	6	0.3	3	25
Mudstone – Carboniferous	23	10	10–50	40	20	10	1		30
Shale – Carboniferous	23	15	5–30	20	5	2	0.5		25
Clay – Cretaceous	18	30	1–4	2		0.2	2	0.7	20
Coal – Carboniferous	14	10	2–100	30		10	2		
Gypsum – Triassic	22	5	20–30	25		20	1		30
Salt – Triassic	21	5	5–20	12		5			
Hornfels	27	1	200–350	250		80			40
Marble	26	1	60–200	100		60	10	32	35
Gneiss	27	1	50–200	150		45	10	30	30
Schist	27	3	20–100	60		20	2		25
Slate	27	1	20–250	90		30	10		25

Delgado et al. (2003)

Geotechnical properties of fine soils and of the sedimentary rocks

Zone		Particle size				Void ratio, e	Soil density (kg/m^3)	
		%Sand	%Silt	%Clay	Q_{50} (mm)		Dry	Bulk
FPZ	Silt	23.1 ± 13.5	61.6 ± 12.7	19.3 ± 10.6	0.0251 ± 0.0156	0.76 ± 0.14	1558 ± 137	1983 ± 85
	Clay	5.0 ± 7.6	56.4 ± 19.9	46.6 ± 13.4	0.0040 ± 0.0047	0.76 ± 0.13	1558 ± 129	1974 ± 80
	Soft subzone	5.1 ± 5.7	65.7 ± 20.3	38.4 ± 9.5	0.0055 ± 0.0049	1.10 ± 0.21	1287 ± 111	1810 ± 98
AFZ	Silt	35.4 ± 17.2	45.6 ± 17.0	22.0 ± 4.1	0.0258 ± 0.0182	0.60 ± 0.25	1750 ± 218	1984 ± 269
	Clay	23.6 ± 8.4	51.5 ± 17.3	34.9 ± 5.6	0.0083 ± 0.0049	0.60 ± 0.10	1716 ± 157	2022 ± 157
SR	Weathered marl	–	–	–	–	0.69 ± 0.11	1634 ± 107	2038 ± 74
	Marl	7.3 ± 7.5	58.5 ± 17.9	39.9 ± 14.1	0.0050 ± 0.0052	0.52 ± 0.08	1770 ± 100	2122 ± 81
	Sandstone	–	–	–	0.3750 ± 0.2946	0.48 ± 0.13	1940 ± 220	2190 ± 170

Zone		c' (kPa)	ϕ' (°)	c (kPa)	ϕ (°)	Qu (kPa)	N (SPT)[a]
FPZ	Silt	12 ± 12	29.1 ± 6.3	26 ± 23	17.8 ± 6.1	66 ± 63	7.1 ± 6.8 (2)
	Clay	5 ± 8	29.6 ± 4.8	52 ± 44	24.3 ± 7.3	121 ± 104	9.3 ± 6.5 (0)
	Soft subzone	17 ± 16	28.3 ± 7.4	26 ± 15	13.6 ± 3.6	40 ± 30	5 ± 3 (0)
AFZ	Silt	7 ± 3	31.5 ± 5.2	97 ± 80	28.0 ± —	194 ± 160	16.1 ± 14 (4)
	Clay	23 ± 10	29.7 ± 3.9	142 ± 117	23.5 ± 7.8	302 ± 235	15.6 ± 15 (8)
SR	Weathered marl	20 ± 11	26.5 ± 3.9	46 ± 23	16.1 ± 3.0	88 ± 56	15 ± 6 (0)
	Marl	14 ± 13	35.5 ± 12.4	151 ± 122	23.3 ± 9.2	339 ± 202	37 ± 10 (41)
	Sandstone	–	–	–	–	6450 ⊥ 2060	37 ⊥ 16 (83)

Q_{50}: Median particle size.
c'/c: Effective/Total stress cohesion; ϕ'/ϕ: Effective/Total stress friction angle; Qu: Unconfined shear strength; N (SPT): SPT blow count.
[a] Numbers in parenthesis represent the percentage of tests with refusal.

Hernan Gavilanes (2003)

Tipo de roca	Peso especifico seco		Porosidad (n)
	(t_f/m^3)	(kN/m^3)	(%)
Ígneas			
Basalto	2,21 - 2,77	21,66 - 27,15	0,22 - 22,06
Diabasa	2,82 - 2,95	27,64 - 28,91	0,17 - 1,00
Gabro	2,72 - 3,0	26,66 - 29,40	0,00 - 3,57
Granito	2,53 - 2,62	24,79 - 25,68	1,02 - 2,87
Metamórficas			
Cuarcita	2,61 - 2,67	25,58 - 26,17	0,40 - 0,65
Esquisto	2,6 - 2,85	25,48 - 27,93	10,00 - 30,00
Gneis	2,61 - 3,12	25,58 - 30,58	0,32 - 1,16
Mármol	2,51 - 2,86	24,60 - 28,03	0,65 - 0,81
Pizarra	2,71 - 2,78	26,56 - 27,24	1,84 - 3,61
Sedimentarias			
Arenisca	1,91- 2,58	18,72 - 25,28	1,62 - 26,40
Caliza	2,67 - 2,72	26,17 - 26,66	0,27 - 4,10
Dolomita	2,67 - 2,72	26,17 - 26,66	0,27 - 4,10
Lutita	2,0 - 2,40	19,60 - 23,52	20,00 - 50,00

Materiales no cohesivos	Ángulo de fricción (ϕ)	Cohesión (kPa)
Arenas	28 - 34	0
Gravas	34 - 37	0
Roca triturada		
Basalto	40 - 50	
Granito	45 - 50	0
Caliza	35 - 40	
Arenisca	35 - 45	

Materiales cohesivos	Angulo de fricción (ϕ)	Cohesión (kPa)
Arcillas	22 - 27	20 - 50
	27 - 32	30 - 70
Rocas		
Igneas	35 - 45	5.000 - 55.000
Metamórficas	30 - 40	20.000 - 40.000
Sediment. duras	35 - 45	10.000 - 30.000
Sediment. blandas	25 - 35	10.000 - 20.000

Hunt (2005)

Shear Strength Parameters of Residual Soil, Weathered Rocks, and Related Materials[a]

			Strength Parameters	
Rock Type	**Weathering Degree (see Table 6.15)**	**c, $\bar{c}$ (tsf)**	**ϕ, $\bar{\phi}$, ϕ_r (deg)**	**Remarks**
		Igneous Rocks		
Granite	Decomposed	C = 0 ϕ_{avg} = 29	ϕ = 27–31	500 tests, Cherry Hill Dam
	Quality index i	C	ϕ	*In situ* direct shear tests.
	15	1	41	Alto Rabagão
	10	2	45–46	
	7	3	49–52	
	5	5	57	
	3	6 13	62 63	
	Weathered, zone IIB		ϕ_r = 26–33	Lab direct shear tests.
	Partly weathered, zone IIB		ϕ_r = 27–31	Alto Lindosa
	Relatively sound, zone III		ϕ_r = 29–32	
	Red earth, zone IB		ϕ = 28	
	Decomposed, zone IC		ϕ_{avg} = 35	
	Decomposed, fine-grained	c = 0 if	ϕ = 25–34	
	Decomposed, coarse-grained	saturated	ϕ = 36–38	
	Decomposed, remolded		ϕ = 22–40	
Quartz diorite	Decomposed; sandy, silty	c = 0.1	ϕ = 30 +	Lab tests, UD samples
Diorite	Weathered	c = 0.3	ϕ = 22	CU triaxial tests
Rhyolite	Decomposed		ϕ = 30	
		Metamorphic Rocks		
Gneiss (micaceous)	Zone IB	c = 0.6	ϕ = 23	Direct shear tests
	Decomposed	c = 0.3	ϕ = 37	
Gneiss	Decomposed, zone IC		ϕ = 18.5	CU triaxial tests
	Decomposed (fault zone)	c = 1.5	ϕ = 27	Direct shear tests on concrete-rock surfaces
	Much decomposed	c = 4.0	ϕ = 29	
	Medium decomposed	c = 6.5	ϕ = 35	
	Unweathered	c = 12.5	ϕ = 60	
Schist	Weathered (mica schist soil)		ϕ = 24½	From analysis of slides
	Partly weathered mica schists and phyllites (highly fractured)	c = 0.7	ϕ = 35	Perpendicular to schistosity
	Weathered, intermediate zone IC	$\bar{c}$, = 0.5 $\bar{c}$, = 0.7	ϕ, $\bar{\phi}$, = 15 ϕ = 18 $\bar{\phi}$, = 21	CU tests, S = 50% CU tests, S = 100%
	Weathered		ϕ = 26–30	Compacted rock fill, field direct shear tests
Phyllite	Residual soil, zone IC	c = 0	ϕ = 24	Perpendicular to schistosity
		c = 0	ϕ = 18	Parallel to schistosity (both from analysts of slides)
		Sedimentary Rocks		
Keuper marl	Highly weathered	$\bar{c}$,≤0.1	$\bar{\phi}$ = 25–32; ϕ_r = 18–24	2% carbonates
	Intermediately weathered	$\bar{c}$,≤0.1	$\bar{\phi}$ = 32–42 ϕ_r = 22–29	14% carbonates
	Unweathered	$\bar{c}$,≤0.3	$\bar{\phi}$ = 40 ϕ_r − 23 32	20% carbonates (all triaxial tests, D and CU and cut planes)

(*Continued*)

Continued

Rock Type	Weathering Degree (see Table 6.15)	Strength Parameters c, $\bar{c}$ (tsf)	$\phi, \bar{\phi}, \phi_r$ (deg)	Remarks
London clay	Weathered (brown)	$\bar{c}$, = 0.1–0.2	$\bar{\phi}$ = 19–22 ϕ_r = 14	
	Unweathered	$\bar{c}$, = 0.9–1.8	$\bar{\phi}$ = 23–30 ϕ_r = 15	
		Joint Filling		
"Black seams"	In zone IC		ϕ_r = 10.5	Seam with slickensides
			ϕ_r = 14.5	Seam without slicken sides (both CU tests)
		Shear Zones[b]		
Metamorphic rocks			ϕ_r = 15–25	Foliation shear
Shales			ϕ = 10–20	Mylonite seam
Fault gouge, general			ϕ_r = 15–30	

[a] From Deere, D.U. and Patton, *Proceedings of the 4th Panamerican Conference on Soil Mechanics and Foundation Engineering*, San Juan, Vol. I, 1971, pp. 87–100.

[b] From Deere, D.U., *Foundation for Dams, ASCE*, New York, 1974, pp. 417–424.

Common Properties of Cohesionless Soils

Material	Compactness	D_R (%)	N[a]	γ dry (g/cm³)[b]	γ dry (pcf)[b]	Void ratio e	Strength[c] ϕ
GW:well-graded gravels, gravel-sand mixtures	Dense	75	90	2.21	138	0.22	40
	Medium dense	50	55	2.08	130	0.28	36
	Loose	25	<28	1.97	123	0.36	32
GP: poorly graded gravels, gravel-sand mixtures	Dense	75	70	2.04	127	0.33	38
	Medium dense	50	50	1.92	120	0.39	35
	Loose	25	<20	1.83	114	0.47	32
SW: well-graded sands, gravelly sands	Dense	75	65	1.89	118	0.43	37
	Medium dense	50	35	1.79	112	0.49	34
	Loose	25	<15	1.70	106	0.57	30
SP: poorly graded sands, gravelly sands	Dense	75	50	1.76	110	0.52	36
	Medium dense	50	30	1.67	104	0.60	33
	Loose	25	<10	1.59	99	0.65	29
SM: silty sands	Dense	75	45	1.65	103	0.62	35
	Medium dense	50	25	1.55	97	0.74	32
	Loose	25	<8	1.49	93	0.80	29
ML: inorganic silts, very fine sands	Dense	75	35	1.49	93	0.80	33
	Medium dense	50	20	1.41	88	0.90	31
	Loose	25	<4	1.35	84	1.0	27

[a] *N* is blows pet loot of penetration in the SPT. Adjustments for gradation are after Burmister (1962). See Table 3.23 for general relationships of D_R vs. *N*.

[b] Density given is for G_s = 2 65 (quartz grains).

[c] Friction angle ϕ depends on mineral type, normal stress, and grain angularity as well as D_R and gradation (see Figure 3.93).

Typical Properties of Formations of Cohesive Materials

Material	Type[a]	Locations	γ_d (pcf)	W (%)	LL (%)	PL (%)	s_u (tsf)	$\bar{c}$ (tsf)	$\bar{\phi}$	Remarks
Clay shales (Weathered)										
Carlisle (Cret.)	CH	Nebraska	92.4	18				0.5	45	ϕ extremely variable
Bearpaw (Cret.)	CH	Montana	89.9	32	130	90		0.35	15	
Pierre (Cret.)		South Dakota	91.7	28				0.9	12	
Cucaracha (Cret.)	CH	Panama Canal		12	80	45				$\phi_r = 10°$
Pepper (Cret.)	CH	Waco, Texas		17	80	58		0.4	17	$\phi_r = 7°$
Bear Paw (Cret.)	CH	Saskatchewan		32	116	92		0.4	20	$\phi_r = 8°$
Modeio (Tert.)	CH	Los Angeles	89.9	29	66	31		1.6		Intact specimen
Modelo (Tert.)	CH	Los Angeles	89.9	29	66	31		0.32	27	Shear zone
Martinez (Tert.)	CH	Los Angeles	103.6	22	62	38		0.25	26	Shear zone
(Eocene)	CH	Menlo Park, California	103.0	30	60	50	Free swell 100%; $P = 10$ tsf			
Residual Soils										
Gneiss	CL	Brazi; buried	80.5	38	40	16		0	40	$e_0 = 1.23$
Gneiss	ML	Brazil; slopes	83.6	22	40	8		0.39	19	c,ϕ
Gneiss	ML	Brazil; slopes	83.6		40	8		0.28	21	Unsoaked
Colluvium										
From shales	CL	West Virginia		28	48	25		0.28	28	$\phi_r = 16°$
From gneiss	CL	Brazil	68.6	36	40	16		0.2	31	$\phi_r = 12°$

(*Continued*)

Continued

Material	Type[a]	Locations	γd (pcf)	W (%)	LL (%)	PL (%)	s_u (tsf)	c (tsf)	ϕ	Remarks
Alluvium										
Back swamp	OH	Louisiana	35.6	140	120	85	0.15			
Back swamp	OH	Louisiana	62.4	60	85	50	0.1			
Hack swamp	MH	Georgia	59.9	54	61	22	0.3			e_s = 1.7
Lacustrine	CL	Great Salt Lake	48.7	50	45	20	0.34			
Lacustrine	CL	Canada	69.3	62	33	15	0.25			
Lacustrine (volcanic)	CH	Mexico City	18.1	300	410	260	0.4			e_s=7, S_t=13
Estuarine	CH	Thames River	48.7	90	115	85	0.15			
Estuarine	CH	Lake Maricaibo		65	73	50	0.25			
Estuarine	CH	Bangkok		130	118	75	0.05			
Estuarine	MH	Maine		DO	60	30	0.2			
Marine Soils (Other than Estuarine)										
Offshore	MH	Santa Barbara, California	52.0	80	83	44	0.15			e_s = 2.28
Offshore	CH	New Jersey		65	95	60	0.65			
Offshore	CH	San Diego	36.2	125	111	64	0.1			Depth = 2 m
Offshore	CH	Gulf of Maine	36.2	163	124	78	0.05			
Coastal Plain	CH	Texas (Beaumont)	86.7	29	81	55	10	0.2	16	ϕ_r=14, e_s=0.8
Coastal Plain	CH	London	99.8	25	80	55	2.0			
Loess										
Silty	ML	Nebraska-Kansas	76.8	9	30	8		0.6	32	Natural *w*%
Silty	ML	Nebraska Kansas	76.8	(35)	30	8		0	23	Prewetted
Clayey	CL	Nebraska-Kansas	78.0	9	37	17		2.0	30	Natural *w*%
Glacial Soils										
Till	CL	Chicago	132.3	23	37	21	3.5			
Lacustrine (varved)	CL	Chicago	105.5	22	30	15	1.0			e_s=0.6 (OC)
Lacustrine (varved)	CL	Chicago		24	30	13	01			e_s=1.2 (NC)
Lacustrine (varved)	CH	Chicago	73.6	50	54	30	0.1			
Lacustrine (varved)	CH	Ohio	60.0	46	58	31	0.6			S_t = 4
Lacustrine) (varved)	CH	Detroit	74.9	46	55	30	08			e_s=13 (clay)
Lacustrine (varved)	CH	New York City		46	62	34	1.0			e_s=1.25 (clay)
Lacustrine (varved)	CL	Boston	84.2	38	50	26	0.8			S_t = 3
Lacustrine (varved)	CH	Seattle		30	55	22			30	ϕ_r = 13°
Marine[b]	CH	Canada–Leda clay	55.5	80	60	32	0.5			S_t = 128
Marine[b]	CL	Norway	83.6	40	38	15	0.13			S_t = 7
Marine[b]	CL	Norway	80.5	43	28	15	0.05			S_t = 75

ROM 0.5-05 (2005)

	Rocks	Specific weight (kN/m³)	Unconfined Comprensive Strength of Fresh Fragments (MPa)	Deformation Modulus (MPa)	
Hard	IGNEOUS METAMORPHIC Gneiss, quartzites SEDIMENTARY Well-cemented sandstones, some more compact limestones and dolomites	26	100	MASSIVE	50.000
				JOINTED	20.000
				HIGHLY JOINTED	10.000
Medium	METAMORPHIC Schists and slates SEDIMENTARY Excepting poorly cemented sandstones, marls and conglomerates	24	50	MASSIVE	20.000
				JOINTED	10.000
				HIGHLY JOINTED	5.000
Soft	SEDIMENTARY Excepting poorly cemented sandstones, marls and conglomerates	22	20	MASSIVE	5.000
				JOINTED	2.000
				HIGHLY JOINTED	1.000

Specific weight: The value indicated can vary by ± 2 kN/m³ or even more in some rocks, particularly if they contain heavy minerals (pyrite, for instance).
Strength: The value may range from less than half to over double the figure indicated.
Deformation modulus: This refers to the equivalent deformation modulus of the rock mass when an area larger than 1 m² is loaded. The modulus value can vary across a wide range – values three times greater or smaller than those indicated can be found. Poisson's ratio may be taken to equal 0.2 for the hardest rocks, 0.25 for medium and 0.3 for soft rocks.

	Soil Type	Compacity	Void Ratio (2)	Cohesion (kPa)	Friction Angle (ϕ^0)	Drained deformation Modulus (5) (MPa)	Permeability Coefficient (3) (cm/s)
Granular Soils (1)	Clean sands and gravels (> 10% sand)	Dense	0,25	0	45	100	10^{-2}
		Medium	0,35	0	40	50	
		Loose	0,45	0	35	20	
		Very losse	0,60	0	30	10	
Granular Soils (1)	Gravel and sands with low silt and/ or clay contents (5-10%) (4)	Dense	0,20	10	40	50	10^{-3}
		Medium	0,30	5	35	20	
		Loose	0,40	2	30	10	
		Very loose	0,60	0	27	5	
	Gravel and sands with high fine soil contents (10-20%) (4)	Dense	0,15	20	35	50	10^{-4}
		Medium	0,25	10	30	20	
		Losse	0,35	5	27	10	
		Very loose	0,50	0	25	5	
Artificial Fills	Dumped pit-run berms and continuously graded (dirty) rockfills	Loose	0,50	0	40	10	-
		Very loose	0.70	0	35	5	

IGME (2006)

PROPIEDADES COMUNES DE LOS SUELOS NO COHESIVOS (HUNT, 1984. Cortesía de McGraw-Hill)

Material	Compacidad	D_r (%)	N (1)	Densidad seca (2) γ_d(g/cm³)	Indice de poros e	Angulo de rozamiento interno
GW: Gravas bien graduadas, mezclas de grava y de arena	Densa	75	90	2,21	0,22	40
	Medianamente densa	50	55	2,08	0,28	36
	Suelta	25	< 28	1,97	0,36	32
GP: Gravas mal graduadas, mezclas de grava y arena	Densa	75	70	2,04	0,33	38
	Medianamente densa	50	50	1,92	0,39	35
	Suelta	25	< 20	1,83	0,47	32
SW: Arenas bien graduadas, arenas con grava	Densa	75	65	1,89	0,43	37
	Medianamente densa	50	35	1,79	0,49	34
	Suelta	25	< 15	1,70	0,57	30
SP: Arenas mal graduadas, arenas con grava	Densa	75	50	1,76	0,52	36
	Medianamente densa	50	30	1,67	0,60	33
	Suelta	25	< 10	1,59	0,65	29
SM: Arenas limosas	Densa	75	45	1,65	0,62	35
	Medianamente densa	50	25	1,55	0,74	32
	Suelta	25	<8	1,49	0,80	29
ML: Limos inorgánicos, arenas muy finas	Densa	75	35	1,49	0,80	33
	Medianamente densa	50	20	1,41	0,90	31
	Suelta	25	< 4	1,35	1,00	27

(1) N es el número de golpes por 30 cm de penetración en el SPT. La Tabla V.5 relaciona D_r y N.
(2) Los valores corresponden a γ_s = 2,65 (partículas de cuarzo).

VALORES REPRESENTATIVOS DE φ' PARA ARENAS Y LIMOS (TERZAGHI Y PECK, 1948. Cortesía de John Wiley and Sons)

Materiales	φ' (grados)	
	Suelto	Denso
Arena, granos redondos, uniformes	27,5	34
Arena, granos angulares, bien graduados	33	45
Gravas arenosas	35	50
Arena limosa	27-33	30-34
Limo inorgánico	27-30	30-35

Bell (2007)

	Gravels	Sands	Silts
Specific gravity	2.5–2.8	2.6–2.7	2.64–2.66
Bulk density (Mg m^{-3})	1.45–2.3	1.4–2.15	1.82–2.15
Dry density (Mg m^{-3})	1.4–2.1	1.35–1.9	1.45–1.95
Porosity (%)	20–50	23–35	—
Void ratio	—	—	0.35–0.85
Liquid limit (%)	—	—	24–35
Plastic limit (%)	—	—	14–25
Coefficient of consolidation (m^2 yr^{-1})	—	—	12.2
Cohesion (kPa)	—	—	75
Angle of friction (deg)	35–45	32–42	32–36

Jaeger et al. (2007)

Rock	Cohesion (kPa)	Friction angle (º)
Bentonitic shale	0	9 - 27
Marble	0	31 - 37
Gneiss	0	31 - 35

Ministerio de Fomento (2009)

TIPOS DE ROCA		PESO ESPECÍFICO SECO (kN/m^3)
Rocas sedimentarias		
Conglomerados		20-25
Areniscas		20-25
Limolitas		20-25
Argilitas		20-25
Margas		18-22
Calizas		18-25
Calizas margosas		18-25
Calcarenitas		20-25
Dolomías		20-26
Yesos		22
Rocas metamórficas		
Pizarras		20-25
Esquistos		20-25
Gneises		20-25
Rocas plutónicas		22-25
Rocas volcánicas		10-30

TIPO DE SUELO		PESO ESPECÍFICO SECO (kN/m^3)	COHESIÓN EFECTIVA c' (kPa)	ÁNGULO DE ROZAMIENTO EFECTIVO ϕ' (^{o})
Tierra vegetal		*	*	*
Coluviones		15-22	0-10	20-40
Acarreos fluviales		17-22	0-10	25-40
Gravas		17-22	0	25-40
Arenas		16-20	0	30-35
Limos		12-18	0-10	25-30
Arcillas normalmente consolidadas		11-16	0-10	15-25
Suelos fangosos y turbas		5-10	0	10-20
Vertidos artificiales		*	*	*
Roca alterada con indicación del grado de alteración (tabla 3.3)		15-22	0-50	15-35

Appendix A2: Empirical relationships between Schmidt hammer rebound and Join Compressive Strength (JCS)

Barton and Choubey (1977)

$$\log JCS = 0.00088\ \gamma_{rock} \cdot r + 1.01$$

JCS: Join Compressive Strength in MN/m^2
γ_{rock} : specific weight in kN/m^3
r: Schmidt hammer rebound of the joint

Aydin and Basu (2005)

References	Proposed correlations*	r	Validity range		
			Rock type	σ_{UCS}	R
Aufmuth (1973)	$\sigma_{UCS}=0.33*(R_L*\rho)^{1.35}$	0.80	25 different lithologies	12–362	10–54
	$E_t=4911.84*(R_L*\rho)^{1.06}$	0.75			
Kahraman (1996: in Yilmaz and Sendir, 2002)	$\sigma_{UCS}=0.00045*(R_N*\rho)^{2.46}$	0.96	10 different lithologies	–	–
Gokceoglu (1996: in Yilmaz and Sendir, 2002)	$\sigma_{UCS}=0.0001*R^{3.27}$	0.84	Marl	–	–
Yasar and Erdogan (2004)	$\sigma_{UCS}=0.000004*R_L^{4.29}$	0.89	Carbonates, sandstone, basalt	40–112	45–55
Dearman and Irfan (1978)	$\sigma_{UCS}=0.00016*R_L^{3.47}$	–	Granite	11–266	23–62
	$E_t=1.89*R_L-60.55$	0.93	(Grade I to IV)		
Xu et al. (1990)	$\sigma_{UCS}=2.98*e^{(0.06*R_L)}$	0.95	Mica-schist	9–56	17–53
	$E_t=1.77*e^{(0.07*R_L)}$	0.96			
	$\sigma_{UCS}=2.99*e^{(0.06*R_L)}$	0.91	Prasinite	8–145	21–64
	$E_t=2.71*e^{(0.04*R_L)}$	0.91			
	$\sigma_{UCS}=2.98*e^{(0.063*R_L)}$	0.94	Serpentinite	–	–
	$E_t=2.57*e^{(0.03*R_L)}$	0.88			
	$\sigma_{UCS}=3.78*e^{(0.05*R_L)}$	0.93	Gabro	–	–
	$E_t=1.75*e^{(0.05*R_L)}$	0.95			
	$\sigma_{UCS}=1.26*e^{(0.52*R_L*\rho)}$	0.92	Mudstone	–	–
	$E_t=0.07*e^{(0.31*R_L*\rho)}$	0.89			
Deere and Miller (1966)	$\sigma_{UCS}=9.97*e^{(0.02*R_L*\rho)}$	0.94	28 different lithologies	22–358	23–59
	$E_t=0.19*R_L*\rho^2-7.87$	0.88			
Beverly et al. (1979: in Xu et al., 1990)	$\sigma_{UCS}=12.74*e^{(0.02*R_L*\rho)}$		20 different lithologies	38–218	–
	$E_t=0.19*R_L*\rho^2-12.71$				
Cargill and Shakoor (1990)	$\sigma^{UCS}=3.32*e^{(0.04*R_L*\rho)}$	0.93	Sandstones		
	$\sigma_{UCS}=18.17*e^{(0.02*R_L*\rho)}$	0.98	Carbonates	35–271	27–49
Kahraman (2001)	$\sigma_{UCS}=6.97*e^{(0.01*R_N*\rho)}$	0.78	Carbonates	4–153	15–70
This study	$\sigma_{UCS}=1.45*e^{(0.07*R_L)}$	0.92	Granite	6–196	20–65
	$E_t=1.04*e^{(0.06*R_L)}$	0.91	(Grade I to IV)		23–76
	$\sigma_{UCS}=0.92*e^{(0.07*R_N)}$	0.94			
	$E_t=0.72*e^{(0.05*R_N)}$	0.92			
Yilmaz and Sendir (2002)	$\sigma_{UCS}=2.27*e^{(0.06*R_L)}$	0.91			
	$E_t=3.15*e^{(0.05*R_L)}$	0.95	Gypsum	15–30	30–44
Katz et al. (2000)	$\sigma_{UCS}=2.21*e^{(0.07*R_N)}$	0.96	Limestone, sandstone	11–259	24–73
	$E_t=0.00013*R_N^{3.09}$	0.99	Syenite, granite		
Kidybinski (1980)	$\sigma_{UCS}=0.52*e^{(0.05*R+\rho)}$		Coal, shale, mudstone, siltstone, sandstone	–	–
Shorey et al. (1984)	$\sigma_{UCS}=0.40*R_N-3.60$	0.94	Coal	3–13	15–40
Haramy and DeMarco (1985)	$\sigma_{UCS}=0.99*R_L-0.38$	0.70	Coal	7–46	12–44
Ghose and Chakraborti (1986)	$\sigma_{UCS}=0.88*R_L-12.11$	0.87	Coal	13–41	28–53
Singh et al. (1983)	$\sigma_{UCS}=2.00*R_L$	0.86	Sandstone, siltstone, mudstone, seatearth	12–73	10–35
O' Rourke (1989)	$\sigma_{UCS}=4.85*R_L-76.18$	0.77	Sandstone, siltstone, limestone, anhydride	14–215	19–52
Sachpazis (1990)	$\sigma_{UCS}=4.29*R_L-67.52$	0.96	33 different carbonates	22–311	16–60
	$E_t=1.94*R_L-33.93$	0.88			
Tugrul and Zarif (1999)	$\sigma_{UCS}=8.36*R_L-416.00$	0.87	Granite	109–193	64–72

Abbreviations:
σ_{UCS}: UCS (MPa); E_t: tangent Young's modulus (GPa) at 50% of σ_{UCS}; ρ: density (gm/cm^3); R_L and R_N: rebound values for L and N hammers; r: regression coefficient.
* Note that some of the above relations were modified from their original forms into one of the general expressions (power/exponential/linear) with common SI units for individual variables.

Others

References	Proposed correlation	r	Rock type
Güney et al. (2005)	$UCS = 4.124 \cdot R_N - 134.33$	0.91	Limestone and marble
Buyuksagis and Goktan (2007)	$UCS = 2.5328 \cdot e^{0.06Rn}$	0.94	Granite, limestone, marble and travertine
Shalabi et al. (2007)	$UCS = 3.201 \cdot R_L - 46.59$	0.76	Low density dolomite and dolomitic limestone
Sabatakakis et al. (2008)	$UCS = 3.1 \cdot e^{0.09Rl}$	0.89	Limestone, marlstone and sandstone

Selected relationships to estimate Join Compressive Strength (JCS) at 2002 Bullas and 2005 La Paca rock slides

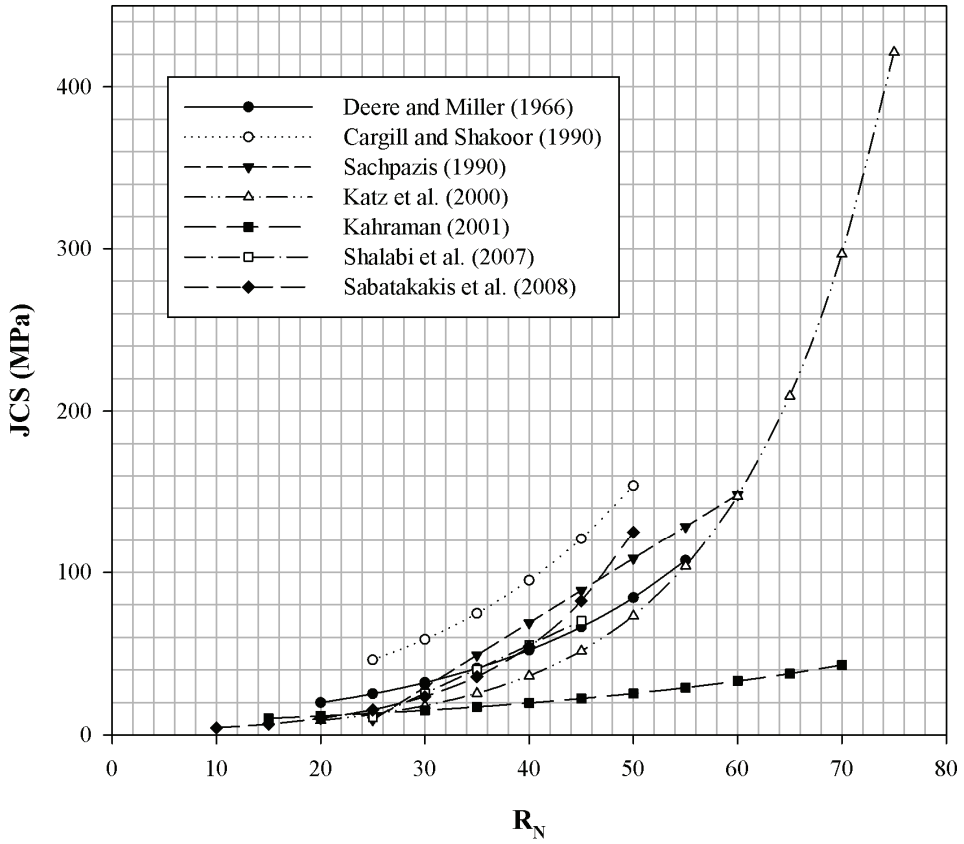

2002 Bullas rock slide

Weathered joint surface		**Unweathered joint surface**	
r_N (0°)	**r_N (0°)**	**R_N (0°)**	**R_N (0°)**
42	61	66	62
60	31	62	34
44	49	54	64
43	47	62	68
29	43	68	60
57	49	64	64
52	53	60	66
62	60	68	60
52	64	56	64
47	53	52	60
41	64	60	40
50	51	59	60
56	55	52	51
60	57	62	55
50	30	60	60
34	53	30	57
60	64	40	55
40	64	56	55
55	51	56	51
58	60	54	68
50	**53**	**57**	**58**
51 ± 2		**57 ± 0.4**	

	JCS (MPa)
Deere and Miller (1966)	80
Barton and Choubey (1977)	84
Cargill and Shakoor (1990)	147
Sachpazis (1990)	114
Katz et al. (2000)	80
Kahraman (2001)	25
Shalabi et al. (2007)	89
Sabatakakis et al. (2008)	139

Mean	**95**
Standard deviation	**39**

2005 La Paca rock slide

Weathered joint surface				Unweathered joint surface			
r_N (0º)	r_N (0º)	r_N (0º)	r_N (0º)	R_N (0º)	R_N (0º)	R_N (0º)	R_N (0º)
21	44	38	51	38	34	41	38
41	26	28	39	43	41	42	43
43	41	44	21	32	41	47	32
21	42	38	14	32	39	30	32
41	28	17	25	23	37	38	23
28	39	51	33	60	41	50	60
33	29	35	22	20	33	32	20
47	40	51	28	54	43	54	54
51	30	57	39	54	46	41	54
51	33	36	39	32	37	49	32
47	25	22	42	33	39	60	33
57	25	45	17	28	45	51	28
30	49	20	26	50	41	34	50
35	41	35	39	30	39	42	30
37	48	45	32	49	48	58	49
47	40	25	30	33	43	64	33
43	29	25	29	48	49	42	48
30	37	47	36	45	32	45	45
37	21	26	17	49	38	58	49
33	36	47	25	45	46	51	45
39	**35**	**37**	**30**	**40**	**41**	**46**	**40**
35 ± 4				**42 ± 4**			

	JCS (MPa)
Deere and Miller (1966)	43
Barton and Choubey (1977)	46
Cargill and Shakoor (1990)	78
Sachpazis (1990)	51
Katz et al. (2000)	26
Kahraman (2001)	18
Shalabi et al. (2007)	41
Sabatakakis et al. (2008)	37

Mean	**43**
Standard deviation	**18**

Appendix A3: Laboratory tests on soil samples

2002 Bullas rock slide

Laboratorios Entecsa calidad acreditada

ACTA DE ENSAYOS DE IDENTIFICACIÓN DE SUELOS

Obra: GR, UNIVERSIDAD
Peticionario: UNIVERSIDAD DE GRANADA
Fecha ensayo: 20/05/2009

Referencia: 091036
Procedencia: traida al laboratorio
Denominacion: gra-1

ENSAYOS ACREDITADOS. JUNTA DE ANDALUCIA

ANÁLISIS GRANULOMÉTRICO POR TAMIZADO (UNE 103-101/95)

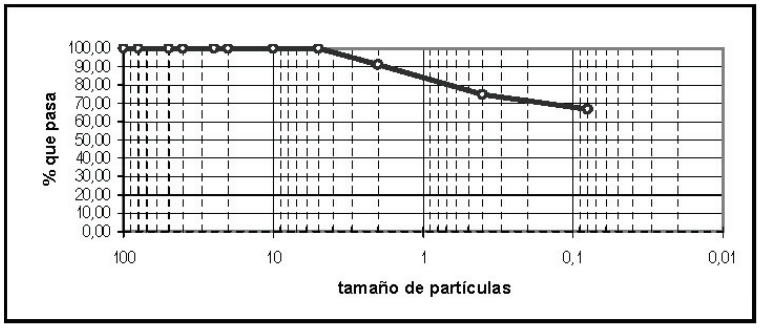

TAMICES (% QUE PASA)

UNE	100	80	50	40	25	20	10	5	2	0,4	0,08
ASTM	4"	3"	2"	1,5"	1"	3/4"	3/8"	N.º 4	N.º 10	N.º 40	N.º 200
% QUE PASA	100,00	100,00	100,00	100,00	100,00	100,00	100,00	100,00	91,26	74,88	66,77

LÍMITES DE ATTERBERG.

LÍMITE LÍQUIDO (UNE 103-103/94): **42,40**
LÍMITE PLÁSTICO (UNE 103-104/93): **24,28**
ÍNDICE DE PLASTICIDAD: **18,12**

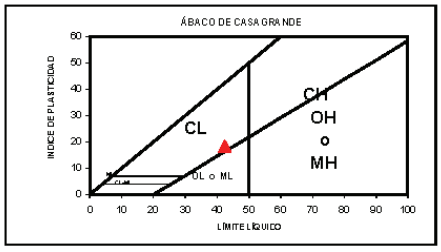

CLASIFICACIÓN DEL SUELO.

USCS/ASTM (ASTM-D 2487/00) **CL**

DESCRIPCIÓN DEL SUELO: **Arcillas inorgánicas de baja plasticidad**

OTRAS PROPIEDADES

HUMEDAD NATURAL % (UNE103-300/93): **1,76**
D. APARENTE (gr/cm3) (UNE 103-301/94): **2,06**
D. SECA (gr/cm3): **2,03**

CAMBIO POTENCIAL DE VOLUMEN (E. LAMBE) (UNE 103600/96)

P.V.C.:
ÍNDICE DE EXPANSIVIDAD (kp/cm2): (MPa):
CLASIFICACIÓN:

ACTA DE RESULTADOS DE ENSAYOS

Laboratorios Entecsa® calidad acreditada

DENSIDAD RELATIVA DE LAS PARTICULAS DE UN SUELO
PESO ESPECÍFICO. UNE-103302:1994 ENSAYO ACREDITADO. JUNTA DE ANDALUCIA

Peticionario: UNIVERSIDAD DE GRANADA
Obra: GR, UNIVERSIDAD
Trabajo Nº: 091036
Fecha: 21/05/2009

Procedencia de la muestra: traida al laboratorio
Descripcion del material: arcillas abigarradas con bolos de carbonatos
Denominación: den-rel-1

	MUESTRA 1	MUESTRA 2	MUESTRA 3
M1	103,102	100,472	106,580
M2	63,221	60,524	60,149
M3	78,386	75,753	75,340
M4	112,740	110,161	116,236
g	2,744	2,749	2,745

PESO ESPECÍFICO **G= 2,742 g/cm3**

ACTA DE RESULTADOS DE ENSAYOS

ENSAYO DE CORTE DIRECTO (UNE 103 401-98)

Laboratorios Entecsa calidad acreditada

ENSAYO ACREDITADO. JUNTA DE ANDALUCIA

Obra: GR, UNIVERSIDAD
Peticionario: UNIVERSIDAD DE GRANADA
Referencia: 091036
Fecha ensayo: 21/05/2009
Denominación: CD-1
Descripción: arcillas abigarradas con cantos
Cota (m): 0

Dimensiones de las probetas.

Diámetro (cm):	5
Altura (cm):	2
Área (cm^2):	19,63
Volúmen (cm^3):	39,27

Párametros del Ensayo.

Velocidad del Ensayo (mm/min):	0,52
Tipo de Ensayo:	UU

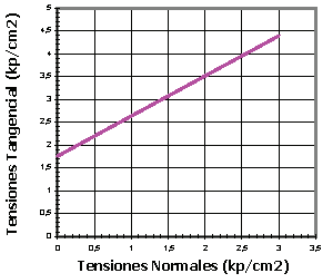

Párametros Físicos de las Probetas.

Probeta	I	II	III
Humedad inicial (%)	11,94	11,94	11,94
Humedad final (%)			
Densidad aparente (g/cm3)	2,02	1,98	2,01
Densidad seca (g/cm3)	1,78	1,75	1,77
Indice de huecos incial	0,54	0,57	0,55
Indice de huecos final	0,87	0,97	0,90
Dens. de las partículas (g/cm3	2,74	2,74	2,74
Grado de saturación (%)	39,51	36,67	38,73

Tensiones aplicadas a la probeta.

Probeta:	I	II	III
T. Normal (kp/cm^2):	0,5	1	1,5
T. Tangencial (kp/cm^2):	2,22	2,59	3,10
T. Residual (kp/cm^2):	0,73	1,40	2,10
Dilatancia (%):	-4,25	-5,10	-4,55

Resultados del Ensayo.

COHESIÓN (kp/cm^2):	1,76
ÁNGULO ROZ. INTERNO (º):	41,3

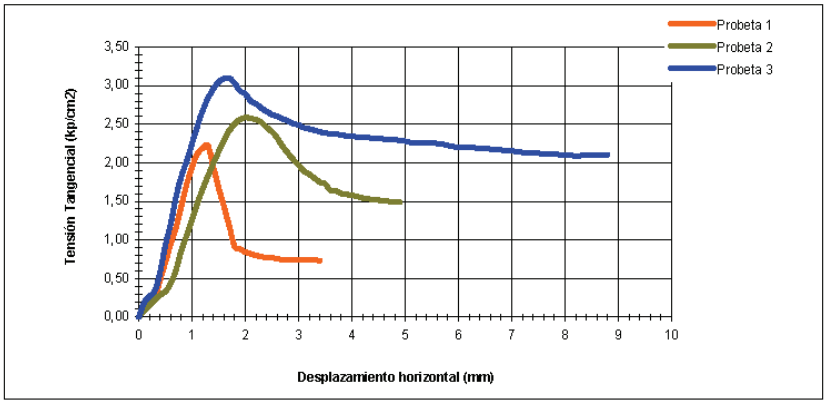

ACTA DE RESULTADOS DE ENSAYOS

ENSAYO DE CORTE DIRECTO (UNE 103 401-98)

Laboratorios Entecsa calidad acreditada

ENSAYO ACREDITADO. JUNTA DE ANDALUCIA

Obra: GR, UNIVERSIDAD
Peticionario: UNIVERSIDAD DE GRANADA
Referencia: 091036
Fecha ensayo: 21/05/2009
Denominación: CD-2
Descripción: arcillas abigarradas con cantos
Cota (m): 0

Dimensiones de las probetas.

Diámetro (cm):	5
Altura (cm):	2
Área (cm^2):	19,63
Volúmen (cm^3):	39,27

Párametros Físicos de las Probetas.

Probeta	I	II	III
Humedad inicial (%)	12,63	12,63	12,63
Humedad final (%)	15,21	14,52	14,88
Densidad aparente (g/cm3)	1,99	1,93	1,84
Densidad seca (g/cm3)	1,74	1,68	1,61
Indice de huecos incial	0,57	0,63	0,70
Indice de huecos final	0,73	0,72	0,60
Dens. de las partículas (g/cm3	2,74	2,74	2,74
Grado de saturación (%)	38,39	33,95	29,01

Párámetros del Ensayo.

Velocidad del Ensayo (mm/min):	0,078
Tipo de Ensayo:	CD

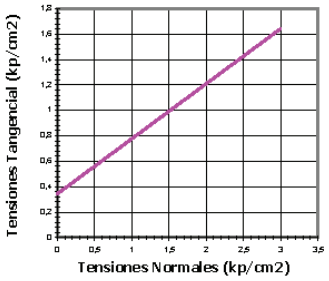

Tensiones aplicadas a la probeta.

Probeta:	I	II	III
T. Normal (kp/cm^2):	0,5	1	1,5
T. Tangencial (kp/cm^2):	0,54	0,81	0,98
T. Residual (kp/cm^2):	0,44	0,69	0,92
Dilatancia (%):	-1,95	-1,20	1,15

Resultados del Ensayo.

COHESIÓN (kp/cm^2):	0,34
ÁNGULO ROZ. INTERNO (º):	23,4

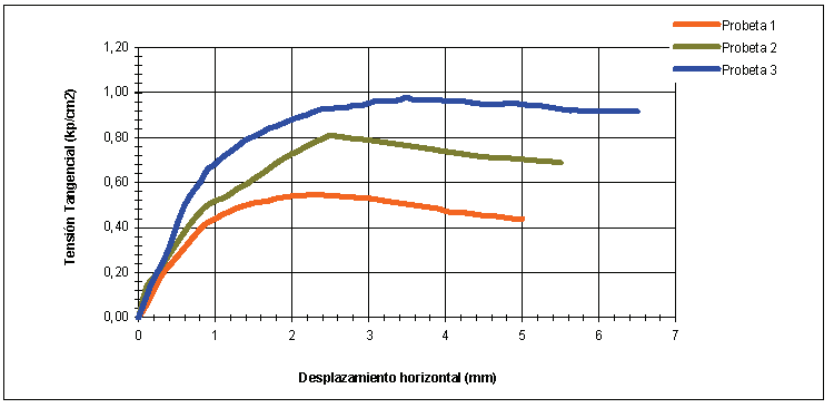

Güevéjar landslide

Laboratorios Entecsa calidad acreditada

ACTA DE ENSAYOS DE IDENTIFICACIÓN DE SUELOS

Obra: GR, G-1 A G-6
Peticionario: UNIVERSIDAD GRANADA
Fecha ensayo: 03/09/2009

Referencia: 091045
Procedencia: GR
Denominacion: G-1

ENSAYOS ACREDITADOS. JUNTA DE ANDALUCIA

ANÁLISIS GRANULOMÉTRICO POR TAMIZADO (UNE 103-101/95)

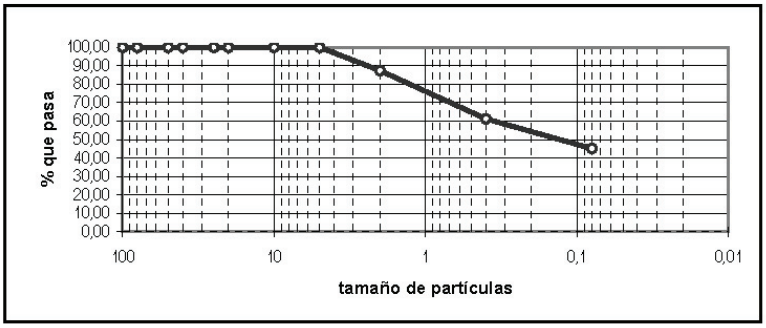

TAMICES (% QUE PASA)

UNE	100	80	50	40	25	20	10	5	2	0,4	0,08
ASTM	4"	3"	2"	1,5"	1"	3/4"	3/8"	N.º 4	N.º 10	N.º 40	N.º 200
% QUE PASA	100,00	100,00	100,00	100,00	100,00	100,00	100,00	100,00	87,40	61,20	45,15

LÍMITES DE ATTERBERG.

LÍMITE LÍQUIDO (UNE 103-103/94): --
LÍMITE PLÁSTICO (UNE 103-104/93): --
ÍNDICE DE PLASTICIDAD: **N.P.**

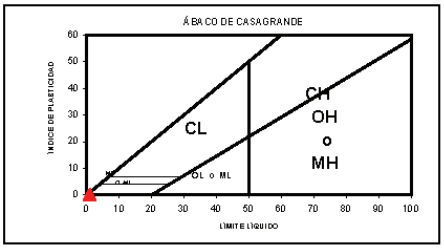

CLASIFICACIÓN DEL SUELO.

USCS/ASTM (ASTM-D 2487/00) **SM**

DESCRIPCIÓN DEL SUELO: **Arenas limosas**

OTRAS PROPIEDADES

HUMEDAD NATURAL % (UNE103-300/93): **5,04**
D. APARENTE (gr/cm3) (UNE 103-301/94): **1,49**
D. SECA (gr/cm3): **1,42**
D. RELATIVA (gr/cm3) (UNE 103-302/94):
SULFATOS SOLUBLES (mg/Kg) (EHE):
ACIDEZ BAUMANN GULLY (mg/Kg) (EHE):

CAMBIO POTENCIAL DE VOLUMEN (E. LAMBE) (UNE 103600/96)

P.V.C.:
ÍNDICE DE EXPANSIVIDAD (kp/cm2): (MPa):
CLASIFICACIÓN:

Laboratorios Entecsa calidad acreditada

ACTA DE ENSAYOS DE IDENTIFICACIÓN DE SUELOS

Obra:	GR, G-1 A G-6	**Referencia:**	091045
Peticionario:	UNIVERSIDAD GRANADA	**Procedencia:**	GR
Fecha ensayo:	03/09/2009	**Denominacion:**	G-1

ENSAYOS ACREDITADOS. JUNTA DE ANDALUCIA

ANÁLISIS GRANULOMÉTRICO POR TAMIZADO (UNE 103-101/95)

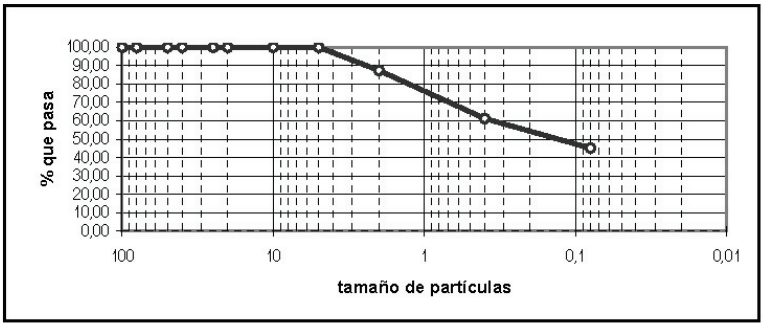

TAMICES (% QUE PASA)

UNE	100	80	50	40	25	20	10	5	2	0,4	0,08
ASTM	4"	3"	2"	1,5"	1"	3/4"	3/8"	N.º 4	N.º 10	N.º 40	N.º 200
% QUE PASA	100,00	100,00	100,00	100,00	100,00	100,00	100,00	100,00	87,40	61,20	45,15

LÍMITES DE ATTERBERG.

LÍMITE LÍQUIDO (UNE 103-103/94): --

LÍMITE PLÁSTICO (UNE 103-104/93): --

ÍNDICE DE PLASTICIDAD: **N.P.**

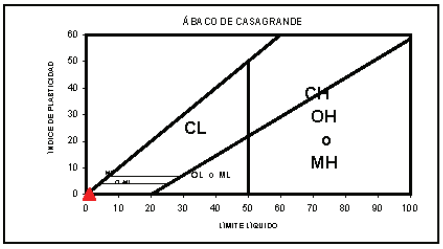

CLASIFICACIÓN DEL SUELO.

USCS/ASTM (ASTM-D 2487/00) **SM**

DESCRIPCIÓN DEL SUELO: **Arenas limosas**

OTRAS PROPIEDADES

HUMEDAD NATURAL % (UNE103-300/93): **5,04**

D. APARENTE (gr/cm3) (UNE 103-301/94): **1,49**

D. SECA (gr/cm3): **1,42**

D. RELATIVA (gr/cm3) (UNE 103-302/94):

SULFATOS SOLUBLES (mg/Kg) (EHE):

ACIDEZ BAUMANN GULLY (mg/Kg) (EHE):

CAMBIO POTENCIAL DE VOLUMEN (E. LAMBE) (UNE 103600/96)

P.V.C.:

ÍNDICE DE EXPANSIVIDAD (kp/cm2): (MPa):

CLASIFICACIÓN:

Laboratorios Entecsa calidad acreditada

ACTA DE ENSAYOS DE IDENTIFICACIÓN DE SUELOS

Obra:	GR, G-1 A G-6	**Referencia:**	091045
Peticionario:	UNIVERSIDAD GRANADA	**Procedencia:**	GR
Fecha ensayo:	03/09/2009	**Denominacion:**	G-3

ENSAYOS ACREDITADOS. JUNTA DE ANDALUCIA

ANÁLISIS GRANULOMÉTRICO POR TAMIZADO (UNE 103-101/95)

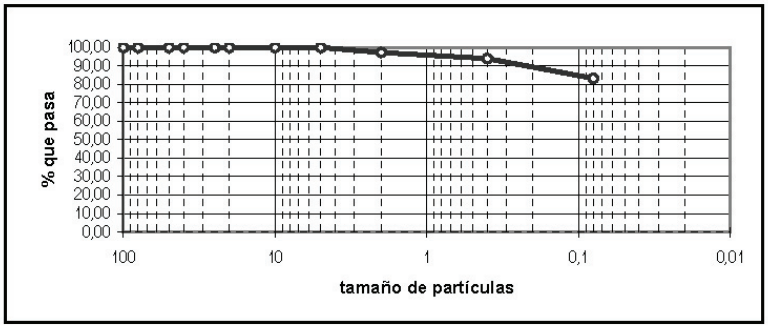

TAMICES (% QUE PASA)

UNE	100	80	50	40	25	20	10	5	2	0,4	0,08
ASTM	4"	3"	2"	1,5"	1"	3/4"	3/8"	N.º 4	N.º 10	N.º 40	N.º 200
% QUE PASA	100,00	100,00	100,00	100,00	100,00	100,00	100,00	100,00	97,26	94,01	83,20

LÍMITES DE ATTERBERG.

LÍMITE LÍQUIDO (UNE 103-103/94): --

LÍMITE PLÁSTICO (UNE 103-104/93): --

ÍNDICE DE PLASTICIDAD: **N.P.**

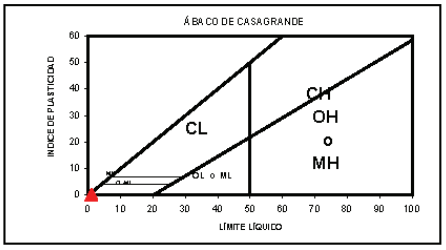

CLASIFICACIÓN DEL SUELO.

USCS/ASTM (ASTM-D 2487/00) **ML**

DESCRIPCIÓN DEL SUELO: **Limos inorgánicos de baja plasticidad**

OTRAS PROPIEDADES

HUMEDAD NATURAL % (UNE103-300/93):	**8,31**
D. APARENTE (gr/cm3) (UNE 103-301/94):	**1,70**
D. SECA (gr/cm3):	**1,57**
D. RELATIVA (gr/cm3) (UNE 103-302/94):	
SULFATOS SOLUBLES (mg/Kg) (EHE):	
ACIDEZ BAUMANN GULLY (mg/Kg) (EHE):	

CAMBIO POTENCIAL DE VOLUMEN (E. LAMBE) (UNE 103600/96)

P.V.C.:		
ÍNDICE DE EXPANSIVIDAD (kp/cm2):		(MPa):
CLASIFICACIÓN:		

Laboratorios Entecsa calidad acreditada

ACTA DE ENSAYOS DE IDENTIFICACIÓN DE SUELOS

Obra:	GR, G-1 A G-6	**Referencia:**	091045
Peticionario:	UNIVERSIDAD GRANADA	**Procedencia:**	GR
Fecha ensayo:	03/09/2009	**Denominacion:**	G-4

ENSAYOS ACREDITADOS. JUNTA DE ANDALUCIA

ANÁLISIS GRANULOMÉTRICO POR TAMIZADO (UNE 103-101/95)

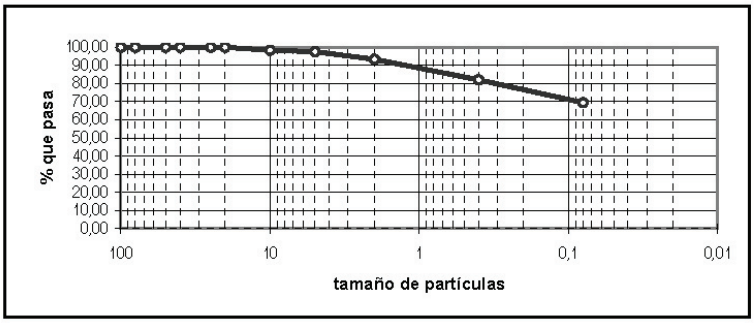

TAMICES (% QUE PASA)

UNE	100	80	50	40	25	20	10	5	2	0,4	0,08
ASTM	4"	3"	2"	1,5"	1"	3/4"	3/8"	N.º 4	N.º 10	N.º 40	N.º 200
% QUE PASA	100,00	100,00	100,00	100,00	100,00	100,00	98,35	97,59	93,40	82,01	69,45

LÍMITES DE ATTERBERG.

LÍMITE LÍQUIDO (UNE 103-103/94): **38,90**
LÍMITE PLÁSTICO (UNE 103-104/93): **22,88**
ÍNDICE DE PLASTICIDAD: **16,02**

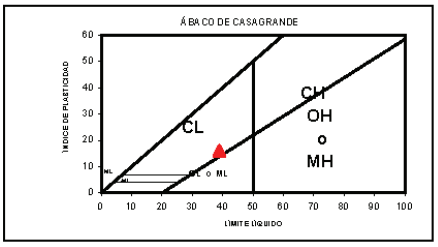

CLASIFICACIÓN DEL SUELO.

USCS/ASTM (ASTM-D 2487/00) **CL**

DESCRIPCIÓN DEL SUELO: **Arcillas inorgánicas de baja plasticidad**

OTRAS PROPIEDADES

HUMEDAD NATURAL % (UNE103-300/93): **8,11**
D. APARENTE (gr/cm3) (UNE 103-301/94): **1,94**
D. SECA (gr/cm3): **1,80**
D. RELATIVA (gr/cm3) (UNE 103-302/94):
SULFATOS SOLUBLES (mg/Kg) (EHE):
ACIDEZ BAUMANN GULLY (mg/Kg) (EHE):

CAMBIO POTENCIAL DE VOLUMEN (E. LAMBE) (UNE 103600/96)

P.V.C.:
ÍNDICE DE EXPANSIVIDAD (kp/cm2): (MPa):
CLASIFICACIÓN:

Laboratorios Entecsa calidad acreditada

ACTA DE ENSAYOS DE IDENTIFICACIÓN DE SUELOS

Obra:	GR, G-1 A G-6	**Referencia:**	091045
Peticionario:	UNIVERSIDAD GRANADA	**Procedencia:**	GR
Fecha ensayo:	03/09/2009	**Denominacion:**	G-5

ENSAYOS ACREDITADOS. JUNTA DE ANDALUCIA

ANÁLISIS GRANULOMÉTRICO POR TAMIZADO (UNE 103-101/95)

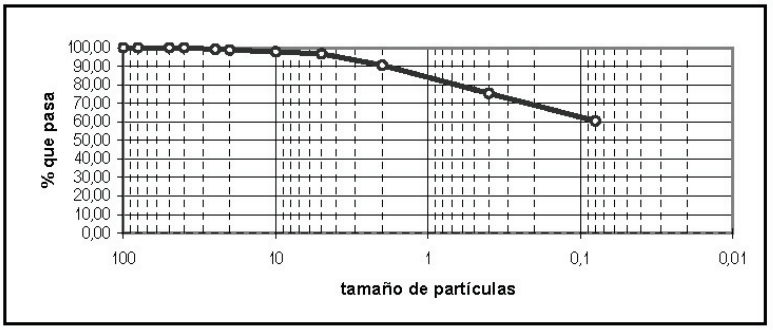

TAMICES (% QUE PASA)

UNE	100	80	50	40	25	20	10	5	2	0,4	0,08
ASTM	4"	3"	2"	1,5"	1"	3/4"	3/8"	N.º 4	N.º 10	N.º 40	N.º 200
% QUE PASA	100,00	100,00	100,00	100,00	99,11	98,75	97,76	96,62	90,49	75,34	60,43

LÍMITES DE ATTERBERG.

LÍMITE LÍQUIDO (UNE 103-103/94):	**33,10**
LÍMITE PLÁSTICO (UNE 103-104/93):	**19,66**
ÍNDICE DE PLASTICIDAD:	**13,44**

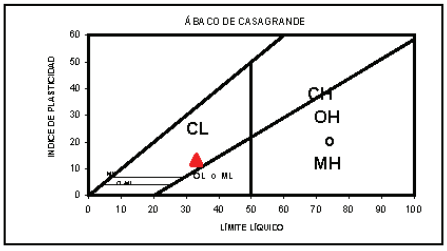

CLASIFICACIÓN DEL SUELO.

USCS/ASTM (ASTM-D 2487/00) **CL**

DESCRIPCIÓN DEL SUELO: **Arcillas inorgánicas de baja plasticidad**

OTRAS PROPIEDADES

HUMEDAD NATURAL % (UNE103-300/93):	**7,65**
D. APARENTE (gr/cm3) (UNE 103-301/94):	**1,98**
D. SECA (gr/cm3):	**1,84**
D. RELATIVA (gr/cm3) (UNE 103-302/94):	
SULFATOS SOLUBLES (mg/Kg) (EHE):	
ACIDEZ BAUMANN GULLY (mg/Kg) (EHE):	

CAMBIO POTENCIAL DE VOLUMEN (E. LAMBE) (UNE 103600/96)

P.V.C.:	
ÍNDICE DE EXPANSIVIDAD (kp/cm2):	(MPa):
CLASIFICACIÓN:	

Laboratorios Entecsa calidad acreditada

ACTA DE ENSAYOS DE IDENTIFICACIÓN DE SUELOS

Obra:	GR, G-1 A G-6	**Referencia:**	091045
Peticionario:	UNIVERSIDAD GRANADA	**Procedencia:**	GR
Fecha ensayo:	03/09/2009	**Denominacion:**	G-6

ENSAYOS ACREDITADOS. JUNTA DE ANDALUCIA

ANÁLISIS GRANULOMÉTRICO POR TAMIZADO (UNE 103-101/95)

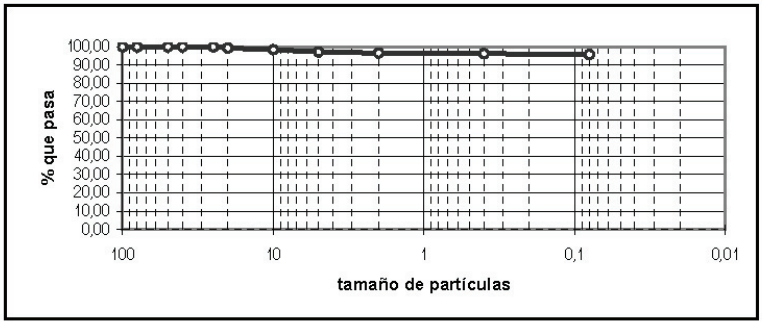

TAMICES (% QUE PASA)

UNE	100	80	50	40	25	20	10	5	2	0,4	0,08
ASTM	4"	3"	2"	1,5"	1"	3/4"	3/8"	N.º 4	N.º 10	N.º 40	N.º 200
% QUE PASA	100,00	100,00	100,00	100,00	100,00	99,39	98,47	97,24	96,57	96,29	95,77

LÍMITES DE ATTERBERG.

LÍMITE LÍQUIDO (UNE 103-103/94):	**51,20**
LÍMITE PLÁSTICO (UNE 103-104/93):	**25,53**
ÍNDICE DE PLASTICIDAD:	**25,67**

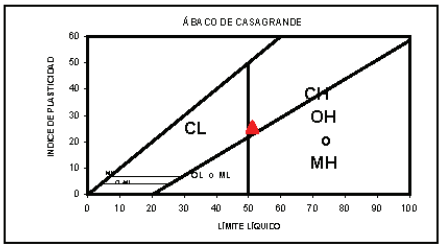

CLASIFICACIÓN DEL SUELO.

USCS/ASTM (ASTM-D 2487/00) **CH**

DESCRIPCIÓN DEL SUELO: **Arcillas inorgánicas de alta plasticidad**

OTRAS PROPIEDADES

HUMEDAD NATURAL % (UNE103-300/93):	**10,01**
D. APARENTE (gr/cm3) (UNE 103-301/94):	**2,07**
D. SECA (gr/cm3):	**1,88**
D. RELATIVA (gr/cm3) (UNE 103-302/94):	
SULFATOS SOLUBLES (mg/Kg) (EHE):	
ACIDEZ BAUMANN GULLY (mg/Kg) (EHE):	

CAMBIO POTENCIAL DE VOLUMEN (E. LAMBE) (UNE 103600/96)

P.V.C.:	
ÍNDICE DE EXPANSIVIDAD (kp/cm2):	(MPa):
CLASIFICACIÓN:	

ACTA DE RESULTADOS DE ENSAYOS

Laboratorios Entecsa calidad acreditada

DETERMINACIÓN DE LA DENSIDAD RELATIVA DE LAS PARTÍCULAS DE UN SULO
SEGÚN NORMA UNE 103-302-94

Peticionario: UNIVERSIDAD DE GRANADA
Obra: GR, G-1 A G-6
Trabajo Nº: 91045
Fecha: 04/09/2009

ENSAYO ACREDITADO. JUNTA DE ANDALUCIA

Procedencia de la muestra: G-1
Descripción del material: ARENAS LIMOSAS
Denominación: 091045-GEO-TNA-SON1-M1

DENSIDAD RELATIVA DE LAS PARTICULAS 2,4082 €

ACTA DE RESULTADOS DE ENSAYOS

Laboratorios Entecsa calidad acreditada

DETERMINACIÓN DE LA DENSIDAD RELATIVA DE LAS PARTÍCULAS DE UN SULO
SEGÚN NORMA UNE 103-302-94

Peticionario: UNIVERSIDAD DE GRANADA
Obra: GR, G-1 A G-6
Trabajo Nº: 91045
Fecha: 04/09/2009

ENSAYO ACREDITADO. JUNTA DE ANDALUCIA

Procedencia de la muestra: G-2
Descripción del material: ARCILLAS
Denominación: 091045-GEO-TNA-SON1-M1

DENSIDAD RELATIVA DE LAS PARTICULAS 2,8154

ACTA DE RESULTADOS DE ENSAYOS

Laboratorios Entecsa calidad acreditada

DETERMINACIÓN DE LA DENSIDAD RELATIVA DE LAS PARTÍCULAS DE UN SULO
SEGÚN NORMA UNE 103-302-94

Peticionario: UNIVERSIDAD DE GRANADA
Obra: GR, G-1 A G-6
Trabajo Nº: 91045
Fecha: 04/09/2009

ENSAYO ACREDITADO. JUNTA DE ANDALUCIA

Procedencia de la muestra: G-3
Descripción del material: LIMOS
Denominación: 091045-GEO-TNA-SON1-M1

DENSIDAD RELATIVA DE LAS PARTICULAS 2,3858

ACTA DE RESULTADOS DE ENSAYOS

Laboratorios Entecsa calidad acreditada

DETERMINACIÓN DE LA DENSIDAD RELATIVA DE LAS PARTÍCULAS DE UN SULO
SEGÚN NORMA UNE 103-302-94

Peticionario: UNIVERSIDAD DE GRANADA
Obra: GR, G-1 A G-6
Trabajo Nº: 91045
Fecha: 04/09/2009

ENSAYO ACREDITADO. JUNTA DE ANDALUCIA

Procedencia de la muestra: G-4
Descripción del material: ARCILLAS
Denominación: 091045-GEO-TNA-SON1-M1

DENSIDAD RELATIVA DE LAS PARTICULAS 2,8049

ACTA DE RESULTADOS DE ENSAYOS

Laboratorios Entecsa calidad acreditada

DETERMINACIÓN DE LA DENSIDAD RELATIVA DE LAS PARTÍCULAS DE UN SULO
SEGÚN NORMA UNE 103-302-94

Peticionario: UNIVERSIDAD DE GRANADA
Obra: GR, G-1 A G-6
Trabajo Nº: 91045
Fecha: 04/09/2009

ENSAYO ACREDITADO. JUNTA DE ANDALUCIA

Procedencia de la muestra: G-5
Descripción del material: ARCILLAS
Denominación: 091045-GEO-TNA-SON1-M1

DENSIDAD RELATIVA DE LAS PARTICULAS 2,6180

ACTA DE RESULTADOS DE ENSAYOS

Laboratorios Entecsa calidad acreditada

DETERMINACIÓN DE LA DENSIDAD RELATIVA DE LAS PARTÍCULAS DE UN SULO
SEGÚN NORMA UNE 103-302-94

Peticionario: UNIVERSIDAD DE GRANADA
Obra: GR, G-1 A G-6
Trabajo Nº: 91045
Fecha: 04/09/2009

ENSAYO ACREDITADO. JUNTA DE ANDALUCIA

Procedencia de la muestra: G-6
Descripción del material: ARCILLAS ALTA PLASTICIDAD
Denominación: 091045-GEO-TNA-SON1-M1

DENSIDAD RELATIVA DE LAS PARTICULAS 2,2194

ACTA DE RESULTADOS DE ENSAYOS
ENSAYO DE CORTE DIRECTO (UNE 103 401-98)

Laboratorios Entecsa calidad acreditada

ENSAYO ACREDITADO. JUNTA DE ANDALUCIA

Obra:	GR, G-1 A G-6		
Peticionario:	UNIVERSIDAD DE GRANADA	**Muestra:**	091045-G-1
Referencia:	091045	**Descripción:**	arenas limosas
Fecha ensayo:	10/09/2009	**Cota (m):**	-

Dimensiones de las probetas.

Diámetro (cm):	5
Altura (cm):	2
Área (cm^2):	19,63
Volúmen (cm^3):	39,27

Párametros del Ensayo.

Velocidad Ensayo (mm/min): 0,24

Tipo de Ensayo: CD

Párametros Físicos de las Probetas.

Probeta	I	II	III
Humedad inicial (%)	5,09	5,09	5,09
Humedad final (%)	4,93	5,03	5,16
Densidad aparente (g/cm3)	1,55	1,57	1,58
Densidad seca (g/cm3)	1,47	1,49	1,50
Indice de huecos incial	0,63	0,61	0,60
Indice de huecos final	0,91	0,68	0,78
Dens. de las partículas (g/cm3	2,40	2,40	2,40
Grado de saturación (%)	11,81	12,38	12,68

Tensiones aplicadas a la probeta.

Probeta:	I	II	III
T. Normal (kp/cm^2):	0,5	1	1,5
T. Tangencial (kp/cm^2):	0,48	0,84	1,52
T. Residual (kp/cm^2):	0,34	0,84	1,26
Dilatancia (%):	-3,40	-0,80	-2,20

Resultados del Ensayo.

		Residual
COHESIÓN (kp/cm^2):	0,00	0,00
ÁNGULO ROZ. INTERNO (º):	46,0	42,7

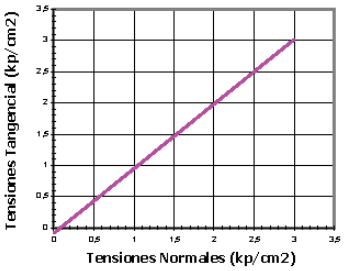

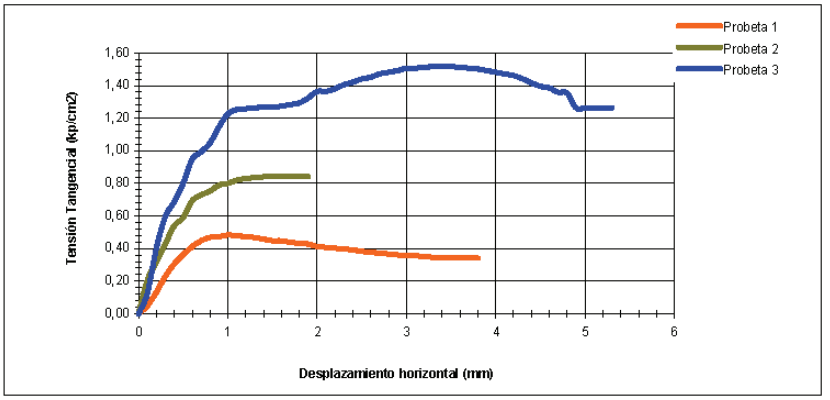

ACTA DE RESULTADOS DE ENSAYOS
ENSAYO DE CORTE DIRECTO (UNE 103 401-98)

Laboratorios Entecsa calidad acreditada

ENSAYO ACREDITADO. JUNTA DE ANDALUCIA

Obra: GR, G-1 A G-6
Peticionario: UNIVERSIDAD DE GRANADA
Referencia: 091045
Fecha ensayo: 16/09/2009
Muestra: 091045-G-2
Descripción: arcillas rojas
Cota (m): -

Dimensiones de las probetas.

Diámetro (cm):	5
Altura (cm):	2
Área (cm^2):	19,63
Volúmen (cm^3):	39,27

Párametros del Ensayo.

Velocidad Ensayo (mm/min): 1,25
Tipo de Ensayo: UU

Párametros Físicos de las Probetas.

Probeta	I	II	III
Humedad inicial (%)	7,32	7,32	7,32
Humedad final (%)	7,29	7,46	7,44
Densidad aparente (g/cm3)	1,78	1,81	1,81
Densidad seca (g/cm3)	1,65	1,68	1,68
Indice de huecos incial	0,70	0,68	0,67
Indice de huecos final	0,98	0,91	0,58
Dens. de las partículas (g/cm3	2,81	2,81	2,81
Grado de saturación (%)	17,26	18,12	18,30

Tensiones aplicadas a la probeta.

Probeta:	I	II	III
T. Normal (kp/cm^2):	0,5	1	1,5
T. Tangencial (kp/cm^2):	0,76	0,94	1,17
T. Residual (kp/cm^2):	0,76	0,94	1,17
Dilatancia (%):	-3,25	-2,75	1,05

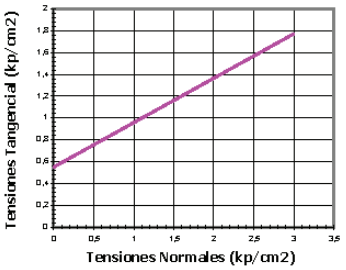

Resultados del Ensayo.

		Residual
COHESIÓN (kp/cm^2):	0,55	0,55
ÁNGULO ROZ. INTERNO (º):	22,1	22,1

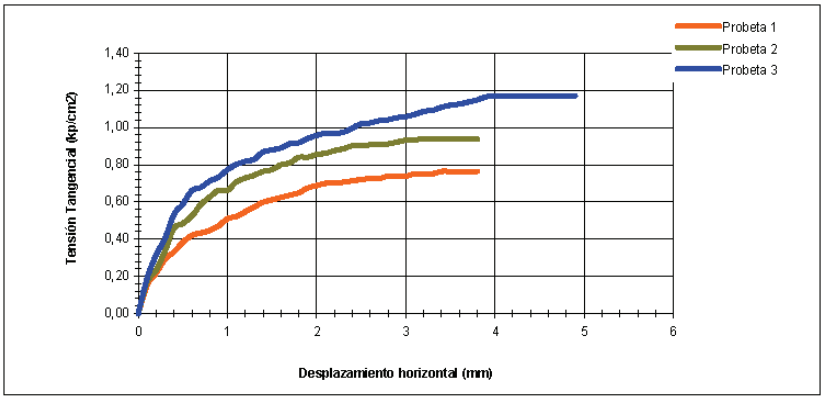

ACTA DE RESULTADOS DE ENSAYOS
ENSAYO DE CORTE DIRECTO (UNE 103 401-98)

Laboratorios Entecsa calidad acreditada

ENSAYO ACREDITADO. JUNTA DE ANDALUCIA

Obra:	GR, G-1 A G-6		
Peticionario:	UNIVERSIDAD DE GRANADA	**Muestra:**	091045-G-2
Referencia:	091045	**Descripción:**	arcillas rojas
Fecha ensayo:	23/09/2009	**Cota (m):**	-

Dimensiones de las probetas.

Diámetro (cm):	5
Altura (cm):	2
Área (cm^2):	19,63
Volúmen (cm^3):	39,27

Párametros del Ensayo.

Velocidad Ensayo (mm/min): 0,29

Tipo de Ensayo: CD

Párametros Físicos de las Probetas.

Probeta	I	II	III
Humedad inicial (%)	7,32	7,32	7,32
Humedad final (%)	7,43	7,37	7,13
Densidad aparente (g/cm3)	1,82	1,83	1,82
Densidad seca (g/cm3)	1,68	1,70	1,69
Indice de huecos incial	0,67	0,66	0,67
Indice de huecos final	0,78	0,68	0,67
Dens. de las partículas (g/cm3	2,81	2,81	2,81
Grado de saturación (%)	18,39	18,94	18,57

Tensiones aplicadas a la probeta.

Probeta:	I	II	III
T. Normal (kp/cm^2):	0,5	1	1,5
T. Tangencial (kp/cm^2):	0,88	1,30	1,78
T. Residual (kp/cm^2):	0,36	1,13	1,77
Dilatancia (%):	-1,30	-0,25	0,00

Resultados del Ensayo.

		Residual
COHESIÓN (kp/cm^2):	0,42	0,00
ÁNGULO ROZ. INTERNO (°):	42,0	54,7

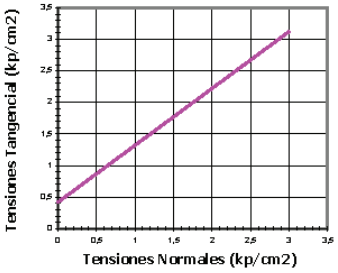

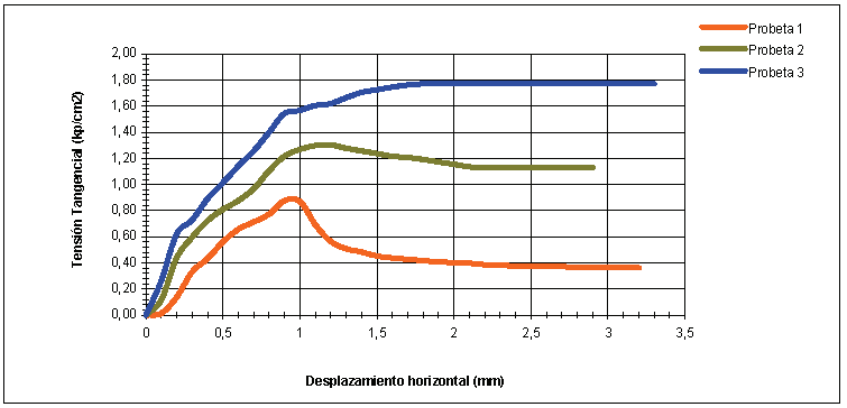

ACTA DE RESULTADOS DE ENSAYOS
ENSAYO DE CORTE DIRECTO (UNE 103 401-98)

Laboratorios Entecsa calidad acreditada

ENSAYO ACREDITADO. JUNTA DE ANDALUCIA

Obra: GR, G-1 A G-6
Peticionario: UNIVERSIDAD DE GRANADA
Referencia: 091045
Fecha ensayo: 30/09/2009
Muestra: 091045-G-3
Descripción: limos arenosos
Cota (m): -

Dimensiones de las probetas.

Diámetro (cm):	5
Altura (cm):	2
Área (cm^2):	19,63
Volúmen (cm^3):	39,27

Párametros del Ensayo.

Velocidad Ensayo (mm/min): 1,25
Tipo de Ensayo: UU

Párametros Físicos de las Probetas.

Probeta	I	II	III
Humedad inicial (%)	8,31	8,31	8,31
Humedad final (%)	8,72	8,51	8,17
Densidad aparente (g/cm3)	1,69	1,68	1,68
Densidad seca (g/cm3)	1,55	1,54	1,54
Indice de huecos incial	0,53	0,55	0,54
Indice de huecos final	0,64	0,60	0,54
Dens. de las partículas (g/cm3	2,38	2,38	2,38
Grado de saturación (%)	24,21	23,24	23,65

Tensiones aplicadas a la probeta.

Probeta:	I	II	III
T. Normal (kp/cm^2):	0,5	1	1,5
T. Tangencial (kp/cm^2):	0,59	0,76	1,03
T. Residual (kp/cm^2):	0,56	0,72	0,83
Dilatancia (%):	-1,45	-0,60	0,00

Resultados del Ensayo.

		Residual
COHESIÓN (kp/cm^2):	0,34	0,43
ÁNGULO ROZ. INTERNO (º):	24,1	15,4

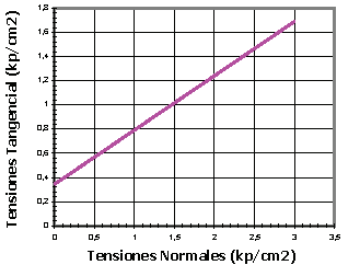

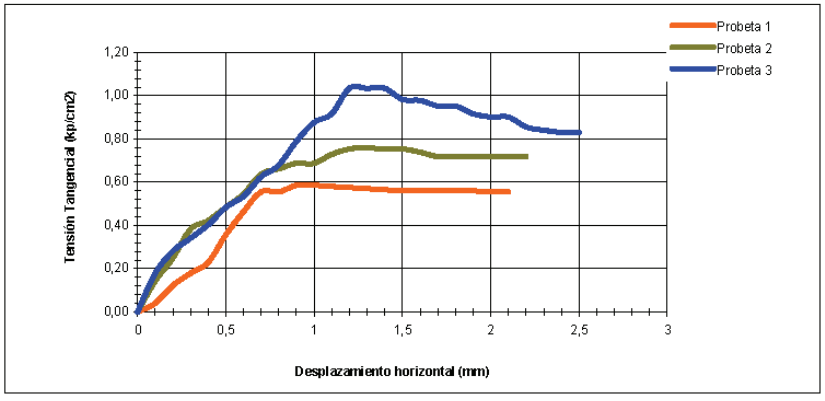

ACTA DE RESULTADOS DE ENSAYOS
ENSAYO DE CORTE DIRECTO (UNE 103 401-98)

Laboratorios Entecsa calidad acreditada

ENSAYO ACREDITADO. JUNTA DE ANDALUCIA

Obra:	GR, G-1 A G-6		
Peticionario:	UNIVERSIDAD DE GRANADA	**Muestra:**	091045-G-3
Referencia:	091045	**Descripción:**	limos arenosos
Fecha ensayo:	06/10/2009	**Cota (m):**	-

Dimensiones de las probetas.

Diámetro (cm):	5
Altura (cm):	2
Área (cm^2):	19,63
Volúmen (cm^3):	39,27

Párametros del Ensayo.

Velocidad Ensayo (mm/min): 0,21

Tipo de Ensayo: CD

Párametros Físicos de las Probetas.

Probeta	I	II	III
Humedad inicial (%)	8,31	8,31	8,31
Humedad final (%)	8,11	8,51	8,46
Densidad aparente (g/cm3)	1,70	1,68	1,69
Densidad seca (g/cm3)	1,56	1,54	1,55
Indice de huecos incial	0,53	0,55	0,54
Indice de huecos final	0,54	0,60	0,56
Dens. de las partículas (g/cm3	2,38	2,38	2,38
Grado de saturación (%)	24,35	23,24	23,79

Tensiones aplicadas a la probeta.

Probeta:	I	II	III
T. Normal (kp/cm^2):	0,5	1	1,5
T. Tangencial (kp/cm^2):	0,58	0,79	1,12
T. Residual (kp/cm^2):	0,46	0,71	1,12
Dilatancia (%):	-0,10	-0,65	-0,20

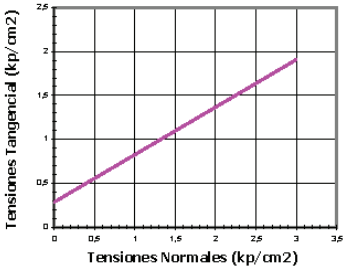

Resultados del Ensayo.

		Residual
COHESIÓN (kp/cm^2):	**0,29**	**0,10**
ÁNGULO ROZ. INTERNO (º):	**28,4**	**33,3**

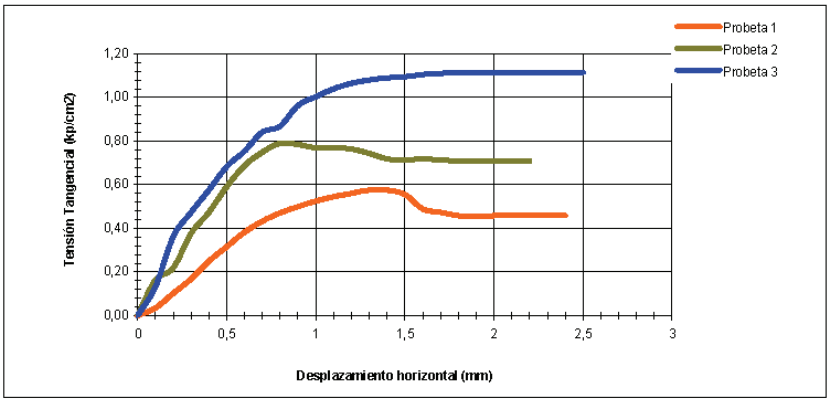

ACTA DE RESULTADOS DE ENSAYOS
ENSAYO DE CORTE DIRECTO (UNE 103 401-98)

Laboratorios Entecsa calidad acreditada

ENSAYO ACREDITADO. JUNTA DE ANDALUCIA

Obra: GR, G-1 A G-6
Peticionario: UNIVERSIDAD DE GRANADA
Referencia: 091045
Fecha ensayo: 13/01/1900
Muestra: 091045-G-4
Descripción: arcillas
Cota (m): -

Dimensiones de las probetas.

Diámetro (cm):	5
Altura (cm):	2
Área (cm^2):	19,63
Volúmen (cm^3):	39,27

Párametros del Ensayo.

Velocidad Ensayo (mm/min): 1,25
Tipo de Ensayo: UU

Párametros Físicos de las Probetas.

Probeta	I	II	III
Humedad inicial (%)	8,11	8,11	8,11
Humedad final (%)	8,57	8,07	8,04
Densidad aparente (g/cm3)	1,99	1,99	1,96
Densidad seca (g/cm3)	1,83	1,83	1,80
Indice de huecos incial	0,53	0,53	0,55
Indice de huecos final	0,73	0,74	0,75
Dens. de las partículas (g/cm3	2,80	2,80	2,80
Grado de saturación (%)	27,99	27,85	26,50

Tensiones aplicadas a la probeta.

Probeta:	I	II	III
T. Normal (kp/cm^2):	0,5	1	1,5
T. Tangencial (kp/cm^2):	0,92	1,11	1,36
T. Residual (kp/cm^2):	0,31	0,87	1,17
Dilatancia (%):	-2,60	-2,70	-2,55

Resultados del Ensayo.

		Residual
COHESIÓN (kp/cm^2):	0,68	0,00
ÁNGULO ROZ. INTERNO (º):	23,9	40,7

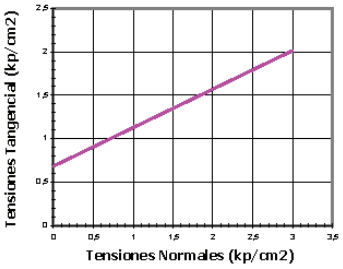

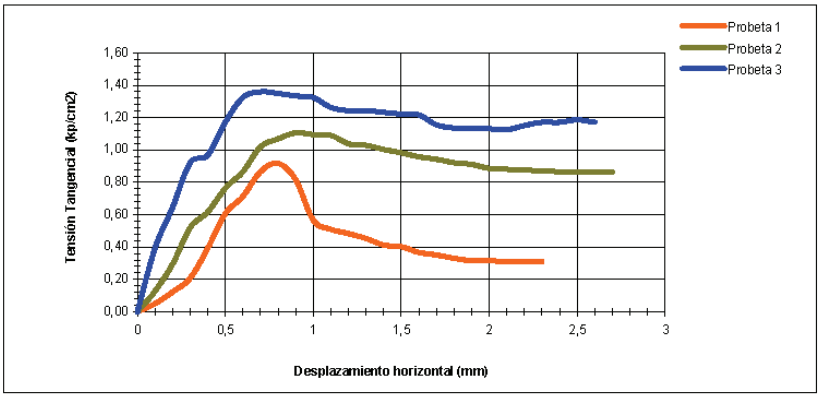

ACTA DE RESULTADOS DE ENSAYOS
ENSAYO DE CORTE DIRECTO (UNE 103 401-98)

Laboratorios Entecsa calidad acreditada

ENSAYO ACREDITADO. JUNTA DE ANDALUCIA

Obra:	GR, G-1 A G-6		
Peticionario:	UNIVERSIDAD DE GRANADA	**Muestra:**	091045-G-4
Referencia:	091045	**Descripción:**	arcillas rojas
Fecha ensayo:	20/10/2009	**Cota (m):**	-

Dimensiones de las probetas.

Diámetro (cm):	5
Altura (cm):	2
Área (cm^2):	19,63
Volúmen (cm^3):	39,27

Párametros del Ensayo.

Velocidad Ensayo (mm/min): 0,17

Tipo de Ensayo: CD

Párametros Físicos de las Probetas.

Probeta	I	II	III
Humedad inicial (%)	8,11	8,11	8,11
Humedad final (%)	8,29	8,10	8,05
Densidad aparente (g/cm3)	1,94	1,95	1,96
Densidad seca (g/cm3)	1,78	1,79	1,80
Indice de huecos incial	0,57	0,56	0,55
Indice de huecos final	0,80	0,61	0,55
Dens. de las partículas (g/cm3	2,80	2,80	2,80
Grado de saturación (%)	25,10	25,73	26,37

Tensiones aplicadas a la probeta.

Probeta:	I	II	III
T. Normal (kp/cm^2):	0,5	1	1,5
T. Tangencial (kp/cm^2):	0,60	1,06	1,39
T. Residual (kp/cm^2):	0,44	1,02	1,36
Dilatancia (%):	-2,85	-0,65	0,00

Resultados del Ensayo.

		Residual
COHESIÓN (kp/cm^2):	0,22	0,01
ÁNGULO ROZ. INTERNO (º):	38,4	42,8

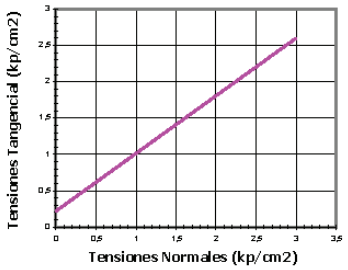

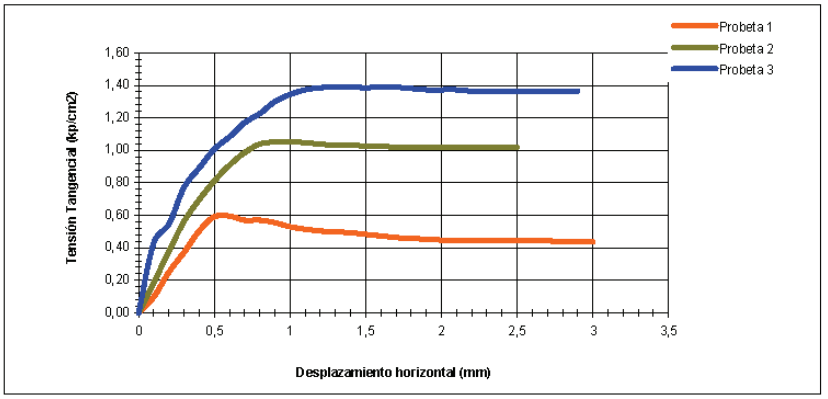

ACTA DE RESULTADOS DE ENSAYOS
ENSAYO DE CORTE DIRECTO (UNE 103 401-98)

Laboratorios Entecsa calidad acreditada

ENSAYO ACREDITADO. JUNTA DE ANDALUCIA

Obra: GR, G-1 A G-6
Peticionario: UNIVERSIDAD DE GRANADA
Referencia: 091045
Fecha ensayo: 26/10/2009
Muestra: 091045-G-5
Descripción: arcillas
Cota (m): -

Dimensiones de las probetas.

Diámetro (cm):	5
Altura (cm):	2
Área (cm^2):	19,63
Volúmen (cm^3):	39,27

Párametros del Ensayo.

Velocidad Ensayo (mm/min): 1,25
Tipo de Ensayo: UU

Párametros Físicos de las Probetas.

Probeta	I	II	III
Humedad inicial (%)	7,65	7,65	7,65
Humedad final (%)	7,67	7,80	7,35
Densidad aparente (g/cm3)	1,99	1,99	2,01
Densidad seca (g/cm3)	1,84	1,84	1,86
Indice de huecos incial	0,42	0,42	0,41
Indice de huecos final	0,80	0,48	0,53
Dens. de las partículas (g/cm3	2,62	2,62	2,62
Grado de saturación (%)	33,13	33,13	34,45

Tensiones aplicadas a la probeta.

Probeta:	I	II	III
T. Normal (kp/cm^2):	0,5	1	1,5
T. Tangencial (kp/cm^2):	0,74	0,87	1,30
T. Residual (kp/cm^2):	0,41	0,57	0,99
Dilatancia (%):	-5,30	-0,75	-1,65

Resultados del Ensayo.

		Residual
COHESIÓN (kp/cm^2):	0,40	0,08
ÁNGULO ROZ. INTERNO (º):	29,5	29,8

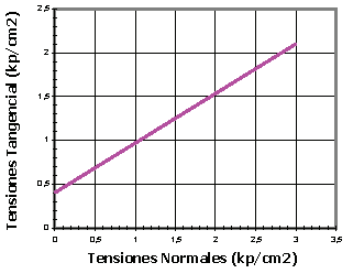

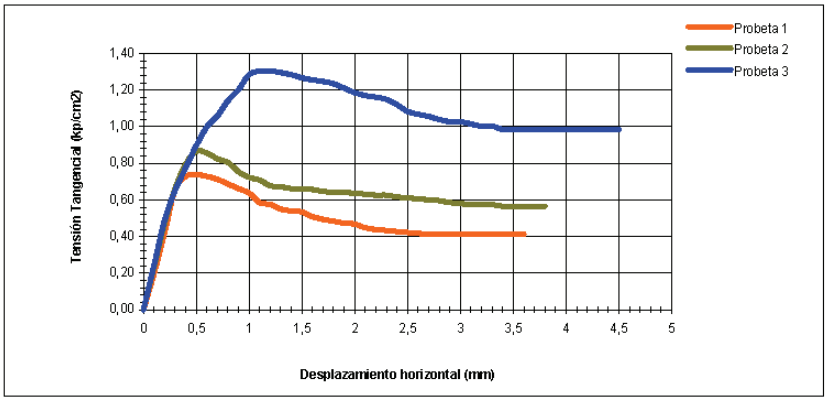

ACTA DE RESULTADOS DE ENSAYOS
ENSAYO DE CORTE DIRECTO (UNE 103 401-98)

Laboratorios Entecsa calidad acreditada

ENSAYO ACREDITADO. JUNTA DE ANDALUCIA

Obra:	GR, G-1 A G-6		
Peticionario:	UNIVERSIDAD DE GRANADA	**Muestra:**	091045-G-5
Referencia:	091045	**Descripción:**	arcillas
Fecha ensayo:	23/10/2009	**Cota (m):**	-

Dimensiones de las probetas.

Diámetro (cm):	5
Altura (cm):	2
Área (cm^2):	19,63
Volúmen (cm^3):	39,27

Párametros Físicos de las Probetas.

Probeta	I	II	III
Humedad inicial (%)	7,65	7,65	7,65
Humedad final (%)	7,67	7,80	7,35
Densidad aparente (g/cm3)	1,99	1,99	2,01
Densidad seca (g/cm3)	1,84	1,84	1,86
Indice de huecos incial	0,42	0,42	0,41
Indice de huecos final	0,55	0,52	0,44
Dens. de las partículas (g/cm3	2,62	2,62	2,62
Grado de saturación (%)	33,13	33,13	34,45

Párametros del Ensayo.

Velocidad Ensayo (mm/min): 0,14

Tipo de Ensayo: CD

Tensiones aplicadas a la probeta.

Probeta:	I	II	III
T. Normal (kp/cm^2):	0,5	1	1,5
T. Tangencial (kp/cm^2):	0,85	1,18	1,35
T. Residual (kp/cm^2):	0,35	0,86	1,22
Dilatancia (%):	-1,80	-1,30	-0,35

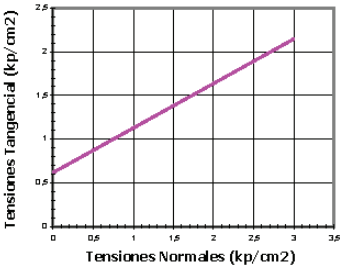

Resultados del Ensayo.

		Residual
COHESIÓN (kp/cm^2):	0,62	0,00
ÁNGULO ROZ. INTERNO (º):	27,0	41,1

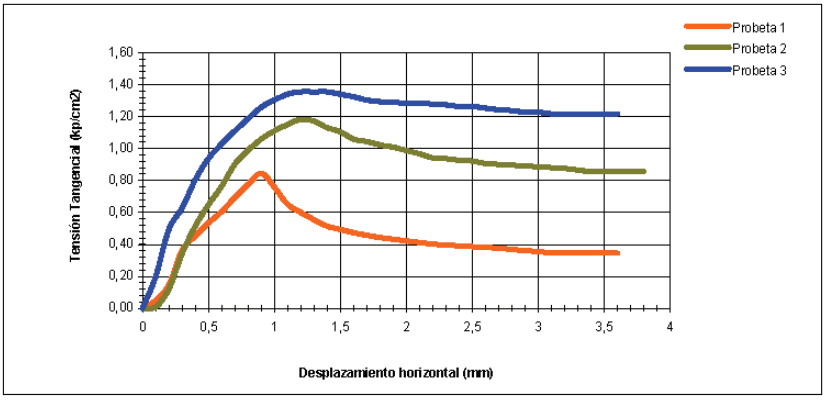

ACTA DE RESULTADOS DE ENSAYOS
ENSAYO DE CORTE DIRECTO (UNE 103 401-98)

Laboratorios Entecsa calidad acreditada

ENSAYO ACREDITADO. JUNTA DE ANDALUCIA

Obra:	GR, G-1 A G-6		
Peticionario:	UNIVERSIDAD DE GRANADA	**Muestra:**	091045-G-6
Referencia:	091045	**Descripción:**	arcillas alta plasticidad
Fecha ensayo:	31/10/2009	**Cota (m):**	-

Dimensiones de las probetas.

Diámetro (cm):	5
Altura (cm):	2
Área (cm^2):	19,63
Volúmen (cm^3):	39,27

Párametros del Ensayo.

Velocidad Ensayo (mm/min): 1,25

Tipo de Ensayo: UU

Párametros Físicos de las Probetas.

Probeta	I	II	III
Humedad inicial (%)	10,01	10,01	10,01
Humedad final (%)	10,56	10,16	9,88
Densidad aparente (g/cm3)	2,10	2,11	2,11
Densidad seca (g/cm3)	1,89	1,90	1,90
Indice de huecos incial	0,39	0,38	0,38
Indice de huecos final	0,96	0,59	0,55
Dens. de las partículas (g/cm3	2,62	2,62	2,62
Grado de saturación (%)	48,77	49,59	50,43

Tensiones aplicadas a la probeta.

Probeta:	I	II	III
T. Normal (kp/cm^2):	0,5	1	1,5
T. Tangencial (kp/cm^2):	0,94	1,45	1,89
T. Residual (kp/cm^2):	0,34	0,72	1,02
Dilatancia (%):	-8,20	-3,05	-2,50

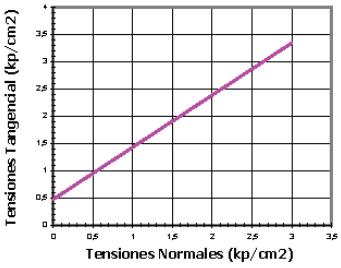

Resultados del Ensayo.

		Residual
COHESIÓN (kp/cm^2):	0,47	0,02
ÁNGULO ROZ. INTERNO (º):	43,8	34,1

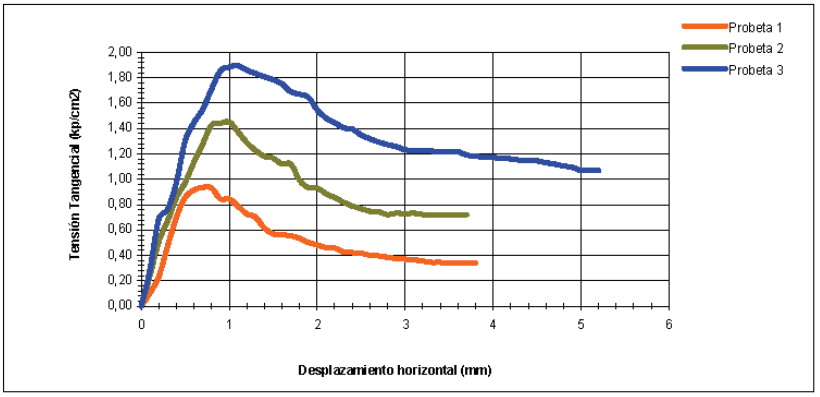

ACTA DE RESULTADOS DE ENSAYOS
ENSAYO DE CORTE DIRECTO (UNE 103 401-98)

Laboratorios Entecsa calidad acreditada

ENSAYO ACREDITADO. JUNTA DE ANDALUCIA

Obra:	GR, G-1 A G-6		
Peticionario:	UNIVERSIDAD DE GRANADA	**Muestra:**	091045-G-6
Referencia:	091045	**Descripción:**	arcillas de alta plasticidad
Fecha ensayo:	26/09/2009	**Cota (m):**	-

Dimensiones de las probetas.

Diámetro (cm):	5
Altura (cm):	2
Área (cm^2):	19,63
Volúmen (cm^3):	39,27

Párametros Físicos de las Probetas.

Probeta	I	II	III
Humedad inicial (%)	10,01	10,01	10,01
Humedad final (%)	10,00	10,23	10,13
Densidad aparente (g/cm3)	2,09	2,12	2,11
Densidad seca (g/cm3)	1,88	1,90	1,90
Indice de huecos incial	0,39	0,38	0,38
Indice de huecos final	0,47	0,44	0,44
Dens. de las partículas (g/cm3	2,62	2,62	2,62
Grado de saturación (%)	47,70	50,72	50,15

Párametros del Ensayo.

Velocidad Ensayo (mm/min): 0,18

Tipo de Ensayo: CD

Tensiones aplicadas a la probeta.

Probeta:	I	II	III
T. Normal (kp/cm^2):	0,5	1	1,5
T. Tangencial (kp/cm^2):	0,69	1,03	1,68
T. Residual (kp/cm^2):	0,46	0,85	1,25
Dilatancia (%):	-1,10	-0,95	-0,85

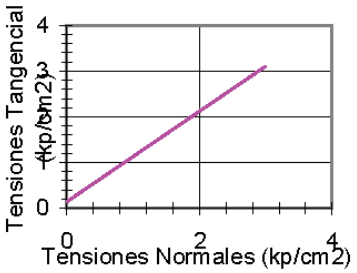

Resultados del Ensayo.

		Residual
COHESIÓN (kp/cm^2):	**0,14**	**0,06**
ÁNGULO ROZ. INTERNO (º):	**44,7**	**38,5**

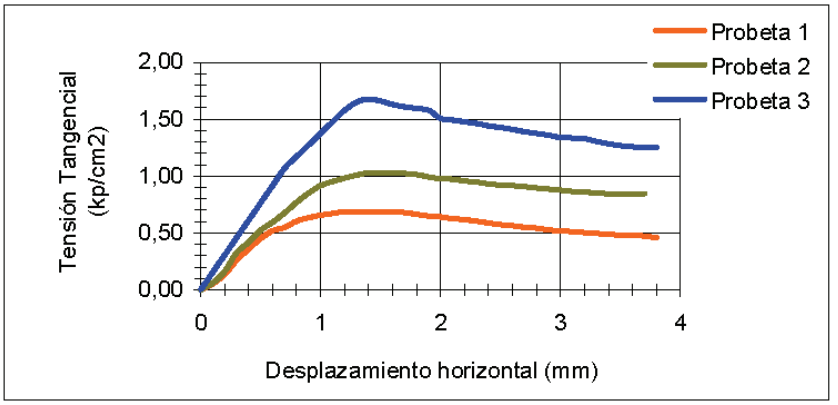

Appendix A4: European Ground Motion Prediction Equations

Reference	GMPE	Magnitude Range	Distance Range (km)	Region
Ambraseys et al. (1996)	$\log PGA = -1.39 + 0.266 \cdot M_s - 0.922 \cdot \log (R^2+35^2)^{½} \pm 0.25$ (PGA in g units)	M_s=4.0-7.5	R≤200 (Fault distance)	Europe and Middle East
Sabetta and Pugliese (1996)	$\log PGA = -1.562 + 0.306 \cdot M_s - \log (R^2+5.8^2)^{½} \pm 0.173$ (PGA in g units)	M_s=4.6-6.8	R≤100 (Fault distance)	Italy
	$\log PGA = -1.845 + 0.363 \cdot M_s - \log (R^2+5^2)^{½} \pm 0.190$ (PGA in g units)		R≤100 (Epicentral distance)	
Cabañas et al. (1999)	$\ln PGA = 8.365 + 0.664 \cdot M_s + (R + 20) - 2.206 \cdot \ln (R + 20)$ (PGA in cm/s^2)	M_s=3.5-6.5	R≤200 (Epicentral distance)	Mediterranean
	$\ln PGA = 0.003 + 1.611 \cdot m_{bl,g} - 1.543 \cdot \ln (R + 10)$ (PGA in cm/s^2)	$m_{bl,g}$=2.0-5.0		Iberian Peninsula
Skarlatoudis et al. (2003)	$\log PGA = 1.07 + 0.45 \cdot M_w - 1.35 \cdot \log (R + 6) \pm 0.286$ (PGA in cm/s^2)	M_w=4.5-7.0	R≤160 (Epicentral distance)	Aegean Region
Cantavella et al. (2004)	$\ln PGA = -2.25 + 1.95 \cdot m_{bl,g} - 1.65 \cdot \ln (R^2 + 6^2)^{½}$ (PGA in cm/s^2)	$m_{bl,g}$=2.5-5.1	R=4-284 (Epicentral distance)	SE Iberian Peninsula
Marin et al. (2004)	$\log PGA = -3.93 + 0.78 \cdot M_L - 1.5 \cdot \log R \pm 0.55$ (PGA in g units)	M_L=2.5-5.6	R= 3-50 (Hipocentral distance)	France
Ambraseys et al. (2005)	$\log PGA = 2.522 - 0.142 \cdot M_w + (-3.184 + 0.314 \cdot M_w) \cdot \log (R^2 + 7.6^2)^{½} - 0.084$ (PGA in m/s^2)	M_w≥5.0	R≤100 (Rupture distance)	Europe and Middle East
Bragato and Slejko (2005)	$\log PGA = -3.27 + (1.95 - 0.202 \cdot M_L) \cdot M_L + (-3.11 + 0.00751 \cdot M_L^3) \cdot \log (R^2 + 8.9^2)^{½} \pm 0.399$ (PGA in g units)	M_L=2.5-6.3	R<130 (Fault distance)	Eastern Alps (Italy)
Tapia et al. (2007)	$\log PGA = -1.8 + 0.45 \cdot M_L - 1.6 \cdot \log (R^2 + 10^2)^{½} - 0.0013 \pm 0.426$ (PGA in g units)	M_L=3.8-5.2	R=7.5-548 (Epicentral distance)	Western Mediterranean
Akkar and Bommer (2007)	$\log PGA = 1.647 + 0.767 \cdot M_w - (0.074 \cdot M_w)^2 + (-3.162 + 0.321 \cdot M_w) \cdot \log (R^2 + 7.682^2)^{½} - 0.045$ (PGA in cm/s^2)	M_w=5.0-7.6	R=5-100 (Epicentral distance)	Europe and Middle East
Massa et al. (2008)	$\log PGA = -3.62 + 0.93 \cdot M_w + (-2.02 \cdot \log (R^2 + 11.71^2)^{½} + 0.12 \pm 0.173$ (PGA in g units)	M_w≤6.5	R≤100 (Epicentral distance)	N Italy
Bindi et al. (2009)	$\log PGA = 3.7691 + 0.0523 \cdot (M_w - 4.5) - 0.1389 \cdot (M_w - 4.5)^2 + (-1.9383 + 0.4661 \cdot (M_w - 4.5) \cdot \log (R^2 + 10.1057^2)^{½} \pm 0.3523$ (PGA in cm/s^2)	M_w>4.0	R≤100 (Epicentral distance)	Italy
	$\log PGA = 3.75 + 0.118 \cdot (M_w - 4.5) - 0.1147 \cdot (M_w - 4.5)^2 + (-1.9267 + 0.4285 \cdot (M_w - 4.5) \cdot \log (R^2 + 10.0497^2)^{½} \pm 0.3555$ (PGA in cm/s^2)		R≤100 (Fault distance)	

Appendix A5: Soil amplification factors

Murcia Region (Benito et al., 2006; Tsige and García-Florez, 2006)

CLASIFICACIÓN RISMUR	DESCRIPCIONES GEOLÓGICAS	DESCRIPCIÓN GEOTÉCNICA	VALOR APROXIMADO Vs (m/s)	CLASIFICACIÓN FEMA
I NULA	Rocas ígneas, basalto, andesita y diabasa, etc. Rocas metamórficas; cuarcitas Rocas sedimentarias, dolomía, Paleozoico y Jurásico.	Rocas muy duras y poco fracturadas	>1500	A
IIa MUY BAJA	Rocas sedimentarias y cobertera Intercalación dolomitas y calizas, filitas y areniscas. Jurásico.	Roca dura y fracturada. Intercalación de rocas muy duras y duras	1500-800	B
IIb BAJA	Rocas sedimentarias, calizas margosas, calizas eolíticas y calizas calcáreas, Cretácico y Terciario.	Roca dura-media muy fracturada e intercaladas	750-450	C
IIIa MEDIA	Rocas sedimentarias, calizas margosas, calizas eolíticas y calizas calcáreas, Cretácico y Terciario.	Roca de resistencia media muy fracturada y con abundantes intercalaciones de rocas más blandas (margas y arcillas)	450-350	C
IIIb MEDIA	Rocas fundamentalmente triasicas de Keuper. Arcillas abirragadas y yeso y sedimentos terciario. Areniscas turbiditicas y arcillas verdes obscura, Conglomerados y areniscas.	Roca blanda con arcillas expansivas Suelos no cohesivos poco cementados	350-250	D
IV ALTA	Sedimentos cuaternarios de origen fluvial y coluviales, pie de monte, etc.	Suelos no cohesivos inestables, gravas y arenas, cantos y costras	250-180	D
V ALTA	Sedimentos cuaternarios de origen fluvial y coluvial, dunas sedimentos eólicos. Depósitos expansivos de margas diatomíticas.	Suelos cohesivos blandos, Arcillas, Limos y Arenas, y No Cohesivos Poco Compactos Arenas, Arenas y Conchas	180-150	E
VI MUY ALTA	Depósitos de playa y cauces del río, marismas, fangos, limos y limos arcillas.	Suelos muy blandos	< 150	F

FACTORES DE AMPLIFICACIÓN RISMUR

Tipo suelo		PGA	SA(0.1s)		SA(0.2s)		SA(0.5s)		SA(1s)
RISMUR	FEMA		≤ 0.1 g	> 0.1 g	≤ 0.1 g	> 0.1 g	≤ 0.1 g	> 0.1 g	
I	A	0,8	0,8	0,8	0,8	0,8	0,8	0,8	0,8
IIa	B	1,0	1,0	1,0	1,0	1,0	1,0	1,0	1,0
IIb - IIIa	C	1,2	1,2	1,2	1,2	1,2	1,4	1,4	1,7
IIIb - IV	D	1,4	1,6	1,6	1,6	1,6	1,9	1,8	2,4
V	E	2,0	2,5	1,5	2,5	1,5	2,9	2,8	3,5
VI	F	2.0*	2.5*	2.2*	2.5*	2.2*	2.9*	2.8*	3.5*

Andalusian Autonomous Region (Navarro et al., 2009; Benito et al., 2010)

Soil type	Geological description	Geothecnical description	V_S^{30} (m/s)
I	Igneous rocks: granites, Gabbra, basalts, andesites, etc. Metamorphic rocks: quartzite, marble, gneiss, etc. Sedimentary rocks: limestone and dolomites (Proterozoic, Paleozoic, Mesozoic)	High and very high hardness rocks slightly fractured	>1,500
II	Sedimentary rocks: dolomites, limestone and greywacke. Metamorphic rocks: schist, micaesquists and slate. (Paleozoic and Mesozoic)	Fractured rocks with high and very high hardness.	1,500–750
III	Metamorphic rocks: filites and metapelites (Paleozoic) Sedimentary rocks: sandstone, clay, limestone, marl, etc. Triassic rocks of Keuper: clay, gypsum, sandstone and limestone (Mesozoic, Cenozoic)	Medium-hard rocks highly fractured and sometimes with abundant intercalation of little toughness rocks Soft rocks with expansive clay.	750–400
IV	Quaternary sediments from river source, colluvial and foot of mount: sand, silt, conglomerates. (Tertiary and Quaternary)	Little or no cohesive soils promptly cemented.	400–200
V	Quaternary sediments from river, coluvial and wind origin: gravel, sand, silt and clay. (Quaternary)	Cohesive soft and loose not cohesive soils.	200–150
VI	Beach deposit, wetlands and river channels: mud, sand dunes, plastic clay and silt organic. (Quaternary)	Very soft soils, sometimes potentially liquefiable soils, sensitive clays, organic soils, soft clays, . . .	< 150

FACTORES DE AMPLIFICACIÓN SISMOSAN						
Tipo suelo		A [PGA]	A [SA(0.1s)]	A [SA(0.2s)]	A [SA(0.5s)]	A [SA(1s)]
SISMOSAN	NEHRP-2003					
I	A	0.87	0.84	0.80	0.80	0.80
II	B	1.00	1.00	1.00	1.00	1.00
III	C	1.20	1.20	1.20	1.39	1.70
IV	D	1.40	1.50	1.60	1.90	2.40
V	E	1.80	2.15	2.50	2.88	3.50
VI	F	2.0*	2.25*	2.5*	2.88*	3.5*

Appendix A6: Intensity-PGA relationships for the Mediterranean zone

Reference	I-PGA relationship	Intensity Range	PGA range	Region
Medvedev and Sponheuer (1969)	$\log PGA = -0.408 + 0.301 \cdot I_{MM}$ (PGA in cm/s^2)	$I_{MM} = 5 - 10$	12 - 800	
Ambraseys (1974)	$\log PGA = -0.16 + 0.36 \cdot I_{MM} \pm 0.7$ (PGA in cm/s^2)	$I_{MM} = 4 - 10$	2 - 600	Eastern Mediterranean
Murphy and O'Brien (1977)	$\log PGA = 0.25 + 0.25 \cdot I_{MM}$ (PGA in cm/s^2)	$I_{MM} = 4 - 8$	10 - 700	Southern Europe, Westwern USA and Japan
Chiaruttini and Siro (1981)	$\log PGA = -0.19 + 0.17 \cdot I_{MM} \pm 0.27$ (PGA in g units)	$I_{MM} = 4 - 8$	19 - 158	Italy
Margottini et al. (1992)	$\log PGA = 0.687 + 0.179 \cdot I_{MCS} \pm 0.24$ (PGA in cm/s^2)	$I_{MCS} = 4 - 8$	20 - 222.8	Italy (General Intensity)
	$\log PGA = 0.525 + 0.22 \cdot I_{MCS} \pm 0.21$ (PGA in cm/s^2)			Italy (Local Intensity)
Theodulidis and Papazachos (1992)	$\ln PGA = 0.28 + 0.67 \cdot I_{MM} + 0.42 \pm 0.59$ (PGA in cm/s^2)	$I_{MM} = 4 - 8$	8.8 - 530	Greece
Decanini et al. (1995)	$\log PGA = 0.594 + 0.237 \cdot I_{MM} \pm 0.35$ (PGA in cm/s^2)	$I_{MM} = 4 - 11$	-	Italy, western USA and Latin America
Koliopoulos et al. (1998)	$\ln PGA = 0.03 + 0.74 \cdot I_{MM}$ (PGA in cm/s^2)	$I_{MM} = 3 - 9$	9 - 600	Greece
NCSE-02 (2002)	$\log PGA = -3.223 + 0.301 \cdot I$ (PGA in g units)	$I_{MM} = 5 - 10$	-	Spain
Faccioli and Cauzzi (2006)	$\log PGA = -1.33 + 0.20 \cdot I_{MCS} \pm 0.29$ (PGA in m/s^2)	$I_{MCS} = 4 - 9$	18 - 600	Mediterranean
Tselentis and Danciu (2008)	$I_{MM} = -0.946 + 3.563 \cdot \log PGA$ (PGA in cm/s^2)	$I_{MM} = 4 - 8$	23 - 316	Greece

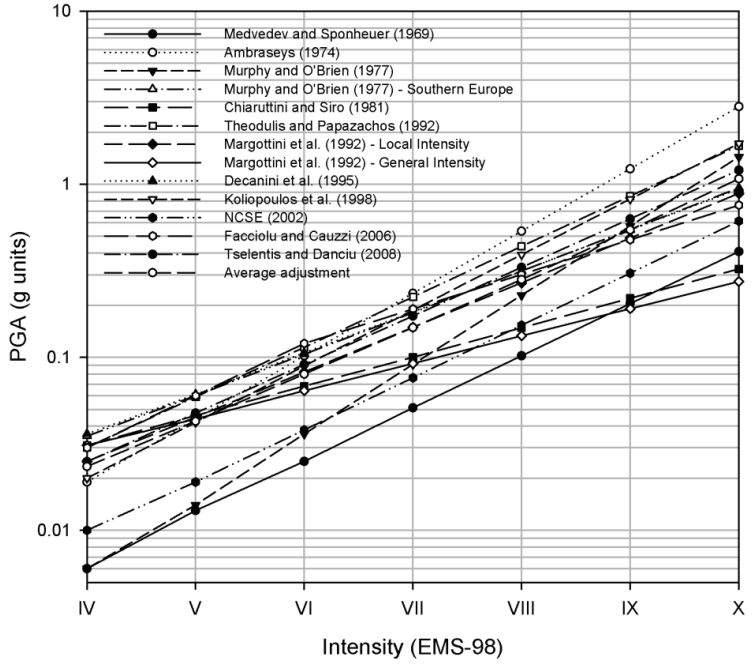

REFERENCES

AENOR (1993). UNE 103-104/93. Test for the plastic limit of a soil. Asociación Española de Normalización y Certificación, Madrid, 2 pp.

AENOR (1994a). UNE 103-301/94. Determination of a soil density. Method of the hydrostatic balance. Asociación Española de Normalización y Certificación, Madrid, 2 pp.

AENOR (1994b). UNE 103-302/94. Determination of the relative density of the particles of a soil. Asociación Española de Normalización y Certificación, Madrid, 3 pp.

AENOR (1994c). UNE 103-103/94. Determination of the liquid limit of a soil by the Casagrande apparatus method. Asociación Española de Normalización y Certificación, Madrid, 9 pp.

AENOR (1998). UNE 103-401/98. Determination of the shear strenght of a soil with the direct shear box. Asociación Española de Normalización y Certificación, Madrid, 34 pp.

AFPS (1995). Guidelines for Seismic Microzonation Studies. French Association for Earthquake Engineering, 7-11.

Akkar, S., Bommer, J.J. (2007). Empirical prediction equations for peak ground velocity derived from strong-motion records from Europe and the Middle East. Bulletin of the Seismological Society of America, 97: 511-530.

Aldaya, F.; Álvarez, F.; Galindo-Zaldívar, J.; González-Lodeiro, F.; Jabaloy, A. and Navarro-Vilá, F. (1991). The Malaguide-Alpujarride contact (Betic Cordilleras, Spain): a brittle extensional detachment. C. R. Acad. Sci. Paris, 313 (Serie II-101): 1447-1453.

Alfaro, P.; Galindo-Zaldívar, J.; Jabaloy, A.; López-Garrido, A.C. and Sanz de Galdeano, C. (2001a). Evidence for the activity and paleoseismicity of the Padul fault (Betic Cordillera, southern Spain). Acta Geologica Hispanica, 36 (3-4): 283-295.

Alfaro, P.; Galindo-Zaldívar, J.; Jabaloy, A.; López-Garrido, A.C. and Sanz de Galdeano, C. (2001b). El sector de El Padul-Nigüelas. In: La Cuenca de Granada. Estructura, Tectónica activa, Sismicidad, Geomorfología y dataciones existentes. Sanz de Galdeano, C.; Peláez Montilla, J.A. and López Garrido. A.C. (Eds.), CSIC-University of Granada, 121-132.

Alonso Chaves, F.M.; Azañón Hernández, J.M.; Azor Pérez, A.; Cantano Martín, M.; Delgado García, J.; García Navarro, E.; Mantero Romero, E.M.; Pérez García, J.L. and Yesares García, J. (2007). Informe final del Análisis de la estabilidad de laderas en el área afectada por el incendio de Sierra Nevada. EGMASA, University of Granada, University of Huelva and University of Jaén, 225 pp.

Ambraseys, N.N. (1974). The correlation of intensity with ground motion. In: Proceedings of the XIV Assembly of the European Seismological Commission. Trieste, Italy, 16-22 September 1974, 335-341.

Ambraseys, N.N.; Douglas, J.; Sarma, S.K. and Smit, P.M. (2005). Equations for the Estimation of Strong Ground Motions from Shallow Crustal Earthquakes Using Data from Europe and the Middle East: Horizontal Peak Ground Acceleration and Spectral Acceleration. Bulletin of Earthquake Engineering, 37: 1-53.

Ambraseys, N.N. and Menu, J.M. (1988). Earthquake-induced ground displacements. Earthquake Engineering and Structural Dynamics, 16: 985-1006.

Ambraseys, N.N. and Srbulov, M. (1994). Attenuation of earthquake-induced ground displacements. Earthquake Engineering & Structural Dynamics, 23(5): 467-487.

Arias, A. (1970). A measure of earthquake intensity. In: Seismic Design for Nuclear Power Plants (R.J. Hansen, Ed.). Massachusetts Institute of Technology Press, Cambridge, 438-483.

Armijo, R. (1977). La Zone des Failles Lorca-Totana (Cordillères Béticas, Espagne), étude tectonique et neotectonique. Ph.D. Thesis, Paris VII, 229 pp.

ASTM (2000). ASTM-D 2487/00. Standard Classification of Soils for Engineering Purposes (Unified Soil Classification System). American Society for Testing and Materials, West Conshohocken, PA, 11 pp.

Ayala Carcedo, F.J. and Corominas, J. (2002). Mapas de susceptibilidad a los movimientos de ladera con técnicas SIG. Fundamentos y Aplicaciones en España. IGME, Serie Medio Ambiente nº 4. Madrid, 191 pp.

Aydin, A. and Basu, A. (2005). The Schmidt hammer in rock material characterization. Engineering Geology, 81: 1-14.

Aydin, A. (2009). ISRM Suggested method for determination of the Schmidt hammer rebound hardness: revised version. International Journal of Rock Mechanics and Mining Sciences, 46(3): 627-634.

Azañón, J.M.; Azor, A.; Booth-Rea, G. and Torcal, F. (2004). Small-scale faulting, topographic steps and seismic ruptures in the Alhambra (Granada, southeast Spain). Journal of Quaternary Science, 19 (3): 219-227.

Azañón, J.M., Azor, A., Cardenal Escarcena, J.F., Delgado García, J., Delgado Marchal, J., Gómez-Molina, A., López-Chicano, M., López-Sánchez, J.M., Mallorqui-Franquet, J.J., Martín, W., Mata de Castro, E., Mateos, R.M., Nieto, F., Peña-Ruano, J.A., Pérez-García, J.L., Puerma-Castillo, M., Rodríguez-Fernández, J., Teixidó-Ullod, T., Tomás-Jover, R., Tsige, M., Yesares, J. (2006) Estudio sobre la predicción y mitigación de movimientos de ladera en vías de comunicación estratégicas de la Junta de Andalucía. Final Report. Instituto Andaluz de Ciencias de la Tierra, CSIC-UGR (Ed.), Granada (Spain), 380 pp.

Azañón, J.M., Azor, A., Yesares, J., Tsige, M., Mateos, R.M., Nieto, F., Delgado, J., López-Chicano, M., Martín, W. and Rodríguez-Fernández, J. (2009). Regional-scale high-plasticity clay-bearing formation as controlling factor on landslides in Southeast Spain. Geomorphology,120: 26-37.

Baena-Pérez, J. (1972). N° 931: Zarcilla de Ramos; Spanish Geologic Map 1:50 000 scale (2ª serie). Instituto Geológico y Minero de España (IGME), Madrid.

Bandis, S.C. (1980). Experimental studies of scale effects on shear strength and deformation of rock joints. Ph.D. Thesis, University of Leeds, Leeds.

Bandel, K., Reicherter, K., Dyrssen, U. and Reiss, S. (2000). Late Neogene lacustrine sedimentary facies and gastropod assemblages (Granada Basin, southern Spain). Mitteilungen Geol.- Paläont, 84. Institut Universität Hamburg, pp. 111-130.

Baptista, M.A., Miranda, P.M.A., Miranda, J.M. and Mendes Victor, L. (1998). Constraints on the source of the 1755 Lisbon tsunami inferred from numerical modeling of historical data on the source of the 1755 Lisbon tsunami. Journal of Geodynamics, 25: 159-174.

Barkan, R., ten Brink, U.S. and Lin, J. (2009). Far field tsunami simulations of the 1755 Lisbon earthquake: Implications for tsunami hazard to the U.S. East Coast and the Caribbean. Marine Geology, 264 (1-2): 109-122.

Barton, N. and Bandis, S. (1990). Review of predictive capabilities of JRC-JCS model in engineering practice. Proc. Int. Conf. Rock Joints, Balkema, Norway, pp 603-610.

Barton, N. and Choubey, V. (1977). The Shear Strength of Rock Joints in Theory and Practice. Rock Mechanics, 10(1-2): 1-54.

Bell, F.G. (2007). Engineering Geology. Second edition. Butterworth-Heinemann (Elsevier), UK, 581 pp.

Benito, B.; Capote, B.; Murphy, P.; Gaspar-Escribano, J.M.; Martínez-Díaz, J.J.; Tsige, M.; Stich, D.; García-Mayordomo, J.; García, M.J.; Jiménez, M.E.; Insua- Arévalo, J.M.; Álvarez-Gómez, J.A. and Canora, C. (2007). An overview of the damaging and low magnitude La Paca earthquake (Mw 4.8) on January 29th, 2005. Context; seismotectonics; and seismic risk implications for Southeast Spain. Bulletin of the Seismological Society of America, 97: 671-690.

Benito, B.; Gaspar-Escribano, J.M.; García-Mayordomo, J.; Jiménez, M.E. and García Rodríguez, M.J. (2006). Proyecto RISMUR: Evaluación de la peligrosidad sísmica. Instituto Geográfico Nacional y Protección Civil de Murcia, Madrid.

Benito B., Navarro, M., Vidal, F., Gaspar-Escribano J.M., García-Rodríguez, M.J. and Martínez-Solares, J.M. (2010). A new seismic hazard assessment in the region of Andalusia (Southern Spain). Bulletin of Earthquake Engineering, DOI 10.1007/s10518-010-9175-9.

Bindi, D.; Luzi, L.; Massa, M. and Pacor, F. (2009). Horizontal and vertical ground motion prediction equations derived from the Italian Accelerometric Archive (ITACA). Bulletin of Earthquake Engineering, DOI 10.1007/s10518-009-9130-9.

Bird, J.F., Bommer, J.J. (2004). Earthquake losses due to ground failure. Engineering Geology, 75: 147-179.

Blumenthal, M. (1927). Versucheiner tektonischen gliederung der Betischen-Cordilleren von central and süd-west Andalusien. Eclogae Geologicae Helvetica, 10: 487-532.

Boatwright, J., Thywissen, K. and Seekins, L.C. (2001). Correlation of Ground Motion and Intensity for the 17 January 1994 Northridge, California, Earthquake. Bulletin of the Seismological Society of America, 91 (4): 739-752.

Booth-Rea, G. (2004). Tectónica Cenozoica en el Dominio Cortical de Alborán. Ph.D. Thesis. University of Granada, 253 pp.

Booth-Rea, G.; Azañón, J. M. and García-Dueñas, V. (2004). Extensional tectonics in the northeastern Betics (SE Spain): case study of extension in a multilayered upper crust with contrasting rheologies. Journal of Structural Geology, 26: 2039-2058.

Booth-Rea, G.; García-Dueñas, V. and Azañón, J.M. (2002). Extensional attenuation of the Malaguide and Alpujarride thrust sheets in a segment of the Alboran Basin folded during the Tortonian (Lorca area, Eastern Betics). C. R. Geoscience, 334: 557-563.

Borcherdt, R.D. (1994). Estimates of Site-Dependent Response Spectra for Design (Methodology and Justification). Earthquake Spectra 10, 617-673.

Bourgois, J., Chauve, P. and Didon, J. (1974) La formation d'argiles a blocs dans la province de Cadix, Cordilleras Betiques, Espagne. Reun. Annu. Sci. Terre 2, 79 pp.

Bousquet, J.C. (1979). Quaternary strike-slip faults in southeastern Spain. Tectonophysics, 52: 277-286.

Buforn, E.; Cesca, S.; Goded, T.; Fresno, C. and del Muñoz, D. (2006). The Bullas (Murcia, SE Spain) earthquake, 29 January 2005. Journal of Seismology, 10: 65-72.

Buforn, E.; Benito, B.; Sanz de Galdeano, C.; Fresno, C.; del Muñoz, D. and Rodríguez, I. (2005). Study of the damaging earthquakes of 1911, 1999, and 2002 in the Murcia, Southeastern Spain region: seismotectonic and seismic-risk implications. Bulletin of the Seismological Society of America, 95: 549-567.

Buforn, E.; Bezzeghoud, M.; Udías, A. and Pro, C. (2004). Seismic sources on the Iberia-African plate boundary and their tectonic implications. Pure and Applied Geophysics, 161: 623-646.

Buforn, E., Sanz de Galdeano, C. and Udías, A. (1995). Sismotectonics of the Ibero-Maghrebian region. Tectonophysics, 248: 247-261.

Buforn, E.; Udías, A. and Madariaga, R. (1991). Intermediate and Deep Earthquakes in Spain. Pure and Applied Geophysics, 136: 375-393.

Buyuksagisa, I.S. and Goktan, R.M. (2007). The effect of Schmidt hammer type on uniaxial compressive strength prediction of rock. International Journal of Rock Mechanics & Mining Sciences, 44: 299-307.

Cabañas, L., Benito, B., Cabañas, C., López, M., Gómez, P., Jiménez, M.E. and Álvarez, S. (1999). Banco de Datos de Movimiento Fuerte del Suelo MFS. Aplicaciones. Física de la Tierra, 11: 111-137.

Cantavella, J.V., Herráiz, M., Jiménez, M.J. and García, M. (2004). Atenuación sísmica en el Sureste de la Península Ibérica. In: Proceedings 4ª Asamblea Hispano-Portuguesa de Geodesia y Geofisica. Figueira da Foz, Portugal, 3-7 February 2004, 289-290.

Capolongo, D.; Refice, A. and Mankelow, J. (2002). Evaluating earthquake-triggered landslide hazard at the basin scale through GIS in the Upper Sele river valley. Surveys in Geophysics, 23: 595-625.

Cargill, J.S. and Shakoor, A. (1990). Evaluation of empirical methods for measuring the uniaxial compressive strength. International Journal of Rock Mechanics & Mining Sciences, 27:495-503.

Carreño, E., Suárez, A., Tordesillas, J.M. and Sánchez, M. (1999). Red Acelerográfica del Instituto Geográfico Nacional. Diez años de registro. In: Proceedings of the 1st Congreso Nacional de Ingeniería Sísmica. Murcia, Spain, 12-16 April 1999, 291-298.

Carro, M., De Amicis, M., Luzi, L. and Marzorati, S. (2003). The application of predictive modeling techniques to landslides induced by earthquakes: the case study of the 26 September 1997 Umbria-Marche earthquake (Italy). Engineering Geology, 69: 139-159.

CEN (Comité Européen of Normalisation) (2004). Eurocode 8: design of structures for earthquake resistance. Part 1: general rules, seismic actions and rules for buildings. EN 1998-1, Brussels.

Cesare, B.; Gómez-Pugnaire, M.T. and Rubatto, D. (2003). Residence time of S-type anatectic magmas beneath the Neogene Volcanic Province of SE Spain: a zircon and monazite SHRIMP study. Contributions to Mineralogy and Petrology, 146: 28-43.

Chen, S.; Lee, S. and Peng, W. (2004). A study on the modelling of the earthquake-induced landslide hazard assessment by cumulative displacement method-A case study. Proceeding of International Symposium on Landslide and Debris Flow Hazard Assessment, 3: 1-15.

Chiaruttini, C. and Siro, L. (1981). The correlation of peak ground horizontal acceleration with magnitude, distance and seismic intensity for Friuli and Ancona, Italy, and the Alpide Belt. Bulletin of the Seismological Society of America, 71: 1993-2009.

Clark, S.P. (Ed.) (1966). Handbook of Physical Constants, Geol. Soc. Am. Mem., 97, 587 pp.

Coral Mocayo, H. (2002). Utilización de métodos experimentales y de simulación numérica para la microzonificación sísmica de áreas urbanizadas en Andorra. PhD Thesis, Universidad Politécnica de Cataluña, Cataluña (Spain), 207pp.

Corominas, J. (ed.) (1989). Estabilidad de Taludes y laderas naturales. Monografía nº 3, Sociedad Española de Geomorfología, Zaragoza, 248 pp.

Cruden, D.M. and Varnes, D.J. (1996). Landslide types and processes. In: Turner, A.K., Schuster, R.L. (eds). Landslides investigation and mitigation. Special Report 247. Transportation Research Board, National Research Council, Washington, pp. 36-75.

De Miguel, F., Vidal, F., Alguacil, G., and Guirao, J.M. (1989). Spatial and energic trends of the microearthquakes activity in the Central Betics. Geodinamica Acta, 3: 87-94.

Deere, D.U. and Miller, R.P. (1966). Engineering classification and index properties for intact rocks. Tech Report. Air Force Weapons Lab., New Mexico, No. AFNL-TR, pp. 65-116. Kirtland.

Decanini, L., Gavarini, C. and Mollaioli, F. (1995). Proposta di definizione delle relazioni tra intensità macrosismica e parametri del moto del suolo. In: Atti del 7° Convegno Nazionale l'Ingegneria Sismica in Italia. Vol. 1, 63-72.

Delgado, J.; Alfaro, P.; Andreu, J.M.; Cuenca, A.; Doménech, C.; Estévez, A.; Soria, J.M.; Tomás, R. and Yébenes, A. (2003). Engineering-geological model of the Segura River flood plain (SE Spain): a case study for engineering planning. Engineering Geology, 68: 171-187.

Delgado, J.; Peláez, J.A.; Tomás R.; Estévez, A.; López Casado, C.; Doménech C. and Cuenca A. (2006). Evaluación de la susceptibilidad de las laderas a sufrir inestabilidades inducidas por terremotos. Aplicación a la cuenca de drenaje del río Serpis (provincia de Alicante). Revista de la Sociedad Geológica de España, 19 (3-4): 197-218.

Doblas, M.; Mahecha, V.; Hoyos, M. and López-Ruiz, J. (1997). Slickenside and fault surface kinematic indicators on active normal faults of the Alpine Betic cordilleras, Granada, southern Spain. Journal of Structural Geology, 19 (2): 159-170.

Dobrin, M.B. and Savit, C.H. (1988). Introduction to Geophysical Prospecting. McGraw-Hill, New York, 867 pp.

Egeler, C.G. (1963). On the tectonics of the eastern Betic Cordilleras (SE Spain). Geologische Rundschau, 53: 260-269.

El Amrani Paaza, N.; Lamas, F.; Irigaray, C. and Chacón, J. (1998). Engineering geological characterization of Neogene marls in the Southeastern Granada Basin, Spain. Engineering Geology, 50: 165-175.

El Amrani Paaza, N.; Lamas, F.; Irigaray, C.; Chacón, J. and Oteo, C. (2000). The residual shear strength of Neogene marly soils in the Granada and Guadix basins, southeastern Spain. Bulletin of Engineering Geology and the Environment, 58: 99-105.

ENADIMSA (1985). Mapa geológico-minero de Andalucía. Dirección General de Industria, Energía y Minas. Consejería de Economía e Industria. Junta de Andalucía, Sevilla, 150 pp.

ESRI (Environmental Systems Research Institute) Inc. (2008). ArcGIS 9.3. Redlands, California, U.S.A. Web site (http://www.esri.com.es). Accessed on 10 June, 2010.

Faccioli, E. and Cauzzi, C. (2006). Macroseismic intensities for seismic scenarios estimated from instrumentally based correlations. In: 1st European conference on earthquake engineering and seismology, Geneva, 3-8 September 2006, Paper no. 569.

Fadil, A., Vernant, P., McClusky, S., Reilinger, R., Gomez, F., Ben Sari, D., Mourabit, T., Feigl K. and Barazangi, M. (2006). Active tectonics of the western Mediterranean: geodetic evidence for rollback of a delaminated subcontinental lithospheric slab beneath the Rif Mountains, Morocco. Geology, 34(7): 529-532.

Fallot, P. (1948). Les Cordillères Bétiques. Estudios geologicos, 4(7-8): 259-279.

Fernández, J., Viseras, C. and Soria, J. (1996). Pliocene-Pleistocene infilling of the Granada and Guadix Basins (Betic Cordillera, Spain): the influence of allocyclic and autocyclic processes on the resulting stratigraphic organization. In: Friend, P.F., Dabrio, C.J. (Eds.), Tertiary Basins of Spain. Cambridge University Press, Cambridge, 366-371.

Fernández-Fernández, E. (2003). Estructura del contacto entre las zonas Externas e Internas en el área de Sierra de María y los Vélez (sector oriental de las Cordilleras Béticas). Ph.D. Thesis, University of Granada, 147 pp.

Fernández-Ibáñez, F. and Soto, J.I. (2008). Crustal rheology and seismicity in the Gibraltar Arc (western Mediterranean). Tectonics, 27: TC2007, doi:10.1029/2007TC002192.

Feriche, M. and Botari, C. (2002). Base de datos de sismos históricos. In Primer Centenario del Observatorio de Cartuja. Congreso Cien años de Sismología en Granada. University of Granada (CD-ROM).

Figueras, S., Macau, A., Goula, X. and González, M. (2005). Aplicación del método de Newmark para el estudio de los movimientos de ladera activados por terremotos en Andorra. VI Simposio Nacional sobre taludes y laderas inestables, Valencia. Vol. 3, 12 p.

Fontboté, J.M. (1986). Las Zonas Internas de las Cordilleras Béticas. In: Libro Homenaje a José María Ríos, Geología de España. IGME, Madrid, Tomo 2, pp. 251-243.

Franklin, J.A. and Dusseault, M.B. (1989). Rock Engineering. McGraw-Hill Publ. Co., New York, 600 pp.

Galindo-Zaldívar, J.; González-Lodeiro, F. and Jabaloy, A. (1989). Progressive extensional shear structures in a detachment contact in Western Sierra Nevada (Betic Cordillera, Spain). Geodinamica Acta, 3: 73-85.

Galindo-Zaldívar, J.; González-Lodeiro, F. and Jabaloy, A. (1993). Stress and paleostress in the Betic-Rif cordilleras (Miocene to the present). Tectonophysics, 227: 105-126.

Galindo-Zaldívar, J.; Jabaloy, A.; Morales, J.; Ruano, P. and Serrano, I. (2001). Estructura y evolución tectónica de la Depresión de Granada en el marco de las Cordilleras Béticas. In: La Cuenca de Granada. Estructura, Tectónica activa, Sismicidad, Geomorfología y dataciones existentes. Sanz de Galdeano, C.; Peláez Montilla, J.A. and López Garrido. A.C. (Eds.), CSIC-University of Granada, 89-108.

García-Cortés, A.; Mansilla, H. and Quintero, I. (1991). Puesta de manifiesto de la Unidad Olistostrómica del Mioceno medio en el sector oriental de las Cordilleras Béticas (provincias de Jaén, Almería, Murcia y Alicante). Boletín Geológico y Minero, 102: 524-535.

García-Dueñas, V. (1967). Unidades paleogeográficas en el sector central de la Zona Subbética. Not. Com. Instituto Geológico y Minero de España, 101-102: 73-100.

García-Dueñas, V.; Balanyá, J.C. and Martínez-Martínez, J.M. (1992). Miocene extensional detachments in the outcropping basement of the northern Alboran Basin and their tectonic implications. Geo-Marine Letters, 12: 88-95.

García-Dueñas, V. and Martínez-Martínez, J.M. (1988). Sobre el adelgazamiento mioceno del Dominio de Alborán: el despegue de los Filabres (Béticas orientales). Geogaceta, 5: 53-55.

García-Hernández, M.; López-Garrido, A.C.; Rivas, P.; Sanz de Galdeano, C. and Vera, J.A. (1980). Mesozoic paleogeographic evolution of the External Zones of the Betic Cordillera. Geologie en Mijnbouw., 59: 155-168.

García-Mayordomo, J. (1998). Riesgo Sísmico en la Cuenca de Alcoy (Alicante). Aproximación a una Zonificación Sísmica. M.Sc. Thesis on Enginerring Geology. University Complutense of Madrid (Spain).

García-Mayordomo, J. (1999). Zonificación Sísmica de la Cuenca de Alcoy mediante un Sistema de Información Geográfico. 1er Congreso Nacional de Ingeniería Sísmica, Murcia, Memorias, Tomo Ib, 443-450.

García-Mayordomo, J. (2005). Caracterización y Análisis de la Peligrosidad Sísmica en el Sureste de España. Ph.D. Thesis. University Complutense of Madrid, Spain, 373 pp.

García-Mayordomo, J.; Gaspar-Escribano, J.M. and Benito, B. (2007). Seismic hazard assessment of the Province of Murcia (SE Spain): analysis of source contribution to hazard. Journal of Seismology, 11(4): 453-471.

García-Mayordomo, J.; Rodríguez-Peces, M.J.; Azañón, J.M.and Insua Arévalo, J.M. (2009). Advances and trends on earthquake-triggered landslide research in Spain. 1st International Workshop on Earthquake Archaeology and Palaeoseismology. Baelo Claudia, Cádiz, Spain, 4 pp.

Gaspar-Escribano, J.M. and Benito, B. (2007). Ground motion characterization of low-to-moderate seismicity zones and implications for seismic design: lessons from recent, M_w~4.8, damaging earthquakes in Southeast Spain. Bulletin of the Seismological Society of America, 97: 531-544.

Gaspar-Escribano, J.M.; Benito, B. and García-Mayordomo, J. (2008). Hazard-consistent response spectra in the Region of Murcia (Southeast Spain): comparison to earthquake-resistant provisions. Bulletin of Earthquake Engineering, 6 (2): 179-196.

Gauyau, F.; Bayer, R.; Bousquet, J.C.; Lachaud, J.C.; Lesquer, A. and Montenat, C. (1977). Le prolongament de l'accident d'Alhama de Murcia entre Murcia et Alicante (Espagne méridionale). Bulletin de la Sociètè Géologique de France, 7 (3): 623-629.

Geli, L.; Bard, P.Y. and Jullien, B. (1988). The effects of topography on earthquake ground motion. A review and new results. Bulletin of the Seismological Society of America, 78 (1): 42-63.

Giani, G.P. (1992). Rock Slope Stability Analysis. Balkema, Rotterdam. 361 pp.

González-Lodeiro, F.; Aldaya, F.; Galindo-Zaldívar, J. and Jabaloy, A. (1996). Superposition of extensional detachments during the Neogene in the internal zones of the Betic cordilleras. International Journal of Earth Sciences, 85 (2): 350-362.

González de Vallejo, L.; Ferrer, M.; Ortuño, L. and Oteo, C. (2002). Ingeniería Geológica. Editorial Prentice Hall. Madrid, 744 pp.

Grandin, R., Borges, J.F., Bezzeghoud, M., Caldeira, B. and Carrilho, F. (2007). Simulations of strong ground motion in SW Iberia for the 1969 February 28 (Ms = 8.0) and the 1755 November 1 (M~ 8.5) earthquakes - I. Velocity model. II. Strong ground motion simulations. Geophysical Journal International, 171(2): 807-822.

Graham, J. (1984). Methods of slope stability analysis. In: Brunsden, D. and Prior, D.B. (eds). Slope Instability. John Wiley & Sons, pp. 171-215.

Güney, A.; Altındag, R.; Yavuz, H. and Saraç, S. (2005). Evaluation of the Relationships between Schmidt Hardness Rebound Number and Other (Engineering) Properties of Rocks. The 19th International Mining Congress and Fair of Turkey, IMCET2005, İzmir, Turkey. pp. 83-89.

Gutscher, M.A., Baptista, M.A. and Miranda, J.M. (2006). The Gibraltar Arc seismogenic zone: Part 2. Constraints on a shallow east dipping fault plane source for the 1755 Lisbon earthquake provided by tsunami modeling and seismic intensity. Tectonophysics, 426: 153-166.

Gutenberg, B. and Richter, C.F. (1956). Earthquake magnitude, intensity, energy and acceleration. Bulletin of the Seismological Society of America, 40: 105-145.

Guzzetti, F., Ardizzone, F., Cardinali, M., Rossi, M. and Valigi, D. (2009). Landslide volumes and landslide mobilization rates in Umbria, central Italy. Earth and Planetary Science Letters, 279: 222-229.

Hanks, T.C. and Kanamori, H. (1979). A moment magnitude scale. Journal of Geophysical Research, 84: 2348-2350.

Harp, E.L. and Jibson, R.W. (1996). Landslides triggered by the 1994 Northridge, California, earthquake. Bulletin of the Seismological Society of America, 86: 319-332.

Harp, E.L. and Jibson, R.W. (2002). Anomalous Concentrations of Seismically Triggered Rock Falls in Pacoima Canyon: Are They Caused by Highly Susceptible Slopes or Local Amplification of Seismic Shaking? Bulletin of the Seismological Society of America, 92 (8): 3180–3189.

Harp, E.L. and Noble, M.A. (1993). An engineering rock classification to evaluate seismic rock-fall susceptibility and its implication to the Wasatch Front. Bulletin of the Association of Engineering Geologists, 30: 293-319.

Harp E.L. and Wilson R.C. (1995). Shaking Intensity Thresholds for Rock Falls and Slides: Evidence from 1987 Whittier Narrows and Superstition Hills Earthquake Strong-Motion Records. Bulletin of the Seismological Society of America, 85 (6): 1739-1757.

Hernan Gavilanes, J. (2003). Parámetros geotécnicos y estabilidad de taludes. Curso de explotación de canteras. Asociación de Ingenieros de Minas del Ecuador.

Hernández-Enrile, J.L.; Martínez-Díaz, J.J.; Masana, E. and Santanach, P. (2000). Resultados preliminares del estudio paleosísmico mediante trincheras de la falla de Alhama de Murcia (Cordillera Bética), Geotemas, 1-4: 335-339.

Herraiz, M.; De Vicente, G.; Lindonaupari, R.; Giner, J.; Simon, J.L.; González-Casado, J.M.; Vadillo, O.; Rodríguez-Pascua, M.A.; Cicuéndez, J.I.; Casas, A.; Cabañas, L.; Rincón, P.; Cortés, A.L.; Ramírez, M. and Lucini, M. (2000). The recent (upper Miocene to Quaternary) and present tectonic stress distributions in the Iberian Peninsula. Tectonics, 19: 762-786.

Hoek, E. (2000). Practical Rock Engineering. Web site (http://www.rocscience.com). Accessed on 10 June, 2010.

Hoek, E. and Bray, J.W. (1981). Rock Slope Engineering, 3rd edition. Institution of Mining and Metallurgy, London.

Hough, B.K. (1957). Basic Soils Engineering. The Ronald Press Co, Nueva York.

Hunt, R.E. (2005). Geotechnical Engineering Investigation Handbook. 2ª Edición. Taylor & Francis, 1088 pp.

IAEG Commission on Landslides (1990). Suggested nomenclature for landslides. Bulletin of Engineering Geology and the Environment, 41: 13-16.

IGME (2000). Caracterización geotécnica y estudio de Peligrosidad sísmica y por inundaciones de la Ciudad de Cartagena. Consejería de Política Territorial y Obras Públicas de la Región de Murcia. Maps scale 1:15.000. Madrid, 5 volumes.

IGME (2006). Manual de Ingeniería de taludes. Madrid, 459 pp.

IGME and Diputación de Granada (2007). Atlas de Riesgos Naturales en la provincia de Granada. Granada, 190 pp.

ITGE (1985). Mapa hidrogeológico de España a escala 1:200.000. Hoja nº 79 Murcia.

ITGE (1991). Mapa neotectónico, sismotectónico y de actividad de fallas de la Región de Murcia (escalas 1:200.000 y 1:100.000). Consejería de Política Territorial y Obras Públicas de la Región de Murcia. 6 mapas, 99 pp.

ITGE (1992). Estudio de peligrosidad y vulnerabilidad sísmica en Lorca y su término municipal. Consejería de Política Territorial y Obras Públicas de la Región de Murcia. Madrid, 201 pp.

ITGE (1994). Mapa Geológico de la Región de Murcia a escala 1:200.000. Consejería de Política Territorial y Obras Públicas de la Región de Murcia. 1 map, 105 pp.

ITGE (1995). Atlas Inventario de Riesgos Naturales de la Comunidad Autónoma de la Región de Murcia. Consejería de Política Territorial y Obras Públicas de la Región de Murcia. Madrid, 5 maps, 138 pp.

Jabaloy, A.; Galindo-Zaldívar, J. and González-Lodeiro F. (1993). The Alpujárride-Nevado-Fibábride extensional shear zone, Betic Cordillera, SE Spain. Journal of Structural Geology, 15 (3-5): 555-569.

Jaeger, J.C.; Cook, N.G.W. and Zimmerman, R.W. (2007). Fundamentals of Rock Mechanics. Blackwell Publishing. 475 pp.

Janbu, N. (1973). Slopes stability computations. In: E. Hirschfield and S. Poulos (Editors). Embankment Dam Engineering (Casagrande Memorial Volume). John Wiley & Sons, New York, pp. 47-86.

Jibson, R.W. (1993). Predicting earthquake-induce landslide displacements using Newmark's sliding analysis. Transportation Research Record, 1411: 9-17.

Jibson, R.W. (1996). Use of landslides for paleoseismic analysis. Engineering Geology, 43: 291-323.

Jibson, R.W. (2007). Regression models for estimating coseismic landslide displacement. Engineering Geology, 91: 209-218.

Jibson, R.W.; Harp, E.L. and Michael, J.A. (2000). A method for producing digital probabilistic seismic landslide hazard maps. Engineering Geology, 58: 271-289.

Jibson, R.W. and Michael, J.A. (2009). Maps showing seismic landslide hazards in Anchorage, Alaska. U.S. Geological Survey Scientific Investigations Map 3077, scale 1:25,000, 11-p. pamphlet. [Available at URL http://pubs.usgs.gov/sim/3077]

Jibson, R.W. and Keefer, D.K. (1993). Analysis of the seismic origin of landslides: Examples from the New Madrid seismic zone. Geological Society of America Bulletin, 105: 521-536.

Jiménez Pintor, J. (2006). El deslizamiento de Güevéjar. M.Sc. Thesis on Engineering Geology. University of Granada, 85 pp.

Jiménez Pintor, J. and Azor, A. (2006). El Deslizamiento de Güevéjar (provincia de Granada): un caso de inestabilidad de laderas inducida por sismos. Geogaceta, 40: 287-290.

Jiménez-Salas, J.A. and Justo-Alpañés, J.L. (1975). Geotecnia y cimientos I. Propiedades de los suelos y las rocas. Editorial Rueda, Madrid.

Johnson, C. (1997). Resolving denudational histories in orogenic belts with apatite fission-track thermochronology and structural data: An example from southern Spain. Geology, 25 (7): 623-626.

Johnston, A.C. (1996). Seismic moment of earthquakes in stable continental regions III. New Madrid 1811-12, Charleston 1886 and Lisbon 1755. Geophysical Journal International, 126: 314-344.

Kahraman, S. (2001). Evaluation of simple methods for assessing the uniaxial compressive strength of rock. International Journal of Rock Mechanics and Mining Sciences, 38: 981-994.

Kampschuur, W., Langenberg, C.W., Baena, J., Velando, F., García-Monzon, G., Paquet, J. and Rondeel, H.E. (1972). N° 932: Coy; Spanish Geologic Map 1:50,000 scale (2nd serie). Instituto Geológico y Minero de España (IGME), Madrid.

Karnik, V. (1971). Seismicity of the European area. Part I. D. Reidel Publishing Company, Dordrecht, Holland, 372 pp.

Katz, O., Reches, Z. and Roegiers, J.C. (2000). Evaluation of mechanical rock properties using a Schmidt Hammer. International Journal of Rock Mechanics and Mining Sciences, 37: 723-728.

Keefer, D.K. (1984). Landslides caused by earthquakes. Geological Society of America Bulletin, 95: 406-421.

Keefer, D.K. (1994). The importance of earthquake-induced landslides to long-term slope erosion and slope-failure hazards in seismically active regions. Geomorphology, 10: 265-284.

Keefer, D.K. (2002). Investigating landslides caused by earthquakes - A historical review. Surveys in Geophysics, 23: 473-510.

Keystone Retaining Wall Systems (2000). Soil Stregth. Technical Notes. 1 p.

Koliopoulos, P.K., Margaris, B.N. and Klims, N.S. (1998). Duration and energy characteristics of Greek strong motion records. Journal of Earthquake Engineering, 2(3): 391-417.

Koloski, J.W.; Schwarz, S.D. and Tubbs, D.W. (1989). Geotechnical properties of geologic materials. In: Galster, R.W., chairman, Engineering geology in Washington. Washington Division of Geology and Earth Resources Bulletin, 78, v. I: 19-26.

Kramer, S.L. (1996). Geotechnical earthquake engineering. Prentice Hall, New Jersey, 653 pp.

Lamas, F.; Irigaray, C. and Chacón, J. (2002). Geotechnical characterization of carbonate marls for the construction of impermeable dam cores. Engineering Geology, 66: 283-294.

Lonergan, L. and Platt, J.P. (1994). The Internal-External Zone Boundary in the eastern Betic Cordillera, SE Spain. Journal of Structural Geology, 16 (2): 175-188.

Lonergan, L. and Platt, J. (1995). The Malaguide-Alpujarride boundary: a major extensional contact in the Internal Zone of the eastern Betic Cordillera, SE Spain. Journal of Structural Geology, 17 (12): 1665-1671.

López Casado, C., Molina Palacios, S., Delgado, J. and Peláez, J.A. (2000). Attenuation of Intensity with Epicentral Distance in the Iberian Peninsula. Bulletin of the Seismological Society of America, 90(1): 34-47.

López Casado, C.; Peláez Montilla, J.A. and Henares Romero, J. (2001). Sismicidad en la Cuenca de Granada. In: La Cuenca de Granada. Estructura, Tectónica activa, Sismicidad, Geomorfología y dataciones existentes, Sanz de Galdeano, C.; Peláez Montilla, J.A. and López Garrido. A.C. (Eds.), CSIC-University of Granada, 148-157.

López Marinas, J.M. (1978). Terremotos históricos acaecidos en las provincias de Murcia y Alicante. Cimbra, 156: 4-16.

Luzi, L. and Pergalani, F. (1996). Applications of statistical and GIS techniques to slope instability zonation (1:50.000 Fabriano geological map sheet). Soil Dynamics and Earthquake Engineering, 15: 83-94

Luzi, L. and Pergalani, F. (2000). A correlation between slope failures and accelerometric parameters: the 26 September 1997 earthquake (Umbria-Marche, Italy). Soil Dynamics and Earthquake Engineering, 20: 301-313.

Luzi, L.; Pergalani, F. and Terlien, M.T.J. (2000). Slope vulnerability to earthquakes at subregional scale, using probabilistic techniques and geographic information systems. Engineering Geology, 58: 313-336.

Machado, F. (1966). Contribução para o estudo do terremoto de 1 de Novembro de 1755. Revista da Faculdade de Ciências de Lisboa, Series C 14, 19-31.

Mankelow, J.M. and Murphy, W. (1998). Using GIS in the probabilistic assessment of earthquake triggered landslide hazards. Journal of Earthquake Engineering, 2(4): 593-623.

Margottini, C., Molin, D. and Serva, L. (1992). Intensity versus ground motion: a new approach using Italian data. Engineering Geology, 33: 45-58.

Marín-Lechado, C.; Galindo-Zaldívar, J. and Rodríguez-Fernández, L.R. (2002). Deformaciones tectónicas desde el Tortoniense en el Campo de Dalías (Cordilleras Béticas). Geogaceta, 32: 171-173.

Martín, A.J., Carreño, E. and Izquierdo, A. (1996). Análisis de la atenuación de aceleraciones de la serie de sismos de Adra de 1993 y 1994. Avances en Geodesia y Geofísica, I (1): 115-123.

Martín-Algarra, A. (1987). Evolución geológica alpina del contacto entre las Zonas Internas y las Zonas Externas de la Cordillera Bética. Ph.D. Thesis. University of Granada, 1171 pp.

Martínez-Díaz, J.J. (1998). Neotectónica y Tectónica Activa del sector centroccidental de Murcia y Sur de Almería, Cordillera Bética (España). Ph.D. Thesis. University Complutense of Madrid, Spain, 466 pp.

Martínez-Díaz, J.J. (2000). Indicios geomorfológicos indicativos de tectónica activa en el sector Lorca-Totana de la Falla de Alhama de Murcia. Boletín Geológico y Minero, 111 (1): 67-76.

Martínez-Díaz, J.J. (2002). Stress field variation related to fault interaction in a reverse oblique-slip fault: the Alhama de Murcia fault, Betic Cordillera, Spain. Tectonophysics, 356: 291-305.

Martínez-Díaz, J.J. and Hernández-Enrile, J.L. (1991). Reactivación de la falla de Alhama de Murcia (sector de Lorca-Totana): cinemática y campos de esfuerzos desde el Messiniense hasta la actualidad. Geogaceta, 9: 38-42.

Martínez-Díaz, J.J. and Hernández-Enrile, J.L. (1992). Tectónica reciente y rasgos sismotectónicos en el sector Lorca-Totana de la Falla de Alhama de Murcia. Estudios Geológicos, 48: 153-162.

Martínez-Díaz, J.J. and Hernández-Enrile, J.L. (1999). Segmentación tectónica de la Falla de Alhama de Murcia y actividad paleosísmica asociada. Contribución a la determinación de la peligrosidad sísmica en la región de Murcia. I Congreso Nacional de Ingeniería Sísmica, Murcia. Memorias Ia, 75-87.

Martínez-Díaz, J.J.; Masana, E.; Hernández-Enrile, J.L. and Santanach, P. (2001). Evidence for coseismic events of recurrent prehistoric deformation along the Alhama de Murcia Fault, southeastern Spain. Acta Geologica Hispanica, 36 (3-4): 315-327.

Martínez-Díaz, J.J., Rigo, A., Louis, L., Capote, R., Hernández-Henrile, J., Carreño, E. and Tsige, M. (2002). Caracterización geológica y sismotectónica del terremoto de Mula (Febrero 1999, Mb 4.8) mediante la utilización de datos geológicos, sismológicos y de interferometría de RADAR (INSAR). Geogaceta, 31: 157-160.

Martínez-Guevara, J.B. (1984). Temblores de tierra en el núcleo sísmico de Lorca-Totana. Estudio de sismicidad histórica. Instituto Geográfico Nacional, Murcia, nº 51, pp.

Martínez-Martínez, J.M., Booth-Rea, G., Azañón, J.M. and Torcal, F. (2006). Active transfer fault zone linking a segmented extensional system (Betics, southern Spain): Insight into heterogeneous extension driven by edge delamination. Tectonophysics, 422: 159-173.

Martínez-Martínez, J.M.; Soto, J.I. and Balanyá, J.C. (2002). Orthogonal holding of extensional detachments: structure and origin of the Sierra Nevada elongate dome (Betics, SE Spain). Tectonics, 21 (3): 1012.

Martínez Solares, J.M. and López Arroyo, A. (2004). The great historical 1755 earthquake. Effects and damage in Spain. Journal of Seismology, 8: 275-294.

Martínez Solares, J.M. and Mezcua, J. (2002). Catálogo sísmico de la Península Ibérica (880 a.c.-1900). Monograph 18. Instituto Geográfico Nacional, Madrid, 253 pp.

Masana, E.; Martínez-Díaz, J.J.; Hernández-Enrile, J.L. and Santanach, P. (2004). The Alhama de Murcia fault (SE Spain), a seismogenic fault in a diffuse plate boundary: Seismotectonic implications for the Ibero-Magrebian region. Journal of Geophysical Research, 109 (1): 17 pp.

Mayne, P.W.; Christopher, B.R. and DeJong, J.T. (2002). Manual on Subsurface Investigations. FHWA Publication No. FHWA NHI-01-031, Washington, D.C., 294 pp.

Medvedev, S.V. and Sponheuer, W. (1969). Scale of seismic intensity. Proceedings of the 4th World Conference of Earthquake Engineering. A-2, Santiago, Chile, 143-153.

Meijninger, B.M.L. and Vissers, R.L.M. (2006). Miocene extensional basin development in the Betic Cordillera,SE Spain revealed through analysis of the Alhama de Murcia and Crevillente Faults. Basin Research, 18: 547-571.

Mezcua, J., Herraiz, M. and Buforn, E. (1984). Study of the 6 June 1977 Lorca (Spain) earthquake and its aftershock sequence. Bulletin of the Seismological Society of America, 74 (1): 167-179.

Mezcua, J., Rueda, J. and García Blanco, R.M. (2004). Reevaluation of Historic Earthquakes in Spain. Seismological Research Letters, 75 (1): 75-81.

Michetti, A.M. et al. (2007). Intensity Scale ESI 2007. In: Guerrieru L and Vittori E (eds.), Mem. Descr. Carta Geol. d'Italia., vol. 74, Servizio Geologico d'Italia - Dipartimento Difesa del Suolo, APAT, Rome, Italy.

Miles, S.B. and Ho, C.L. (1999). Rigorous landslide hazard zonation using Newmark's method and stochastic ground motion simulation. Soil Dynamics and Earthquake Engineering, 18(4): 305-323.

Ministerio de Fomento (2009). Guía de cimentaciones en obras de carretera (3rd ed.). Dirección General de Carreteras. Centro de Publicaciones, 304 pp.

Montenat, C. (ed.); Ott d'Estevou, Ph. and Delort, T. (1990). Les Bassins néogènes du domaine Bétique oriental (Espagne), Documents et Travaux de l'Institut Geologique Albert de Lapparent, 12-13: 261-280.

Montenat, C. and Ott d'Estevou, P. (1999). The diversity of late Neogene sedimentary basins generated by wrench faulting in the Eastern Betic Cordillera, SE Spain. Journal of Petroleum Geology, 22(1): 61-80.

MOP (1971). Estudio previo de terrenos, Autopista del Mediterráneo, tramo Murcia-Lorca. Dirección General de Carreteras, División de Materiales, Madrid, 2 maps, 125 pp.

Morales, J., Singh, S.K. and Ordaz, M. (1996). Analysis of the Granada (Spain) earthquake of 24 June, 1984 (M = 5) with emphasis on seismic hazard in the Granada Basin. Tectonophysics, 257: 253-263.

Morales, J., Serrano, I., Vidal, F. and Torcal, F. (1997). The depth of the earthquake activity in the Central Betics (Southern Spain). Geophysical Research Letters, 24(24): 3289-3292.

Morgenstern, N.R. and Price, V.E. (1965). The analysis of the stability of general slip surfaces. Geotechnique, 15(1): 79-93.

Mulas, J., Ponce de León, D., Martínez, M., and Pardo, J.M. (2001). Diseño de una metodología para la zonificación de la inestabilidad de laderas naturales producidas por terremotos. Aplicación a una zona del Pirineo Central (Huesca). V Simposio Nacional sobre Taludes y Laderas Inestables, Vol. III: 1241-1252.

Mulas, J.; Ponce de León, D. and Reoyo, E. (2003). Microzonación sísmica de movimientos de ladera en una zona del Pirineo Central. 2º Congreso Nacional de Ingeniería Sísmica, 13-26.

Muñoz, D. and Udías, A. (1981). Estudio de los parámetros y serie de replicas del terremoto de Andalucía del 25 de Diciembre de 1884 y la sismicidad de la región de Granada-Málaga. In: El Terremoto de Andalucía de 25 de Diciembre de 1884. Instituto Geográfico Nacional (Ed.), Madrid (Spain), 95-139.

Muñoz, D., Cisternas, A., Udías, A., Mezcua, J., Sanz de Galdeano, C., Morales, J., Sánchez-Venero, M., Haessler, H., Ibáñez, J., Buforn, E., Pascual, G. and Rivera, L. (2002). Microseismicity and tectonics in the Granada Basin (Spain). Tectonophysics, 356: 233-252.

Murphy, P. (2005). Informe macrosísmico de los terremotos de Lorca de Enero de 2005. Instituto Geográfico Nacional, Madrid, 45 pp.

Murphy, W. (2006). The role of topographic amplification on the initiation of rock slopes failures during earthquakes. In: Evans et al. (Ed.), Landslides from Massive Rock Slope Failure, p. 139-154.

Murphy J.R. and O'Brien, L.J. (1977). The correlation of peak ground acceleration amplitude with intensity and other physical parameters. Bulletin of the Seismological Society of America, 67: 877-915.

Murphy, W., Petley, D.N., Bommer, J. and Mankelow, J.M. (2002). Uncertainty in ground motion estimates for the evaluation of slope stability during earthquakes. Quarterly Journal of Engineering Geology and Hydrogeology, 58: 271-289.

Murphy, W. and Mankelow, J.H. (2004). Obtaining probabilistic estimates of displacements on a landslide during future earthquakes. Journal of Earthquake Engineering, 8: 133-157.

Navarro, M.; Góngora, A.; Vidal, F.; Dominguez, S.; Benito, B. and Alcalá, F. (2009). A proposal on soil classification for site effect estimation in Andalusia region (southern Spain) applicable to seismic risk management. 8th International Workshop on Seismic Microzoning and Risk Reduction Workshop Abstract and Short Paper CD (ISBN 978-84-691-9107-1), Almería, Spain, pp. 25-35.

NCSE-02 (2002). Norma de Construcción Sismorresistente: Parte general y edificación. Comisión Permanente de Normas Sismorresistentes. B.O.E. de 11 de octubre de 2002 (35898-35967).

NEHRP (National Earthquake Hazards Reduction Program) (2003). Recommendation prevision for seismic regulation for new buildings and other structures, In: Building Seismic Safety Council, Washington, D.C. Federal Emergency. FEMA.

Neumann, F. (1954). Earthquake Intensity and Related Ground Motion, University Press, Seattle, Washington, 77 pp.

Newmark, N.M. (1965). Effects of earthquakes on dams and embankments. Geotechnique, 15 (2): 139-160.

Nieto, L.M. and Rey, J. (2003). Magnitude of lateral displacement of the Crevillente Fault Zone (Betic Cordillera, SE Spain): stratigraphical and sedimentological considerations. Geol. Jour., 38: 1-16

Nobel, F.A.; Andriessen, P.A.M.; Hebeda, E.H.; Priem, H.N.A. and Rondeel, H.E. (1981). Isotopic dating of the post-Alpine Neogene volcanism in the Betic Cordilleras, southern Spain. Geologie en Mijnbouw, 60: 209-214.

Nuttli, O.W. (1985). Average seismic source-parameter relations for plate-margin earthquakes. Tectonophysics, 118: 161-174.

Oteo Mazo, C. (2001) Informe sobre el deslizamiento de Diezma (A-92) y las soluciones para estabilizarlo. Consejería de Obras Públicas y Urbanismo de la Junta de Andalucía, Madrid (Spain), 60 pp.

Oteo Mazo, C. (2003) Diseño y ejecución del tratamiento para estabilizar el deslizamiento de Diezma (Granada): Special Volume of the III Congreso Andaluz de Carreteras, 7-10 October 2003, Sevilla, vol. 3, pp. 40-52.

Ott d'Estevou and Montenat, C. (1985). Evolution structurale de la zone bétique orientale (Espagne) du Tortonien à l'Holocène. C.R. Acad. Sci. París. T. 300, série II, 8: 363-368.

Panza, G.F., Cazzaro, R. and Vaccari, F. (1997). Correlation between macroseismic intensities and seismic ground motion parameters. Annali di Geofisica, 40(5): 1371-1382.

Pedersen, H.; Le Brun, B.; Hatzfeld, D.; Campillo, M. and Bard, P.Y. (1994). Ground-motion amplitude across ridges. Bulletin of the Seismological Society of America, 84: 1786-1800.

Peláez Montilla, J.A.; Sanz de Galdeano, C. and López Casado, C. (2001). Potencialidad sísmica de las fallas de la Cuenca de Granada. In: La Cuenca de Granada. Estructura, Tectónica activa, Sismicidad, Geomorfología y dataciones existentes, Sanz de Galdeano, C.; Peláez Montilla, J.A. and López Garrido. A.C. (Eds.), CSIC-University of Granada, 158-174.

Pérez-López, A. and Sanz de Galdeano, C. (1994). Tectónica de los materiales triásicos en el sector central de la Zona Subbética (Cordillera Bética). Revista de la Sociedad Geológica de España, 7: 141-153.

Platt, J.P. and Vissers, R.L.M. (1989). Extensional collapse of thickened continental litosphere: A working hypothesis for the Alboran Sea and Gibraltar Arc. Geology, 17: 540-543.

Rapolla, A., Paoletti, V. and Secomandi, M. (2010). Seismically-induced landslide susceptibility evaluation: Application of a new procedure to the island of Ischia, Campania Region, Southern Italy. Engineering Geology, 114(1-2): 10-25.

Reicherter, K.R. (2001). Paleoseismologic advances in the Granada basin (Betic Cordilleras, southern Spain). Acta Geologica Hispanica, 36 (3-4): 267-281.

Reicherter, K.R.; Jabaloy, A.; Galindo-Zaldívar, J.; Ruano, P.; Becker-Heidmann, P.; Morales, J.; Reiss, S. and González-Lodeiro, F. (2003). Repeated palaeoseismic activity of the Ventas de Zafarraya fault (S Spain) and its relation with the 1884 Andalusian earthquake. International Journal of Earth Sciences (Geologische Rundschau), 92: 912-922.

Reid, H.F. (1914). The Lisbon earthquake of November 1, 1755. Bulletin of the Seismological Society of America, 4(2): 53-80.

Rey Pastor, A. (1949). Comarca sísmica de Caravaca y el sismo del 23 de junio de 1948. Instituto Geográfico y Catastral, Madrid, pp. 21-33.

Rocscience Inc. (2003). Slide 5.0 User's Guide. Part I. 199 pp.

Rodríguez, C.E.; Bommer, J.J. and Chandler, R.J. (1999). Earthquake-induced landslides: 1980-1997. Soil Dynamics and Earthquake Engineering, 18(5): 325-346.

Rodríguez-Estrella, T. and Almoguera, J. (1986). La neotectónica del noreste de Lorca (Murcia) y su incidencia en el canal del trasvase Tajo-Segura. En: I Jornadas de Estudio del Fenómeno Sísmico y su incidencia en la ordenación del territorio. IGN.

Rodríguez-Estrella, T. and Mancheño, R. (1993). La Neotectónica de Lorca y sus alrededores en relación con la actividad actual de la Falla de Alhama de Murcia. Análisis de las grietas del Túnel de Lorca y de los barrios altos de esta ciudad. Problemática Geoambiental y Desarrollo, 1: 709-715.

Rodríguez-Fernández, J. and Sanz de Galdeano, C. (2006). Late orogenic intramontane basin development: the Granada basin, Betics (southern Spain). Basin Research, 18: 85-102.

Rodríguez Ortiz, J.M..; Serra, J. and Oteo, C. (1986). Curso Aplicado de Cimentaciones. Colegio Oficial de Arquitectos. Madrid. 266 pp.

Rodríguez-Peces, M.J. (2008). Evaluación regional de inestabilidades de ladera por efecto sísmico: mapas de desplazamiento de Newmark para la Cuenca de Lorca, Cuenca de Granada y Sierra Nevada. M.Sc. Thesis on Geology. University of Granada (Spain), 254 pp.

Rodríguez Peces, M.J.; García Mayordomo, J.; Azañón-Hernández, J.M. and Jabaloy Sánchez, A. (2008). Evaluación regional de inestabilidades de ladera por efecto sísmico en la Cuenca de Lorca (Murcia): Implementación del método de Newmark en un SIG. Boletín Geológico y Minero, 119 (4): 459-472.

Rodríguez-Peces, M.J.; García-Mayordomo, J.; Azañón-Hernández, J.M. and Jabaloy-Sánchez, A. (2009). Comparing Newmark's method at regional and local scales: La Paca earthquake induced rock-fall case (Murcia, SE Spain). Geophysical Research Abstracts, 11, EGU2009-7949-3, European Geoscience Union General Assembly 2009, Vienna, Austria.

Rodríguez Peces, M.J.; García Mayordomo, J. and Azañón, J.M (2009). Comparación del método de Newmark a escala regional, local y de emplazamiento: el caso del desprendimiento de la Paca (Murcia, SE España). Geogaceta, 46: 151-154.

ROM 0.5-05 (2005). Geotechnical recommendations for the design of maritime and harbour works. Puertos del Estado, Ministerio de Fomento, Madrid (Spain). 546 pp.

Romeo, R. (2000). Seismically induced landslide displacements: a predictive model. Engineering Geology, 58: 337-351.

Rueda, J. and Mezcua, J. (2001). Sismicidad, sismotectónica y peligrosidad sísmica en Galicia. Instituto Geográfico Nacional, Madrid, 64 pp.

Rueda J. and Mezcua J. (2002). Estudio del terremoto de 23 de Septiembre de 2001 en Pego (Alicante). Obtención de una relación mbLg-Mw para la Península Ibérica. Revista de la Sociedad Geológica de España, 15(3-4): 159-173.

Sabatakakis, N.; Koukis, G.; Tsiambaos, G. and Papanakli, S. (2008). Index properties and strength variation controlled by microstructure for sedimentary rocks. Engineering Geology, 97: 80-90.

Sabetta, F. and Pugliese, A. (1996). Estimation of Response Spectra and Simulation of Nonstationary Earthquake Ground Motions. Bulletin of the Seismological Society of America, 86 (2): 337-352.

Sachpazis, C.I. (1990). Correlating Schmidt hardness with compressive strength and Young's modulus of carbonate rocks. Bulletin of the International Association of Engineering Geology, 42: 75-83.

Sanz de Galdeano, C. (1973). Geología de la transversal Jaén-Frailes (provincia de Jaén). Ph.D. Thesis, University of Granada, 274 pp.

Sanz de Galdeano, C. (1983). Los accidentes y fracturas principales de las Cordilleras Béticas. Estudios Geológicos, 39: 157-165.

Sanz de Galdeano, C. (1990). Geologic evolution of the Betic Cordilleras in the Western Mediterranean, Miocene to the present. Tectonophysics, 172: 107-119.

Sanz de Galdeano, C. (1996). The E-W segments of the contact between the External and Internal Zones of the Betic and Rif Cordilleras and the E-W corridors of the Internal Zone (A combined explanation). Estudios Geológicos, 52: 123-136.

Sanz de Galdeano, C. (2001a). Las fallas del sector nororiental de la Cuenca de Granada. In: La Cuenca de Granada. Estructura, Tectónica activa, Sismicidad, Geomorfología y dataciones existentes, Sanz de Galdeano, C.; Peláez Montilla, J.A. and López Garrido. A.C. (Eds.), CSIC-University of Granada, 117-120.

Sanz de Galdeano, C. (2001b). El borde meridional de la Cuenca de Granada, desde Jayena a Zafarraya. In: La Cuenca de Granada. Estructura, Tectónica activa, Sismicidad, Geomorfología y dataciones existentes, Sanz de Galdeano, C.; Peláez Montilla, J.A. and López Garrido. A.C. (Eds.), CSIC-University of Granada, 139-142.

Sanz de Galdeano, C. and Alfaro, P. (2004). Tectonic significance of the present relief of the Betic Cordillera. Geomorphology, 63 (3-4): 175-190.

Sanz de Galdeano, C. and Buforn, E. (2005). From strike-slip to reverse reactivation: The Crevillente Fault System and seismicity in the Bullas-Mula area (Betic Cordillera, SE Spain). Geologica Acta, Vol.3, Nº 3: 241-250.

Sanz de Galdeano, C. and López Garrido. A.C. (2000). Las fallas neotectónicas entre Granada y la Costa: El límite occidental del Nevado-Filábride y de las unidades alpujárrides inferiores. Revista de la Sociedad Geológica de España, 13 (3-4): 519-528.

Sanz de Galdeano, C. and Vera, J.A. (1991). Una propuesta de clasificación de las cuencas neógenas béticas. Acta Geologica Hispanica, 26: 205-227.

Sanz de Galdeano, C. and Vera, J.A. (1992). Stratigraphic record and palaeogeographical context of the Neogene basins in the Betic Cordillera, Spain. Basin Research, 4: 21-36.

Sanz de Galdeano, C.; Peláez Montilla, J.A. and López Casado. C. (2003). Seismic Potential of the Main Active Faults in the Granada Basin (Southern Spain). Pure and Applied Geophysics, 160: 1537-1556.

Sanz Pérez, E. (1992). El deslizamiento de ladera de Güevéjar (Granada) durante los terremotos de Lisboa (1755) y Andalucía (1884). III Simposio Nacional sobre Taludes y Laderas Inestables. La Coruña (Spain), 195-203.

Sepúlveda, S.A.; Murphy, W. and Petley, D.N. (2005a). Topographic controls on coseismic rock slides during the 1999 Chi-Chi earthquake, Taiwan. Quarterly Journal of Engineering Geology and Hydrogeology, 38 (2): 189–196.

Sepúlveda, S.A.; Murphy, W.; Jibson, R.W. and Petley, D.N. (2005b). Seismically induced rock slope failures resulting from topographic amplification of strong ground motions: The case of Pacoima Canyon, California. Engineering Geology, 80: 336-348.

Serpelloni, E., Vannucci, G., Pondrelli, S., Argnani, A., Casula, G., Anzidei, M., Baldi, P. and Gasperini, P. (2007). Kinematics of the Western Africa-Eurasia plate boundary from focal mechanisms and GPS data. Geophysical Journal International, 169: 1180-1200.

Shalabi, F.; Cording, E.J. and Al-Hattamleh, O.H. (2007). Estimation of rock engineering properties using hardness tests. Engineering Geology, 90:138-147.

Silva, P.G. (1994). Evolución geodinámica de la Depresión del Guadalentín desde el Mioceno Superior hasta la actualidad: Neotectónica y Geomorfología. Ph.D. Thesis, University Complutense of Madrid, 642 pp.

Silva, P.G.; Goy, J.L.; Somoza, L.; Zazo, C. and Bardají, T. (1993). Landscape response to strike-slip faulting linked to collisional settings: quaternary tectonics and basin formation in the Eastern Betics, Southeast Spain. Tectonophysics, 224: 289-303.

Silva, P.G.; Goy, J.L. and Zazo, C. (1992). Características estructurales y geométricas de la falla de desgarre de Lorca-Alhama. Geogaceta, 12: 7-11.

Silva, P.G., Goy, J.L., Zazo, C., Lario, J. and Bardají, T. (1997). Paleoseismic indications along 'aseismic' fault segments in the Guadalentín Depression (SE Spain). Journal of Geodynamics, 24 (1-4): 105-115.

Silva, P.G., Goy, J.L., Zazo, C. and Bardají T. (2003). Fault-generated mountain fronts in southeast Spain: geomorphologic assessment of tectonic and seismic activity. Geomorphology, 50: 203-225.

Skarlatoudis, A.A., Papazachos, B.N., Margaris, N., Theodulidis, C., Papaioannou, I., Kalogeras, E.M., Scordilis, E.M. and Karakostas, V. (2003). Empirical peak ground-motion predictive relations for shallow earthquakes in Greece. Bulletin of the Seismological Society of America, 93(6): 2591-2603.

Smoltczyk U. (editor) (2002). Geotechnical Engineering Handbook. Volumen 1: Fundamentals. Alemania, 751 pp.

Stagg, K.G. and Zienkiewicz, O.C. (1968). Mecánica de rocas en la ingeniería práctica. Editorial Blume, pp. 16-29 y 45.

Stich, D., Batlló, J., Morales, J., Macià, R. and Dineva, S. (2003). Source parameters of the Mw= 6.1 1910 Adra earthquake (southern Spain). Geophysical Journal International, 155: 539-546.

Stich, D.; Serpelloni, E.; Mancilla, F. and Morales, J. (2006). Kinematics of the Iberia-Maghreb plate contact from seismic moment tensors and GPS observations. Tectonophysics, 426: 295-317.

Taramelli, T. and Mercalli, G. (1886). I terremotti andalusi cominciati il 25 diciembre 1884. Atti Reale Accademia dei Lincei (Roma), vol. III, serie 4, 116-222.

Terzaghi, K.; Peck, R.B. and Mesri, G. (1996). Soil Mechanics in Engineering Practice (3rd ed.). John Wiley & Sons, New York. 512 pp.

Theodulidis, N.P. and Papazachos, B.C. (1992). Dependence of strong ground motion on magnitude-distance, site geology and macroseismic intensity for shallow earthquakes in Greece: I, peak horizontal acceleration, velocity and displacement. Soil Dynamics and Earthquake Engineering, 11: 387-402.

Trifunac, M.D. and Brady, A.G. (1975). On the correlation of seismic intensity scales with the peaks of recorded strong .ground motion. Bulletin of the Seismological Society of America, 65: 139-162.

Tse, R. and Cruden, D.M. (1979). Estimating joint roughness coefficients. International Journal of Rock Mechanics and Mining Sciences & Geomech. Abstr., 16: 303-307.

Tselentis, G. and Danciu, L. (2008). Empirical Relationships between Modified Mercalli Intensity and Engineering Ground-Motion Parameters in Greece. Bulletin of the Seismological Society of America, 98(4): 1863-1875.

Tselentis, G. and Danciu, L. (2010). Probabilistic seismic hazard assessment in Greece – Part 1: Engineering ground motion parameters. Natural Hazards and Earth Systems Sciences, 10: 1-15.

Tsige, M. and García Flórez, I. (2006). Propuesta de clasificación geotécnica del "efecto sitio" (amplificación sísmica) de las formaciones geológicas de la Región de Murcia. Geogaceta, 40: 39-42.

Turner, S.P.; Platt, J.P.; George, R.M.M.; Kelley, S.P.; Pearson, D.G. and Nowell, G.M. (1999). Magmatism associated with orogenic collapse of the Betic-Alboran Domain, SE Spain. Journal of Petrology, 40 (6): 1011-1036.

Udías, A. and Muñoz, D. (1979). The Andalusian earthquake of 25 December 1884. Tectonophysics, 53: 291-299.

Udías, A. and Buforn, E. (1991). Regional stresses along the Eurasia-Africa plate boundary derived from focal mechanism of large earthquakes. Pure Applied Geophysics, 136: 433-448.

USGS (2008). Web site (http://earthquake.usgs.gov/eqcenter/eqinthenews/2008/us2008ryan/). Accessed on 10 June, 2010.

Van Bemmelen, R.W. (1927). Bijdrage tot de geologie der Betisch Ketens in de provincie Granada. Ph.D. Thesis. University of Delft, Delft.

Van Westen, C.J. and Terlien, M.T.J. (1996). An approach towards deterministic landslide hazard analysis in GIS. A case study from Manizales (Colombia). Earth Surface Processes and Landforms, 21: 853-868.

Van Westen, C.J. (2000). The modelling of landslide hazards using GIS. Surveys in Geophysics, 21: 241-255.

Van Westen, C.J. (2004). Geo-information tools for landslide risk assessment: an overview of recent developments. In: Lacerda, W.A., Ehrlich, M., Fontoura, S., Sayão, A. (Eds.), Landslides: Evaluation and Stabilization, vol. 1, pp. 39-56.

Varnes, D.J. (1978). Slope movement types and processes. In: Krizek, R.J., Schuster, R.L. (eds). Landslides: Analysis and Control. Special Report, 176. Transportation Research Board, National Research Council, Washington, pp. 11-33.

Vazquez Carretero, N.J. (2001). Cálculo de la subsidencia unidimensional debida a los descensos del nivel piezométrico. Aplicación al casco urbano de Murcia y a los efectos sobre sus edificios. Ph.D. Thesis. University of Sevilla, 476 pp.

Vera, J.A. (2000). El Terciario de la Cordillera Bética: Estado actual de conocimientos. Revista de la Sociedad Geológica de España, 13: 345-373.

Vera, J.A. (editor) (2004). Geología de España. SGE-IGME, Madrid, 890 p.

Vidal, F. (1986). Sismotectónica de la región Bética-Mar de Alborán. Ph.D. Thesis, University of Granada, 450 pp.

Wald, D.J., Quitoriano, V., Heaton, T.H. and Kanamori, H. (1999). Relationships between peak ground acceleration, peak ground velocity, and modified Mercalli intensity in California. Earthquake Spectra, 15: 557-564.

Wang, K.L. and Lin, M.L. Development of shallow seismic landslide potential map based on Newmark's displacement: the case study of Chi-Chi earthquake, Taiwan. Environmental Earth Sciences, 60(4): 775-785.

Waltham, A.C. (2002). Foundations of Engineering Geology. 2nd Edition. Spon Press. London.

Wasowski, J.; Del Gaudio, V.; Pierri, P. and Capolongo, D. (2002). Factors controlling seismic susceptibility of the Sele valley: The case of the 1980 Irpinia earthquake re-examined. Surveys in Geophysics, 23: 563-593.

Weijermars, R.; Roep, Th.B.; van den Eeckhout, B.; Postma, G. and Kleverlaan, K. (1985). Uplift history of a Betic fold nappe inferred from Neogene-Quaternary sedimentation and tectonics (in the Sierra Alhamilla and Almería, Sorbas and Tabernas Basins of the Betic Cordilleras, SE Spain). Geologie en Mijnbouw, 64: 397-411.

Wells, D.L. and Coppersmith, K.J. (1994). New empirical relationships among magnitude, rupture lenght, rupture width, rupture area, and surface displacement. Bulletin of the Seismological Society of America, 84 (4): 974-1002.

Wieczorek, G.F.; Wilson, R.C. and Harp, E.L. (1985). Map showing slope stability during earthquakes in San Mateo County California. U.S. Geological Survey Miscellaneous Investigations Map I-1257-E, escala 1:62500.

Wilson, R.C. and Keefer, D.K. (1983). Dynamic analysis of a slope failure from the 6 August 1979 Coyote Lake, California, earthquake. Bulletin of the Seismological Society of America, 73: 863-877.

Wilson, R.C. and Keefer, D.K. (1985). Predicting areal limits of earthquake-induced landsliding. En: Evaluating Earthquake Hazards in the Los Ángeles Region: An Earth-Science Perspective (ed. Ziony, J.I.). U.S. Geological Survey Professional Paper, 1360: 317-345.

Xu, Q., Fan, X., Huang, R. and Van Westen, C. (2009). Landslide dams triggered by the Wenchuan Earthquake, Sichuan Province, south west China. Bulletin of Engineering Geology and the Environment, 68: 373-386.

Yang, Z.Y., Lo, S.C. and Di, C.C. (2001). Reassessing the joint roughness coefficient (JRC) estimation using Z2. Rock Mechanics and Rock Engineering, 34(3): 243-251.

Yin, Y., Wang, F. and Sun, P. (2009). Landslide hazards triggered by the 2008 Wenchuan earthquake, Sichuan, China. Landslides, 6(2): 139-152.

Youd, T.L. (1978). Major cause of earthquake failure is ground failure. Civil Engineering, ASCE, Vol. 48, No.4.